Author:
Sun, Rujie

Title:
Mechanical Metastructures with Integrated Flexible Electronics Systems

Mechanical Metastructures with Integrated Flexible Electronics Systems

Rujie Sun

Department of Aerospace Engineering

UNIVERSITY OF BRISTOL

A dissertation submitted to the University of Bristol in accordance with the requirements for award of the degree of DOCTOR OF PHILOSOPHY in the Faculty of Engineering

May 2019

Word Count: 45800

ABSTRACT

Rapid advances in material and manufacturing contribute to the wide applications of integrated flexible electronics, such as sensors, actuators, energy harvesting, etc. Piezoelectric materials have great potential in bio-medical applications because of their self-powered capacities. However, the soft and highly deformable surfaces of most tissues in the human body restrict the wide use of piezoelectric materials, which feature low stretchability.

This thesis explores the Kirigami techniques in applications of various electronic systems, including stretchable piezoelectric strain sensors, self-powered health monitoring devices, tunable sensing systems, and 3D architecture metastructures.

The Kirigami technique with linear cut patterns has been employed to design a stretchable piezoelectric sensor with enhanced piezoelectricity. A parametric study is performed to investigate its mechanical behaviour, followed by experimental tests. An inter-segment electrode connection approach is proposed to further enhance the piezoelectric performance of the sensor. A series of dynamics tests under a range of loading conditions, including variable frequencies and strains, are carried out to evaluate the performances of the Kirigami-based sensors, and the results validate the promising potential as stretchable electronic systems for biomedical applications.

Then, in terms of applications in health monitoring, an integrated sensing system is developed in conjunction with a wireless communication interface for data transmission. With the superior performances of mechanical stretchability by Kirigami designs, the devices can be mounted on different surfaces as either wearable or implantable systems without mechanical irritation. The outstanding mechanical and electrical performances have been validated by experiments for cardiac monitoring and wearable body tracking, offering insights into future implantable and wearable healthcare applications.

A non-uniform Kirigami pattern is further studied and its potential applications in tunable sensing performances are investigated. A class of highly tunable mechanical metastructures with controlled and predictable spatial deformations by prescribed non-uniform Kirigami patterns is proposed and verified by combined numerical simulation and experimental tests. A demonstration application of the non-uniform Kirigami pattern in piezoelectric sensors shows that this type of metastructure design paves new ways to the developments of stretchable electronics.

A 3D vibration platform based on Kirigami cut topologies is proposed based on the design of metastructures subjected to compressive buckling. The tunable dynamic performances of the vibration systems can be achieved by changing the compressive strains and Kirigami cut patterns. Following the presented platform, a 3D energy harvester is designed and its energy harvesting performance in multi-directional vibrations within a wide frequency range is evaluated.

To My Loving Parents

DEDICATION AND ACKNOWLEDGEMENTS

I would like to sincerely appreciate all who have given me valuable advices and constant help during my PhD stage, making it an unformattable experience in my life.

I would like firstly to express my appreciations to my supervisors, Professor Fabrizio Scarpa and Professor Jonathan Rossiter. Whenever I had questions and felt confused, they always provided valuable suggestions, and helped me figure out the key issues. In a flexible working environment, I enjoyed my research life and learnt a lot during the past years. My supervisors not just gave me the solutions, but more focused on the way how to solve the problems and to be an independent researcher. I could always get inspirations from the discussions with them. In addition to the academic supervision, they also gave me much help in paper writing and career developments.

Many thanks to Professor John Rogers at Northwestern University in the US. During the one-year research in his group, I participated in several challenging and exciting projects, learning a lot of practical techniques in the area of flexible electronics and relevant biomedical applications. This research experience had significant influence on my following PhD research.

Thanks to Dr Ian Farrow for valuable advices and help on my PhD projects. Thanks to Professor Paul Weaver in ACCIS CDT. During my first-year study, Professor Weaver gave me many advices and useful suggestions on the PhD projects. Thanks to Sarah Hallworth who gave me many suggestions during the first-year CDT life. Thanks to Dr Nathan Lepora for his reviews and suggestions during my annual PhD reviews. Thanks to Dr Andrew Murray and Dr Germinal Magro who gave me a lot of support for my experimental setup.

I would also like to acknowledge the support from the China Scholarship Council, and the Engineering and Physical Sciences Research Council through the EPSRC Centre for Doctoral Training in Advanced Composites for Innovation and Science (Grant No. EP/L016028/1).

Thanks to my colleagues in ACCIS and Soft Robotics groups for their support in research. Thanks to Dr Sara Correia Carreira, Dr Chaoqun Xiang, Dr Xiao-Chong Zhang, Dr Bing Zhang, Dr Xun Wu, Dr Ningbo Xie, Dr Chenchen Zhu, Dr Jianglong Guo, Logan Wang, Yanjun He, Yi Wang. Thanks to my friends, LuLu Xu and Yan Chen, for their valuable advices.

Many thanks to my colleagues and friends in Rogers' group. Thanks to Professor Xinge Yu, Professor Yi Zhang, Professor Xueju Wang for their valuable advices and help in research and life.

I would like to express my special thanks to my friends, Dr Chen Zhou and Dr Lanwei Zhou, who have been giving me constant support during my whole PhD life.

Finally, and most importantly, I would like to express my sincere thanks to my family who have been giving me support, trust, and encouragement in my whole life. Thanks to their constant love without which I would not be able to better focus on my PhD research and enjoy the life in UK.

AUTHOR'S DECLARATION

I declare that the work in this dissertation was carried out in accordance with the requirements of the University's Regulations and Code of Practice for Research Degree Programmes and that it has not been submitted for any other academic award. Except where indicated by specific reference in the text, the work is the candidate's own work. Work done in collaboration with, or with the assistance of others, is indicated as such. Any views expressed in the dissertation are those of the author.

SIGNED:……DATE:…… ……

CONTENTS

LIST OF FIGURES

LIST OF TABLES

Journal Publications

Part work in this thesis have been published in peer-reviewed journals. Namely, Chapter 3 and Chapter 4 are based on Paper 1 and Paper 2 respectively.

1. **R. Sun**, S. Carreira, Y. Chen, C. Xiang, B. Zhang, I. Farrow, F. Scarpa, J. Rossiter. Stretchable Piezoelectric Sensing Systems for Self-powered and Wireless Health Monitoring. *Advanced Materials Technologies*, 2019: 1900100
2. **R. Sun**, B. Zhang, L. Yang, W. Zhang, I. Farrow, F. Scarpa, J. Rossiter. Kirigami Stretchable Strain Sensors with Enhanced Piezoelectricity Induced by Topological Electrodes. *Applied Physics Letters*. 2018, 112(25):251904. (Highlight, Featured Paper)
3. X. Yu, H. Wang, X. Ning, **R. Sun**, H. Albadawi, M. Salomao, A.C. Silva, Y. Yu, L. Tian, A. Koh, C.M. Lee, A. Chempakasseril, P. Tian, M. Pharr, J. Yuan, Y. Huang, R. Oklu and J.A. Rogers, Needle-shaped Ultrathin Piezoelectric Microsystem for Guided Tissue Targeting via Mechanical Sensing. *Nature Biomedical Engineering*. 2018, 2, 165–172. (Cover Paper)
4. X. Ning, X. Yu, H. Wang, **R. Sun**, R.E. Corman, H. Li, C.M. Lee, Y. Xue, A. Chempakasseril, Y. Yao, Z. Zhang, H. Luan, Z. Wang, W. Xia, X. Feng, R.H. Ewoldt, Y. Huang, Y. Zhang and J.A. Rogers, Mechanically Active Materials in Three-Dimensional Mesostructures. *Science Advances*. 2018, 4: eaat8313. (Highlight Paper)
5. X. Zhao, H. Shen, **R. Sun**, Q. Luo, X. Li, Y. Zhou, M. Tai, J. Li, Y. Gao, X. Li, H. Lin. Bending Durable and Recyclable Mesostructured Perovskite Solar Cells Based on Superaligned ZnO Nanorod Electrode. *Solar RRL*, 2018, 2(5), 1700194.
6. C. Mu, Y. Song, W. Huang, A. Ran, **R. Sun**, W. Xie, H. Zhang. Flexible Normal-Tangential Force Sensor with Opposite Resistance Responding for Highly Sensitive Artificial Skin. *Advanced Functional Materials*. 2018, 28(18), 1707503.
7. X. Wang, X. Guo, J. Ye, N. Zheng, P. Kohli, D. Choi, Y. Zhang, Z. Xie, Q. Zhang, H. Luan, K. Nan, B. H. Kim, Y. Xu, X. Shan, W. Bai, **R. Sun**, Z. Wang, H. Jang, F. Zhang, Y. Ma, Z. Xu, X. Feng, T. Xie, Y. Huang, Y. Zhang, J. A. Rogers. Freestanding 3D Mesostructures, Functional Devices, and Shape-Programmable Systems Based on Mechanically Induced Assembly with Shape Memory Polymers. *Advanced Materials*. 2018, 1805615
8. C. Mu, J. Li, Y. Song, W. Huang, A. Ran, K. Deng, J. Huang, W. Xie, **R. Sun**, H. Zhang. Enhanced Piezocapacitive Effect in $CaCu_3Ti_4O_{12}$–Polydimethylsiloxane Composited Sponge for Ultrasensitive Flexible Capacitive Sensor. *ACS Applied Nano Materials*. 2018, 1(1), 274-283.
9. X. Ning, H. Wang, X. Yu, J. A. N. T. Soares, Z. Yan, K. Nan, G. Velarde, Y. Xue, **R. Sun**, Q. Dong, H. Luan, C. M. Lee, A. Chempakasseril, M. Han, Y. Wang, L. Li, Y. Huang, Y. Zhang, J. A. Rogers, 3D Tunable, Multiscale, and Multistable Vibrational Micro-Platforms Assembled by Compressive Buckling. *Advanced Functional Materials*. 2017, 1;27(14).

Literature review in Chapter 2 is partially based on XP report:

R. Sun. Recent progress in wearable electronics: design considerations and characteristics, Nov. 2015, University of Bristol (internal unpublished document).

CHAPTER 1 - INTRODUCTION

With an increasing aging population and emphasis on maintaining acceptable health and living conditions for the elderly population, it is important to develop technologies that support the sustainability of existing medical systems.

Bio-integrated devices with health monitoring systems have emerged as one potential solution to mitigate the above concerns. Recorded data from these devices normally include a broad range of mechanical and chemical information, which is important to predict potential health issues and evaluate the overall health status. Flexible and stretchable electronics are attracting increasing attention as recent advances in materials, mechanics, and manufacturing techniques create new opportunities for the integration of various high-quality electronics and multi-functional sensing systems into a single miniaturized device. Most organs and tissues in the human body possess soft, curvilinear, and time-dynamic surfaces. To conformably bio-integrate with the human body, the next generation of wearable electronics for health monitoring should be highly flexible, stretchable, and sensitive.

Wearable sensing systems may experience multiple mechanical loadings, such as bending, tension, and torsion, synchronizing with the behaviors of skin and tissue. Therefore, it is essential for these systems to provide stable and reliable electrical outputs, which are not affected by various complex deformations. From the mechanical perspectives, most current electronic systems are relatively rigid and stiff, thus mechanically incompatible with biological systems. The mechanical properties of biomaterials are critical factors to influence the functions and responses of biological systems. In terms of physical properties, the Young's modulus and Poisson's ratio are important to characterize basic elastic behaviours. Most biological systems, such as the heart tissues, have Young's moduli varying from tens to hundreds of kilopascals, much lower than that of rigid piezoelectric materials, e.g. lead zirconate titanate (PZT) of around 70 gigapascals. As for the Poisson's ratio, conventional elastic materials possess positive values, while some biomaterials with negative Poisson's ratios are promising in biomedical areas [1]. Moreover, stretchability is another fundamental requirement for bio-integrated devices, and to achieve stretchable electronics is generally more complicated than to obtain flexibility. For conventional well-developed inorganic materials, such as silicon, flexibility can be achieved by reducing its thickness with advanced microfabrication techniques. However, ultra-thin films of intrinsically non-stretchable materials do not guarantee stretchability. This mechanical mismatch remains a fundamental challenge for the

development of wearable devices that can seamlessly integrate and conform to biological surfaces. To obtain an intimate interface to skin or organs, exploring advanced techniques to develop flexible and stretchable electronics that can be mechanically compatible with biological systems is of significant importance for electrophysiological measurements and health monitoring.

In addition to establishing a desirable interface between electronics and human tissues and skins, there are a range of parameters in the human body that need to be detected and measured as health indicators, which can be categorized into two main types: physical and chemical signals. Aligned with monitoring various physiological signals, sophisticated sensing components are required based on different working mechanisms. A physical sensor converts a physical stimulus change into an electrical output which can be measured and stored. In particular, mechanical sensors for strain and pressure measurement have broad applications in health monitoring, such as heart rate, wrist pulse, respiration rate, voice recognition, finger motion, tissue modulus, cancer biomarkers, etc. As for mechanical sensors, several types of sensing mechanisms have been studied in the past decades, including three typical ones, i.e. piezoelectricity, piezoresistivity, and capacitance-based principles. More recently, several new transduction methods, such as triboelectricity, magnetics and optics, have also been explored. Comprehensive research has been carried out to enhance the fundamental performances of sensing systems, such as sensitivity and stretchability, based on material syntheses and structural designs. Moreover, in order to meet the demand of rapid growth in the commercial market of medical wearables, providing sustainable power is another important requirement for bio-integrated electronics. For wearable devices, batteries are currently one of the most versatile options, thus further increasing the properties (mainly capacity and stability) of batteries is still imperative. However, especially for implantable electronics, periodically replacing the power source is undesirable where surgeries increase pain and risks to patients. Consequently, the technique of energy harvesting is promising for the development of self-powered devices. It efficiently overcomes the limitations of battery-based power. In addition, most traditional electronics currently rely on wired connections with instrument to monitor and record vital information of human body, and it would be inconvenient for wearable devices and even impossible for long-term implants to have wires always connecting to external machines. Using wireless sensing techniques, it is possible to continuously monitor health status by wirelessly transmitting health data to external devices, such as smart phone, and to hospital for remote personalized medicine. To develop wireless technology in bio-integrated electronics is of vital significance to improve healthcare and clinical efficiency.

Bio-integrated electronics is an extremely interdisciplinary field that relies on converging technologies including electronics, optoelectronics, mechanics, materials, applied physics,

chemistry, microfabrication and biology. Recent advances in sensing components, energy harvesting/battery technology, and wireless communication interfaces have contributed to the development of fully integrated, multi-functional, and bio-compatible electronic systems. Significant improvements have been achieved in improving the basic performance of sensing systems, such as sensitivity and stretchability. Sensitivity, the ratio between electrical changes and external stimulus changes, is one of the most crucial parameters for sensing systems. Currently, two typical strategies are explored to increase the sensitivity of sensing systems. The first method replies on the improvement of material intrinsic properties. For example, in the area of piezoelectric based sensors, significant work has focused on the employment of nanowires or/and nanoparticles to increase the piezoelectric coefficients. The second method is based on microstructural designs to increase the electrical outputs. Stretchability is another important parameter that determines the feasibility of the sensing systems under various conditions. For epidermal electronics, the device should possess at least 30 % stretchability without affecting its electrical performances as the dynamic strain of human skin could reach more than 30% [2]. There are two main ways to improve stretchability, either by developing intrinsically stretchable materials, or by tailoring geometric designs. However, there remains a challenge to simultaneous improvement of both sensitivity and stretchability. It is of significance to develop applicable methodologies to combine these two parameters in a good balance. Self-power is another desirable property for bio-integrated electronics, eliminating the dependence on external batteries. By exploiting advances in material science, several self-powering technologies based on piezoelectric, triboelectric, and thermoelectric effects have shown promising applications in self-powered electronics. In recent years, wireless technologies have received attention in the applications of bio-integrated electronics, and many well-known communication technologies, such as near-field communication (NFC), Bluetooth, and WiFi, have great potential to be integrated with biomedical devices to enable wireless data transmission capabilities.

This thesis aims to explore the methodologies inspired from mechanical metamaterials, to develop integrated flexible electronic systems. The Kirigami technique will be adopted to design a stretchable structural platform, and its mechanical properties will be studied comprehensively. Based on the proposed concept, by integrating piezoelectric materials and NFC-based wireless interface, a multi-functional and self-powered sensing system will be developed for wireless health monitoring. A further study will be focused on the properties and deformation behaviors of non-uniform Kirigami structures with representative application investigations. The Kirigami technique also has great potential in developing multi-modal and multi-directional vibration-based energy harvesters.

CHAPTER 2 - LITERATURE REVIEW AND THESIS OUTLINE

Bio-integrated electronics are attracting increasing attention as rapid developments in material science, mechanics and microfabrication techniques create new opportunities for the integration of various high-quality electronic, and optoelectronic systems into a single miniaturized device. Most tissues and skins in human body possess soft, curvilinear, and time-dynamic surfaces. To conformably bio-integrate with the human body, next generation of wearable devices for human physiological information monitoring should be highly flexible, stretchable, and sensitive. Sensing systems are core components to provide reliable feedback on body conditions, directly determining therapy choices. This section will provide a review of research developments on bio-integrated electronics, from transduction mechanisms to performance evaluations. The thesis motivations and objectives are then introduced, followed by a detailed thesis outline.

2.1 INTEGRATED ELECTRONIC SYSTEMS

Bio-integrated devices with health monitoring systems are regarded as one of the potential solutions to future healthcare systems. Recorded data from these devices is important to predict potential health issues and subsequent diagnostics and therapy. Rapid advances in material science, manufacturing techniques, and miniaturization of electronics have facilitated the development of multi-functional materials that have the potential to couple sensing, actuation, computation, and communication [3]. Next-generation bio-integrated devices will integrate compliant sensor systems to monitor body health (e.g., temperature, strain, blood-pressure, and heartbeat), memory modules to store recorded data during continuous, long-term monitoring, battery modules, wireless power/data transmission, actuation parts to deliver feedback and physical therapy [4]. Current emerging electronic technologies for the human body can be classified into three categories: soft, injectable, and bioresorbable electronics [5]. The surfaces of most tissues inside the human body and skins are soft and curvilinear. Therefore, soft electronics aim to develop low-stiffness epidermal systems to enable intimate conformity to their surfaces. Injectable electronics are extensions of current surface-mounted devices. Such techniques allow the delivery of soft bioelectronics into deep regions of biological systems in a non-invasive fashion. Bioresorbable electronics are promising for implantable devices, which can maintain high-performance operation for a defined period and eventually be dissolved in biofluids. Figure 2.1 shows representative functionalities in some recently developed bio-integrated electronics.

2.2 TRANSDUCTION MECHANISM

Sensing components are core constituents in bio-integrated electronics, which communicate directly with various external stimuli. Traditional sensing technologies, e.g. piezoelectricity, piezoresistivity, and capacitance, are widely used but suffer from considerable drawbacks, such as low sensitivity, high hysteresis, single modality, etc. The design principles and recent progress are discussed in several thorough reviews [6, 7]. Some improvements based on these traditional methods are discussed in the following parts, using nano- and micro- technologies and bio-inspired structures. Other recently developed mechanisms, such as triboelectricity, optics, and magnetics, are also briefly discussed.

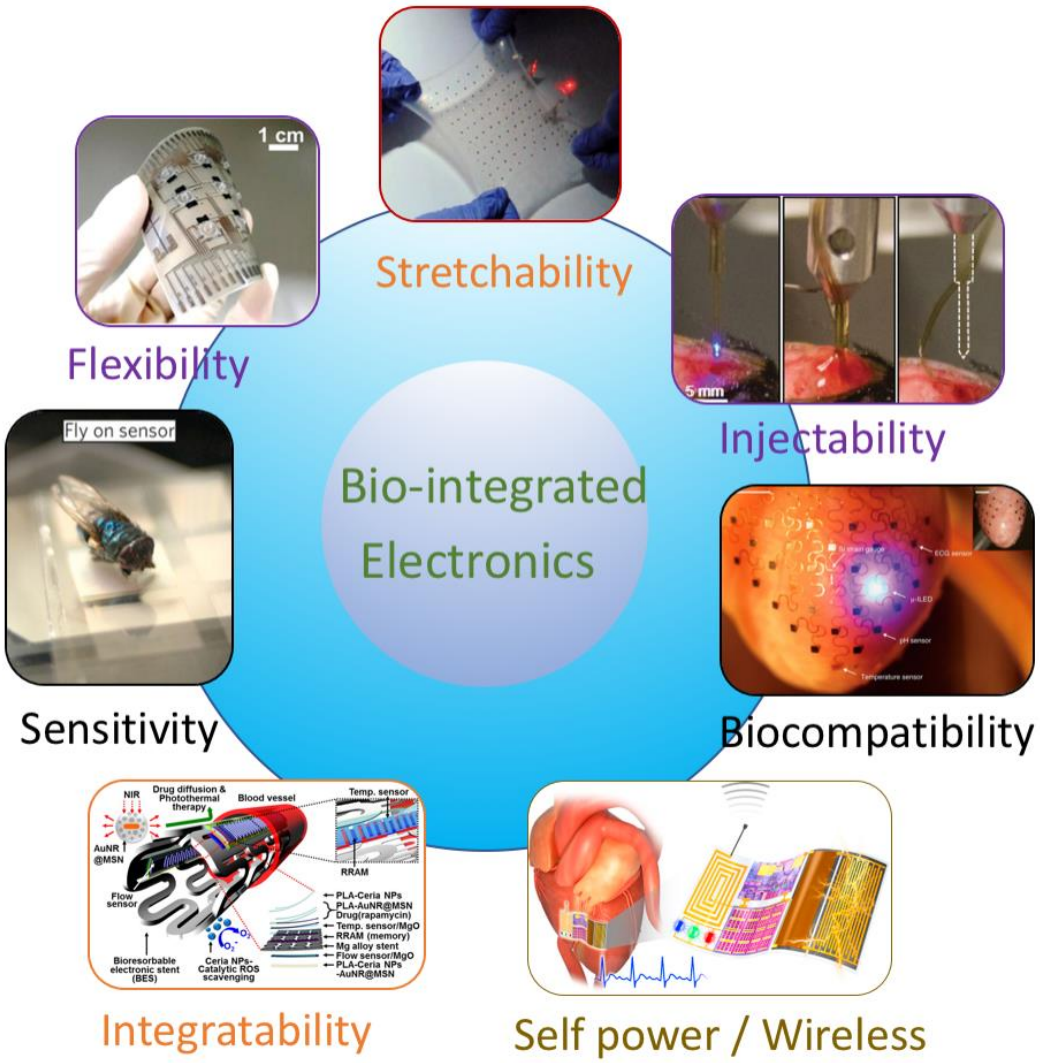

Figure 2.1 Illustrations of the diverse functions of recently developed bio-integrated devices. "Flexibility" reproduced with permission from [8]. Copyright 2014 American Chemical Society. "Stretchability" reproduced with permission from [9]. Copyright 2013, Springer Springer Nature Publishing Group. "Injectability" reproduced with permission from [10]. Copyright 2013, American Association for the Advancement of Science. "Biocompatibility" reproduced with permission from [11]. Copyright 2014, Springer Nature Publishing Group. "Self-power / Wireless" reproduced with permission from [12]. Copyright 2015, Elsevier Ltd. "Integratability" reproduced with permission from [4]. Copyright 2015, American Chemical Society. "Sensitivity" reproduced with permission from [13]. Copyright 2010, Springer Nature Publishing Group.

2.2.1 Piezoelectricity

For most current sensing systems based on several traditional methods, a common limitation is the requirement of external power sources, which limits deployment and operating lifetime. Since the first introduction of piezoelectric zinc oxide (ZnO) based nanogenerators [14], self-powered sensing systems have attracted a great deal of attention [15] with potential in wearable and implantable electronics [16, 17].

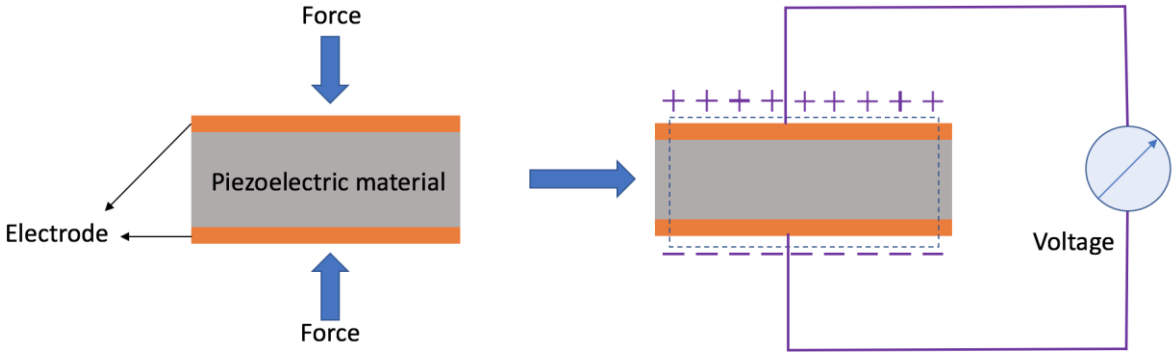

Figure 2.2 The schematic of direct piezoelectric effect. Electric change produced on crystal surfaces when external mechanical stimuli is applied.

Piezoelectric effect, an electromechanical interaction, is the basic mechanism for piezoelectric sensors. Piezoelectricity is the electric charge produced on crystal surfaces when external mechanical stimuli is applied on piezoelectric materials as shown in Figure 2.2. A range of piezoelectric materials have been extensively studied in recent years, which are classified into two typical types: inorganic and organic materials. For inorganic-based piezoelectric materials, some common examples, such as PZT [18-20], ZnO [14], barium titanate ($BaTiO_3$) [21], PMN-PT [22], and many others [23], have been extensively investigated to utilize the high piezoelectric constants. However, inorganic-based materials are generally rigid and in bulk state with ultra-high stiffness, which is not compatible with the human body. Broad efforts have been devoted towards improving the mechanical flexibility, and it has been demonstrated that such type of brittle materials in thin-film [18-21] or nano-wire [14, 22] forms show good flexibility that is applicable to flexible electronics. Unfortunately, thin-film forms are costly to produce and require complicated fabrication techniques, such as chemical mechanical polishing (CMP) [24], limiting their widespread applications. Organic piezoelectric materials are normally polymer-based materials, which exhibit inherent flexibility, high biocompatibility, and are compatible with low-cost fabrication techniques, making them preferable for flexible electronics with seamless conformity to curvilinear surfaces. Extensively studied examples in recent years include polyvinylidene difluoride (PVDF) [25-28] and polyvinylidene fluorid-trifluoroethylene (P(VDF - TrFE)) [29-31]. To combine the superior piezoelectric performances and mechanical flexibility from inorganic and organic materials respectively, hybrid composite systems, composed of inorganic piezoelectric fillers and polymer matrices such as P(VD - TrFE)/$BaTiO_3$ [32], PDMS/$BaTiO_3$ [33], PVDF/ZnO [34], has been developed. This is an efficient strategy to enhance both electric and mechanical properties. Piezoelectric devices with excellent self-powered sensing performances have great potential in a wide range of applications, e.g. arterial pulse monitoring

[20], tissue modulus measurement [35], gastrointestinal motility sensing [36], robotics interfaces [37], and many others [38-40]. Piezoelectric sensors are promising candidates to develop self-powered devices in virtue of the advantages of high sensitivity and fast response for dynamic measurements, but not feasible to static stimulus measurements due to charge leakage of piezoelectric materials.

2.2.2 Piezoresistivity

Piezoresistive systems are typically based on the piezoresistive transduction, where the resistance can be affected by external mechanical stimuli. The resistance of a piezoresistive sensor is defined as

$$R = \rho \frac{l}{A} \qquad 2.1$$

Where R is the resistance, ρ is the resistivity of the material, l is the length, and A is the cross-section area. An external stimulus could induce the changes in either the geometry or resistivity [41]. Piezoresistivity has been commonly adopted for pressure and strain sensors with intrinsic advantages, including low-cost fabrication process, low energy consumptions, and simple structures. However, the disadvantage of mechanical hysteresis hinders its applications in the fabrication of high-performance sensors.

Constant efforts have been made to develop advanced technologies in material sceince and structural designs to improve the performance of piezoresistive sensing systems. Recently, several novel concepts have been intensively studied, mainly based on two strategies: conventional materials with novel structural patterns, and new material systems. For metallic based sensors, the gauge factor is normally around 2 [42]. However, when micro-cracks are introduced into the thin metal films with elastomer as the substrate, the gauge factor can be significantly enhanced to be over 200 [43]. Based on brittle conductive materials, the outstanding sensitivity is attributed to the geometry feature of cut-through fractures upon stretching. The crack concept is also feasible for non-metal materials, such as carbon nanotube [44, 45], graphene [46, 47], and graphite [48]. Conductive composites, as novel synthesised materials, can be designed as piezoeresistive sensors based on the tunnelling effect [49-51]. For example, carbon nanotubes are widely used as the nanofiller for conductive nanocomposites. Once the concentration of carbon nanotube reaches a certain level percolation, the tunnelling paths between adjacent CNTs are created. When mechanical stimulus is applied, the electron tunnelling in the CNT network is changed, thus affecting the resistance of the sensing system.

2.2.3 Capacitance

In general, the key of capacitive-type sensing systems is the capacitor properties. The configuration of a capacitor is generally based on a dielectric layer with two parallel plates. The capacitance is expressed as follows

$$C = \varepsilon \frac{s}{d} \qquad 2.2$$

Where C is the capacitance, ε is the dielectric permittivity, s is the effective electrode area, d is the distance between plates. An elastic polymer is widely adopted as the dielectric material. When a mechanical stimulus is applied, the distance d and/or the effective electrode area s change, affecting the capacitance.

Currently, most research is focused on two directions, stretchable electrodes and dielectric properties, to improve the sensing performances. For stretchable sensing applications, stretchable electrodes are essential components. The stretchability of electrodes can be achieved by either structural designs, e.g. serpentine layout [52], or composite sysnthesis [53-55]. Modifying the material property and structural configuration of dielectric layer is an efficient way to improve the performance of capacitive sensors. Polydimethylsiloxane (PDMS) is widely used as dielectric layers due to its biocompatibility and tunable elastic properties. Several micro-structured concepts with PDMS dielectric have been demonstrated to be efficient ways for the improvement of the sensitivity and response time, such as micro-pillars [56, 57], micro-pyramids [58, 59], and porous structures [60, 61]. The dielectric constant plays a vital role in determining the sensing performances, and several novel materials have been explored to increase the dielectric constant, e.g. ion gel [59, 62], graphene oxide [63], and conductive filler/polymer nanocomposite [64-66].

2.2.4 Triboelectricity

Recently, many other concepts have been developed to improve the sensing performances. The triboelectric effect has been extensively studied, and it is regarded as a promising source for self-powered pressure sensing [67]. A basic triboelectric nanogenerator (TENG) generally consists of two layers, one is liable to lose electrons and the other readily gains electrons. Relative sliding by external deformation induces the establishment of an electric potential between these two electrodes. Fan et al [68] developed a transparent and self-powered pressure sensing system using a triboelectric process and demonstrated that micro-pyramid features can significantly contribute to the improvement of triboelectricity efficiency. It is promising as a high-performance sensor with the advantage of its low-cost fabrication process. Triboelectric sensors can also be used to scan surface topography using a combination of contact-electrification and electrostatic inductions [69].

A membrane-structured TENG with contact-separation mode is designed at the root of a whisker, whose deflection caused by detected objects would induce an electric output current/voltage, and its magnitude depends on the bending degree of the whisker. In the area of wearable devices, human skin can be regarded as a natural triboelectric layer. To utilise this feature, a skin-based TENG system was presented using a contact and separation working mode [70]. PDMS film with micropyramid surface was one triboelectric layer and human skin was the other triboelectric layer with high tendency to lose electrons. This device has demonstrated high performance as a self-powered tactile sensor. Several reviews about triboelectric based technologies have been published [4, 71, 72], including fundamental theories, recent application areas (e.g. pressure/touch sensing, vibration sensing, motion sensing, physiological activities sensing, and chemical/environmental sensors), and future perspectives.

2.2.5 Other mechanisms

In addition to the abovementioned methods, there are several other working principles for tactile and strain sensing. The transistor is another suitable option with intrinsic advantages, including flexibility, low-cost processability, and integrated capacity of signal transduction and amplification [73, 74]. In general, a typical transistor consists of source, drain, and gate terminals [75]. The voltage at gate terminal modulates the channel conductivity, thus controlling the current between drain and source terminals. External stimuli would affect the gate terminal properties, such as charge density, capacitance, conductivity, and applied terminal voltage. The change in the gate terminal leads to a change of drain-source current, which can be used as the sensor signal. Transistor-type sensors exhibit easy signal amplification by optimizing the gate terminal properties. Bao et al [76] developed skin-like polymer transistor array with intrinsical stretchability for pressure mapping. This device can reach a significantly high density of 347 transistors per square centimetre with silicon-comparable performances from scalable fabrication. A graphene transistor with air-dielectric layers has been demonstrated to efficiently widen the pressure range for tactile sensors [77].

An alternative approach based on polymer waveguides without any electronic components in sensing areas is proposed for dynamic response detection [78]. The waveguides underneath the touch layer scatter upon a pressure touch, and by monitoring the light intensity the force could be detected. Magnetic field can also be used for tactile sensor. By measuring the change of magnetic field, external stimulus can be detected [79]. Based on magnetoelastic effect, external strain effectively affects the magnetization direction in ferromagnetic materials, and the resistance between two ferromagnetic layers also depends on their relative angle due to magnetoresistance effect. By combining magnetoelastic and magnetoresistance effects, a flexible magnetoresistive

sensor has been developed for in-plane mapping of strain directions [80]. Resonant frequency has been found to be another good indicator to measure mechanical stimulus, as demonstrated in a developed wireless device for continuous pressure monitoring [81].

2.2.6 Additional physiological signals

In addition to the previous sensing mechanisms mainly for tactile sensing, several other physiological information, such as temperature, sweat, and electrophysiological signals, is important to reflect the health status.

Several types of temperature sensing mechanisms have been developed in recent years, such as the Seebeck effect [82], resistive temperature detectors (RTDs) [83], and transistors [84]. The Seebeck effect, encompassed within the thermoelectric effect, is the conversion from heat to electrical signal. A graphene-based thermal sensing system was developed by leveraging graphene's tunable Seebeck coefficient [82]. In RTDs, the temperature is measured as a function of the resistance of a RTD element. Some polymer composites exhibit significant resistivity changes with temperature, but the problems are temperature sensitivity and reproducibility. To address these two challenges, a Ni microparticle-filled composite with binary polymer matrix is presented [83]. In a semiconductor, the field-effect mobility is generally temperature dependent, showing potential applications in thermal sensing. However, thermal instability and limited thermal sensitivity are major issues. Adding polar groups in the polymer chain is demonstrated to be an efficient way to overcome the above limitations. Wu et al [84] developed a thermally stable transistor, and the dielectric layer consists of a three-arm stereocomplex polylactide with strong polar groups. The sensitivity can be enhanced significantly based on the mechanism of charge-trapping effect due to the polar group.

Sweat is a representative biofluid of the human body. It is attractive to health monitoring due to a wealth of biomarkers it contains and noninvasive collection of samples. It has been recognized that the concentrations of various components in sweat (metabolites and electrolytes) are closely linked with health status and disease. For example, the concentration of chloride can be indicator of cystic fibrosis [85], the glucose concentration is useful for diabetes care [86], sweat lactate can be used to monitor the performances of physical activities and pressure ischemia [87], and the loss of some minerals, such as sodium [88], potassium [89], zinc [90], and calcium [91], through sweat can potentially serve as marker of physiological status. Tremendous research has been devoted to investigating wearable sweat electronics via two typical methods: electrochemical and optical technologies [92, 93]. The electrochemical sensor uses appropriate electrodes to convert targeted analyte in sweat to electrical signals through chemical reactions, and the optical method is based

on colorimetric assays and acquire the concentration results from image analysis. Gao et al [94] proposed an integrated sensor system for multiplexed sweat monitoring. This electronic system integrated sensing, signal processing, and wireless transmission to simultaneously and selectively monitor multiple analytes, including metabolites and electrolytes, in sweat. Using colorimetric assay principle, Rogers et al [95, 96] recently developed skin-interfaced microfluidic systems to simultaneously measure and quantify sweat rate/loss, pH, lactate, glucose, and chloride in a wireless and battery-free mode.

Electrophysiological signals are also important to diagnose and manage human health. For example, electrocardiogram (ECG) can provide information about cardiac diseases, electromyography (EMG) can evaluate muscle health, and electroencephalogram (EEG) aims to record the electrical activity [97]. Rogers group developed various soft and epidermal electronic systems to track electrophysiological signals [98-100]. Such type of system is normally composed of three capacitive electrodes, including measurement, reference, and ground electrodes, coupled to the skin. The measurement is captured as the differential amplitude between measurement and reference electrodes, and the ground electrode is to reduce unwanted signals from the body [98].

Moreover, there is great potential to develop integrated electronics with the ability of detecting various stimuli simultaneously, as the human skin possesses. At present, some research has achieved part of the multifunctionalities, such as hydration and strain [101], temperature and pressure [102], three-axis tactile/slip forces and temperature [8], static/dynamic pressure and temperature [103], and temperature, humidity, and strain [104].

2.3 PERFORMANCE EVALUATION

To achieve high performance for bio-integrated electronics typically requires a combined design in material science and structural engineering. In different application conditions, there are corresponding requirements for sensing systems, including some basic parameters, such as sensitivity and stretchability, and other desirable properties, e.g. self-powered and wireless communication capacities. Material selections and structural configurations have a vital effect on the sensing performances. This section will discuss recent developments in the designs of sensing systems.

2.3.1 Sensitivity

Flexible sensing systems with high sensitivity and low hysteresis are desirable for future generation of wearable devices. To evaluate the sensing performance, there remain several challenges to overcome, among which high sensitivity and low hysteresis are two important but competing goals.

Soft material with a low modulus is promising to improve the sensitivity. However, low modulus generally induces large viscoelasticity, leading to long response time. Based on the abovementioned sensing mechanisms, various approaches are proposed to improve the sensing performances. Microstructured design offers a potential solution to achieve the above two goals simultaneously. Recent research shows that unique microstructures are promising in various sensing systems.

Porous structure

To overcome the poor sensitivity of conventional pressure-sensitive rubber (PSR)-based sensors, porous structures are introduced into piezoresistive material to increase its deformability [105]. Reverse micelles are water droplets with surrounding emulsifiers. They are used to introduce micropores into PSR structure through the heat treatment of evaporation process. The introduced pores can decrease the modulus, and external stimuli is thus easy to induce large resistance changes.

In self-powered sensing systems, the power output performance could be enhanced by using porous structures [106]. A mesoporous piezoelectric film was developed by casting ZnO nanoparticles into the polymer and the particles can be removed using hydrochloric acid (HCl) solution to introduce pores. High-porosity films could induce large electric output due to the large film displacement under small external stimuli. For triboelectric nanogenerator, sponge-type micro/nanostructured films also enhance the electrical output dramatically due to the increase of the surface area-to-volume ratio [107].

Porous sponges or foams are considered as alternative materials to enhance the sensitivity for both the capacitive [54, 108] and resistive [109-111] pressure sensors. Using elastomeric foam as the dielectric layer in a capacitive sensor, the working performances (sensitivity and operating pressure range) depend on the foam density which can be adjusted to meet various applications, and soft sensors with high porosity are 6 times more sensitive than those with stiff foam [108]. Endowing flexible sponges or foams with electronic conductivity is promising for piezoresistive sensors. Yao and co-workers [109] improved the sensitivity of a piezoresistive sensor, which was composed of coated polyurethane (PU) sponge with fractured microstructure design. After the softening treatment and compression process, a conductive sponge with fractured microstructures is created and its high sensitivity is attributed to giant contact area variation between fragmentised pieces under compression stress, thus affecting the number of conductive pathways and further changing contact resistance. A further study based on fragmentised graphene foam (FGF) is investigated to design highly stretchable strain sensors with tuneable sensitivity by using the GF/PDMS composite [110]. The presented microstructure contributed to an extremely high gauge factor of 15 to 29 due to more conductive pathways induced by FGFs. Metal foam was served as a template

and graphene was grown on its skeleton via a chemical vapor deposition (VCD) process, a common method to produce graphene foam. A graphene foam structure can be generated after the metal template was etched out in acid. Samad et al [111] developed a graphene-foam-based sensor with adjustable sensitivity by a three-step fabrication method. Graphene oxide was firstly dip-coated on nickel foam, then reduced, and finally the nickel foam was removed. It is demonstrated that further heat treatment on the graphene foam would increase and adjust the sensing sensitivity. An alternative approach based on PU is presented to investigate graphene foam sensors [112]. This facile fabrication technique avoided general chemical etching process in previous metal-based methods by the decomposition of PU foam in nitrogen atmosphere at 1000 °C and subsequent evaporation release.

Aerogel-inspired methods are promising to develop pressure sensors with superior microstructures. An ultrasensitive pressure sensor was developed by combining the designs of aerogel and pyramid pattern [113]. The conductive aerogel combined alginate and nitrogen-doped carbon-nanotube-supported silver, and then highly porous aerogel was fabricated by a freeze-drying process. A similar concept was adopted to design a conductive aero-sponge as pressure sensors [114]. In this research, a polypyrrole/silver nanowire hybrid-based 3D network was prepared and further processed into porous materials. The resulting aero-sponge showed high performance as a piezoresistive sensor.

Bio-inspired Structure

Nature provides much inspirations for engineering designs. In sensing systems, pursuit of high sensitivity and multi-modal sensing capacities is of great significance for better health monitoring. From recent research, it can be seen that mimicking certain biological systems is of tremendous interest to achieve the abovementioned goals.

❖ *Interlocked structures*

Human skin is an excellent tactile sensor system. It is flexible and stretchable and at the same time capable of sensing various stimuli, including pressure, temperature and humidity. On further investigation of the mechanism of human skin, an interlocked structure between epidermis and dermis layers can be found. Various sensor receptors are distributed in the layers, enabling the perception of external stimuli [115]. Inspired by the working principle of human skin, several types of sensing systems have been investigated.

In general, high sensitivity, fast response time, and less temperature-dependence are always the objectives in piezoresistive sensors. Part et al [51] proposed an electric skin based on CNT-composite elastomers featuring interlocked microdome arrays. Under applied pressure, the contact

area between the interlocked microdome arrays increases significantly, leading to a giant tunnelling piezoresistance. The results validated the performances of presented sensor design with high sensitivity, rapid response time, and negligible temperature dependence.

Interlocked architectures also exhibit potential in detecting different types of mechanical loads. Based on this architecture, a flexible sensing platform with interlocked arrays of Pt-coated nanofibers was presented and capable of detecting pressure, shear, and torsion [116]. Due to the special geometry of interlocked structures, the interaction of surrounding nanofibers is related to external stimuli which would further affect the contact resistance of the system. Therefore, each mechanical stimulus exhibits a unique strain gauge factor which can be quantified and used for the differentiation of different mechanical stimuli. The material choice and microstructure shape of the interlocked arrays also have a vital influence on the performance of the sensing systems. For the CNT-composite-based microdome array, five mechanical stimuli were detected and differentiated, including normal, shear, stretch, bending, and twisting forces [115]. To detect static and dynamic pressure simultaneously, Ha et al [117] presented a pressure-sensitive system using hierarchical ZnO nanowire arrays. This design enables it to discriminate static and dynamic stimuli. The piezoelectric transduction based on the bending of ZnO nanowires is used for the dynamic pressure detection whose vibration frequency can reach 250 Hz, and contact resistance variations between ZnO nanowires is for static stimulus measurements.

To fabricate the abovementioned microdome arrays, a micro-patterned silicon mould by the photolithography technique is normally required, which is an intrinsically expensive and complex process. Some organisms in nature, however, could provide a facile, efficient, and low-cost moulding method. Mimosa leaves have a surface morphology comprising a protuberant microdome pattern with a microscale diameter [118]. Such naturally microstructured leaves could serve as a template to make an inverse-mimosa mould, which can be further used to make a thin film with replicated surface patterns as the leaves possess. The pressure sensor using this bio-inspired fabrication techniques shows great advantages, including high sensitivity, rapid responding time, and durable stability. Similar process is also demonstrated on flexible electronic skin with a rose petal moulding technique [119].

❖ *Electronic Whisker*

Mammalian whiskers serves an important sensor component in biological systems, which possess airflow detection and tactile sensing for navigation. Several approaches have been investigated on artificial electronic whiskers (e-whiskers) to achieve highly sensitive sensing systems.

Takei et al [120] developed an artificial e-whisker with high sensitivity to mechanical stimulus. This e-whisker was based on high-aspect-ratio elastic fibres, coated by tunable composites of CNT and silver nanoparticle. The combination of nanowires and nanoparticles contributed to an improved strain sensitivity, and its modulation can be readily achieved by adjusting the compositions of the composites. A further study on an integrated sensing system by a cost-effective printing method was carried out to achieve temperature distribution and three dimensional strain mapping simultaneously [121]. Based on a similar principle as in the previous work [120], the sensitivity can be tuned in different occasions by changing the composition ratio of sensing composites. A reconfigurable e-whisker system was developed based on shape memory polymers [122]. Using the presented air assembly method, in which 2D precursors can be transformed into shape tunable 3D configurations under warm air flow, the 3D e-whisker electronics enable multimodal sensing capacities, including temperature, tactile forces, and surface roughness.

❖ *Other bio-inspired structures*

There are several other bio-inspired designs that have potential application in sensing systems. Inspired by the spider's sensory system with crack slit mechanisms, Kang et al [123] developed a nanoscale crack sensor with ultrahigh sensitivity. The high resistance variation through a disconnection-reconnection process contributes to the sensitivity improvement of the system, enabling it to be applied to sound pattern recognition and physiological signal detection even in a noisy environment. Inspired by Gecko architectures, microhairy structures have been adopted as an effective methodology to enhance sensor performance [124]. Pang et al developed highly sensitive pressure sensors for weak pulse measurement based on an interfacial layer with microhairy structures. The sensitivity, hysteresis, and signal-to-noise ratio are adjustable through the design of microhair properties, specifically the material and aspect ratio between the height and radius.

Other micro-structured patterns

Microstructure-based designs have been extensively explored in the sensing fields in the past decade. In addition to the strategies discussed above, several other concepts have also been studied.

In capacitive sensing systems, the dielectric layer is an important element that determines the capacitance amplitude, thus affecting the sensing performance, including sensitivity and hysteresis. Recent work demonstrated that appropriate dielectric designs can significantly enhance sensing properties. Micropyramid-structured dielectrics have been demonstrated to be an efficient approach to obtain superior sensing performances, including unprecedented pressure sensitivity

and rapid response time [13]. Tee et al [125] further investigated the effect of structural geometries and spatial locations of dielectric layer on the sensitivity of capacitive pressure sensors. A comparative study on different microstructures demonstrated that pyramid pattern is an optimal configuration which can significantly reduce the mechanical stiffness.

Besides capacitive sensors, micropyramid structures also show potential in resistive sensors [126]. A stretchable electrode is fabricated based on a micropyramid surface. This type of micro-patterns efficiently improves the contact sensitivity between two electrodes, and even a tiny force would induce a giant geometric change, thus reducing the contact resistance significantly. Moreover, micropyramid-featured nanogenerators can significantly improve the electrical output by increasing the triboelectric effect and the capacitance change [68, 127].

Wrinkled structures are also promising options for tactile sensors. Luo et al [128] presented a highly sensitive pressure sensor where wrinkled conductive polypyrrole film was used as resistive component. With the help of nanostructured insulating spacers, the conductive paths within polypyrrole films increases significantly when an external pressure is applied. Shape memory polymer is also adopted to introduce wrinkling based on the shrinking when it was heated over its glass transition temperature. By sandwiching two conductive wrinkling films together, a giant change of contact surface area would occur under external pressure due to the rough surface morphology induced by wrinkling process, thereby reducing the resistance and improving pressure sensitivity [129].

The surface morphology of sandpaper is a desirable option as a mould to introduce roughness into surfaces, which have been demonstrated to be efficient to improve sensor properties. This sandpaper-based fabrication technique features the advantages of simple and cost effective process, and have potential applications in resistive pressure sensors [130-132] and triboelectric generators [133].

2.3.2 Stretchability

Flexibility and stretchability are two important features for bio-integrated electronics, which enable them to match the soft and stretchable surface properties of most tissues and skins of human body. Stretchability is challenging as it is difficult to simultaneously achieve both excellent mechanical robustness and electrical performance. A great deal of attention has been focused on the development of stretchable electronics, and there are two typical ways to achieve it: structures inducing stretch and materials inducing stretch [134].

Structural Design

For intrinsically brittle material, unique structural designs and geometrical patterning are regarded as promising techniques to achieve stretchability without affecting the properties of the pristine materials.

Two strategies are mainly employed to develop stretchable electronics: wavy structure and island-bridge design. The second approach can be further divided into two types: serpentine and fractal patterns. The wavy/wrinkled structure is a direct way to achieve stretchability while the island-bridge method is based on stretchable interconnection of conductive materials. The unique mechanics of each strategy based on analytical models is discussed [135].

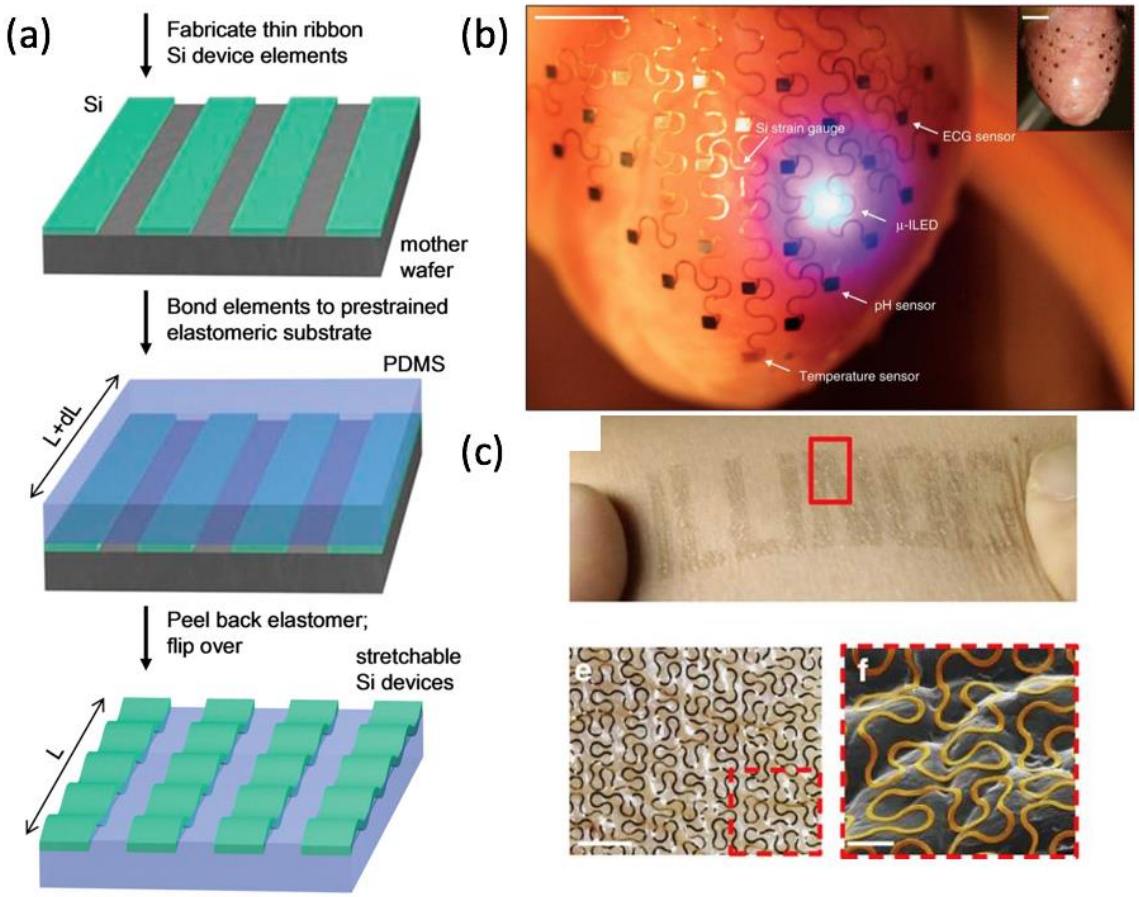

Figure 2.3 Various structural strategies for stretchable electronics. (a) Schematic illustration of the process for the wavy silicon. Reproduced with permission. [136] Copyright 2006, American Association for the Advancement of Science. (b) Multifunctional electronic systems with serpentine interconnects. [11] Reproduced with permission. Copyright 2014, Springer Nature Publishing Group. (c) Stretchable electronics with fractal configurations. [137] Reproduced with permission. Copyright 2014, Springer Nature Publishing Group.

❖ *Wavy configuration*

Inorganic material has broad applications in the developments of high-performance electronics. For example, ferroelectric ceramic with excellent piezoelectric and ferroelectric properties is indispensable to develop a range of electronic devices, such as sensor, actuator, energy converter, etc. Besides, several organic materials, such as CNTs with excellent electric conductivity and high thermal stability, have proved to be feasible electrode materials. However, such types of materials are generally brittle with a fracture strain of approximately 1%, which poses a large limit on their applications.

Recent advances in mechanical and microfabrication techniques enable conventional rigid materials to be stretchable. The wavy configuration is a promising method to achieve a large stretchability without any loss of the intrinsic properties (e.g. conductivity, piezoelectricity). A typical fabrication procedure of buckled wavy nanoribbons consists of three main steps: (i) preparation of elastomer substrate and free-standing 2D precursors, (ii) bonding 2D precursors onto pre-strained elastomer and (iii) releasing the elastomer pre-strain, followed by the formation the periodic, wavy configuration, as shown in Figure 2.3(a) [136]. It has been demonstrated that CNTs embedded in elastomer substrate with a pre-strain of 100% in the wavy form has only 4.1% increase in resistance when it is stretched to the pre-strain [138], enabling it to be a superior conductor. A supercapacitor based on periodically sinusoidal single-walled carbon nanotube (SWNT) macrofilms shows a stable electrochemical performance under 30% applied tensile strain [139]. Feng et al [140] confirmed that the wavy fabrication process does not degrade ferroelectric and piezoelectric properties of PZT nanoribbons. A similar concept is further developed for the transformation of 2D planar structures into various 3D architectures [141], and the final shape can be governed by three parts: (i) the material properties and geometry of the 2D precursors; (ii) the bonding pattern on the substrate; and (iii) the pre-strain in the substrate (magnitude and direction). The buckling configuration is further applied in discrete nanostructures with plasmonic nanodisks [142]. Compared with those in continuous nanofilms, the buckling in discrete nanodisks has distinct features: larger critical strain to trigger buckling, much smaller wavelengths and amplitudes, and different buckling coexisting.

❖ *Serpentine island- bridge configuration*

The island-bridge design is another efficient way to achieve stretchability, in which active components are referred as islands and electrical interconnects serve as the bridges, as illustrated in Figure 2.3(b). Serpentine configuration is efficient as the bridge pattern which can accommodate large applied strain while ensuring the mechanical integrity of the functional materials on the

islands. This method avoids out-of-plane deformation or the pre-strain of an elastomer substrate, which makes it more attractive to meet some special requirements. However, in certain areas with high levels of deformations, the buckling of interconnects and pre-strain in the substrate could further enhance the stretchability.

In this design, the interconnects can be either non-bonded, partially or fully bonded to the substrate. The non-bonding pattern could enlarge the stretchability due to the minimal constrains imposed by the substrate. Zhang et al [143] carried out comprehensive research on the critical buckling and postbuckling behaviours in serpentine interconnects which are not bonded to the elastomer substrate, and these behaviours can be modulated by geometric parameters of the interconnects, providing the straightforward design of optimal island-bridge structures with high areal coverage and large biaxial stretchability. An analytical study based on curved beam theory was performed to study the relation between the serpentine shape and the stretchability [144]. For the freestanding ribbons, this work shows that a larger arc radius and angle with a narrow width would induce lower strain by reducing the effective stiffness. In some cases, the interconnect ribbons need to be bonded on the substrate, and the interconnect-substrate interaction of bonding effect cannot be neglected which could limit the stretchability to some extent. The prestrained strategy can significantly enhance the stretchablity [145]. A comparative study shows that the elastic range for non-prestrained samples is 54 % and for 40 %-prestrained ones the elastic range increases to 120 %. In the prestrained strategy, attention should be paid to the boundary effect in the edge unit of island-bridge cells which could lead to incomplete prestrain absorption [146]. For practical applications, serpentine interconnects can be integrated with various functional materials for different applications, such as sensor/actuator for continuous thermal management of human skin [147], SWNT-based memory units and logic devices [148]. The serpentine mesh also offers new opportunities to develop integrated and multi-functional cardiac membranes that can precisely conform to the shape of heart epicardium [11]. By integrating diverse sensor and actuator components within one single platform, this device could spatiotemporally monitor and modulate cardiac behaviours.

❖ *Fractal island-bridge configuration*

Fractal design, also referred to a 'self-similar' design, consists of small pieces that resemble the whole configuration in Figure 2.3(c). The fractal inspired concept could efficiently improve the space utilization with the increment of the self-similar order, making it an effective strategy to alleviate the competing goals for stretchable electronics: enhanced stretchability and high utilization of active components simultaneously.

Based on conventional serpentine configuration, self-similar serpentine interconnects offer significant stretchability improvement [149]. In this work, an analytical model to study the flexibility and stretchability of self-similar serpentine interconnects provided theoretical guidance for an optimization design of stretchable structures. With active devices occupying 50 % and 70 % surface filling ratio, the system stretchability could reach 90 % and 50 % respectively. This analytical study is limited to in-plane bending, and buckling is not considered due to the relative thick interconnects. To consider postbuckling effect which would further improve the stretchability, conventional nonlinear methods would be cumbersome for such complex microstructures in high self-similar order. A hierarchical computational model was established based on an ordered unraveling mechanism [150]. In this method, there is only one order structure experiencing stretching and the remaining lower order is modelled as straight beams with bending and stretching, which substantially saves the computation efforts. Bonding configuration is also an important factor to determine the final deformation of fractal designs. A postbuckling analysis was carried out for partially bonded and non-bonded fractal serpentine interconnects and the comparative result of stretchability show ~165% for non-bonded system, and ~76% for partially bonded system [151]. Another study based on analytical approach was developed to investigate the elastic stiffness of fractal-inspired interconnect with different orders and several shapes [152]. There are a range of options for the topology of the fractal constructs, e.g. Peano, Greek cross, Vicsek, etc. The utility of these configurations to yield stretchable electronics provides broad design possibilities, such as epidermal sensors and actuators [137]. The electronics with fractal meshes are able to conform to complex surface of curved auricle and mastoid, to provide continuous electroencephalogram measurements [99]. Pursuing stretchability in energy storage devices without the loss of capacity densities is important to offer desirable power for bio-integrated electronics. Xu et al [9] designed stretchable batteries integrated with wireless recharging systems based on self-similar serpentine interconnects. The results reveal 300% reversible stretchability with 50% coverage of active materials. In a multifunctional skin prosthesis, hybrid serpentine and fractal designs were adopted, with a thermal actuator in fractal meshes for uniform heating and multi-electrode arrays and sensors in serpentine formats for nerve stimulation and external stimulus perception [153]. A further study for 3D cardiac membrane [11] based on fractal design was developed [154]. As a core component of the device, the fractal-geometry electrodes exhibit advantages: an increase of surface area by a factor of 14 for better cardiac electrical stimulation, low impedance due to Greek cross geometry, and non-uniform current distribution on the electrode surface.

❖ *Other structural methods*

Apart from the abovementioned patterns, other innovative designs are also explored. The Archimedean spiral pattern is demonstrated to be more stretchable than certain serpentine-based structures [155], and its improved stretchability is attributed to the small curvature of the construct. Overstretching sometimes needs to be avoided, which might lead to the failure of the system with a short lifetime. For certain biological tissue systems with non-linear mechanical properties, the 'J-shaped' stress-strain response, featuring low stiffness for small strains and sharp transition to higher stiffness for large strains, can protect the tissue from excessive strain effectively [156]. This strain-limiting structure was recently embedded in a core/shell architecture for stretchable electronics, which offered an efficient interface to protect the active components from fractures [157]. Lanzara et al [158] developed a spider-web-like network integrated with thousands of temperature sensors and strain gauges. This concept enables the conversion from microscale to macroscopic space with an expansion level of 26500 %. Designs based on the integration of two or more stretchable methods could provide more feasible application solution. Yang et al [159] developed a flexible nanogenerator by assembling a wavy-structured film and serpentine electrodes to enable both compressible and stretchable operational modes.

Material Design

Human skin is a good target for stretchability demonstration. It is intrinsically and mechanically compliant with low modulus allowing free bending, twisting, and stretching without any damage, and capable of sensing multiple stimuli simultaneously, e.g. tactile sensation, humidity, temperature, etc. For epidermal electronics, it is essential to resemble these properties to enable them to intimately conform to human skin. Recent advances in material sciences and fabrication techniques provide new possibilities for stretchable devices.

Intrinsically stretchable materials are effective for stretchable electronics [160]. Due to the intrinsic fluidity, liquids can deform freely and continuously without permanent deformations. Therefore, liquid metal with high conductivity provides new routes to fabricate stretchable devices. At present, Eutectic gallium-indium (EGa-In) stands out because of its attractive attributes: rheological behaviour at room temperature, low resistivity, low viscosity, and low toxicity [161]. The rheological behaviour of EGa-In when injected into microfluidic devices was analysed. Structural stability can be maintained due to the naturally formed oxide layer on the surface. However, the oxide layer also makes it difficult to fabricate EGa-In alloys by inkjet printing. Inkjet printing is a promising method for scalable additive manufacturing but not applicable to the bulk material in an oxygen-containing environment. Boley et al [162] overcame this limitation by a modification of

EGa-In based on a mechanically sintered method. Regarding its applications, EGa-In can be a good candidate for embedded interconnection to achieve stretchability. In a demonstration of μ-light-emitting diodes (μ-LEDs), EGa-In was embedded in a soft film to establish the electrical connection between active elements [163]. The entire device could reach 70 % uniaxial strain without affecting the performances of μ-LEDs. Numerical simulation technique is a complementary tool to optimize the design of soft liquid-embedded structures. Overvelde et al [164] developed an effective 3D FEA technique for the analysis of mechanical and electrical responses of soft liquid-embedded sensing systems, which offers opportunities for soft sensor designs. GaInSn with a lower melting point, is also attractive in stretchable electronics, and has potential applications in stretchable electrodes for strain sensing [165] and heterojunction sensors [166].

A composite system with conductive nanofillers dispersed in an elastic polymer matrix is another efficient method for making stretchable electronics, such as stretchable electrodes [167-169], and strain sensors [170-172]. There are several parameters that control the electrical performances of hybrid composites, e.g. dispersibility, and percolated pathways of nanofillers [160]. Currently, a range of nanomaterials to formulate stretchable conductors have been extensively studied, including silver nanowires [169, 172], copper nanowires [173, 174], carbon nanotubes [170, 171], and graphene [167, 168]. For example, silver nanowires, with excellent electrical, mechanical, and optical properties, have the potential to develop high-performance sensing systems. In a sandwich-structured configuration, silver nanowires can be used as the conductive network, which is embedded between two elastomer layers [172]. This device has been demonstrated with excellent performances, including high linearity, low hysteresis, and strong piezoresistivity, under both static and dynamic load conditions.

Molecular material provides a more direct methodology to achieve intrinsic stretchability [175]. Molecularly stretchable materials are normally based on π-conjugated polymers. For some conjugated polymers, the molecular structures allow significant tensile strain without affecting the electronic function, which is important to achieve stretchability. Savagatrup et al [176] developed a conjugated polymer based on poly(3-alkylthiophene)s (P3ATs).The alkyl side chain in P3ATs plays an important effect on its mechanical and electrical performances. By optimizing the side chain lengths in molecular structures, the synthesized polymer exhibited an optimal combination of mechanical compliance and electrical performances.

Recently, a different material system, heterogeneous composite, has been developed to overcome the modulus mismatch between the soft substrates and rigid components. A novel design based

on heterogeneous composite systems is proposed with five orders differences of elastic properties through the thickness [177]. This unique mechanical behaviour of soft-to-hard transition could effectively protect the active material on top from the external tensions. Xu et al [178] used soft microfluidics as suspensions to mechanically isolate rigid electronics from compliant enclosures.

The techniques to develop intrinsically stretchable materials have been receiving constant attention, and exhibit potential applications in different fields, such as light-emitting devices [179, 180], transistor arrays [181, 182], photodetectors [183, 184], and many others [185-187].

2.3.3 Other desirable properties

Bio-integrated electronics should ideally integrate diverse active components that are capable of continuously monitoring and managing human body health. Apart from the abovementioned parameters, there are several other desirable properties that are essential for bio-integrated systems.

❖ *Wireless communication interface*

In conventional medical devices, a wired connection is essential for the recorded data transmission from sensing components to external machine for data analysis and visualizations. However, this traditional wired approach is not desirable in specific conditions, such as for long-time implanted devices, and babies' vital signs monitoring. Wireless communication technology could efficiently mitigate the wired issues to provide more effective healthcare. Currently, there are diverse wireless technologies having potential to be employed in wireless sensing systems, such as Bluetooth, NFC, RFID, ZigBee, and WiFi [188]. Among them, Bluetooth and NFC predominate in recently developed bio-integrated electronics. Bluetooth, as an active device, can continuously communicate with the reader or other sensors in the network over a long distance, but cannot work without power supply. NFC-based sensing system normally work in a passive and battery-free mode, which does not require power on board. However, the operational distance is limited, typically within centimetres. In recent years, Rogers group have developed a range of wireless devices based on NFC technology, including optoelectronic systems for skin characteristics [189], wearable pulse oximetry [190], pressure sensor for the brain [191], optoelectronic implants for optogenetics [192], and other fields [95, 193-195]. Bluetooth technology has also been widely used as the wireless communication interface for diverse applications, such as biosensor for saliva monitoring [196], real-time monitoring of sodium intake [197], flow measurement through ventricular shunt [198], and electrophysiological sensors [199]. A recent study based on a combined NFC and Bluetooth technology further contributed to the development of advanced epidermal electronic systems for neonatal intensive care [200].

❖ *Self-power*

In general, electronic systems cannot work without power. Traditional wearable devices typically rely on batteries as power supplies, whose lifetime, size, and weight remain big challenges to overcome. Self-powered capacity is desirable for bio-integrated electronics to avoid the need of external power supplies. The human body can be regarded as a potential energy source where energy is normally neglected and dissipated into the environment. Several types of energy sources exist in human body, including mechanical, thermal, and chemical ones, among which mechanical energy is ubiquitous in our daily activities and regarded as one of the most sufficient energy sources.

As discussed in Section 2.2, piezoelectricity and triboelectricity are two commonly adopted techniques to scavenge mechanical energy. In piezoelectric energy harvesting, PVDF and PZT are two high-performance materials that have been extensively explored in various applications, e.g. cardiac pacemaker [38], brain stimulation [24], and arterial pulse monitoring [20]. Triboelectric nanogenerator also exhibits significant potential in a range of areas, such as tactile sensing [201], finger motion monitoring [127], and proximity and pressure sensing [202].

The human body is also a natural heat source, and thermoelectric energy harvesting is of interest to collect the thermal energy from human body. There is a natural temperature difference between surrounding environment and human body, where this difference can be converted into electric voltage due to the Seebeck effect. As current devices pursue miniaturization, it is challenging to improve the efficiency of heat conversion. Recently, Nan et al [203] developed compliant and stretchable devices based on 3D thermoelectric coils. The proposed open 3D structure increased heat flow through the system.

Biofuel cells has emerged as a promising avenue to extract electrical power from various biofluids in human body [204]. A biofuel cell typically consists of anode and cathode electrodes which convert biochemical energy into electrical power through redox reactions. Among various biofluids in human body, sweat is an appealing choice due to its non-invasive collection and energy generation efficiency. Wang group has undertaken comprehensive research on sweat-based wearable biofuel cells in various forms, such as epidermal tattoos [205, 206] and wearable textiles [207, 208], demonstrating it as a promising wearable power source.

2.4 MECHANICAL METAMATERIALS CONCEPTS

Mechanical metamaterial is an emerging discipline that exhibits unusual mechanical properties through rationally structural designs, providing new opportunities to expand material design spaces. Zadpoor [209] summarized several types of mechanical metamaterials, including extremal, negative, and ultra-property materials. For example, in mechanical metamaterials, Poisson's ratio can be

tuned to meet diverse applications. Natural materials typically possess positive Poisson's ratios, and will shrink if a tension strain is exerted in the perpendicular direction. Auxetic materials however have negative Poisson's ratios, meaning stretching in one direction would induce expansion in the perpendicular direction. These demonstrate how material intrinsic properties could be tailed through structural topology designs. There are several topology structural designs in auxetic structures with certain types of mechanical properties, including re-entrant, chiral, and rotating rigid structures [210], and these approaches generally feature uniform topology. Recently, non-uniform topology patterns based on auxetic unit cells have been adopted in the designs of mechanical metamaterials with unprecedented properties, such as independent tailoring of elastic modulus and Poisson's ratio [211, 212], and shape-matching metamaterials [213, 214]. Auxetic mechanical metamaterials show great potential in biomedical applications, and this concept has been recently adopted in research, including stretchable strain sensor with enhanced sensitivity by auxetic mechanical metamaterials [215], and auxetic cardiac patch with desirable mechanical properties conforming to heart shape [1].

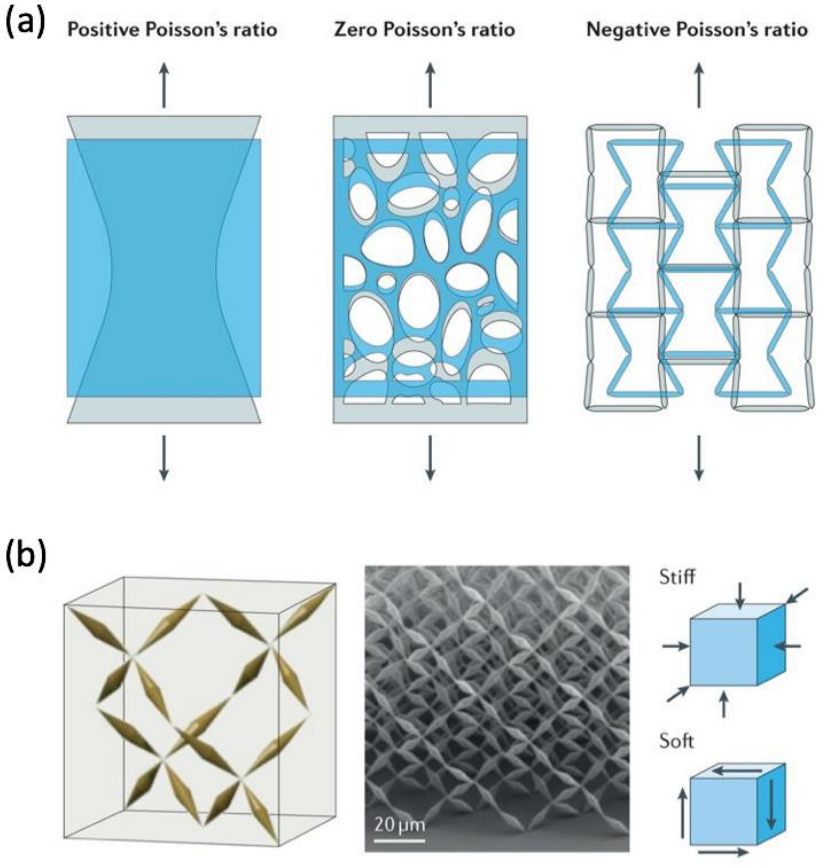

Figure 2.4 Examples of mechanical metamaterials designs. (a) Tunable Poisson's ratios can be achieved by designed architectures. (b) Extremal metamaterials. The structure is designed to be stiff against isotropic compression but soft under shear force. [216] Copyright 2017, Springer Nature Publishing Group.

Among various design principles in mechanical metamaterials, Origami and Kirigami techniques have been extensively studied due to the simple fabrication process and predictable shape control. These two techniques start from planar sheets, which allows a range of patterning on 2D precursors. For Origami-inspired metamaterials, flat sheets folds into 3D configurations based on the predefined crease patterns, and Kirigami introduces additional cuts into the sheets, which brings additional properties, such as extreme stretchability and diverse deformed configurations. Zadpoor et al reviewed the underlying mechanisms to create 3D curved structures from flat sheet based on Origami and Kirigami techniques and diverse potential applications [217]. The Kirigami-based concept has been demonstrated to have high feasibility in a variety of areas, such as stretchable conductor [218, 219], energy harvesting [220, 221], optical devices [222, 223], and many others [224-226].

2.5 RESEARCH MOTIVATIONS AND OBJECTIVES

2.5.1 Piezoelectric-based mechanism

In Section 2.2, several types of transduction mechanisms for sensing systems have been investigated. Each of these mechanisms shows different characteristics, and choosing an appropriate method is important to meet different requirements of health monitoring. The diverse performances of sensing systems were also comprehensively summarized in Section 2.3, including the basic parameters of sensitivity and stretchability, and other desirable properties of self-powered and wireless communication capacities. Considering the practical applications of health monitoring, for example implantable devices, certain features such as self-powered capacity are desirable to remove battery dependence, and piezoelectric transduction mechanism is a feasible option to develop self-powered sensing systems.

2.5.2 Kirigami-based metastructures

Electronic devices typically require specific designs to meet different requirements in various fields. For example, in biological systems, bio-integrated electronics should be highly flexible and stretchable to intimately conform to the biological surfaces. However, most electronic materials lack enough stretchability to meet the dynamic behaviours of biological systems. Mechanical metamaterials, especially the Kirigami technique as discussed in Section 2.4, offer the potential to create novel design concepts to improve structural performance without affecting the intrinsic properties of the underlying materials.

Kirigami-based metastructures presented in this thesis is a type of structural system that possess unusual mechanical properties based on Kirigami designs. The Kirigami technique has been

demonstrated great potential in the field of stretchable electronics, and it can apply to a wide range of advanced materials for various functional devices. The key point is to apply linear cut patterns onto the 2D precursors, and the stretchability can be achieved when the external stretching is compensated by locally out-of-plane bending, thus protecting the intrinsic material properties. Piezoelectric materials show promising applications in self-powered electronics, however they typically lack sufficient stretchability to be integrated with biological systems, such as cardiac patch. Inspired by the Kirigami design concept, Kirigami-based metastructures using piezoelectric PVDF films is promising as a self-powered and stretchable sensing system. The locally out-of-plane bending is able to generate significant voltage outputs by combining a specific electrode design.

Moreover, Kirigami-based metastructures can be designed as a vibration platform with improved dynamic properties. Well-defined Kirigami cut patterns are applied on 2D precursors. Then, the resulting 3D configuration can be created through a mechanical assembly process based on compressive buckling. This Kirigami-based concept provides an efficient way to achieve tunable and predictable structural performances for various applications. Designated Kirigami patterns can contribute to 3D structures with multi-modal and multi-directional vibration properties. Using piezoelectric PVDF materials, this system can be used as an efficient vibration platform in the field of high-performance energy harvesting.

2.5.3 Objectives

Motivated by the aforementioned observations, this thesis explores Kirigami techniques applied to various electronic systems, including stretchable piezoelectric strain sensors, self-powered health monitoring devices, tunable sensing capacities, and energy harvesting systems. There are four objectives in this thesis:

1. To explore the Kirigami technique with linear cut patterns to design a stretchable piezoelectric sensor with enhanced piezoelectricity.

2. The development of an integrated self-powered sensing device, with a flexible, stretchable, and biocompatible sensing part that could be conformably and compliantly mounted on skin and tissue surfaces, and an ultra-miniaturized wireless system for data collection and transmission.

3. The study of Non-uniform Kirigami patterns and their potential application in tunable sensing performances are investigated. Numerical simulations and experimental tests will be conducted to evaluate the proposed sensing system.

4. To develop a Kirigami-based energy harvester. The Kirigami technique with compressive buckling is introduced to explore flexible 3D metastructures for multi-modal and multi-directional vibration energy harvesting.

2.6 THESIS OUTLINE

Chapter 3 investigates Kirigami stretchable strain sensors with enhanced piezoelectricity induced by topological electrodes. A Kirigami technique with linear cut patterns has been employed to design a stretchable piezoelectric sensor with enhanced piezoelectricity. A parametric Finite Element Analysis study is first performed to investigate its mechanical behaviour, followed by experiments. An inter-segment electrode connection approach is proposed to further enhance the piezoelectric performance of the sensor. The voltage output shows superior performance compared to conventionally continuous electrodes. Dynamic tests with a range of frequencies and strains are performed to validate the sensor design.

Chapter 4 focuses on stretchable piezoelectric sensing systems for self-powered and wireless health monitoring. A Kirigami approach to realize a novel stretchable strain sensor is introduced through a network of cut patterns in a piezoelectric thin film, exploiting the anisotropic and local bending that the patterns induce. The resulting pattern simultaneously enhances the electrical performance of the film and its stretchability while retaining the mechanical integrity of the underlying materials. The power output is enhanced from the mechano-electric piezoelectric sensing effect by introducing an intersegment, through-plane, electrode pattern. By additionally integrating wireless electronics, this sensing network could work in an entirely battery-free mode. The Kirigami stretchable piezoelectric sensor is demonstrated in cardiac monitoring and wearable body tracking applications.

In Chapter 5, mechanical metastructures with non-uniform Kirigami is studied. A class of highly tunable mechanical metastructures with controlled and predictable spatial deformations by prescribed non-uniform Kirigami patterns is proposed. A parametric investigation is performed to study the mechanical response of different non-uniform Kirigami designs. Combined numerical and experimental results show the relationship between nominal mechanical properties and Kirigami geometric parameters. Finally, the applications of non-uniform Kirigami in a piezoelectric sensor have been demonstrated.

Chapter 6 explores Kirigami technique in the application of 3D multi-functional vibration energy harvesting via compressive buckling. Tunable mechanical properties have been achieved in the presented energy harvester, where piezoelectric materials are integrated and strategically designed into compliant 3D architected metastructures. This approach enables energy scavenging from

vibrations not only in multiple directions but also across a broad frequency bandwidth, thus increasing the energy harvesting efficiency. The proposed system comprises a buckled ribbon with optional Kirigami cuts. This platform enables the induction of vibration modes across a wide range of resonance frequencies and in arbitrary directions, mechanically coupling with four cantilever piezoelectric beams to capture vibrations. The multi-modal and multi-directional harvesting performance of the proposed configurations has been demonstrated in comparison with planar systems.

In Chapter 7, the summary of this thesis is described, followed by some potential research directions and future work in the field.

CHAPTER 3 - KIRIGAMI STRETCHABLE STRAIN SENSORS WITH ENHANCED PIEZOELECTRICITY INDUCED BY TOPOLOGICAL ELECTRODES

Piezoelectric materials have recently received considerable attention for biomedical applications. A variety of sensors using either organic or inorganic piezoelectric materials have been developed as self-powered systems to avoid battery requirements. However, one of the main barriers hindering the application of piezoelectric sensors is their low stretchability, as most tissues in the human body possess soft and highly deformable surfaces. In this chapter, a novel stretchable piezoelectric sensor was developed using the Kirigami approach, an ancient Japanese art of paper cutting and folding. Tunable mechanical properties can be obtained through a parametric exploration of Kirigami patterns with linear cuts. The Kirigami-induced buckling leads to a moderate stress growth within a large strain, thus increasing the stretchability. Kirigami patterns with linear cuts are introduced to piezoelectric polyvinylidene fluoride (PVDF) films with polyethylene terephthalate (PET) films as the substrate. Furthermore, a novel inter-segment electrode connection is proposed to improve the generated voltage by avoiding charge cancellation. Dynamic tests under various loading conditions are conducted to validate the efficiency and robustness of the Kirigami stretchable sensors. For the first time, the feasibility of making a stretchable sensor with improved piezoelectricity is demonstrated, showing great potential in implantable devices.

3.1 INTRODUCTION

Implantable biomedical devices have recently received significant interest in healthcare. However, most implantable electronics are powered by internal batteries whose life-span restricts long term operations. Additional surgery for the battery replacement is undesirable due to increased pain and risks to the patients. A sustainable power source derived from the biological system itself is therefore crucial for implantable devices. Piezoelectric materials are viable candidates for such implantable sensing systems, since they can be used as self-powered battery-free sensors with intrinsic mechano-electric energy harvesting ability [227]. Many efforts have been dedicated to the development of piezoelectric sensors for health monitoring, as discussed in recent review papers [15, 17, 228]. Two main types of piezoelectric materials are widely used, organic and inorganic. For inorganic ones, such as lead zirconate titanate (PZT) and Barium titanate ($BaTiO_3$), they are quite stiff and brittle in the bulk state, thus not well-suited to flexible biomedical systems directly. Many approaches have been explored to solve this challenge, including the fabrication of thin films [18, 39], and nanowires [229, 230] from these materials. The aforementioned methods generally involve complicated microfabrication processing steps. Organic materials are preferable for biomedical applications; their natural flexibility enable them to conform to the soft surface of human tissues. PVDF and its copolymer poly[(vinylidenefluoride-co-trifluoroethylene) [P(VDF-TrFE)] are two of the most commonly used organic piezoelectric materials, and have shown promise for biomedical applications due to their outstanding piezoelectric characteristics, mechanical ductility, and biocompatible properties [231].

Extensive work has been conducted to improve the piezoelectric properties by facilitating the formation of β phase crystals. This can be achieved by incorporating particles, such as ferrite nanoparticles [232], carbon nanotubes [233], and hybrid nanocomposites [234], into the polymer matrix. A mesoporous PVDF film with ZnO nanoparticles as sacrificial template represents an innovative method to induce the formation of the β phase due to the interactions between PVDF dipoles and the ZnO surface [106]. Such an implantable piezoelectric device exhibits outstanding performances in vivo, and it is also fully compatible with the biological environment [231]. Surface morphology also plays a key role in elevating the power output, and a smooth and flat surface of P(VDF-TrFE) film results in an eight-fold increase in voltage output over a rough surface [227].

In addition to high sensitivity, a health monitoring system also requires high stretchability to offer 3D shape changing within the human body. However, traditional PVDF films show extremely low stretchability, thus limiting their applications in implantable devices. Recently, the Kirigami approach, the Japanese art of cutting and folding paper, has been proven to be a versatile

technology to design diverse mechanical metamaterials with multiple functionalities [217, 235]. The mechanical properties of a Kirigami structure can be tuned and programmed based on a tailored pattern of cuts. For example, a hierarchical fractal cut is demonstrated to be an effective method to design highly stretchable metamaterials [236-238]. Unit cut geometry and hierarchical levers are two important parameters that determine the mechanical behavior. Moreover, the sheet thickness significantly affects the transition from in-plane deformation to out-of-plane deformation, and a thin sheet is prone to trigger mechanical instabilities with induced buckling, forming a variety of three dimensional (3D) architectures [218, 239-241]. The Kirigami approach effectively broadens the design possibilities for a wide range of flexible materials, with the length scale spanning from nanometers to centimeters. The remarkable features of Kirigami structures have recently been introduced in a variety of applications. To improve the power generation of flat solar cells, a simple linear cut pattern is made into thin films of gallium arsenide, and the angle of the tilted panel can be controlled by the stretching strain in order to track the sun's position [221]. With a similar Kirigami pattern, the stretchability of nanocomposite based conductors has been improved from 2% to beyond 100%, with stable conductivity [219, 242]. By introducing different functional materials, a variety of applications have been achieved, such as stretchable graphene transistors [225], mechanical actuators [225, 243], stretchable batteries [244], supercapacitors [220] and deployable reflectors [222, 223]. A recent study has shown ultrastrechable bioprobes with a Young's modulus of 3.6 KPa and stretchability of 840%, which could intimately follow the shape changes of biological tissues. In vivo tests demonstrate that this Kirigami based device could record the electrocardiogram signals of a beating mouse's heart whose volume and surface area experience large and rapid changes [224]. This work has validated the potential of the Kirigami approach in biomedical applications.

Here, we propose a Kirigami piezoelectric sensor with high stretchability and enhanced piezoelectricity. Combined numerical and experimental results demonstrate that tunable and programmable mechanical behavior can be achieved by adjusting the geometric parameters of the cut patterns. We have then fabricated a piezoelectric sensor by making a linear cut pattern into a thin PVDF film. To enhance the electric performance, an inter-segment electrode design is explored through finite element analysis (FEA) and experiments. Finally, dynamic tests at various frequencies and tensile strain levels have been performed on the stretchable piezoelectric sensor system.

3.2 STRUCTURAL DESIGN AND MECHANICAL ANALYSIS

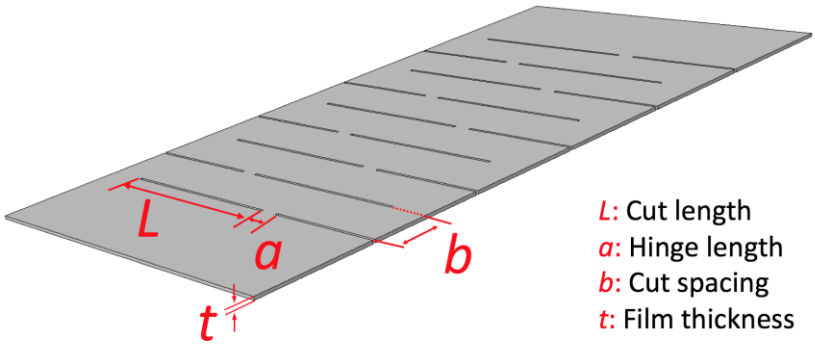

Figure 3.1 Schematic of the Kirigami structure where L, a, b and t indicate cut length, hinge length, cut spacing, and film thickness.

The patterns of cuts in the Kirigami structure need to be algorithmically designed to obtain a specific mechanical performance. We use here a simple and effective linear pattern of cuts in a thin flat film, forming the Kirigami structure. As shown in Figure 3.1, the configuration features a linear cut pattern with uniform layouts. To understand the overall mechanical deformation of the Kirigami configurations, thin polyethylene terephthalate (PET) films was adopted, and this type of linear cut pattern was introduced into this film to analyze the mechanical properties of the Kirigami structure. A uniaxial tensile load was applied on the structure to obtain the stress-strain curves, and the boundary conditions were applied with one end clamped and the tensile loading introduced via the other end.

To validate the test results, FEA was also used to analyze the stress-strain response of the Kirigami structure. The material property is required for numerical simulation studies, and the material properties of the pristine PET film were obtained by performing a test based on the ASTM D882 standard with a tensile test machine (Shimadzu with 1KN load cell). The test specimen has a whole length of 180 mm, a gauge length of 130 mm and 10 mm in width. It is completely clamped at both ends. The tensile speed was set at 0.1 mm/s. To capture the change of width and length during the tensile loading, the displacements of the markers on the PET film were recorded by an iMETRUM video gauge. The data was then collected by a National Instruments card (NI USB-6211). The Poisson's ratio was calculated by the ratio of the transversal strain and longitudinal strain. The stress-strain curves of the PET films are shown in Figure 3.2.

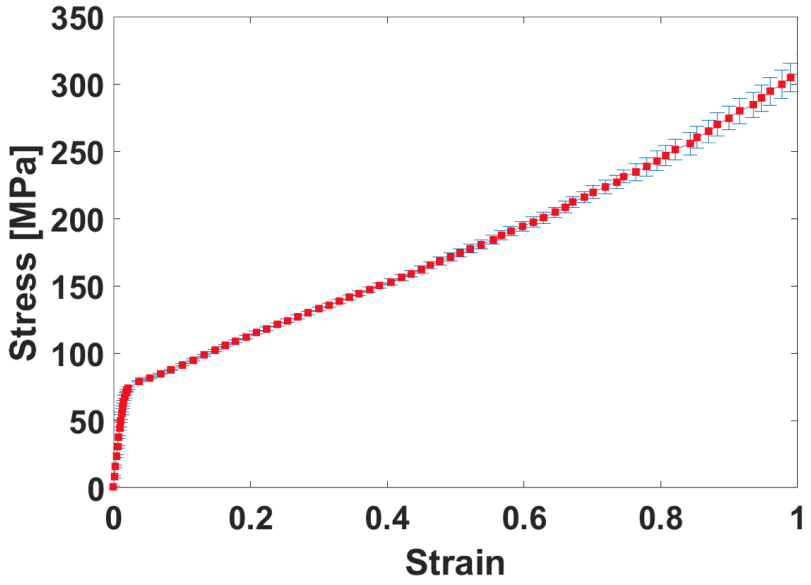

Figure 3.2 The mechanical properties of pristine PET films (125 μm) for five samples under uniaxial tensile tests.

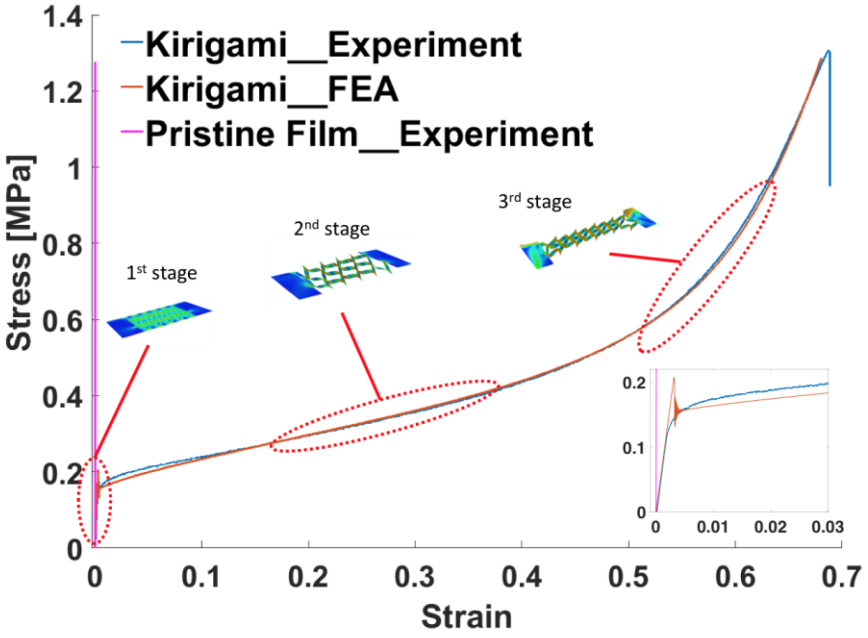

Figure 3.3 Stress-strain curves for the pristine film, and Kirigami patterned film obtained by numerical simulations and experiments. The inset shows the initial stage.

The FE predictions correlate very well with the experimental measurements, and the comparison results are illustrated in Figure 3.3. The typical stress-strain curves of the Kirigami structure show three different stages. During the first stage, the structure undergoes an initial elastic deformation

which is restricted within the in-plane stretching. The effective stiffness of the structure is governed by the in-plane bending of the hinges. Once the applied force reaches the critical buckling load, a mechanical instability is triggered, with a transition from in-plane deformation to out-of-plane buckling (second stage). The out-of-plane bending and rotation of the cut strips lead to a moderate stress growth within a high strain, thus enhancing the stretchability. The third stage occurs with further loading, and the subsequent deformation mode switches from bending back to stretching again. Stress concentration is localized in the edge of the cuts, leading to a sharp increase in the effective stiffness, and finally to fracture.

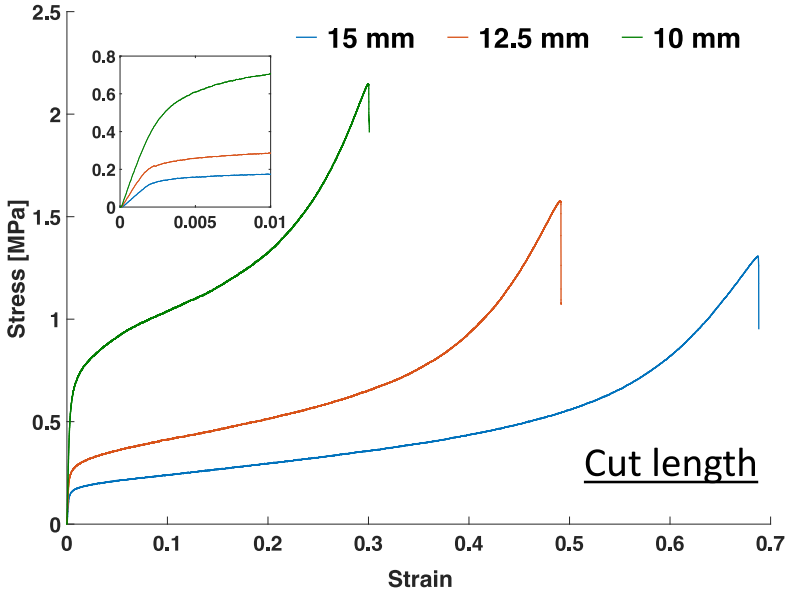

Figure 3.4 Experimental obtained stress- strain curves by varying single geometric parameter of the cut length. The inset shows the initial stage.

Analytical studies have been performed on a range of linear cut patterns, showing that there are several geometric parameters and material properties that determine the mechanical behavior of this type of Kirigami structures. The fundamental parameters are the cut length L, the hinge length a, the spacing between the cuts b, the film thickness t, and the Young's modulus E of the underlying material [240]. The effective modulus of the whole structure is a key emergent metric to be evaluated through a parametric exploration. For biomedical devices, a low effective modulus would be preferable to enable an adaptation to the deformation of the tissue. We carried out a series of experiments with different geometry parameters to characterize the mechanical response. The effective modulus is calculated from the ratio between the nominal stresses and strains within

a 0.5% to 10% strain range to avoid the nonlinear buckling effect of the initial stage. The modulus is adopted as the indicator for the comparison.

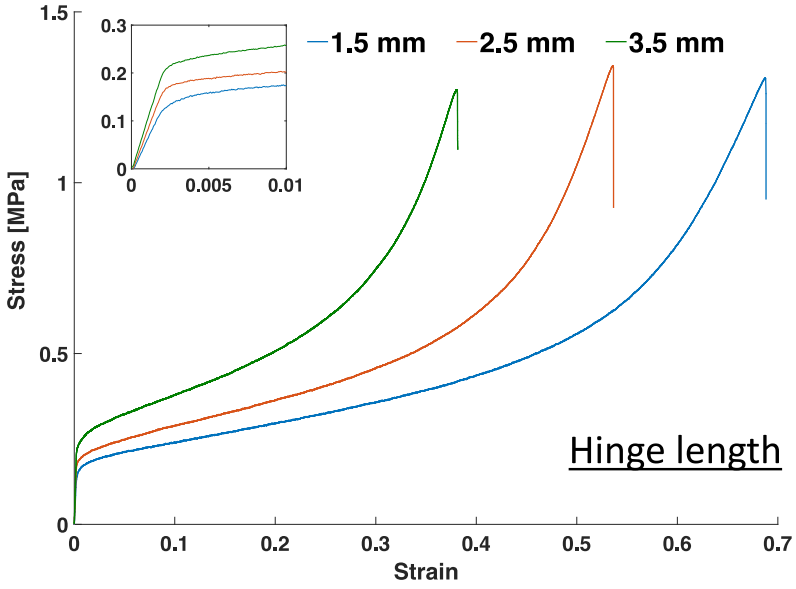

Figure 3.5 Experimental obtained stress- strain curves by varying single geometric parameter of the hinge length. The inset shows the initial stage.

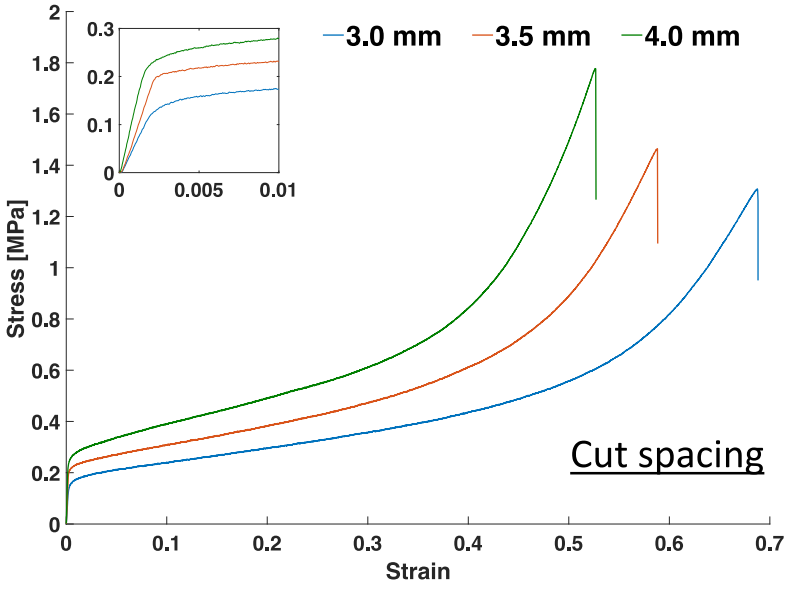

Figure 3.6 Experimental obtained stress- strain curves by varying single geometric parameter of the cut spacing. The inset shows the initial stage.

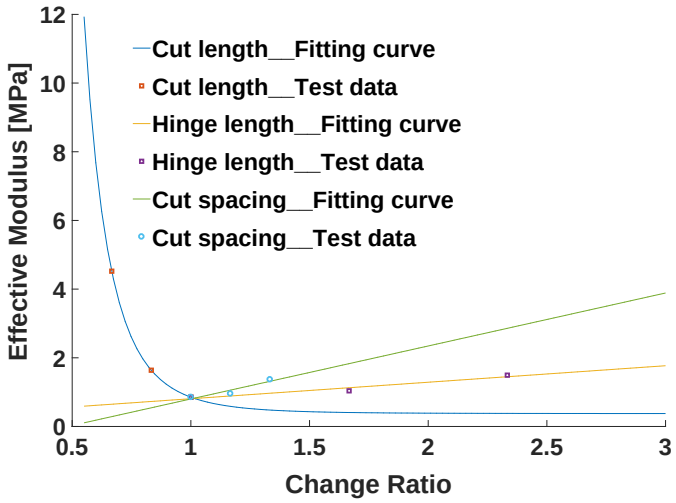

Figure 3.7 Summary of the dependence of effective modulus on the geometric parameters, where the change ratio indicates the normalized value of each parameter relative to its control value

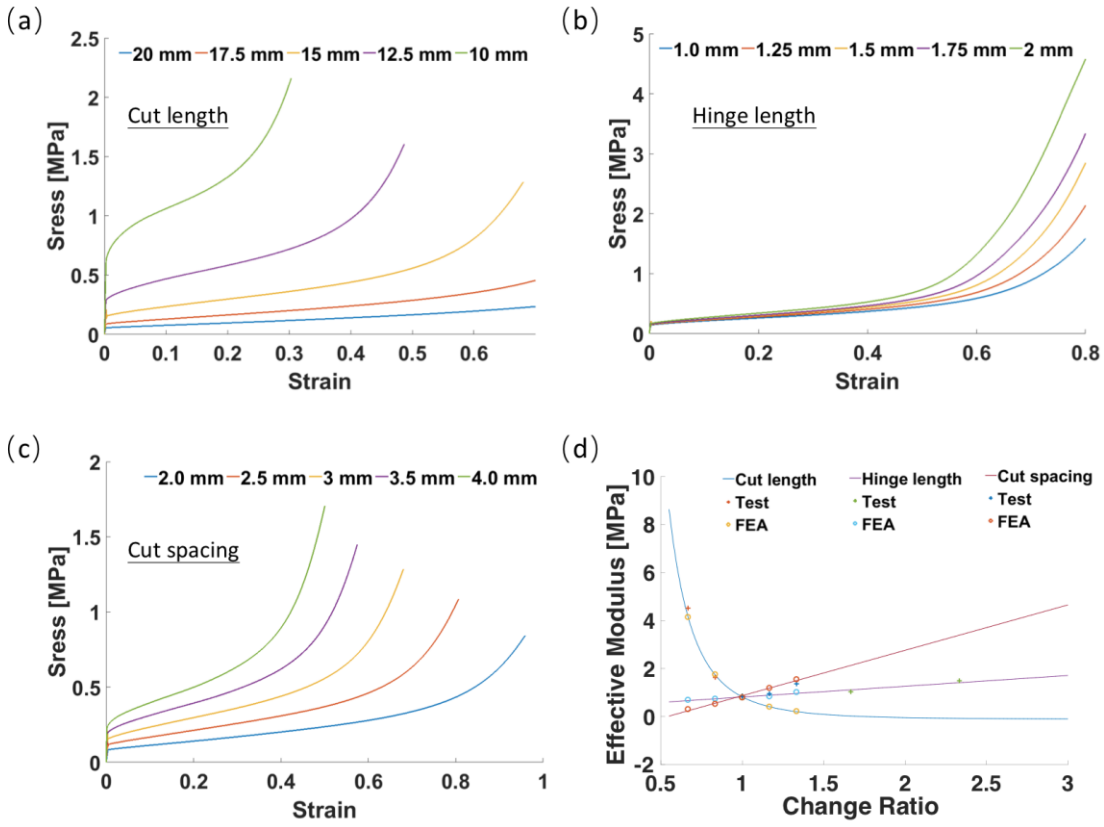

Figure 3.8 FEA study of the stress-strain curves of the Kirigami structure by varying geometric parameters, including the cut length in (a), the hinge length in (b) and the cut spacing in (c), where the control Kirigami parameters are L = 15 mm, a = 1.5 mm, and b = 3mm, respectively; (d) summary of the dependence of effective modulus on the geometric parameters, where the change ratio indicates the normalized value of each parameter relative to its control value. Experimental results correlate very well with the FE prediction.

Figure 3.4 - Figure 3.7 summarized the relationship between the mechanical properties and geometry parameters from tests. Figure 3.4 shows that an increase of the cut length L would soften the structure with a low effective modulus. In Figure 3.5 and Figure 3.6, increasing the hinge length a and the cut spacing b would make the structure more rigid, leading to a higher effective modulus. From Figure 3.7, it can be seen that the hinge length has an exponential effect on the mechanical behavior, while the other parameters exhibit a linear relationship with the effective modulus. The results from Figure 3.7 show that the effective modulus could be readily tuned by controlling the geometry parameters, and the control Kirigami parameters are L = 15 mm, a = 1.5 mm, and b = 3mm, respectively. These parametric studies were also performed by FEA, and as seen in Figure 3.8 the general trends shown in experiments are replicated in FEA as well.

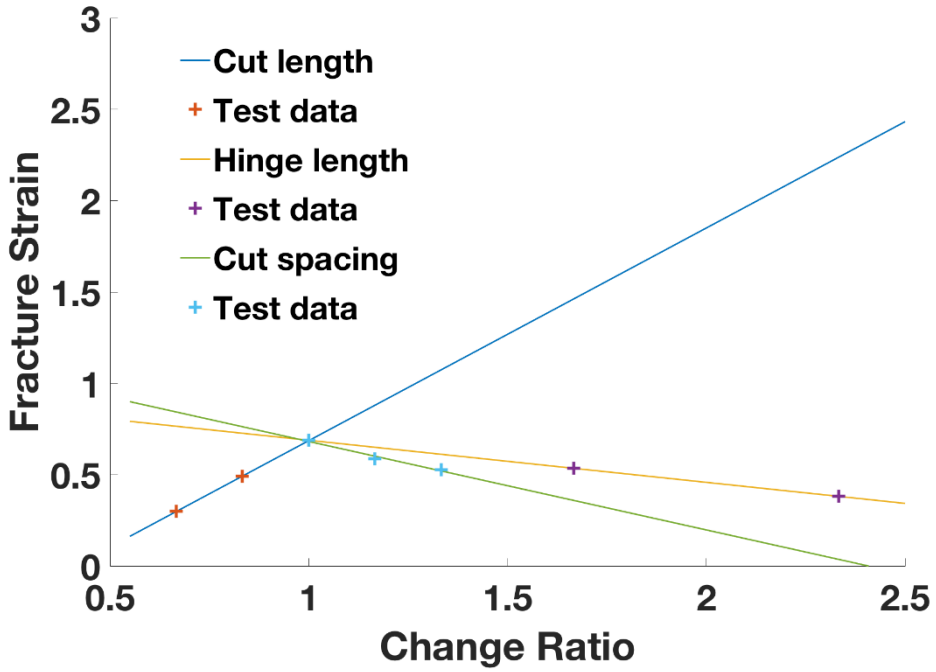

Figure 3.9 Summary of the dependence of fracture strain on the geometric parameters, where the change ratio indicates the normalized value of each parameter relative to its control value. The control Kirigami parameters are L = 15 mm, a = 1.5 mm, and b = 3mm, respectively.

The strain at failure is also an important factor for sensor design, and the relation between the limit strain and the geometric parameters based on the test data is summarized in Figure 3.9. It shows the fracture strain has a linear relationship with the cut length while linear increases of hinge length and cut spacing decrease the fracture strain.

3.3 ELECTRICAL DESIGN AND SYSTEM EVALUATION

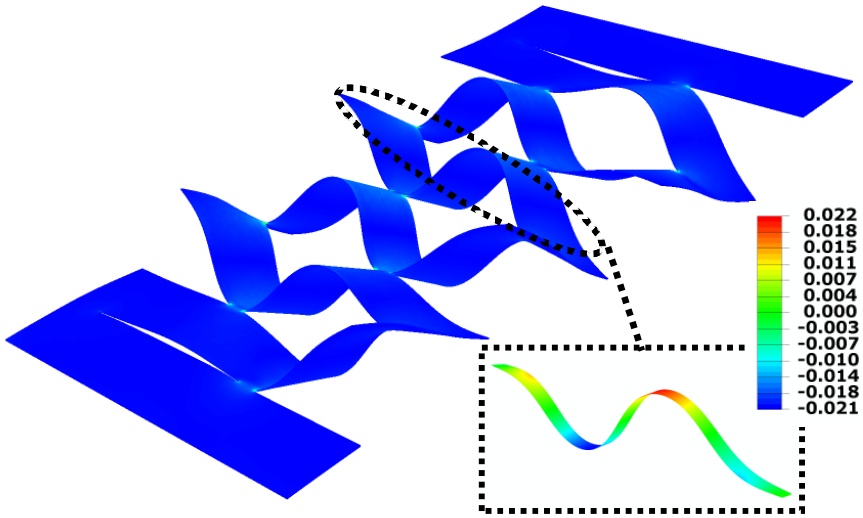

Figure 3.10 The FEA analysis of the mechanical response of the Kirigami structure. The inset is the local strain distribution on a unit strip.

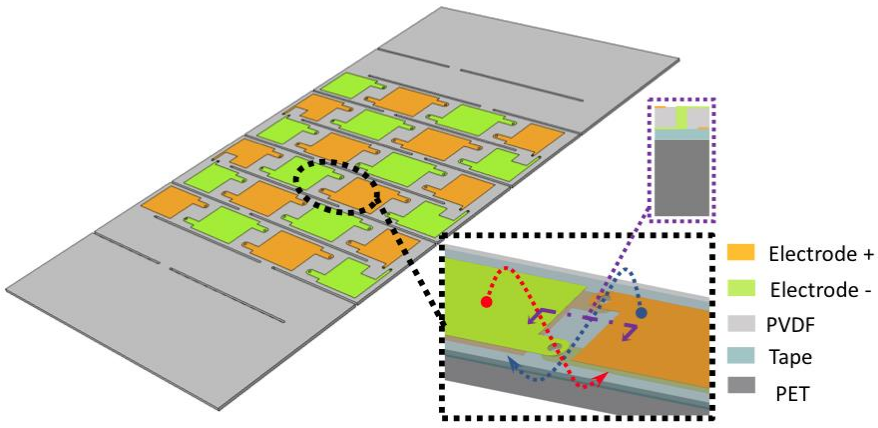

Figure 3.11 The inter-segment electrode pattern with reverse connections for adjacent parts through holes.

We then introduce the linear Kirigami cut pattern into a thin PVDF film to design a stretchable piezoelectric strain sensor. A FEA study was first performed to optimize the electrode design of the Kirigami piezoelectric sensors. For the wavy unit of the Kirigami structure, the local strain distribution along its neutral axis is variable, with compression in red areas and tension in blue areas coexisting on the same surface, as shown in Figure 3.10. If the Kirigami pattern is directly introduced into the PVDF film with continuous electrode, a charge cancellation would occur due to the opposite strain distribution on the same side of the electrodes. An inter-segment electrode

pattern is therefore proposed to improve the electric performance [245]. Rather than using a continuous electrode over the surface, we use only a segment corresponding to one quarter of the wavelength of the buckled section and located in the highest strain region. Then, the opposite electrodes between segments are reversely connected through holes, as illustrated in Figure 3.11.

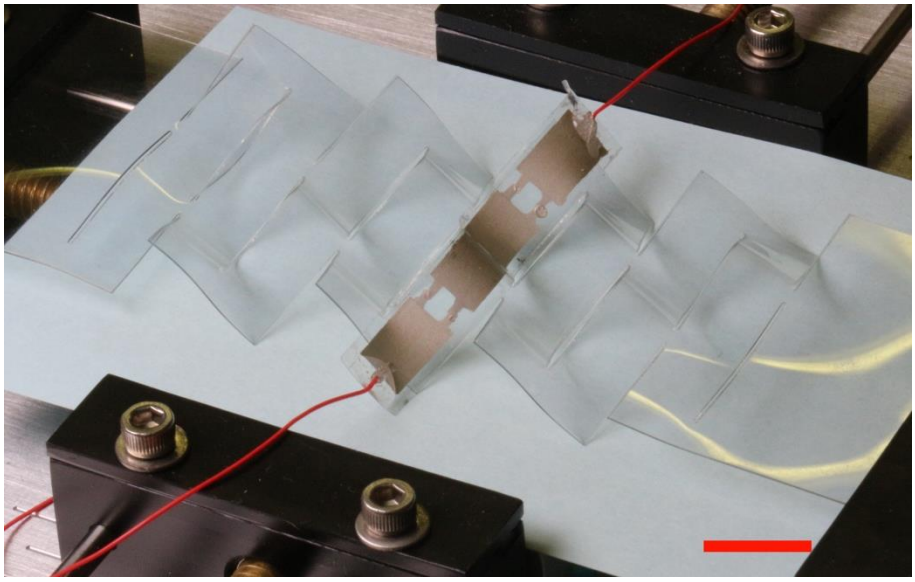

Figure 3.12 The electrode pattern using inter-segment connections within one-unit strip of the Kirigami structures, scale bar 2 cm.

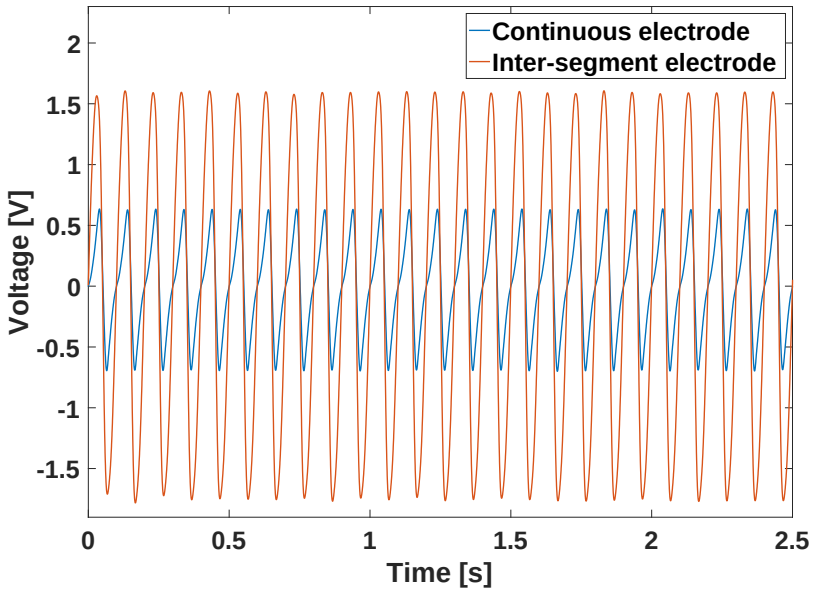

Figure 3.13 The voltage output using the electrode patterns in Figure 3.12 from experimental tests.

In order to validate the proposed inter-segment connection mechanism, an experimental comparative study was performed between the proposed design and the conventional continuous configuration. The Kirigami-based piezoelectric sensor has a two-layer topology, with a 125 μm thickness of PET film as the substrate and a 28 μm thickness of PVDF film. The parameters of the cut patterns are: cut length L=22.5 mm, hinge length a=2.25 mm, and spacing between cuts b=8.25 mm. Kirigami based piezoelectric sensors with these two electrode designs were fabricated with one strip of PVDF film with either continuous or reverse connected electrode integrated, Figure 3.12, and then cyclically stretched. The continuous electrode pattern has an effective area of 43 mm × 6 mm, and the inter-segment connection electrode has an effective surface of 9 mm × 6 mm in a single, quarter wavelength, unit. The experimental results, Figure 3.13, substantially validated the efficiency of the inter-segment connection design, with a resulting 1.63 V generated voltage compared with 0.63 V generated voltage by the continuous electrode pattern under a given frequency of 10 Hz and a tensile strain of 10 %. As seen in Figure 3.13, the output voltage from both inter-segment and continuous electrode designs are not sine-shaped (Figure 3.14). This is due to the relation between the global applied strain and local strain on the strip is not linear, as clearly depicted in Figure 3.14(b).

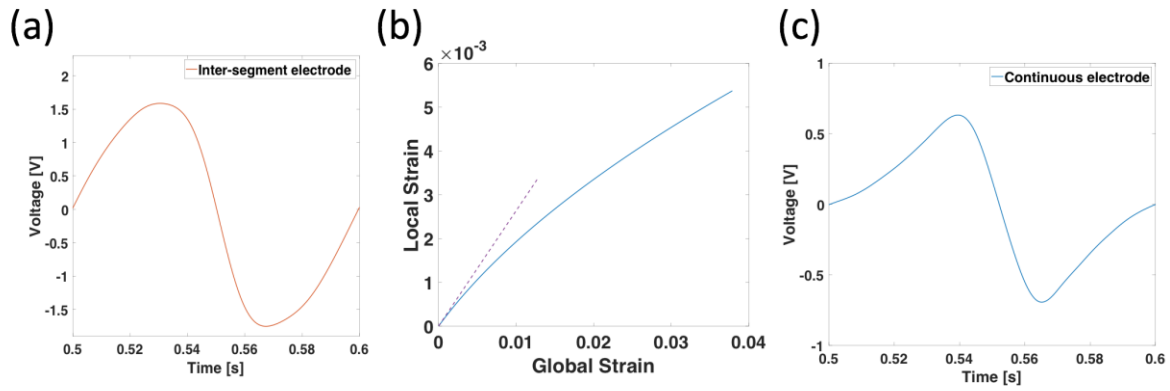

Figure 3.14 (a) Zoom-in of voltage output based on the inter-segment connection electrode; (b) the relation between global and local strains on one-unit electrode of the strip; (c) zoom-in of the voltage output of the continuous electrode.

By using the optimized electrode design, the electric performance of the proposed sensor is explored under dynamic tests with controlled frequency excitation and strain ranges. Figure 3.15(a) shows the output voltage time histories at 10 Hz and tensile strain range between 2 % and 10 %. The voltage increases linearly with applied strain in Figure 3.15(b). The output voltage time series at constant 1% tensile strain and frequency range from 3 Hz to 24 Hz are shown in Figure 3.15(c).

In this case also in Figure 3.15(d), the voltage output shows an almost linear dependency to the frequency increase under the fixed strain.

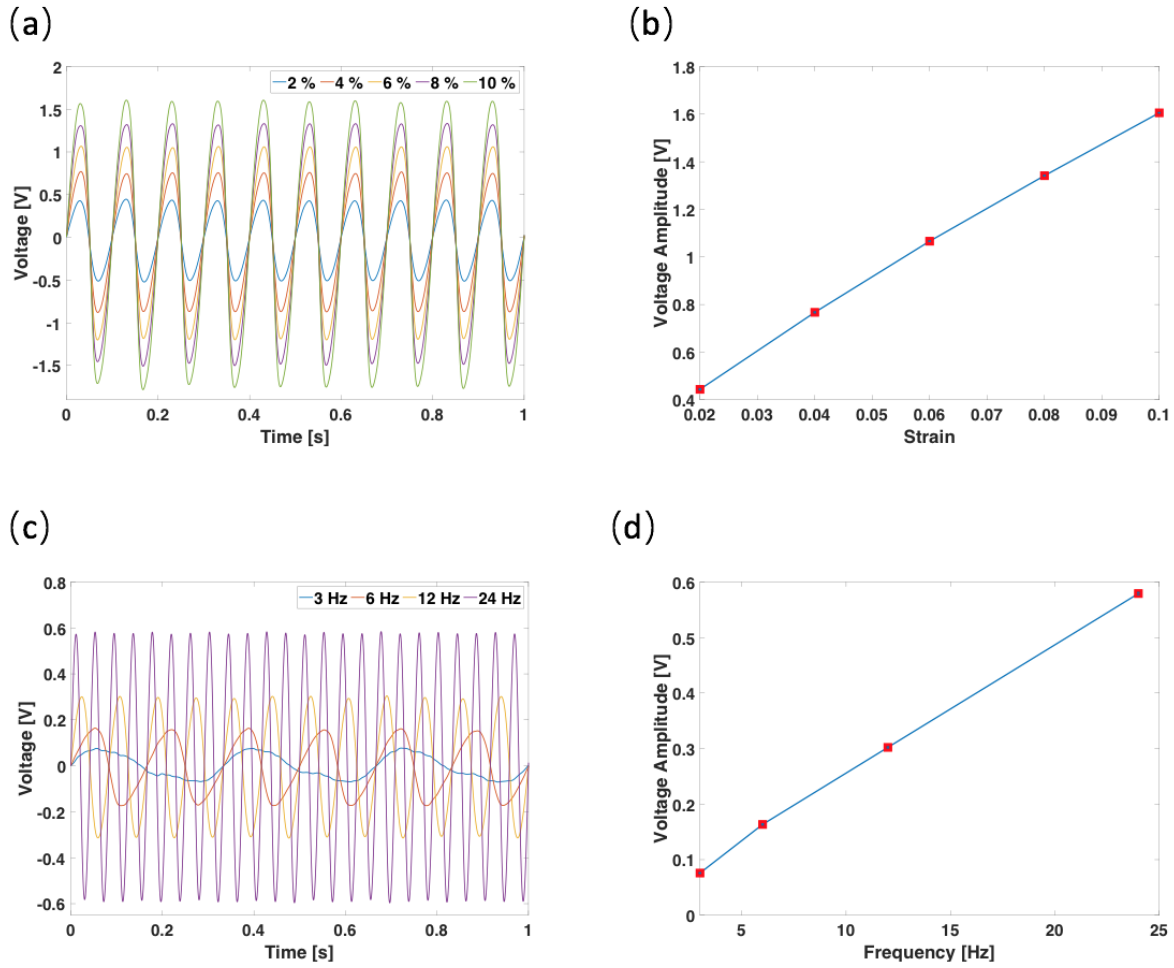

Figure 3.15 (a) Voltage output of the Kirigami piezoelectric sensor under a given frequency of 10 Hz and a strain range from 2 % to 10 %, and (b) the effective sensitivity. (c) Voltage output under a given strain range of 1 % and a frequency range from 3 Hz to 24 Hz, and (d) a corresponding plot of amplitude versus frequency

3.4 Materials and Methods

Materials. Polyvinylidene fluoride (PVDF) thin film with silver electrodes in a thickness of 28 μm was obtained from TE Connectivity Measurement Specialties (Digi-Key). Polyethylene terephthalate (PET) films with a thickness of 125 μm were obtained from Sigma-Aldrich. 3M™ Adhesive Transfer Tape 7952MP was purchased from Stickytapes. Gorilla Epoxy Glue was purchased from OneCall. Silver Conductive Paint was purchased from RS Components.

Preparation of the inter-segment electrode pattern. To reversely connect the adjacent electrodes, holes with dimeter of 0.1 mm were cut on PVDF film using a Speedy Laser engraver. A shadow mask was patterned in water soluble tape (Aquasol) by laser engraver. Then, with the shadow mask, the silver electrodes on both sides of PVDF films were patterned by acetone solvent, and the process is shown in Figure 3.16. Through-hole connections were achieved by silver paint.

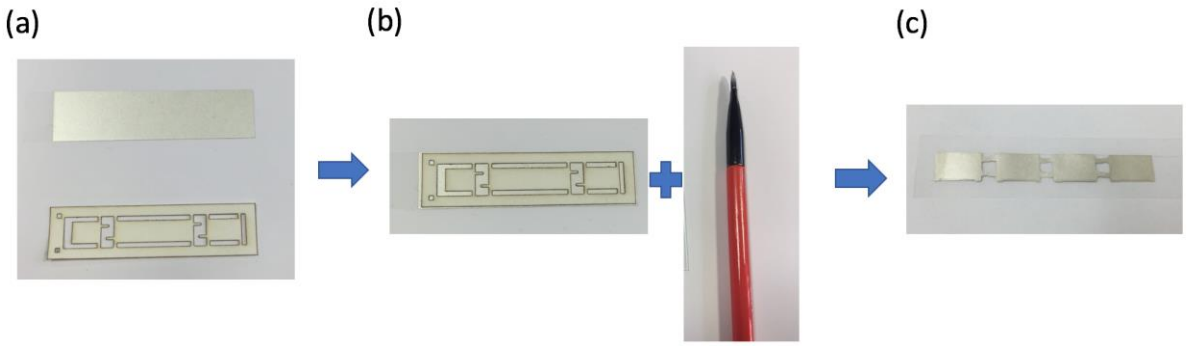

Figure 3.16 The process of electrode patterning with acetone. (a) The mask and PVDF film with unpatterned silver ink electrodes; (b) Pattern the electrodes using brush dipped with acetone; (c) PVDF film with patterned electrodes.

Preparation of Kirigami based piezoelectric sensor. The substrates of 125 μm PET film were cut with the Kirigami linear pattern by the laser engraver. Then, the prepared PVDF film with the patterned electrodes were bonded to the PET surface with adhesive tape. A wire connection was made for the electrodes using silver paint. The electrode collections were encapsulated with epoxy, dried at room temperature.

Finite element analysis. The commercial package Abaqus\Standard 6.14 (Dassault Systems) was used to conduct the mechanical simulation for the parametric study of Kirigami structures and piezoelectric analysis for electrode design.

For the mechanical analysis of the Kirigami structure, a 2D elasto-plastic model (*Elastic and *Plastic Material in Abaqus) with the material properties obtained in Figure 3.2 were used. 2D shell element (S4R) was adopted. The analysis includes two steps. In order to trigger the instability to induce the buckling, an imperfection was introduced with a small bias displacement in the center of the cut edge at the first step. Then, an implicit dynamic step in Abaqus was conducted to analyze the mechanical responses. The global mesh size was set as 0.5 mm with a mesh convergence study. The stress was consistent for further mesh refinement of 0.2 mm mesh size.

Dynamic test and voltage measurements. The electrical response of the piezoelectric sensing system was investigated. The dynamic test under variable frequency and strain ranges at room temperature was carried out using a dynamic mechanical analysis system (MetraviB). USB oscilloscope (PicoScope 2000) was used to collect the voltage output.

3.5 CONCLUSIONS

In conclusion, a stretchable piezoelectric sensor system with enhanced piezoelectric performance and high stretchability was designed and fabricated by introducing Kirigami patterns into a thin PVDF film with a PET film as the substrate. We introduce an inter-segment electrode design to avoid charge cancellation and improve the piezoelectric generator effect. Experimental tests validated the significant improvement in voltage output with the adopted electrode pattern. Moreover, the Kirigami technique vastly extends the strain range of the sensor, while the piezoelectric performance remains stable. Dynamic tests under variable frequencies and strains also validated the efficiency and robustness of the sensing performance. The high stretchability and excellent piezoelectric operation of this Kirigami based piezoelectric sensor suggests its high suitability for implantable, self-powered biomedical devices and sensor systems. This will be furthered explored in Chapter 4 through the development of an integrated sensing system.

CHAPTER 4 - STRETCHABLE PIEZOELECTRIC SENSING SYSTEMS FOR SELF-POWERED AND WIRELESS HEALTH MONITORING

Bio-integrated electronics that integrate high-performance sensing systems and communication interfaces are of increasing importance for their potential applications in health monitoring and wearable devices. Existing approaches reveals challenges to manage the mechanical mismatch between rigid electronics and biological systems. For implantable devices, a miniaturized interface for wireless data collection is of great significance to achieve constant monitoring of physiological information. The concepts presented in this chapter overcome these limitations, to establish an integrated self-powered sensing system, with a flexible, stretchable, and biocompatible sensing part that could be conformably and compliantly mounted on skin and tissue surfaces, and a miniaturized wireless system for data collection and transmission. The combination of structural optimization and a creative inter-segment electrode design contributes to the simultaneously enhanced properties in mechanical and electrical performance. Systematic experimental and simulation studies reveal the ultra-stretchability and self-powered capacities of this system. Successful demonstrations including in vitro, ex vivo, and on-body validate the performance in bio-mechanical and body activities monitoring. The results presented here serve as foundations for next-generation of bio-integrated electronics for human physiological monitoring.

4.1 INTRODUCTION

Wearable electronics are attracting increasing attention as recent developments in materials, mechanics, and manufacturing techniques create new opportunities for the integration of high-quality electronic systems into a single miniaturized device [94, 246, 247]. Most tissues in the human body possess soft, curvilinear, and dynamic-deforming properties, while conventional sensors are generally based on rigid and stiff electronics that are mechanically incompatible with biological systems. Bio-integrated devices with health monitoring systems are regarded as one potential solution to mitigate the above concerns. To conformably integrate with the human body the next generation of devices for human physiological monitoring should be highly flexible, stretchable, sensitive and untethered. Moreover, wireless communication and self-powered capabilities are of great importance, especially for implantable electronics. In this chapter, a piezoelectric sensing solution with high stretchability is presented which encompasses all these properties.

For wearable biomedical devices to offer reliable and precise information of health, flexible and stretchable electronics that could conformably and compliantly interact at the surfaces of human skin and internal organs have received growing attention in recent years [1]. There are generally two conceptually different strategies to achieve stretchability [134]: On the one hand, recent advances in material synthesis provide a promising option to develop intrinsically stretchable materials, such as metal/ionic liquids [166], semiconductor/elastomer hybrid networks [248], and conductor/elastomer hybrid networks [249]. Alternatively, in order to maintain the high electrical performance of conventional rigid materials, geometric designs are employed, such as mesh networks [250], wavy/buckled shapes [136], and segmented island-bridge layouts with serpentine [251, 252] or fractal [9, 137] interconnects. In these geometric designs, strains applied to the sensor would result in distributed changes in wave amplitudes and wavelength in wavy structures or distributed deformation of the interconnecting structure in island-bridge configurations, thereby preventing the materials from local high strains and subsequent failure. However, high cost and complexity of the fabrication process limit use and the required interconnect patterns would also occupy spaces, thus reducing the area density of active component. In recent years Kirigami, the Japanese art of paper cutting, has inspired materials scientists and mechanical designers to enhance the stretchability in materials substrates. The fabrication process of Kirigami structures involves a sequence of predefined cut patterns, and a broad range of desired shapes and mechanical behaviours have been achieved through specific algorithmic cut designs. The Kirigami approach has been applied across a broad range of length scales, spanning from DNA Kirigami at nanoscale [253], to graphene [225] and nanocomposites [218] at microscale, and various functional materials

at macroscale [220-223, 243, 254]. Another advantage of Kirigami is that it could transform a variety of advanced materials and planar systems, that were previously limited in application, into mechanically tunable two and three-dimensional (3D) architectures with broad geometric diversity [226, 255]. Owing to their predictable mechanical behaviors, a high degree of material choices, and a broad range of dimension scales, Kirigami techniques have been used in a variety of applications. For example, with an elegant design of linear cut patterns in thin-film solar cells, a solar-tracking system with tilting surface elements is achieved and controlled by stretching to induce buckling and a resultant feature angle change [221]. Similarly, Kirigami patterns have also been used in deployable reflectors [222, 223], energy storage devices [220], stretchable conductors [219, 222], transistors [225], bioprobes [224], mechanical actuators [243], and sensors [256].

Rapid developments in sensing systems and bio-integrated electronics have imposed a challenge on power sources, which are mainly based on batteries. However, for implantable biomedical devices, battery-powered sensors generally have limited lifetimes and require surgery for battery replacement. To overcome this challenge, techniques to extend battery life and further reduce the energy requirement of sensing systems are under development. However, it is more elegant to provide a sustainable power source generated by the human body itself. Recently, self-powered systems have attracted much attention, and dedicated efforts have been made to develop energy-harvesting systems to extract energy from the body, including electrochemical energy, thermal energy, and mechanical energy, as discussed in recent review papers [17, 228, 257, 258]. Among these power sources, mechanical energy is regarded as a promising option to offer sufficient power for embedded electronics [228]. Many studies have aimed to develop mechanically flexible and biocompatible sensing and energy harvesting systems based on two commonly used techniques: piezoelectricity [19, 36, 39, 259, 260] and triboelectricity [261-263]. Piezoelectric sensors, the focus of this chapter, exploit the mechanical-to-electrical conversion of piezo materials where electrical charge is induced upon mechanical strain. Piezoelectric materials are typically classified into two types, inorganic and organic materials. For inorganic ones, e.g. lead zirconate titanate (PZT), they are brittle and rigid in their bulk state, thus not inherently suitable to biomedical applications. Recently, however, efforts have been devoted to developing thin piezoelectric films of these materials in order to realize the needed flexibility, which normally involves complicated micro fabrication techniques [19, 36, 39]. Alternatively, organic piezoelectric materials, such as polyvinylidene fluoride (PVDF), are widely adopted based on their natural flexibility [259, 260]. However, current designs based on piezoelectric sensors still retain a critical lack of stretchability, impeding applications in areas where large strains occur.

Here, inspired by the Kirigami concept, we present an integrated stretchable sensing system in conjunction with wireless electronics for continuous health monitoring. This device is composed of two subsystems, a Kirigami-based stretchable and self-powered sensing component, and a wireless communication interface for data transmission. A linear Kirigami cut pattern is adopted for its simple manufacturing process. This design delivers significantly improved mechanical and electrical performances. The properties of this type of Kirigami configurations are investigated with numerical and experimental studies. We show that the elasticity of the proposed stretchable sensor can be programmable to match the target subject and can provide a reliable interface between electronics and human body. Simulation analysis validates the superior mechanical properties of Kirigami structures without inducing significant constraints on the measured surface compared with traditional planar structures. To enhance the sensing and power output of Kirigami-based piezoelectric systems, a novel inter-segment electrode pattern is adopted and evaluated by a comparative study. The electrical performances and energy harvesting abilities of this type of piezoelectric sensors have been demonstrated under different mechanical inputs over a range of frequencies and strains. The devices can be mounted on different surfaces as either wearable or implantable systems without mechanical irritation. The effectiveness of this approach for implantable devices is demonstrated by measuring the surface of a deforming balloon and ex vivo pig heart, and as a wearable sensor by measuring knee flexion. To demonstrate the capability for wireless sensing, an integrated sensing system with near-field communication (NFC) and self-powered capabilities is designed. Experiments with balloons and pig hearts illustrate the sensor signals under multiple conditions are successfully collected and wirelessly transmitted to external devices for real-time monitoring. We demonstrate that this type of sensing system with outstanding mechanical and electrical performances has great potential in future implantable and wearable healthcare applications.

4.2 FEATURES OF INTEGRATED SENSING SYSTEMS

The stretchable sensing system introduced here provides a self-powered strain monitoring system with wireless communications for both implantable devices and wearable electronics. The key features of this system include its noninvasive conformity to various types of curved surfaces through a creative Kirigami patterning and corresponding electrode interconnection design, and an interface based on NFC technology [95, 189] to wirelessly transmit strain information to external devices.

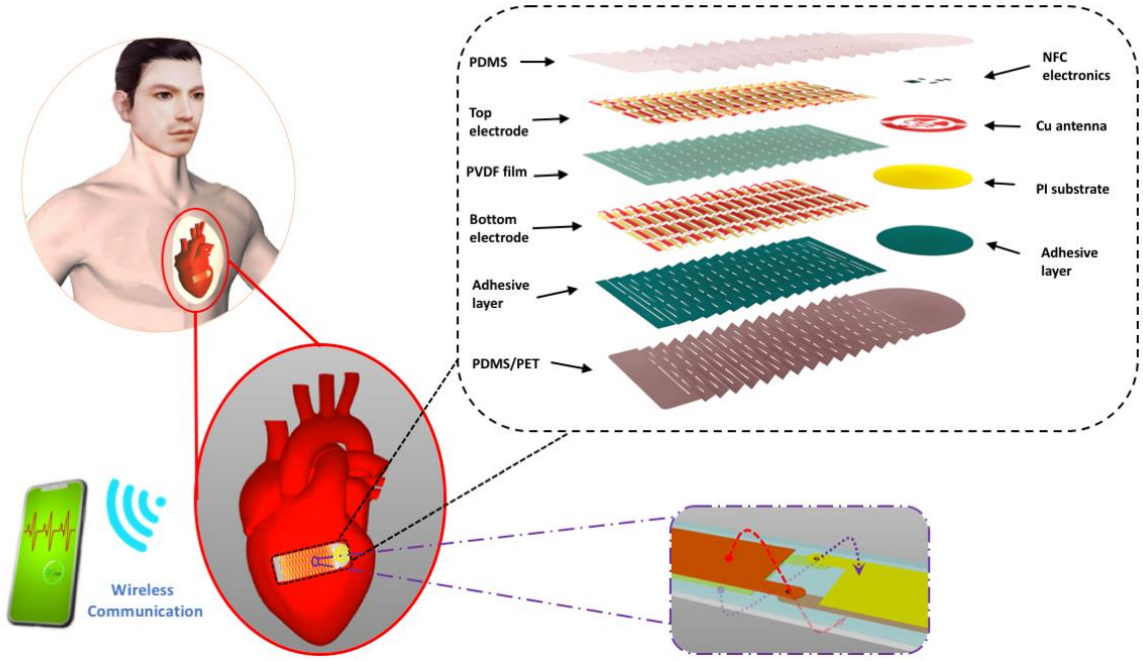

Figure 4.1 Schematic illustration of the integrated device with multi-layered structures between two subsystems: the stretchable sensor and wireless patch, and enlarged electrode patterns.

Figure 4.1 gives the schematics of the Kirigami sensing system for application in wireless cardiac monitoring. The device is composed of two subsystems: (i) a stretchable piezoelectric film as the active sensing component to conform to the subject surface for strain measurements, and (ii) a flexible and millimetre-scale wireless interface for NFC communications. The advantage of this Kirigami-based stretchable sensor is its tuneable mechanical properties for various application areas, thus mitigating any mismatch between the sensor and the subject to be measured[31]. The sensing system consists of a bottom Polydimethylsiloxane (PDMS) layer, covering the Polyethylene terephthalate (PET) substrate (~ 75 μm), followed by a PVDF film (28 μm) with inter-segment electrodes (Ti/Au: 10 nm / 150 nm) with an adhesive layer (~ 50 μm), and top encapsulating PDMS layer (~ 80 μm). After lamination the Kirigami pattern is introduced by laser cutting.

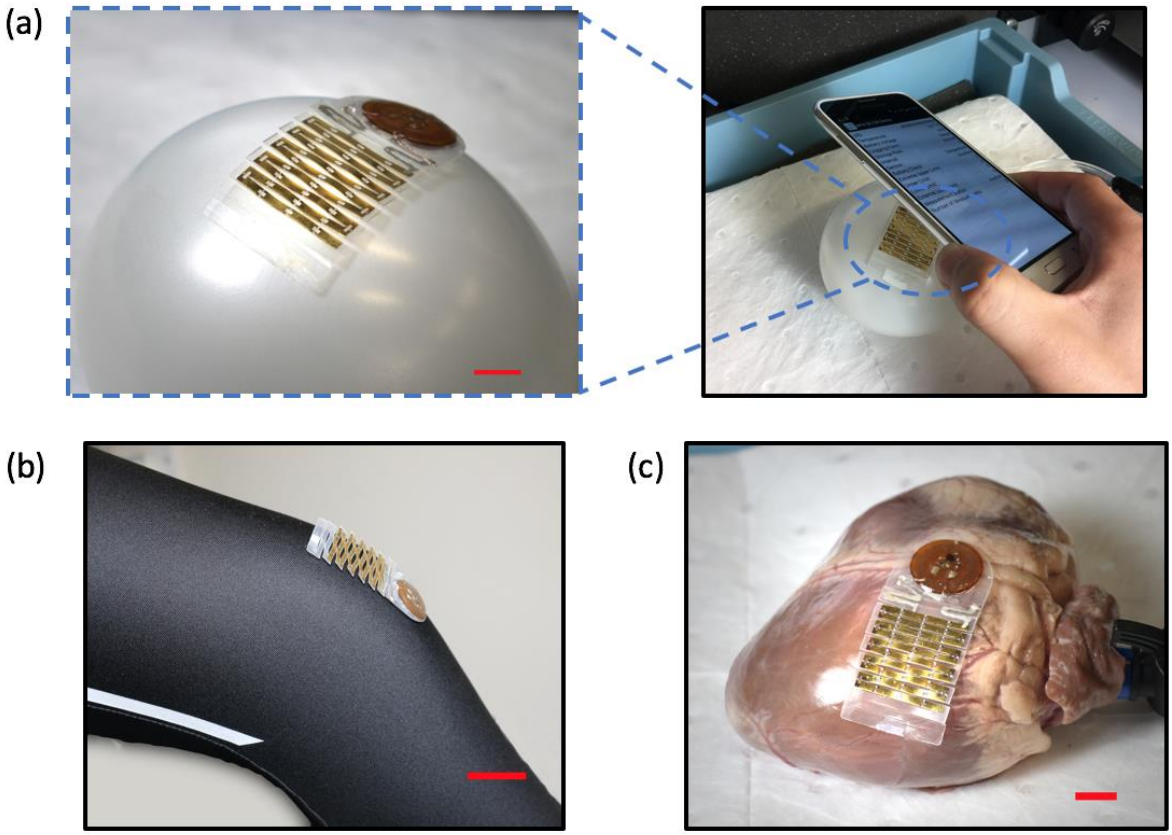

Figure 4.2 (a) Demonstration of the system on curved balloon surface with wireless communication capacity transmitting to external devices with NFC functionality, e.g. smartphone. Scale bar: 1 cm. Several potential application areas including (b) skin (clothes) surface as wearable devices and (c) tissue (pig heart) surface as implantable sensor. Scale bars 2 cm and 1cm respectively.

The wireless interface consists of a die NFC chip, antenna, and resistors. The NFC chip (~2.3 mm × 2.3 mm; ~100 μm thickness) features an analog voltage input, which provides a channel for reading and transmission of the output from the piezoelectric sensing system. The substrate for the wireless interface is a thin and flexible polyimide layer with a patterned cooper circuit on top. The wireless interface is bonded to the bottom PET layer of the sensor system, and silver ink connections are used to electrically connect the sensing subsystem and the wireless interface. A thin PDMS top layer covers the entire device to seal it.

The whole wireless sensing system has a size of 28 mm × 60 mm, and can be easily mounted on various surfaces, and at many points on the human body (Figure 4.2(b)-(c)). As seen in the balloon demonstration (Figure 4.2(a)), this sensing system is compatible with curved and soft balloon surfaces without inducing extra constrains on the balloon deformations due to its high stretchability. A stable wireless communication is created between the platform and a smartphone with NFC functionality even during the large dynamic deformations of the balloon. Temperature

information is also obtained from the NFC chip (ams SL 13A), which could be used as an extra health indicator. This platform is also demonstrated as a wearable device mounted on the human knees (Figure 4.2(b)), recording the daily activities and exercise. The Kirigami induced 3D buckling could also be exploited to improve textile breathability, allowing heat and moisture vapor to be dissipated through the open structures. The developed sensor system delivers both a self-powered sensing function and wireless data transmit capability, two significant requirements for implantable electronics, e.g. for self-powered cardiac monitoring (Figure 4.2(c)).

4.3 BIOCOMPATIBILITY TEST

COS7 fibroblasts have been used as a generic cell model to investigate the biocompatibility of both the sensing and the communication part of the device. The Alamar Blue assay is chosen as a testing method because it allows the assessment of cell viability at several time points and over prolonged periods of time. The active ingredient in this assay is resazurin (also referred to as Alamar Blue), a cell-permeable and non-fluorescent molecule. Within living cells Alamar Blue is converted to fluorescent resorufin. Fluorescence intensity in the medium is therefore an indicator of cell viability. Here, COS7 cells have been cultured on samples of either the sensor or the communication part of the device and cell viability is measured after 24, 48 and 72 h of contact with the devices.

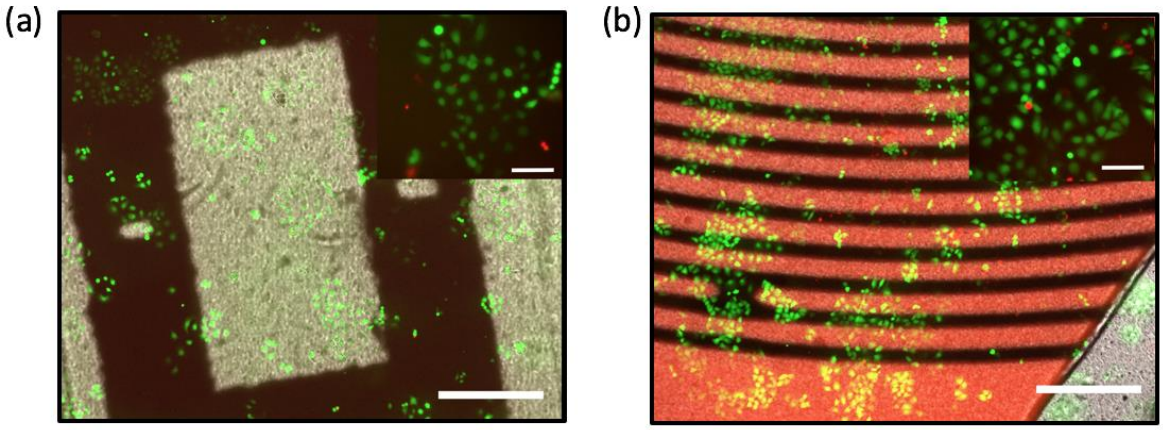

Figure 4.3 Biocompatibility tests. Live/dead staining of COS7 cells cultured on samples of (a) the sensor and (b) communication part. Green and red fluorescence indicates live and dead cells respectively. Insets show cells at a larger magnification. Scale bar of main images 0.5 mm, scale bar of insets 100 μm.

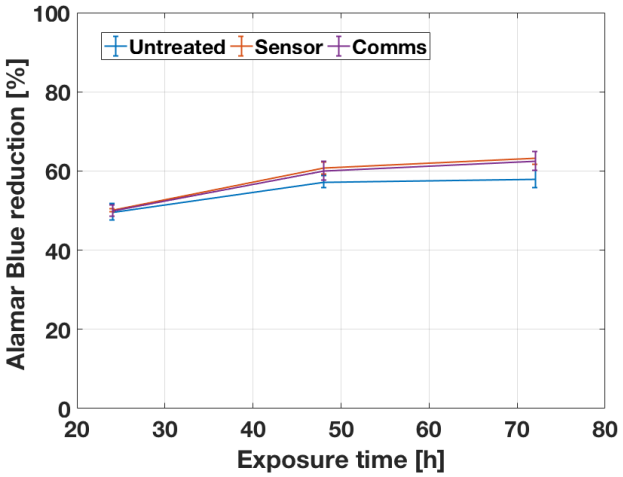

Figure 4.4 Alamar Blue reduction measured in untreated cells and cells grown on the sensor and communication parts of the devices for 24, 48 and 72h. Average and standard deviation of n=4 samples per group are shown.

COS7 cells have also been stained with calcein and ethidium homodimer III and imaged with a fluorescence microscope. Calcein is a cell-permeable molecule that is converted to a green fluorescent dye within living cells, while ethidium homodimer III is a DNA-binding, red fluorescent dye that cannot permeate cells unless their cell membrane is damaged, and they are dead or dying. Microscopy of the stained cell layers cultured on the sensor and communication devices for 48 h reveals that COS7 cells remain viable throughout the culture period (Figure 4.3). This corroborates the results of the Alamar Blue assay and further confirms the biocompatibility of both device parts. The percentage of Alamar Blue reduction in cells grown on the devices does not differ between untreated cells and cells grown on the devices. This indicates very good biocompatibility of both the sensor and the communication part of the device (Figure 4.4). We analyzed the variations between these three groups using one-way analysis of variance (ANOVA). ANOVA provides a statistical test for the null hypothesis that the means of the data are the same. For 24, 48 and 72 h, the probability values for the *F*-test are 0.909, 0.058, and 0.012 respectively, which are larger than the significance level of 0.01. The results indicate that these three group means are equal to each other. PDMS encapsulation is a well-known strategy to render body-interfacing devices biocompatible [264], and the results here confirm this.

4.4 Designs to optimise the mechanical and the electrical performances

The surfaces of major biological systems are soft, irregular and time-dynamic. In contrast, current electronics are generally dominated by hard and planar forms. New designs for soft-hard integration are needed to overcome the mechanical mismatch between electronics and biological

systems. Flexibility and stretchability are therefore of vital importance for bio-integrated electronics. Kirigami provides an approach to achieve flexibility and stretchability simultaneously.

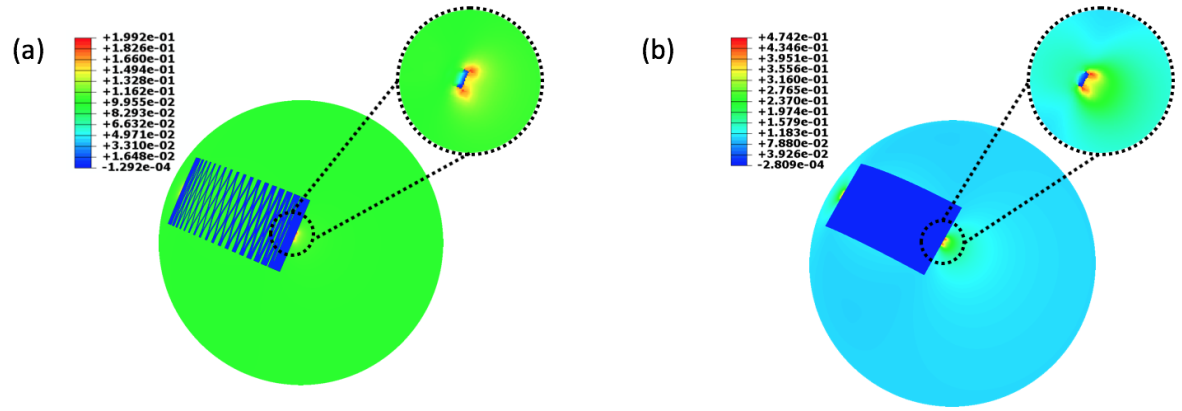

Figure 4.5 Mechanical and electrical optimisation designs with simulation study. Two types of structures, (a) Kirigami and (b) planar structures, on a curved balloon surface after its inflation showing strain distributions on the balloon surface around the bonding areas.

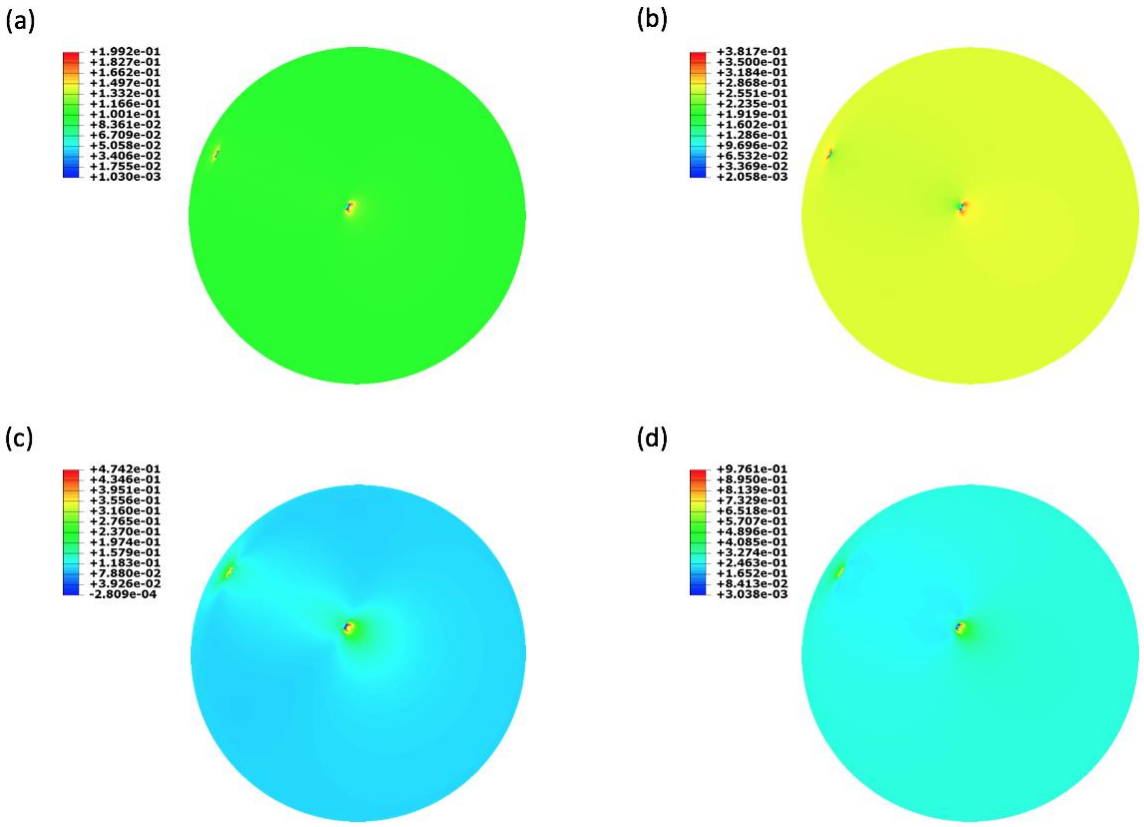

Figure 4.6 Mechanical analysis of the structural design of the stretchable sensor. (a) The strain distribution on the balloon with Kirigami structure bonding on its surface when the balloon was inflated with the volume to 540 ml, and (b) corresponding stress distribution. (c) The strain distribution on the balloon with planar structure bonding on its surface when the balloon was inflated with to volume of 540 ml, and (d) corresponding stress distribution.

A hyperelastic balloon, as a soft and stretchable surface demonstration, has been modelled using the finite element analysis (FEA) to explore the design of sensor structures. Two different patterns for sensors have been evaluated: one is a Kirigami structure (Figure 4.5(a)), and the other is a commonly-used planar configuration (Figure 4.5(b)). The balloon is modelled using a neo-Hookean hyperelastic material using the commercial software Abaqus, and the sensor structures are modelled as 2D shell elements. Non-linear effects due to the larger deformation are considered during the analysis. These two sensor configurations have the same geometry in relaxed form, and both are bonded onto the balloon surface through tie constrains in the center of two opposite edges. The balloon has an initial 400 ml volume of water inside and is then inflated by an infusion process at a fixed filling speed to the final state with 450 ml water inside. In the final state, the Kirigami structure has imposed less restrictions on the balloon inflation compared to the planar structure, as seen in Figure 4.6. The maximum unwanted strain on the balloon surface with Kirigami structure is 0.2, which is two times less than the 0.47 strain provided by the planar configuration. For a free balloon with no sensors, the average stress around the bonding area reaches 0.275 MPa. With the Kirigami structure, the average stress is 0.328 MPa (an increase of 19.3%), while for the planar structure, the average stress is 0.822 MPa (a significantly larger increase of 198.8%) (Figure 4.7). The free deformations are also compared under these three cases.

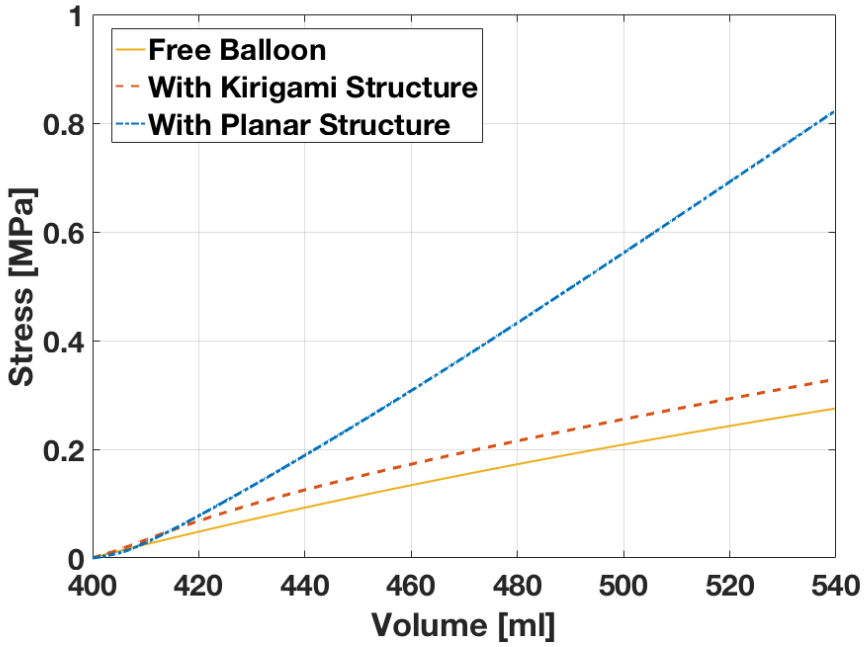

Figure 4.7 A comparative study with the above two structural designs, and the average stress comparison around the bonding areas of the balloon during the inflation process in three cases: no sensing structure on balloon structure; Kirigami structure bonded to balloon surface; planar structure bonded to balloon surface.

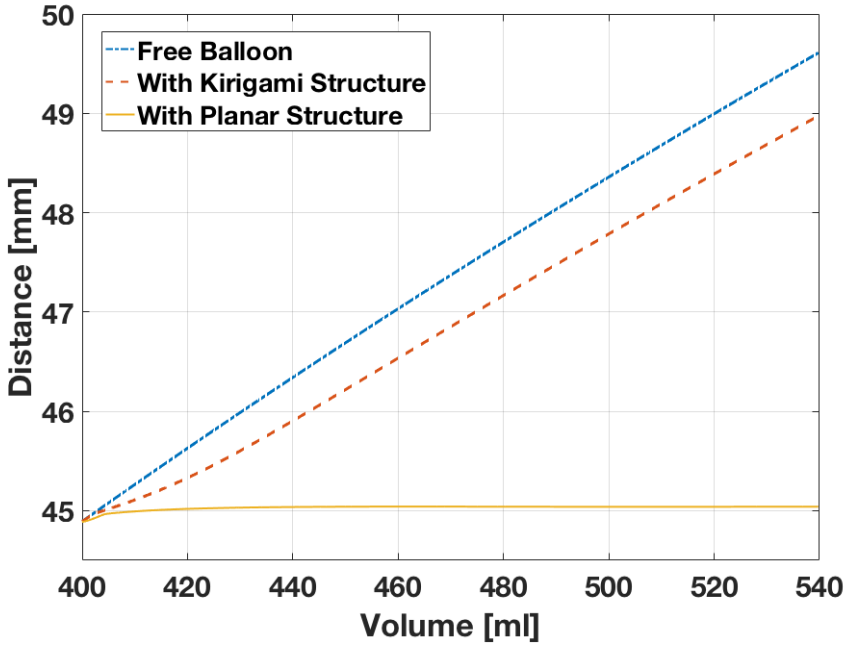

Figure 4.8 The distance change between two bonding areas during the balloon inflation process in the above three cases.

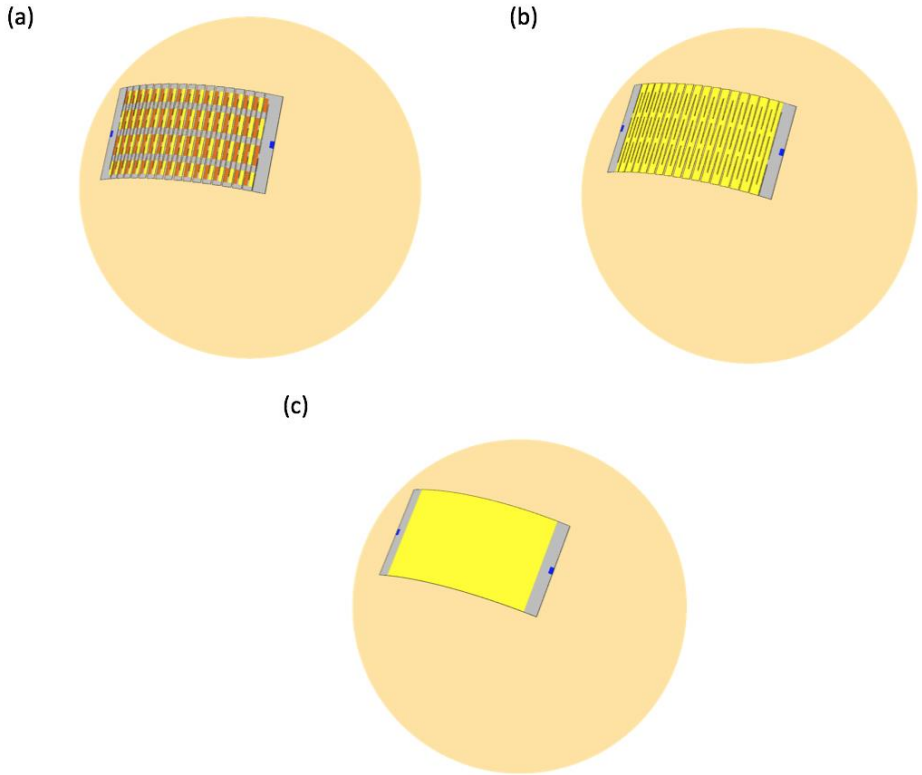

Figure 4.9 The electrode design for the optimization of electrical performance. (a) The Kirigami structure with inter-segment electrode patterns. (b) the Kirigami structure with continuous electrode patterns. (c) the planar structure with continuous electrode patterns

The change of the arc distance between the two bonding areas is used to evaluate the deformation (Figure 4.8). For the free balloon, the distance increases from 45.0 mm to 49.6 mm. The final distance with the Kirigami structure is 49.0 mm, (a reduction of 13.0% compared to the free balloon). For the case of the planar structure, this change of distance is extremely small, from 45 mm to 45.04 mm (a reduction of 97%), meaning that the planar configuration severely restricts the deformation of the balloon. These comparative results demonstrate that a Kirigami structure can efficiently mitigate the interfacial stress caused by the mismatch between rigid sensing electronics and soft biological surfaces.

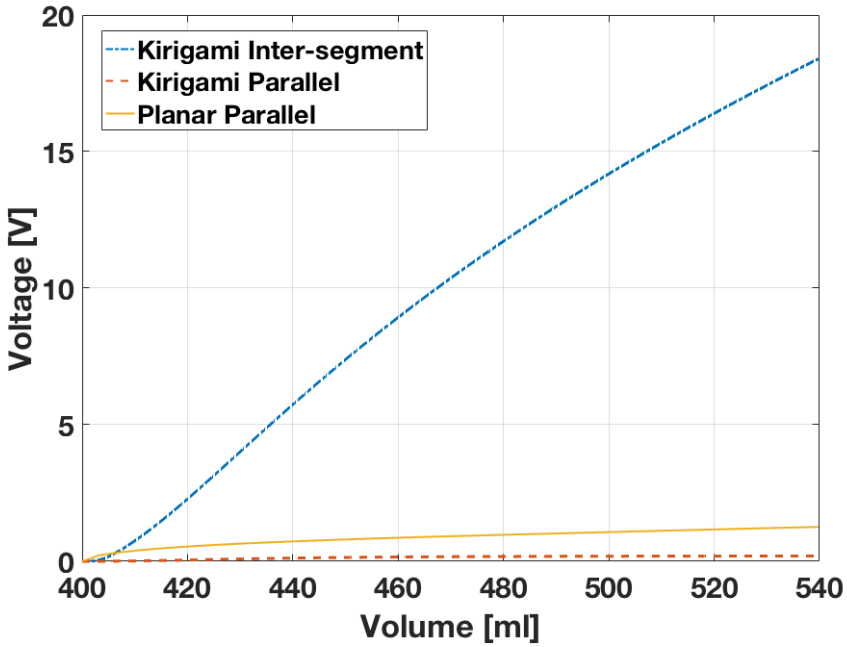

Figure 4.10 Piezoelectric analysis of the electrode design for the sensing system in three designs: the Kirigami structure with inter-segment electrode pattern to reversely connect the adjacent segments to avoid charge cancellation; the Kirigami structure with continuous electrode pattern; the planar structure with continuous electrode pattern. The voltage output during the balloon inflation process.

Mechanical strength and electrical performance are generally two conflicting requirements in bio-integrated electronics. Design optimization has been performed on the electrode patterns of the piezoelectric sensors. 3D eight-node solid element has been adopted for the sensor component, which consists in a two-layer structure: a 28 μm piezoelectric layer and a 75 μm plastic substrate. The electrode is not considered for the mechanical analysis. Three different configurations have been analyzed for comparison (Figure 4.9): a Kirigami structure with inter-segment electrodes; another Kirigami configuration with continuous electrodes; and a planar structure with continuous electrodes. An infusion process similar to the one mentioned above has been applied to inflate the

balloon, and the open-circuit voltages are calculated to evaluate the electrical performances with these three configurations (Figure 4.10). The Kirigami structure with continuous electrode structure shows the lowest voltage output, 0.19 V. This low performance is the result of charge cancellation in the Kirigami-induced 3D buckling structures. The planar structure with continuous electrodes has a better electrical response, with an output voltage output of 1.26 V. The Kirigami structure with inter-segment electrodes, however, has a significantly increased open-circuit voltage (18.4 V). This remarkably large improvement in electrical performance is due to the reverse connections between adjacent segments, which serve to rectify and reinforce the charges between neighboring sensor segments with opposite bending direction (and hence opposite induced charge).

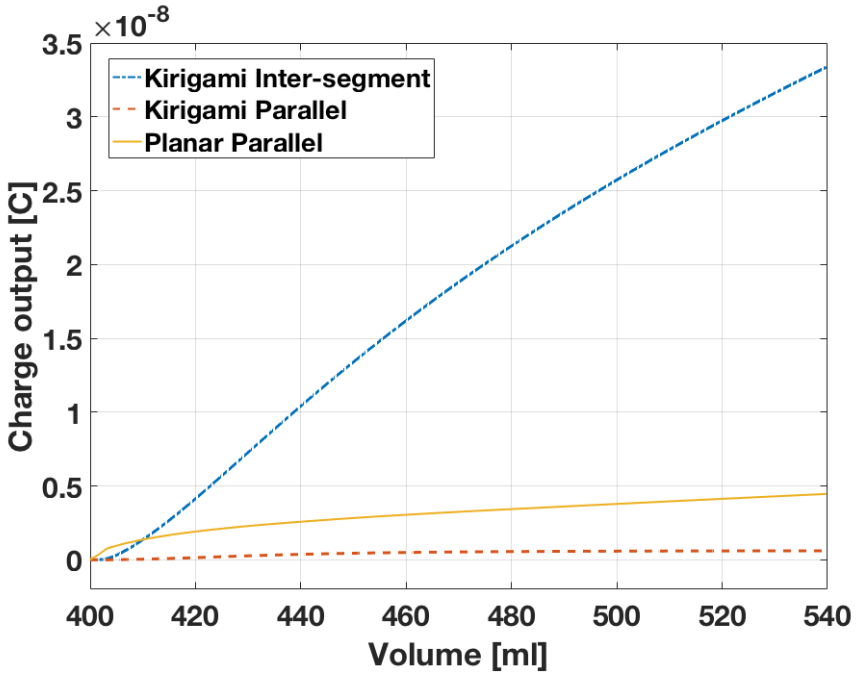

Figure 4.11 The charge output considering the electrode areas in the above three cases in Figure 4.10.

When this type of inter-segment electrodes is introduced the electrode areas would be slightly reduced due to the imperfections involved in the manufacturing process, thus inducing a small increase of the sensor impedance. Considering the electrode area effects, the charge outputs have been compared (Figure 4.11), as calculated by

$$Q = \frac{\varepsilon_r \varepsilon_0 A}{t} V \qquad 4.1$$

where ε_0 is the air permittivity, $\varepsilon_r = 12$ is the relative permittivity of piezoelectric film, t is the film thickness, V is the voltage output, and A is the electrode area. The electrode areas are 478.04

mm^2, 835.18 mm^2, and 933.5 mm^2 for the Kirigami inter-segment electrode, the Kirigami continuous electrode, and the planar continuous electrode respectively. The charge output of the Kirigami structure with inter-segment electrodes is 3.33×10^{-8} C, which is 7.5 times larger than that provided by the planar configuration with continuous electrodes (4.46×10^{-9} C), and 54 times larger than the one featured by the Kirigami structure with the continuous electrodes (6.07×10^{-10} C).

4.5 OUTPUT PERFORMANCE AND CHARACTERIZATION OF THE SELF-POWERED SENSING SYSTEMS

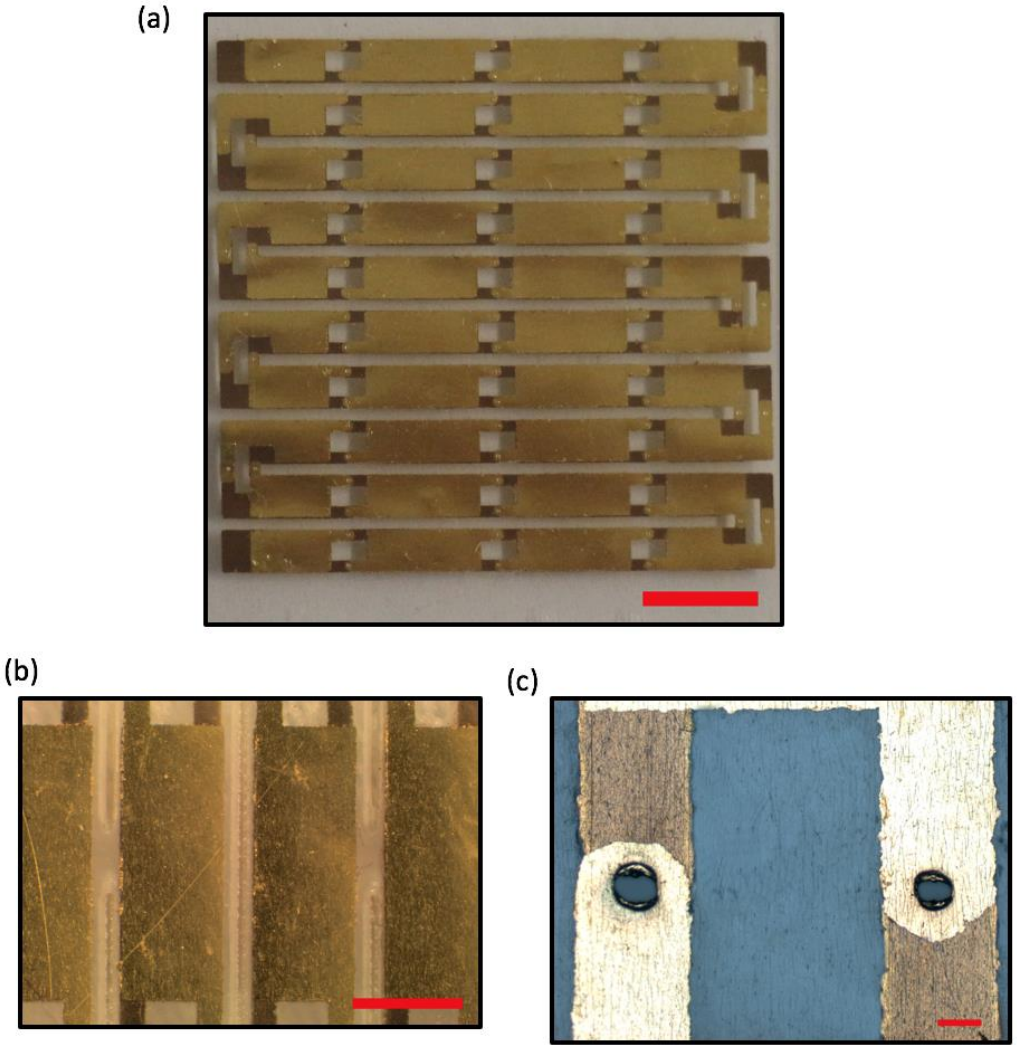

Figure 4.12 (a) The electrode patterns of the sensing system. Scale bar 5 mm. (b) The Kirigami structure achieved by a tailed cut between the electrodes using laser. Scale bar 2 mm. (c) The inter-segment electrode pattern to reversely connect the adjacent segments. Scale bar 0.2 mm.

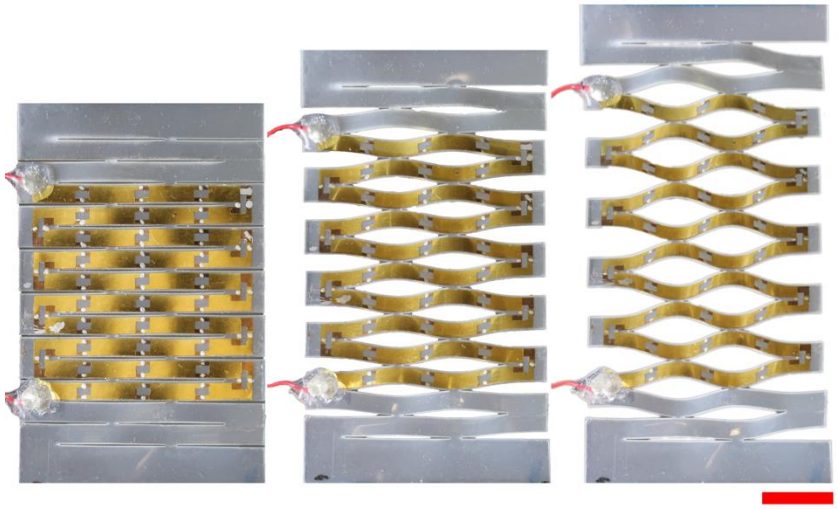

Figure 4.13 The different stages of the stretchable sensors under a tensile test. The strains are 0 %, 15 %, and 30 % respectively. Scale bar: 1 cm

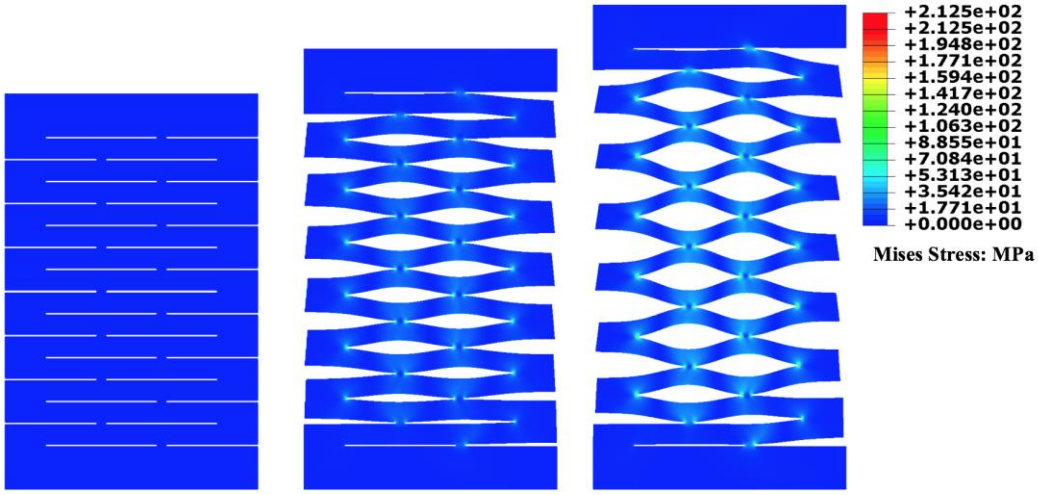

Figure 4.14 The simulation results under the same three strains, and the stress distribution on the Kirigami structure.

To evaluate the performance of the proposed sensing platform we have fabricated the stretchable sensor using the Kirigami structural designs with the inter-segment electrodes, as shown in Figure 4.12. A material testing machine (Instron 8872) is used to apply various tensile conditions on the system. The stretchability of this system is mainly attributed to the induced out-of-plane bending to accommodate the in-plane stretching (Figure 4.13). The experimental results have also been replicated by FEM analysis (Figure 4.14). In practical biomedical applications, encapsulation is an essential requirement to avoid biofluids eroding the sensing electronics and to minimize unwanted cytological effects. PDMS, due to its biocompatibility, is a good package material to encapsulate the device. The electrical output has been analyzed before and after sensor encapsulation. A sine-shape strain input at 1.5 Hz (a representative value of the normal resting heart rate 60–100 bpm [72]) and 10% maximum strain amplitude was applied to analyze the output performances. The

open-circuit voltage (V_{oc}) and short-circuit current (I_{sc}) in Figure 4.15 were 4.04 V and 6.16×10^{-8} A respectively before encapsulation, and 3.72 V and 5.70×10^{-8} A respectively after encapsulation. The comparisons of the electrical output of the sensing system with and without encapsulation under a range of strains and frequencies are given in Figure 4.16.

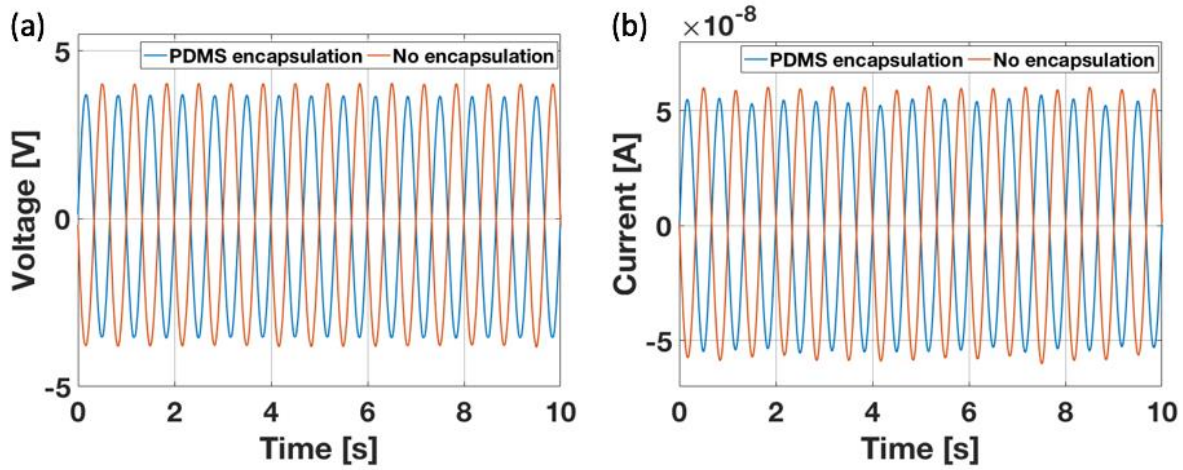

Figure 4.15 The comparisons of (a) the open-circuit voltage and (b) short-circuit current versus time before and after PDMS encapsulation at 1.5 Hz and 10 % strain.

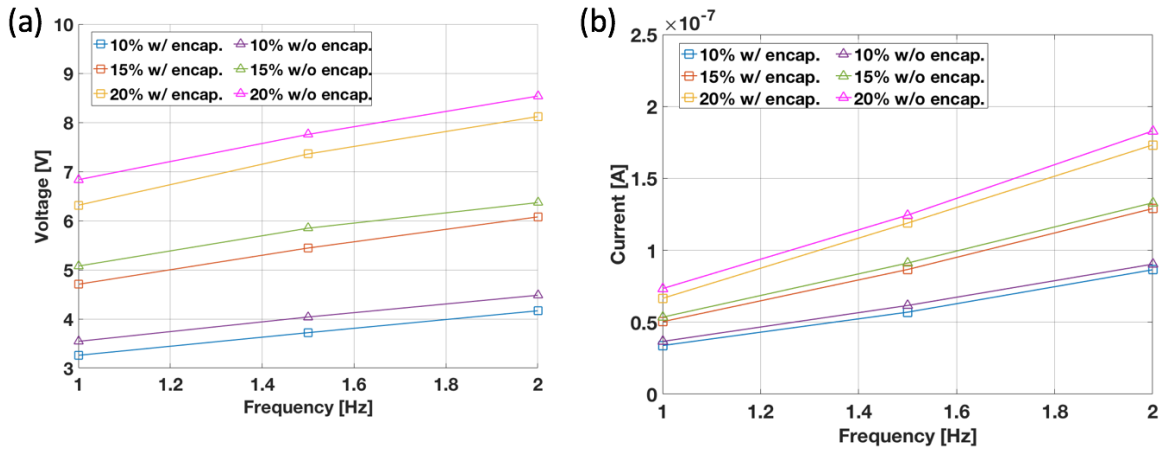

*Figure 4.16 (a) The open-circuit voltage comparisons under a range of strains and frequencies, and **(b)** corresponding short-circuit current.*

To evaluate the sensing performances in various conditions, the electrical outputs under a range of frequencies and strains were tested. Both V_{oc} and I_{sc} show a predominantly linear relationship within a frequency range of 0.5 Hz to 3 Hz, and under strain amplitudes between 5% and 30% (Figure 4.17 and Figure 4.18).

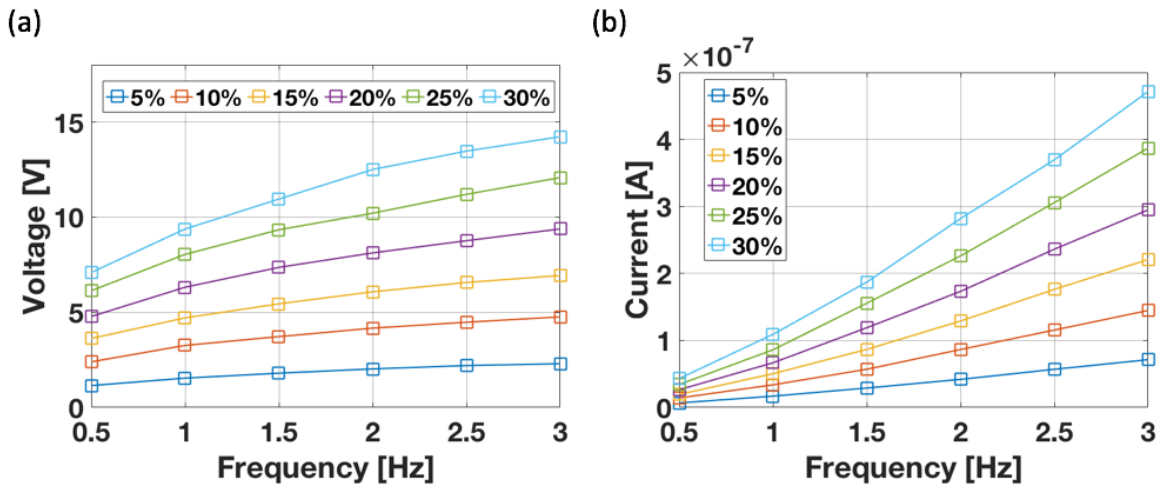

Figure 4.17 (a)The open-circuit voltage and (b) short-circuit current of the sensing system under a range of loading conditions, strain range from 5% to 30%, and frequency range from 0.5 Hz to 3.0 Hz.

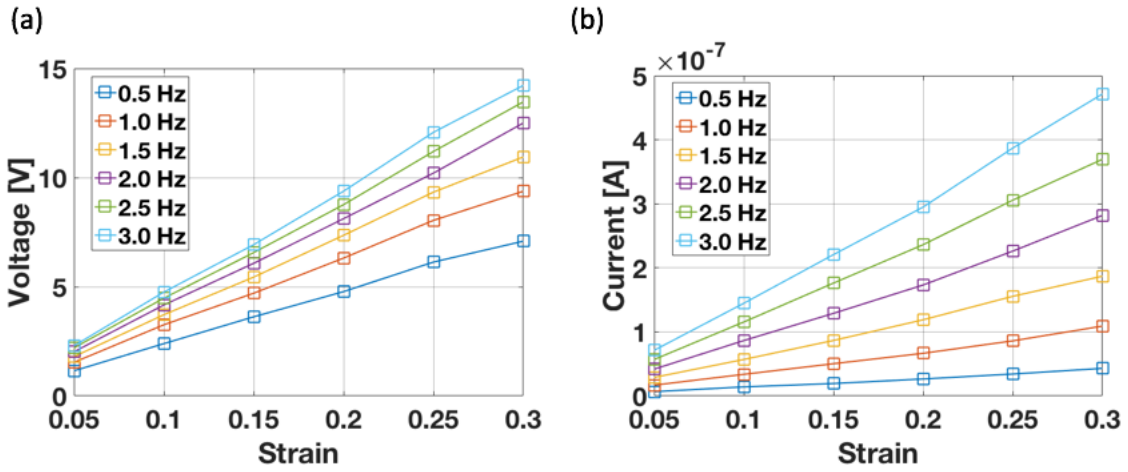

Figure 4.18 The electrical characteristics of the sensing system under a series of loading conditions. (a) The relationship between the open-circuit voltage and the applied strain under variable frequencies. (b) The relationship between the short-circuit current and the applied strain under variable frequencies.

A cyclic tensile test has also been performed to validate the endurance of the sensing capabilities (Figure 4.19). No notable change in voltage output is observed after 1500 cycles at 1.5 Hz, and the average output under three strain conditions, 10%, 15%, and 20% shows a linear relationship with the strain.

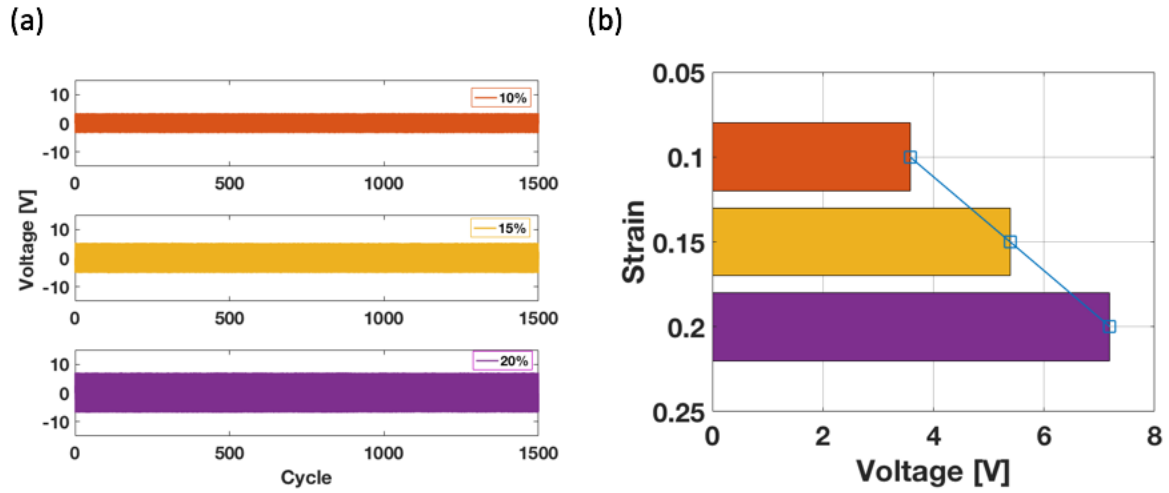

Figure 4.19 (a) *A cycle test of the sensing system at 1.5 Hz and three strains: 10%, 15%, and 20%, and (b) corresponding voltage amplitude comparison*

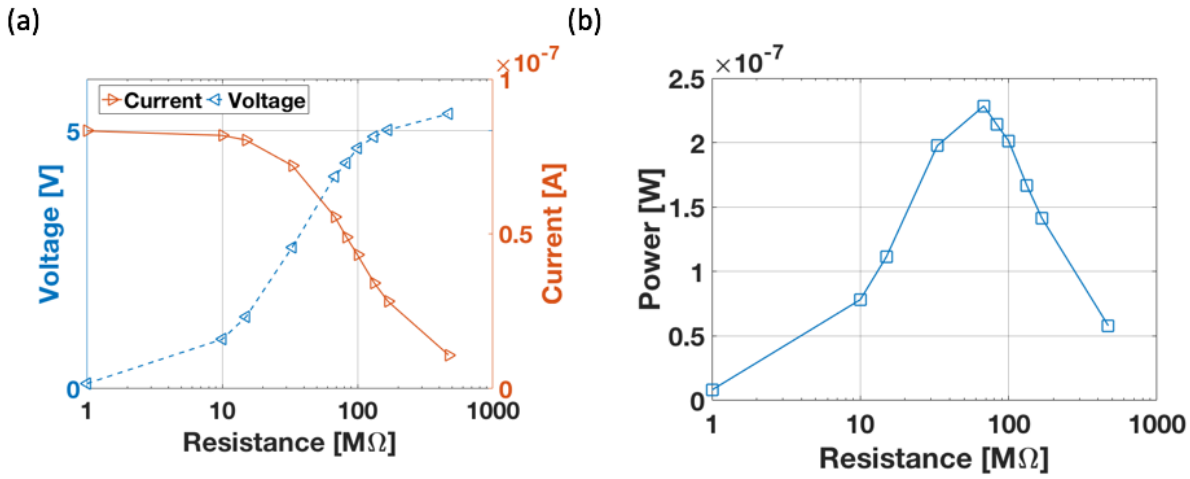

Figure 4.20 The power output performance of the sensing system at 1.5 Hz and 15% strain. (a) The measured voltage and current outputs across the load resistor under a range of resistances from 1 MΩ to 470 MΩ. (b) the instantaneous power output calculated by multiplying the voltage and current with various load resistances.

The electrical performance of the piezoelectric sensor with the external resistors has also been investigated to assess the instantaneous power output at 1.5 Hz and 15% strain (Figure 4.20). The load resistors range between 1 MΩ and 470 MΩ; the voltage increases with the resistance and reaches 5.32 V when the resistance is 470 MΩ, which is close to its corresponding V_{oc} of 5.44 V. The current decreases as the resistance increases, with a value of 8.32×10^{-8} A at 1 MΩ that is also close to its corresponding I_{sc} of 8.66×10^{-8} A. The output power is calculated by multiplying the measured voltage and current, reaching a maximum of 228 nW under the load resistance of 68 MΩ. Energy harvesting performance is also an important characteristic for self-powered sensors,

and the collected energy could also be used as a supplementary power source for other implantable devices such as pacemakers. A 10 μF capacitor has been used to store the harvested energy from the mechanical deformation (Figure 4.21). A silicon bridge rectifier is used to convert the piezoelectric AC output to DC signals before charging the capacitor, and three different frequencies (1 Hz, 1.5 Hz, and 2 Hz) at 15 % strain amplitude have been applied to investigate the charge performance. The sensor could charge the capacitor to 1 V within 200 s at a frequency of 2 Hz. These results indicate that the featured sensing system is a promising stretchable self-powered sensor for implantable electronics applications. The energy harvesting performance of the sensing system under a series of loading conditions are also summarized in Figure 4.22.

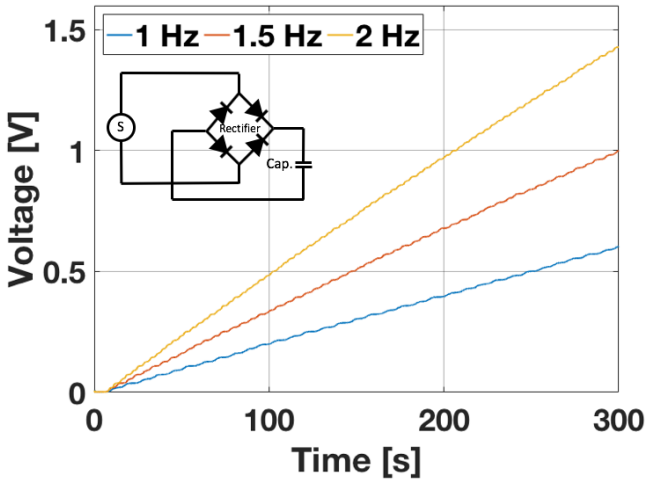

Figure 4.21 The charging of a capacitor (10 μF) from the rectified voltage output of the sensor under 15 % strain. The inset is the circuit diagram of the energy harvesting and storage system.

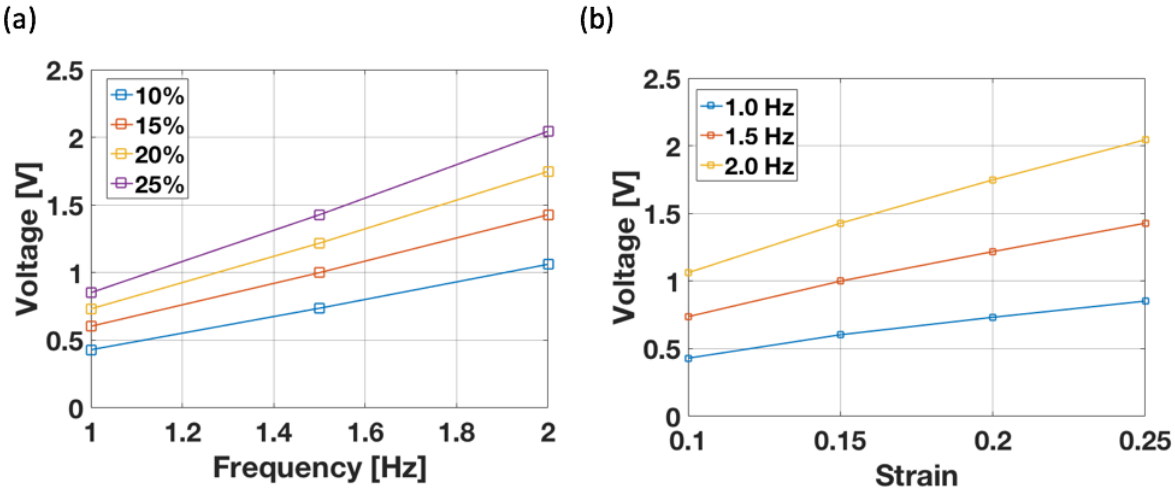

Figure 4.22 The energy harvesting performance of the sensing system under a series of loading conditions. (a) The voltage on the 10 μF capacitor when charged by 300 s and the relationship between the voltage and applied frequency under four strains: 10 %, 15 %, 20% and 25 %. (b) the relationship between the voltage and applied strain under three frequencies: 1.0 Hz, 1.5 Hz, and 2.0 Hz.

4.6 SENSING CAPABILITY ASSESSMENT IN MULTIPLE CONDITIONS

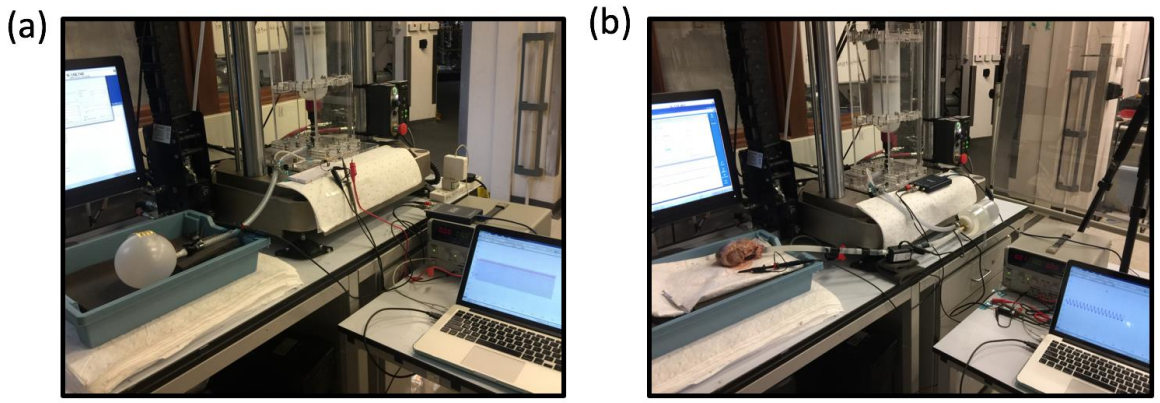

Figure 4.23 The setup for the (a) in vitro and (b) ex vivo tests with air and water as the infusion medium respectively.

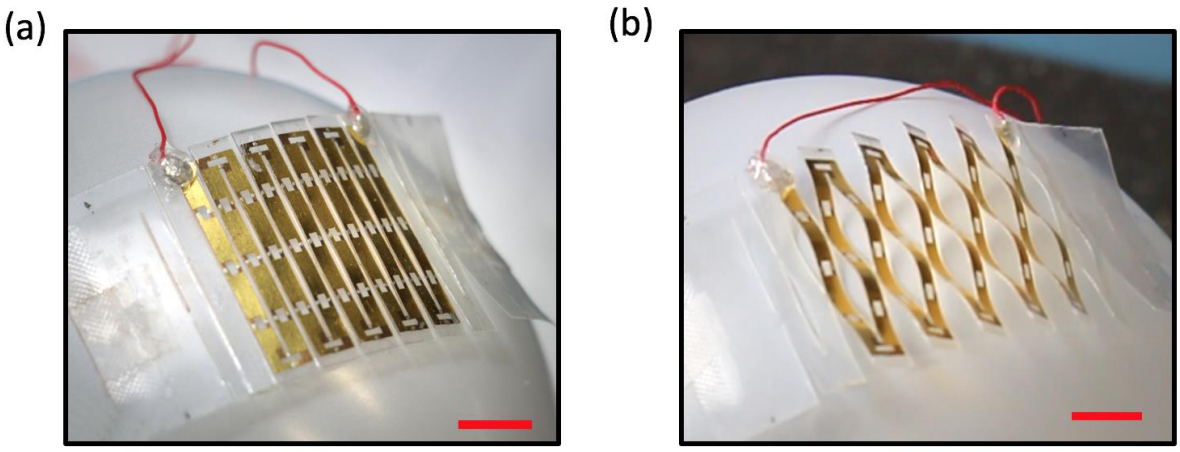

Figure 4.24 The use of the stretchable sensor on the balloon surface (a) before and (b) after deformation. Scale bar: 1 cm.

To further validate the functionality of the device, a series of tests, including in vitro, ex vivo, and on body, have been performed. For in vitro assessment, a stretchable balloon has first been used to investigate the performances of the Kirigami sensor on a soft medium. Two types of fluid, air and water, have been infused into a balloon to inflate it through a controllable setup (Figure 4.23). A syringe, whose movement is controlled by the Instron machine, is used to inject and extract air or water into the balloon via a polyvinyl chloride (PVC) tube. In the air-driven platform, a pressure gauge is used to record the pressure change inside the balloon, and the sensor outputs varying with

the pressure change are subsequently analyzed. The Kirigami sensor conforms to the balloon surface well while still maintaining its free deformations (Figure 4.24). Two types of control signals (sine and heartbeat-like shapes) have been applied to the syringe movements to evaluate the sensing performance with balloon deformations under various conditions. For the case of sine wave inflation, with increasing frequency and pressure (4.0 kPa to 5.7 kPa, and 0.5 to 1.5 Hz, respectively), the voltage outputs increase linearly (Figure 4.25, Figure 4.27). For the case of the heartbeat-like inflation, the detailed characteristics of balloon expansion and contraction are replicated in the voltage signals (Figure 4.26). Linear relationships between the sensor output and frequency and pressure have been obtained (Figure 4.27) in the range of frequencies 0.5 Hz to 1.5 Hz and pressures 3.4 kPa to 4.4 kPa. For water as the infusion material, a flowmeter is used to record the volume change of the balloon. The results illustrate that the sensor output changes with a linear relationship with the change of frequency and water volume (Figure 4.28-Figure 4.29).

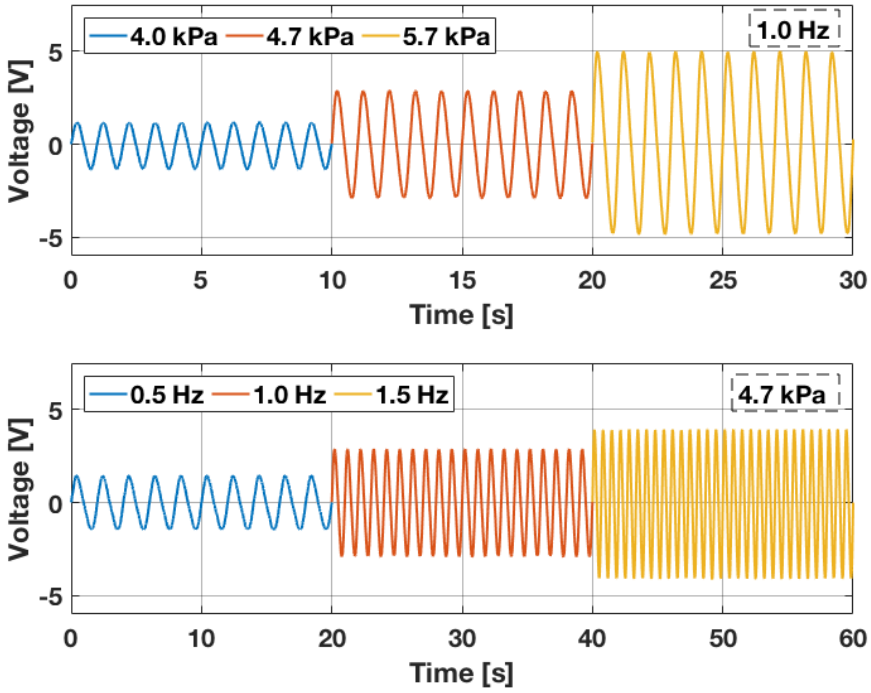

Figure 4.25 The voltage output of the sensor bonded to the balloon under different frequencies and pressures for a sine-shape input on air-driven platform

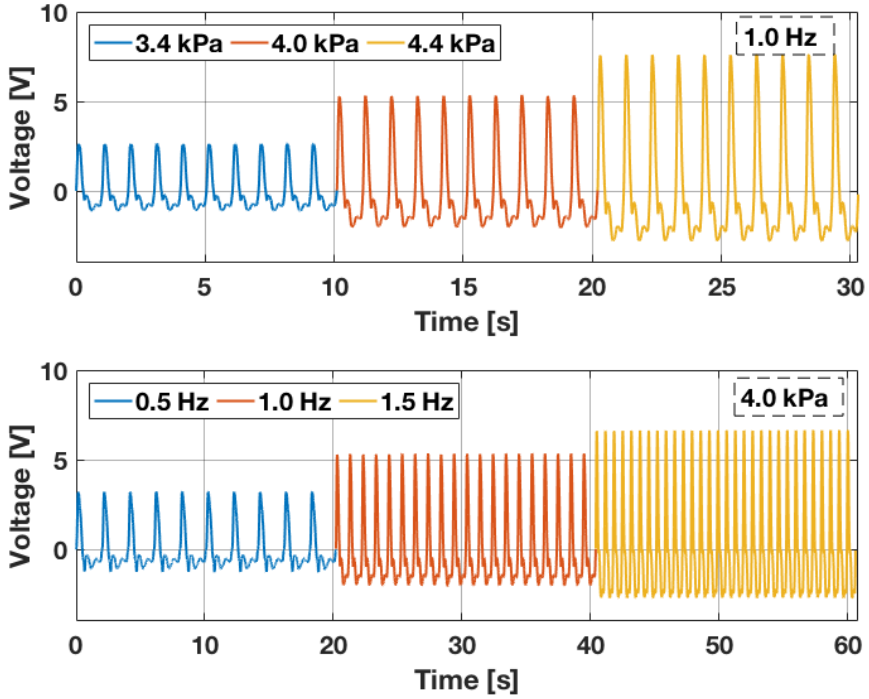

Figure 4.26 The voltage output of the sensor on the balloon under different frequencies and pressures under a heartbeat-like input on air-driven platform.

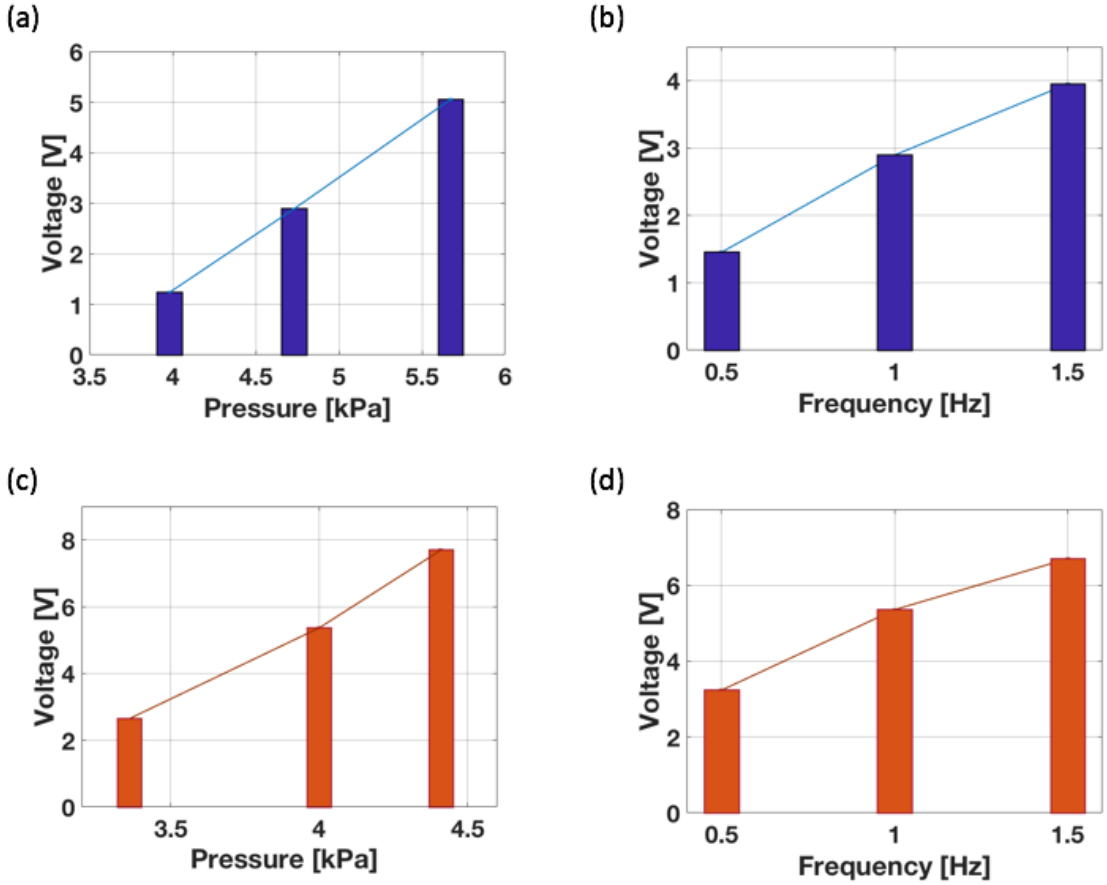

Figure 4.27 The output of the sensing system on the balloon under different loading conditions with air driven platform. (a) the relationship between voltage amplitude and the applied pressure with the sine-shape input under 1.0 Hz, and (b) the relationship between voltage amplitude and the applied frequency with the sine-shape input under the pressure of 4.7 kPa. (c)-(d) The similar relationship between voltage amplitude and (c) the applied pressure under 1.0 Hz and (d) the frequency under the pressure of 4.0 kPa with the heart-beat-shape input.

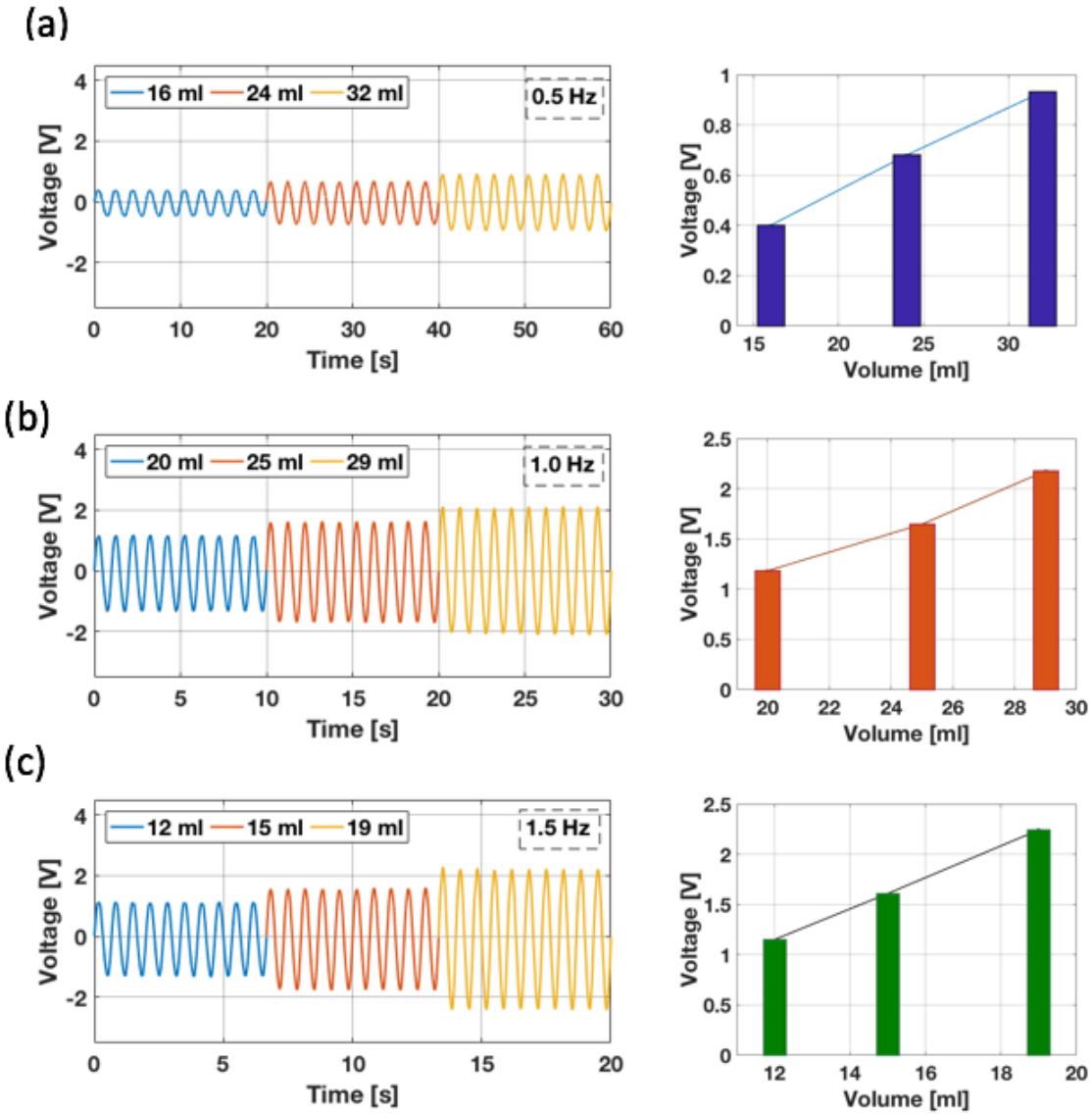

Figure 4.28 The output of the sensing system on the balloon surface under different loading conditions with water driven platform and sine-shape input. The voltage output with different infusion water volumes at three frequencies: (a) 0.5 Hz, (b) 1.0 Hz, (c) 1.5 Hz. and corresponding relationship between them.

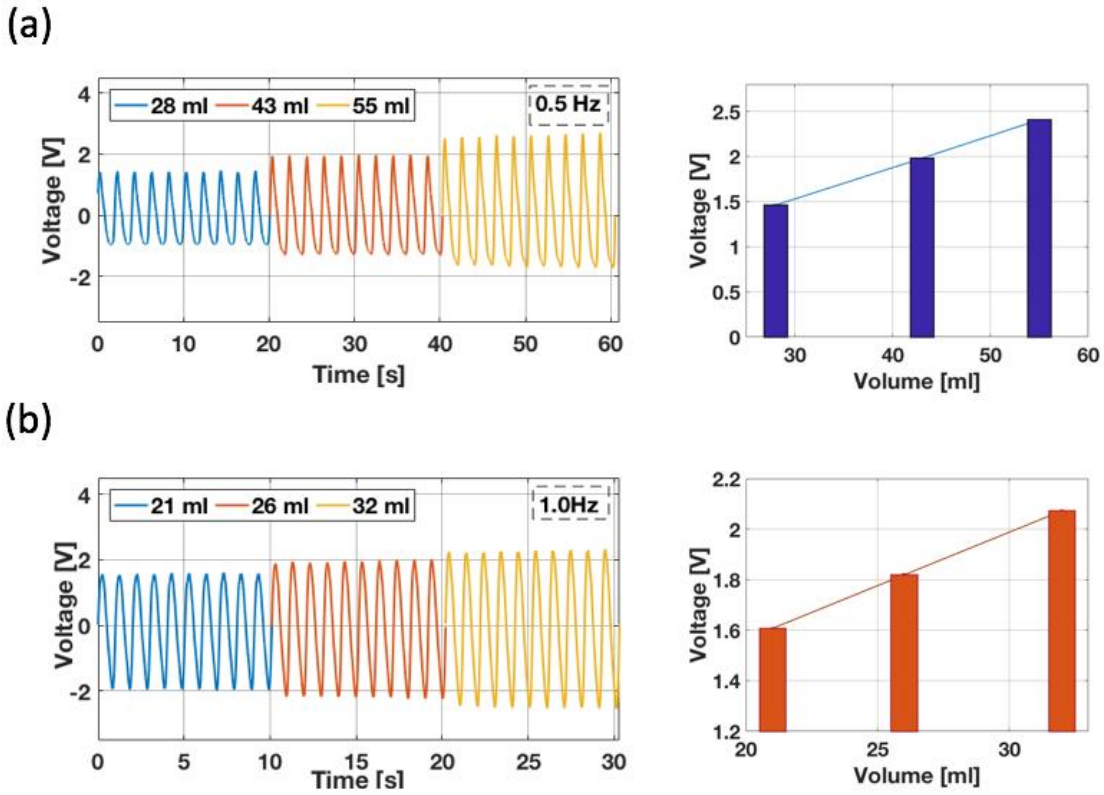

Figure 4.29 The output of the sensing system on the balloon surface under different loading conditions with water driven platform and heart-beat-shape input. The voltage output with different infusion water volume at two frequencies: (a) 0.5 Hz, (b) 1.0 Hz, and corresponding relationship between them. The heart-beat-shape input is not clearly replicated in the voltage output due to the air compressibility as the frequency increase when driving the water movement.

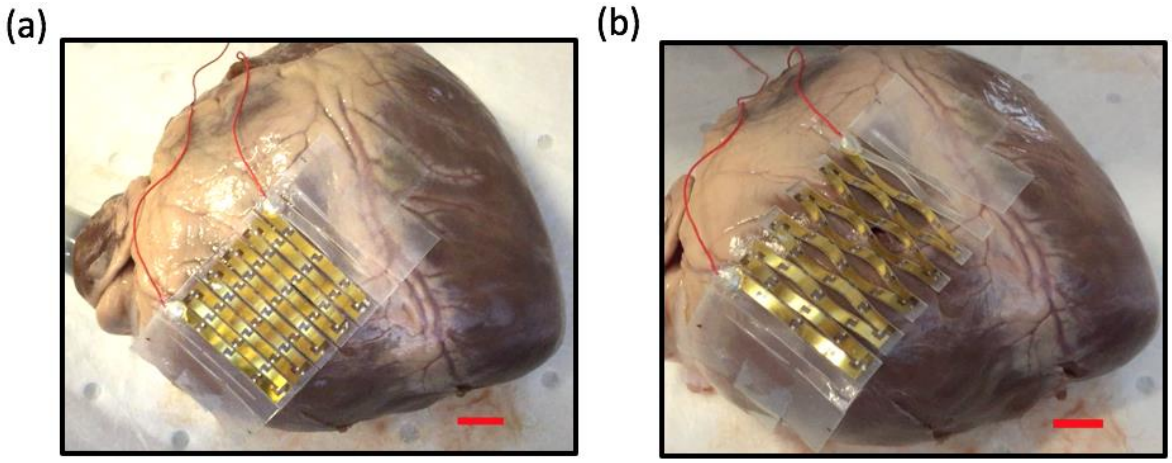

Figure 4.30 The use of the stretchable sensor on the heart surface (a) before and (b) after deformation. Scale bar: 1 cm.

Ex vivo tests are also performed using the in vitro test set-up by substituting the balloon with a fresh pig heart to simulate the in vivo environment. One chamber of the heart is inflated by either water or air. The sensor shows a good conformability to the pig heart surface before and after deformation (Figure 4.30). Two types of signals, pulse (Figure 4.31) and heartbeat-like (Figure 4.32) shapes, have been applied to inflate the heart under a range of frequencies and pressures using air. For the heartbeat-like input, the characteristics of the heart deformations in diastole and systole are clearly embodied in the signal outputs. The average amplitude of the generated voltage also features a linear relationship with pressure and frequency for the pulse waveform (Figure 4.33). A similar relationship between the voltage output and the infused water volume and applied frequency is observed for the water-driven case (Figure 4.34).

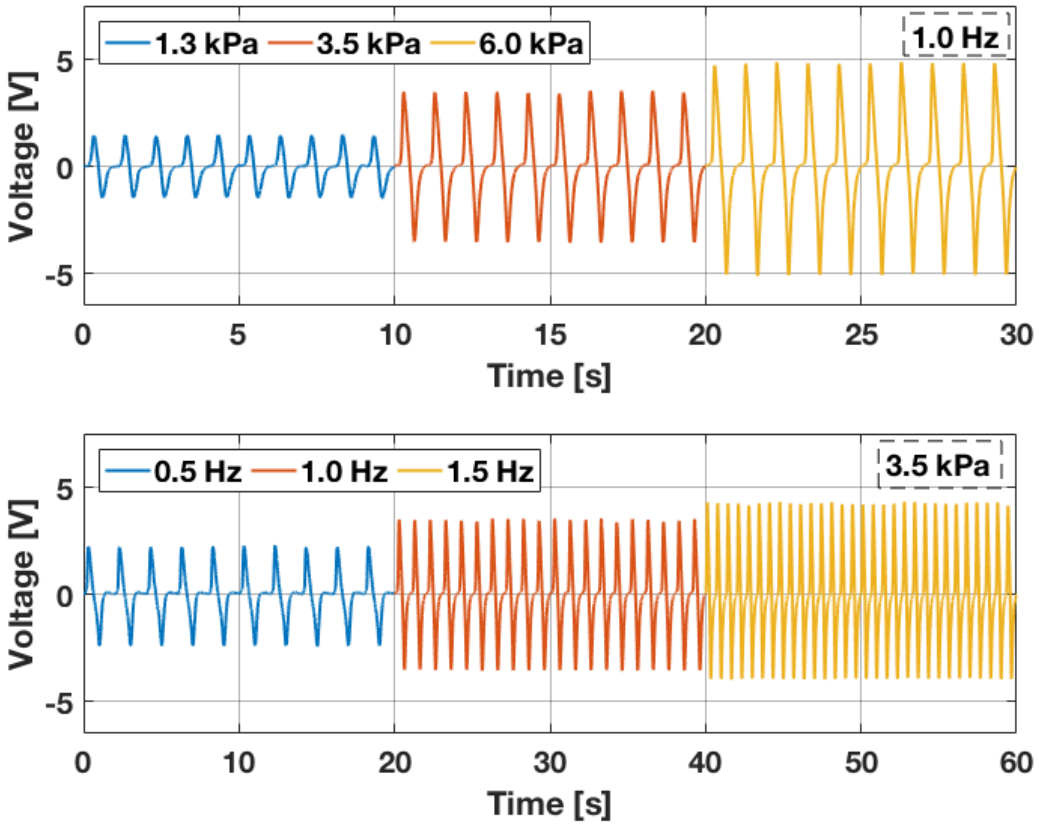

Figure 4.31 The voltage output of the sensor on the pig heart under different frequencies and pressures with pulse inputs on air-driven platform.

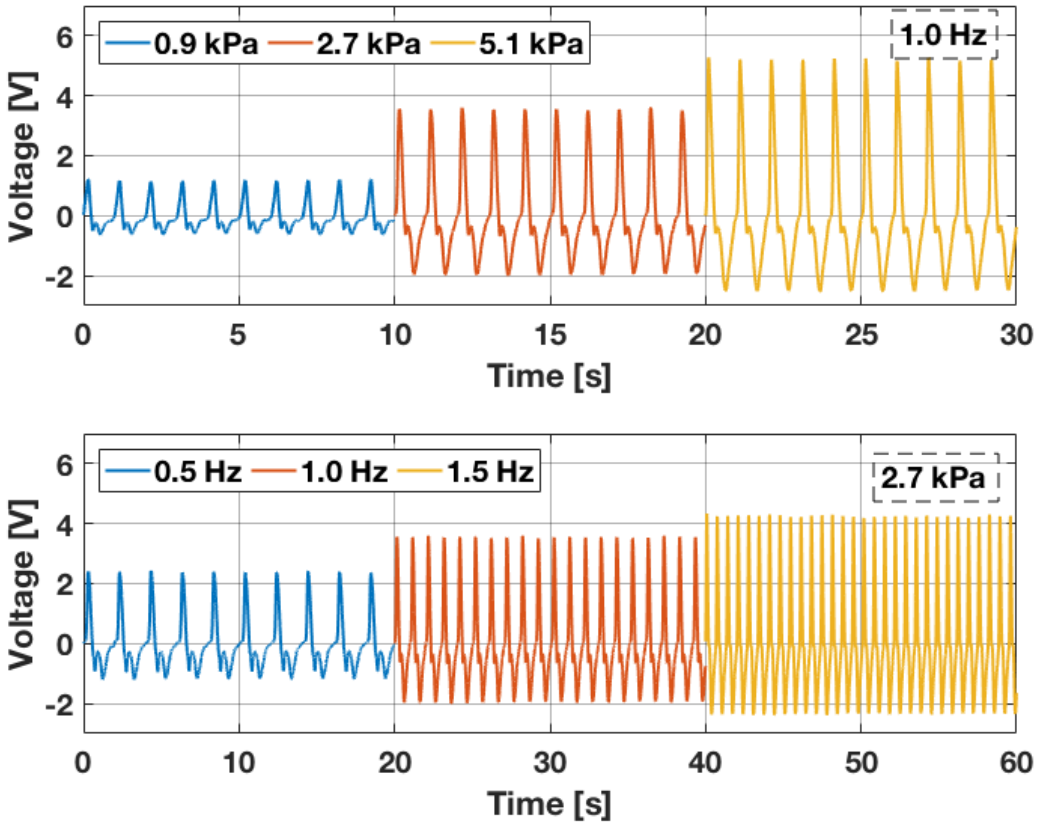

Figure 4.32 The voltage output of the sensor on the pig heart under different frequencies and pressures with heartbeat-like inputs on air-driven platform.

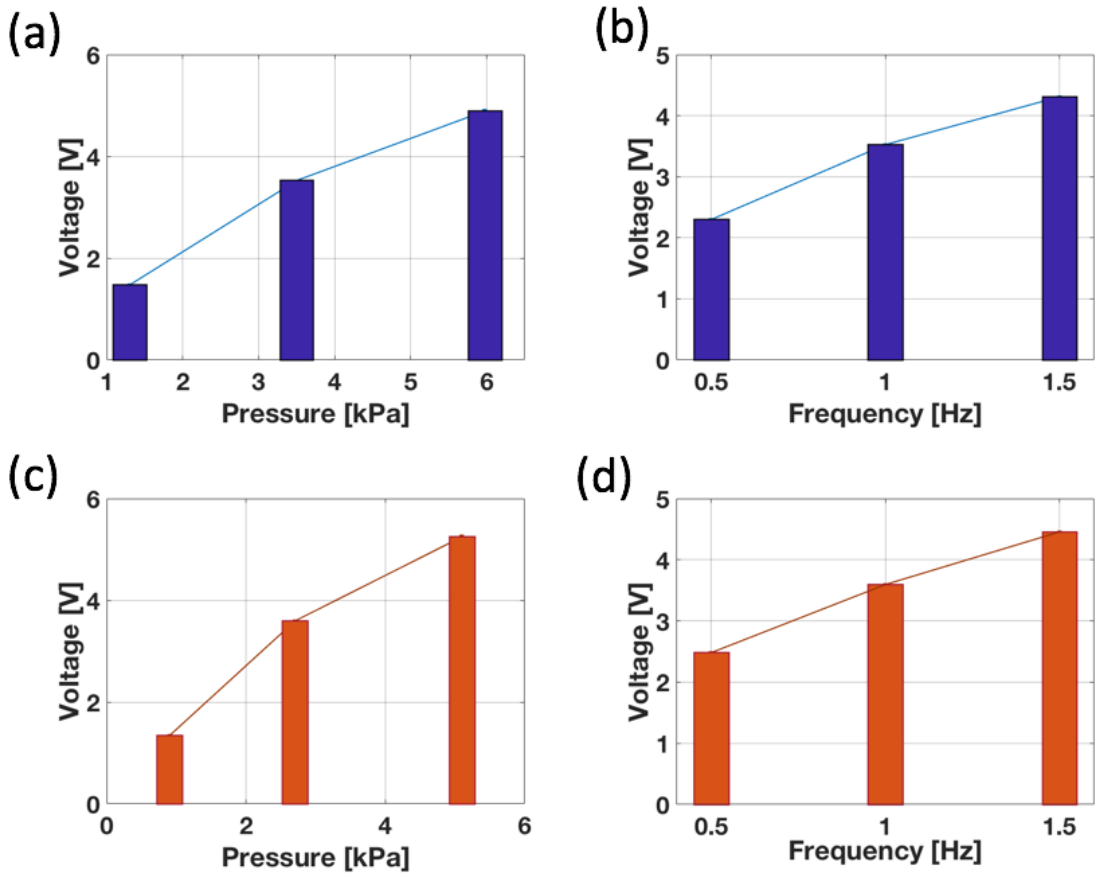

Figure 4.33 The output of the sensing system on the heart surface under different loading conditions with air driven platform. (a) The relationship between voltage amplitude and the applied pressure with the pulse-shape input under 1.0 Hz, and (b) The relationship between voltage amplitude and the applied frequency with the pulse-shape input under the pressure of 3.5 kPa. The similar relationship between voltage amplitude and (c) the applied pressure under 1.0 Hz and (d) the frequency under the pressure of 2.7 kPa with the heart-beat-shape input.

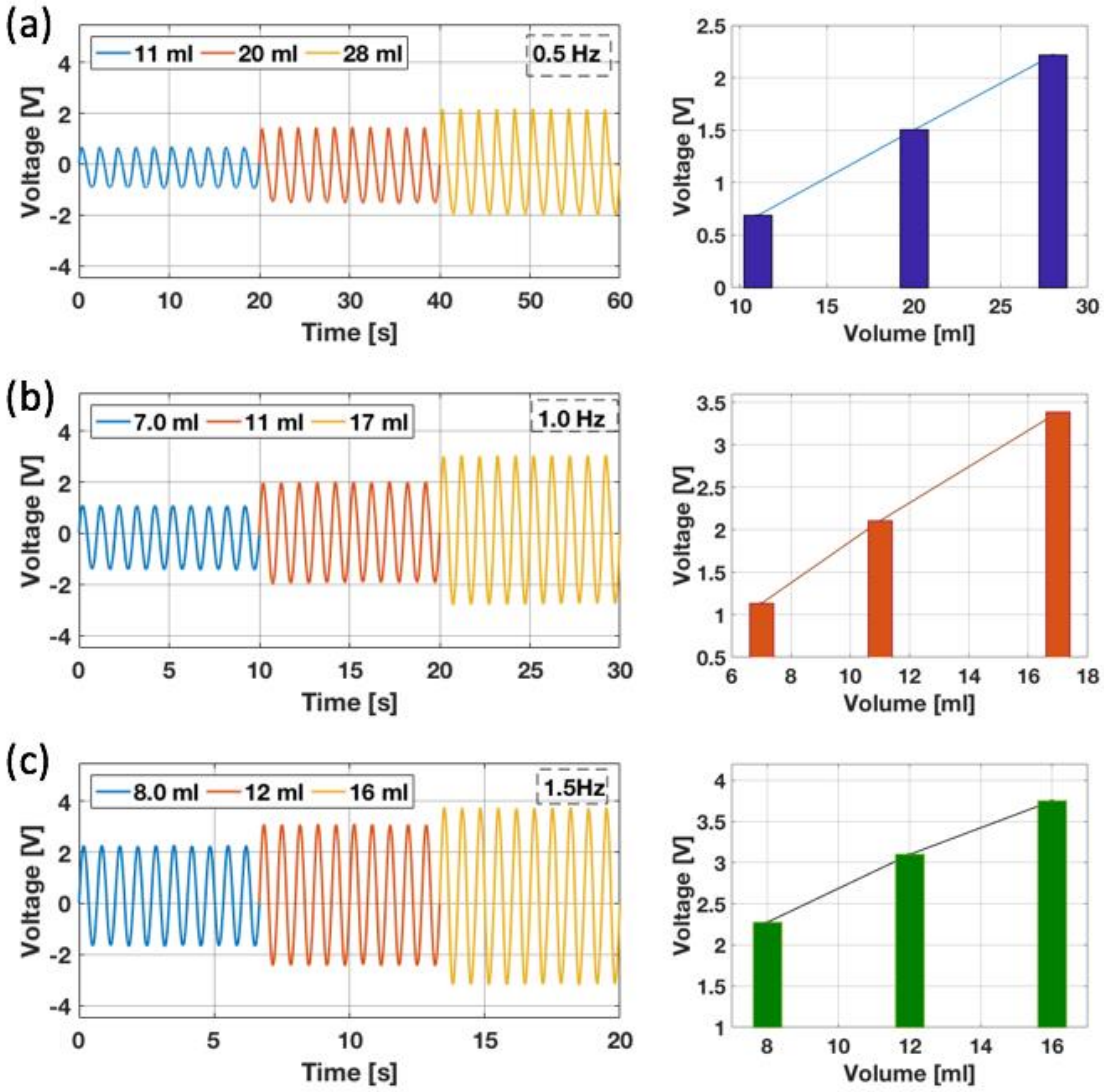

Figure 4.34 The output of the sensing system on the heart surface under different loading conditions with water driven platform and sine-shape input. The voltage output with different infusion water volume at three frequencies: (a) 0.5 Hz, (b) 1.0 Hz, (c) 1.5 Hz, and corresponding relationship between them.

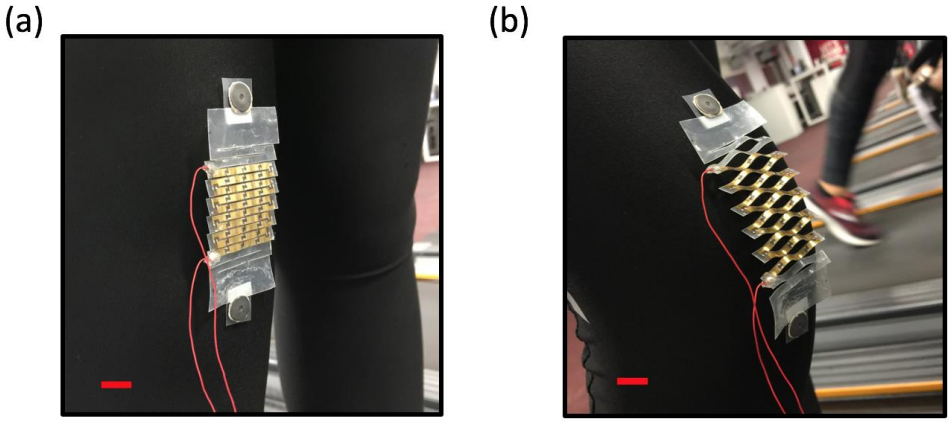

Figure 4.35 The use of the stretchable sensor on the knee joint surface (a) before and (b) after deformation. Scale bar: 1 cm.

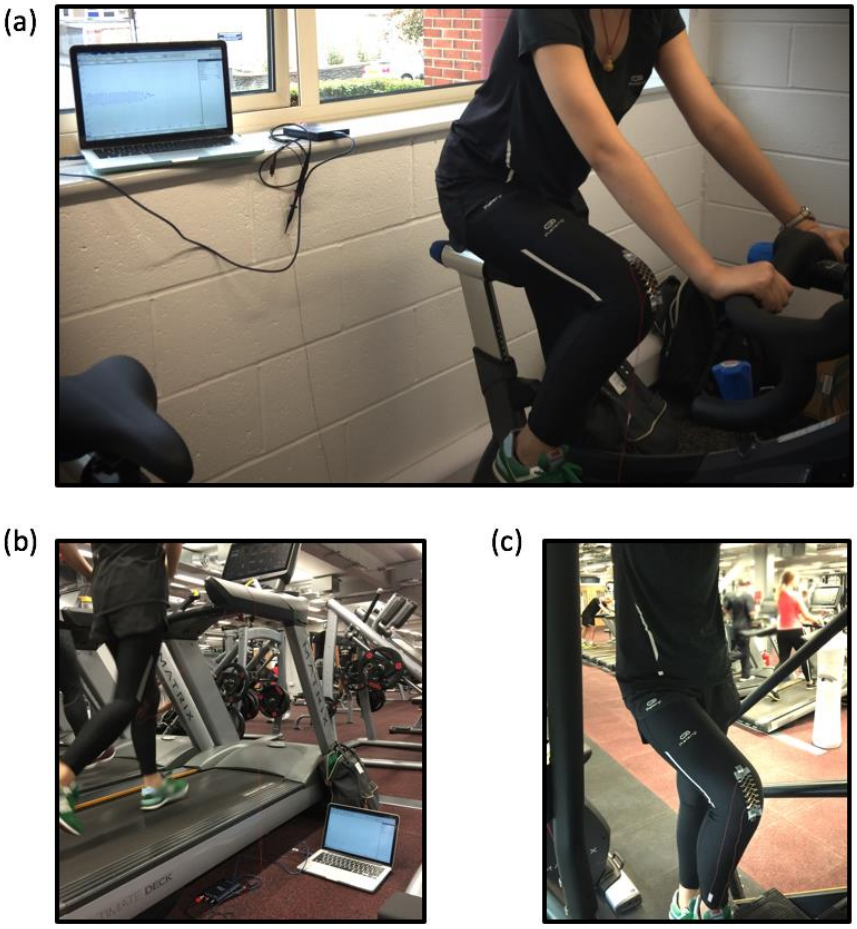

Figure 4.36 The demonstrations of the sensing system under different exercises. (a) cycle, (b) running, (c) climb.

In addition to reliable applications for implantable devices, this sensing system also shows great potential for wearable electronics to record daily activities. To monitor daily exercises, this sensor can be readily mounted on body joints where large deformation occurs, such as the knees (Figure 4.35). Different types of exercises, as shown in Figure 4.36, including cycle, running, and climbing, have been performed to evaluate the sensing performance. For each type of motion, the device illustrates a clearly different voltage waveform, which provided a facile way to distinguish the motion type (Figure 4.37). In addition, when the running speed increases gradually, the voltage amplitude shows a gradual increase (Figure 4.38). Moreover, due to the open 3D buckling structure introduced by Kirigami cutting, the design featured here is intrinsically breathable, and can therefore be incorporated into performance textiles where breathability is essential.

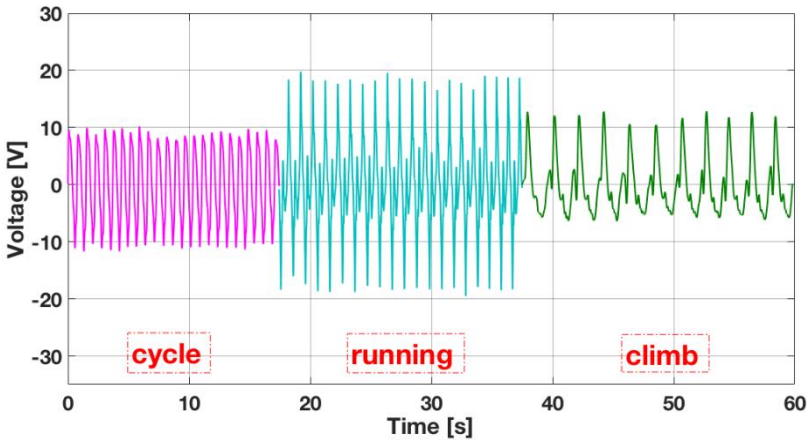

Figure 4.37 The voltage output of the sensor mounting on the knee areas for three types of exercise: cycling, running, and climbing.

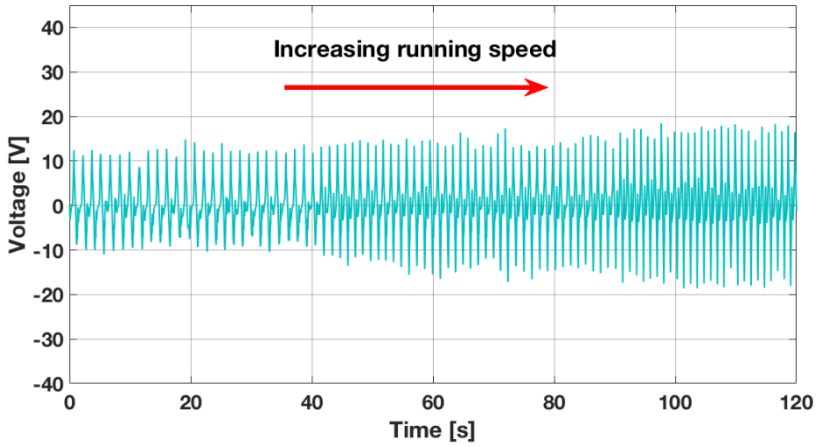

Figure 4.38 The voltage output of the sensor when the running speed increases gradually.

4.7 ASSESSMENT OF INTEGRATED SYSTEMS FOR WIRELESS SENSING CAPACITIES

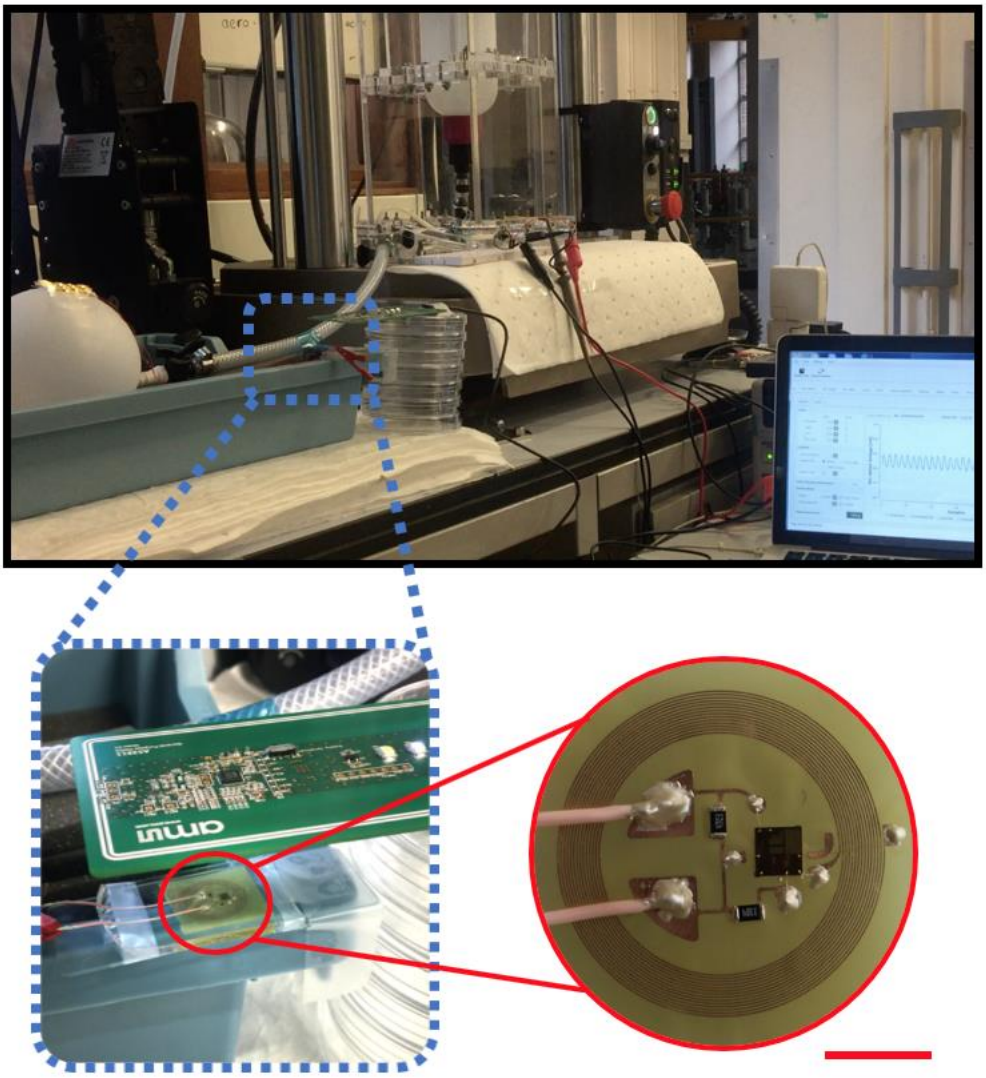

Figure 4.39 The setup for the comparison between wire and wireless results. Enlarged images show the wireless patch, and the communication between the wireless patch and external reader. Scale bar: 5 cm

Considering implantable biomedical devices in real applications, wireless communication is an indispensable capability. NFC technology is therefore explored for integration with our Kirigami sensor to collect the strain outputs and transmit the data to external devices. This provides a convenient way to monitor in-body and on-body conditions in real-time with portable devices, such as a smart phone with NFC functionality. A miniaturized wireless interface with the radius

of ~ 8 mm have been designed and fabricated (Figure 4.39) to capture and transmit the analog voltage signal from the sensor, and an external NFC reader is used to acquire the data. The effective communication distance between the current reader and the wireless interface could reach 25 mm (Figure 4.40). As the analog voltage input of the NFC chip is from 300mV to 600mV, a bias circuit is designed to match this range (Figure 4.41). For in vitro assessment, the previously described air-driven testing platform is used to demonstrate the wireless communication abilities. The sensor is directly connected to the wireless interface using two signal wires. Similar tests as above for balloon deformations under a series of frequencies and pressures have been performed to evaluate the performance of the integrated sensor-communication system. For a fixed balloon pressure, the signal output acquired from the NFC reader is stable, and its amplitude increases with an increase in frequency (Figure 4.42). The results from the wireless NFC interface are then compared with those using wired connections to an oscilloscope, and the results from the two measuring methods are consistent with each other (Figure 4.43). A heartbeat-like input has also been applied to simulate the real heart beating, and the results from the wireless interface illustrated its successful acquisition of the signal characteristics at a representative frequency of 1 Hz (Figure 4.44). The trend of the voltage/pressure signals match the sensor signal obtained from the wired platform (Figure 4.45). Ex vivo tests were also conducted on the pig heart with the same test platform. Reliable results from the NFC interface are observed at a representative frequency of 1 Hz (Figure 4.46).

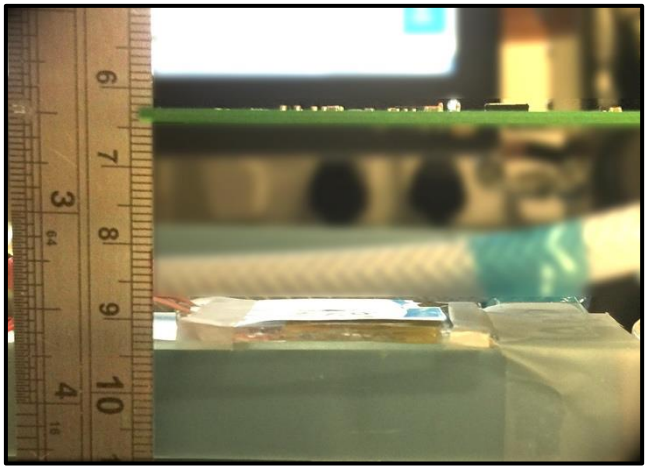

Figure 4.40 The working distance between the wireless patch and external reader to transmit the collected data wirelessly.

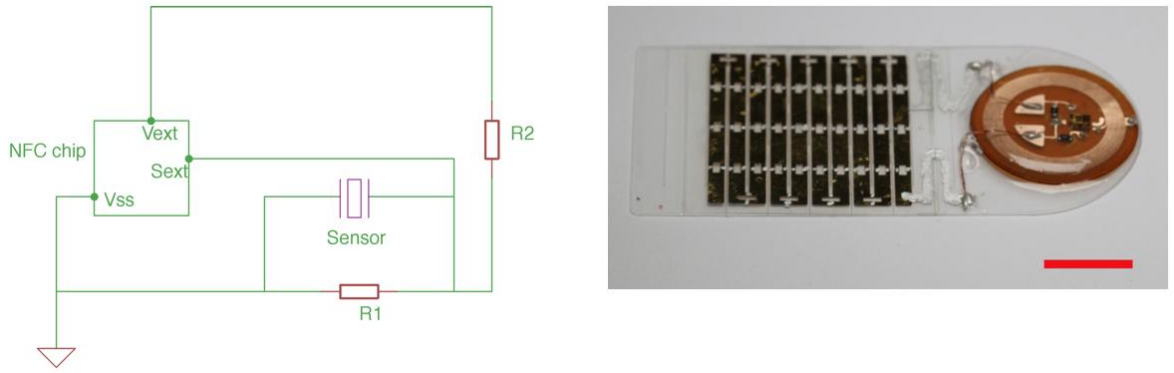

Figure 4.41 The diagram of the working circuit of the wireless communication interface to collect the sensing results. R*1=470 k*Ω*,* R*2=3.3M*Ω*. Scale bar: 1cm.*

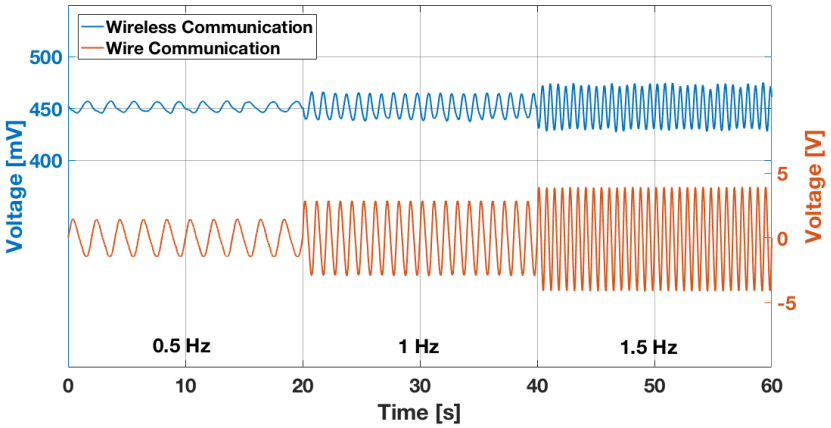

Figure 4.42 The comparative results between the wire and wireless measurement methods with sine-shape input under 4.0 kPa and three frequencies: 0.5 Hz, 1.0 Hz, and 1.5 Hz on air-driven platform.

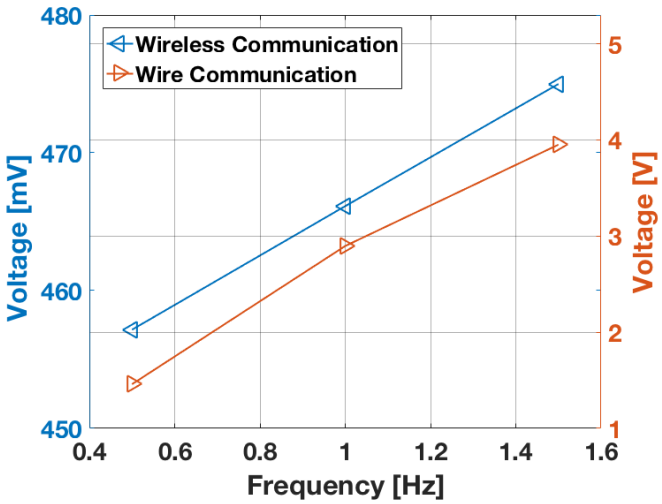

Figure 4.43 The comparative study of the sensing system under wire and wireless measuring ways with sine-shape inputs.

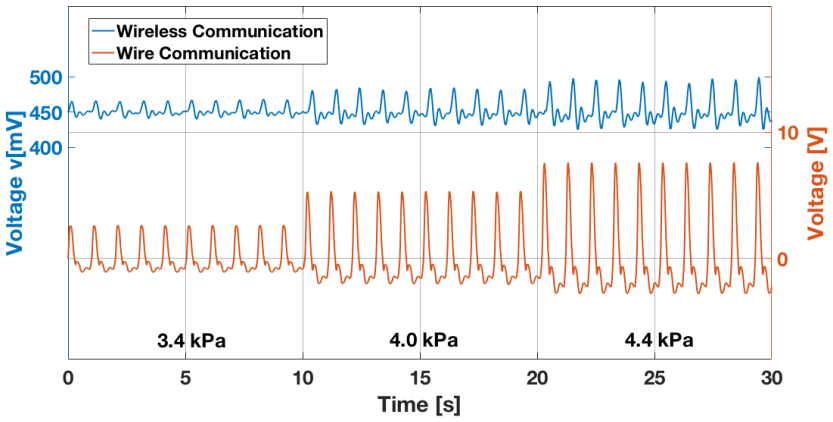

Figure 4.44 The comparative results between the wire and wireless measurement methods with heartbeat-like input at 1 Hz and for three pressures.

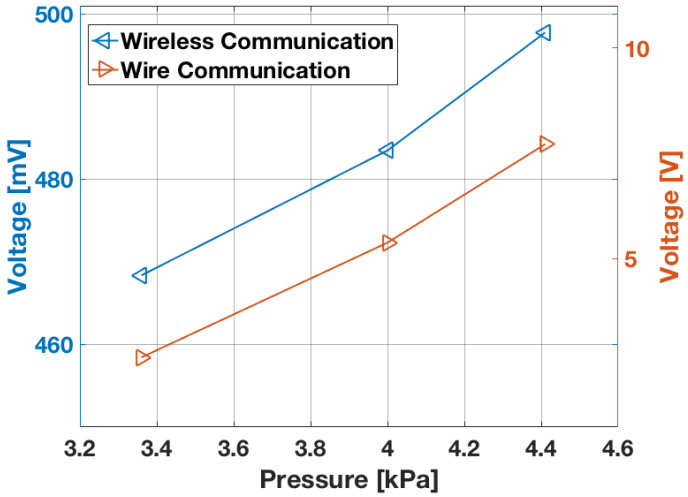

Figure 4.45 The comparative study of the sensing system under wire and wireless measuring ways with heart-beat-shape inputs.

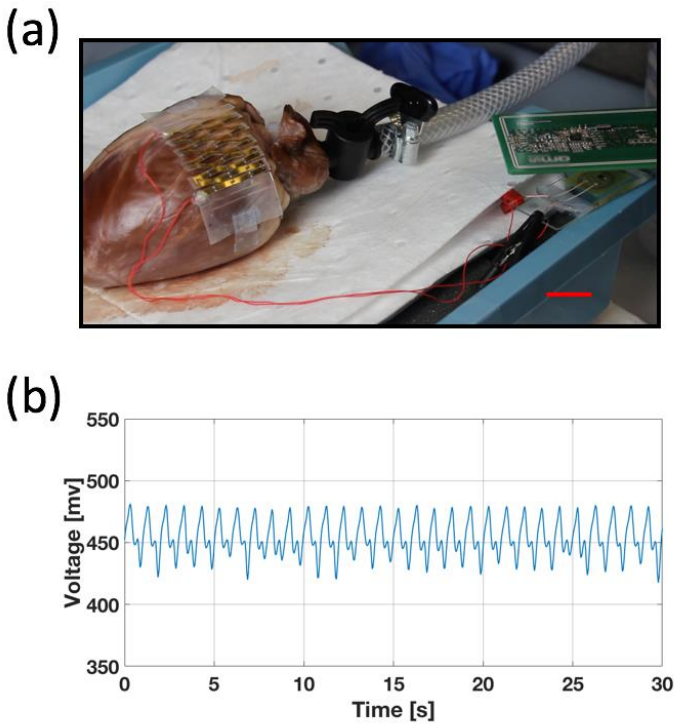

Figure 4.46 The experimental image of the wireless communication demonstration on the pig heart, and the measured signal from the NFC reader. Scale bar: 2 cm

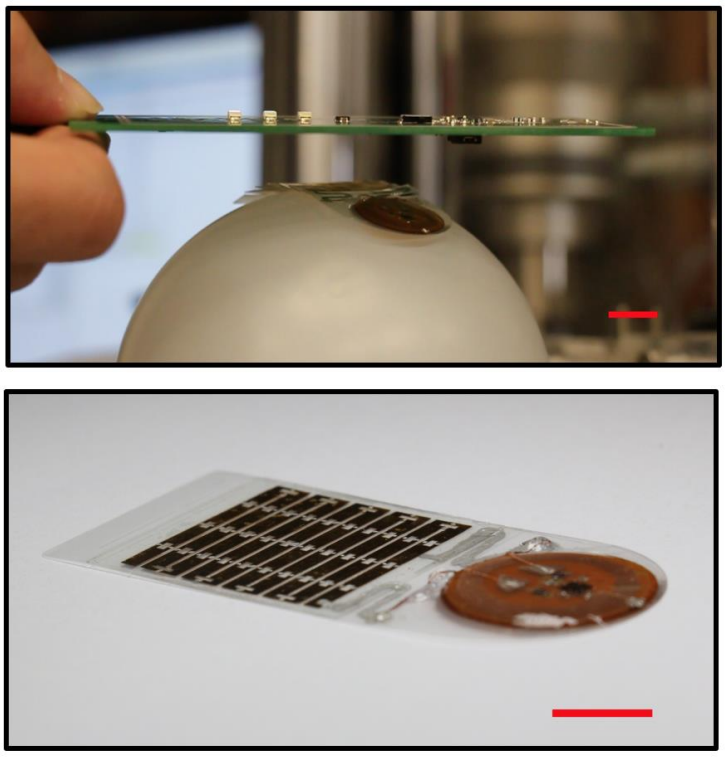

Figure 4.47 The fully integrated sensing and communication system, and its evaluation on the balloon surface. Scale bar: 2 cm, and 1 cm.

Finally, we demonstrate the complete self-contained biosensor by integrating the Kirigami sensor and NFC interface into a single module (Figure 4.47). The sensor size is further optimized to match the dimension of the wireless component to achieve a miniaturized and flexible integrated sensing system. A series of tests has been performed to evaluate the operation of this integrated system at three frequencies and three pressures (Figure 4.48). The acquired results validate the reliability of this integrated system and illustrate the near-linear relationship between the input (frequency and pressure) and output (voltage) (Figure 4.49).

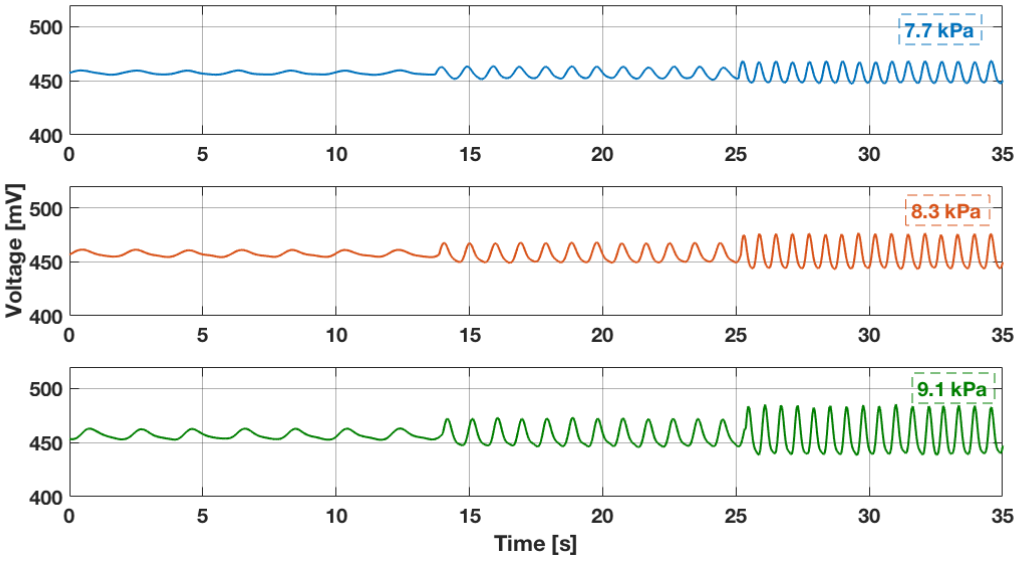

Figure 4.48 The wirelessly transmitted data from the integrated system under a series of conditions, including frequency and pressure changes,

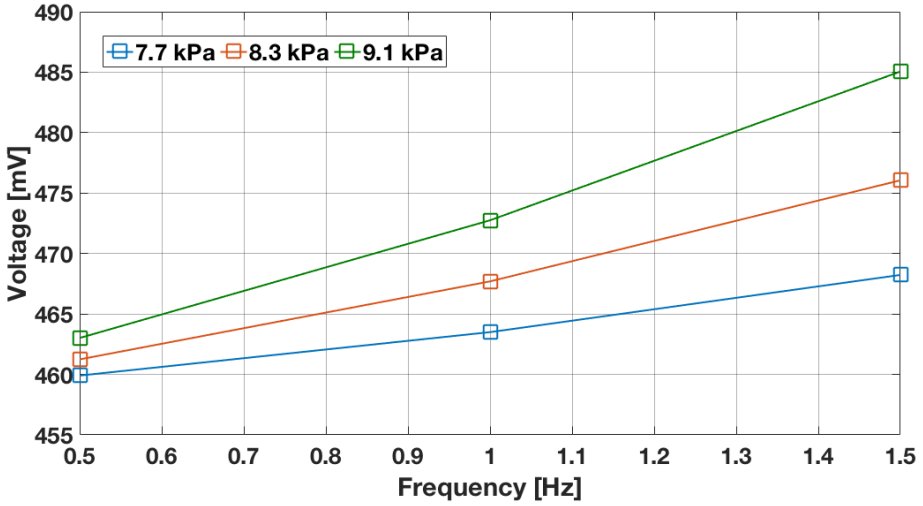

Figure 4.49 The voltage amplitude comparison with the changing parameters.

4.8 METHODS

4.8.1 Finite element analysis

Numerical simulation was adopted for the mechanical structural design and piezoelectric electrode optimization of the sensing systems with the commercial software Abaqus (Abaqus/Standard 6.14). The balloon with hyperplastic materials was established based on a Neo Hooke model, with the parameters of shear modulus (μ_0=0.5 MPa) and bulk modulus (K_0= 250 MPa) [36]. To simulate the process of fluid infusion into the balloon, a fluid cavity was defined to model the fluid-filled balloon. The initial fluid volume was set as 400 ml, and 140 ml was added into the cavity using the keywords *FLUID FLUX in Abaqus at a constant mass flow rate.

For the mechanical analysis of structural designs, 2D shell element (S4R) was adopted to model the Kirigami and planar structures with PET material properties [256]. For the Kirigami structural design, three steps were applied to finish the complete deformation process. In the first *Static step, an imperfection was introduced by adding a small bias displacement of 0.01 mm in the middle point of the top edge of each cut to trigger the buckle instability, and the cut was modelled as a 0.2 mm slot to account for the finite laser beam diameter. In the second step, the Kirigami structure was bent to match the curved surface of the balloon, and TIE constraints were then applied between the balloon and the middle areas of the two end edges of the Kirigami structures. In the final step, the inflation process of the balloon was performed, and due to the balloon deformation, the tied Kirigami structure also experienced the stretching and induced 3D buckling. For the planar structural design, only the last two steps in Kirigami structural designs were applied as there was no need to introduce the imperfection for buckle instability. A mesh convergence study was conducted to set the global mesh size 0.5 mm.

In the piezoelectric analysis of the electrode design, the modelling of the balloon was the same as the above section. Considering the piezoelectric effects, 3D solid element (C3D8R for PET substrate and C3D8E for PVDF layer) was adopted for the sensing part with two layers, 28 μm top layer of piezoelectric material and 75 μm bottom layer of the substrate. Electrical potential in boundary conditions was used to define the electrode patterns (Figure 4.9, each color shares the same potential). Due to the use of hyperelastic material, all steps considered the nonlinear effects (Nlgeon = on in Abaqus). The analysis for Kirigami and planar structures were similar to the above section, with three steps and two steps respectively.

4.8.2 Fabrication of integrated stretchable sensing system with wireless interface

The integrated sensor system included two subsystems, the sensing component and the wireless module. These two parts were fabricated separately, and then assembly together with two electrical connections.

The sensing part was based on a 28 μm thickness of PVDF film (Precision Acoustics Ltd, UK). Holes 0.1 mm in diameter were patterned on the film for the reverse connection of the electrodes (Figure 4.12). The film was then cleaned with Ethanol and DI water before electrode deposition (Ti/Au: 10 nm/150 nm) by sputter coater (Leybold L560) on both sides. The electrodes were patterned using a shadow mask. Water-soluble tape was used as the mask material, and it was cut to the designed pattern, and bonded onto the surface of the piezoelectric film. Once the electrode deposition was complete, the water-soluble tape mask was removed by warm water, leaving the reverse-connected electrode patterns as designed.

The standard photolithography technique was used to fabrication the wireless component. A sheet of polyimide with annealed cooper on top (DuPont Pyralux AC 182500R) served as the substrate of the flexible circuit board. This sheet was firstly cleaned with Acetone, IPA, and DI water. Then the antenna geometry and interconnects were patterned by photolithography (photoresist S1813, spin speed 2000 rpm for 40s, bake at 115 °C for 1 min, UV exposure for 8 seconds with power density of 20 mW/cm^2, development for 45 seconds with MF-319 developer, and post bake for 3 minutes at 115 °C). The patterned cooper film was etched for ~ 15 min in copper etchant (MG Chemicals Ferric Chloride) with gentle stirring. The NFC chip was then bonded on the board, connecting with the copper antenna and accessory electronic components through wire bonder (TPT HB16, gold wire with ball bonding), and strengthened with solder paste (CHIPQUIK, Sn42/Bi57.6/Ag0.4). Accessory resistors were bonded on the board using solder paste. Two wires that electrically connect the wireless interface and sensing part were bonded onto two pads on the wireless board with conductive adhesive (CHEMTRONICS, CW2400), and cured for 10 mins at 70 °C. A layer of PDMS (Dow Corning, Sylgard 184; 10:1) was coated on the wireless patch to encapsulate the active components, followed by one-hour curing at 70 °C.

The substrate of the sensing part as well as the platform to assemble the above two subsystems was a 75 μm thickness of PET film. The PET film was cut into the final outline shape for the next step of assembly. It was then cleaned with Ethanol and DI water. The piezoelectric film with patterned electrode and the wireless patch were bonded side-by-side onto the PET film with an adhesive (3M Adhesive7952MP, 50 μm). Silver paint (Electrolube, SCP03B) was used to electrically connect these two parts. A layer of PDMS was then coated on the device (spin

parameters: 1000 rpm for 40 s and room temperature curing) to encapsulate all active components, electrodes, and interconnects. Finally, the tailed Kirigami cuts were patterned by laser engraver (Speedy 100) with precise alignment to match the electrode patterns.

4.8.3 Mechanical test setup

A materials test machine (Instron 8872) was used to perform the mechanical tests with a range of loading conditions. A displacement control, for different shapes of input including sine, pulse, and heartbeat-like signals, was adopted with various frequencies controlled by software (Bluehill 3). The piezoelectric film was fixed on both ends with grips, and the top grip was moved during tensile tests.

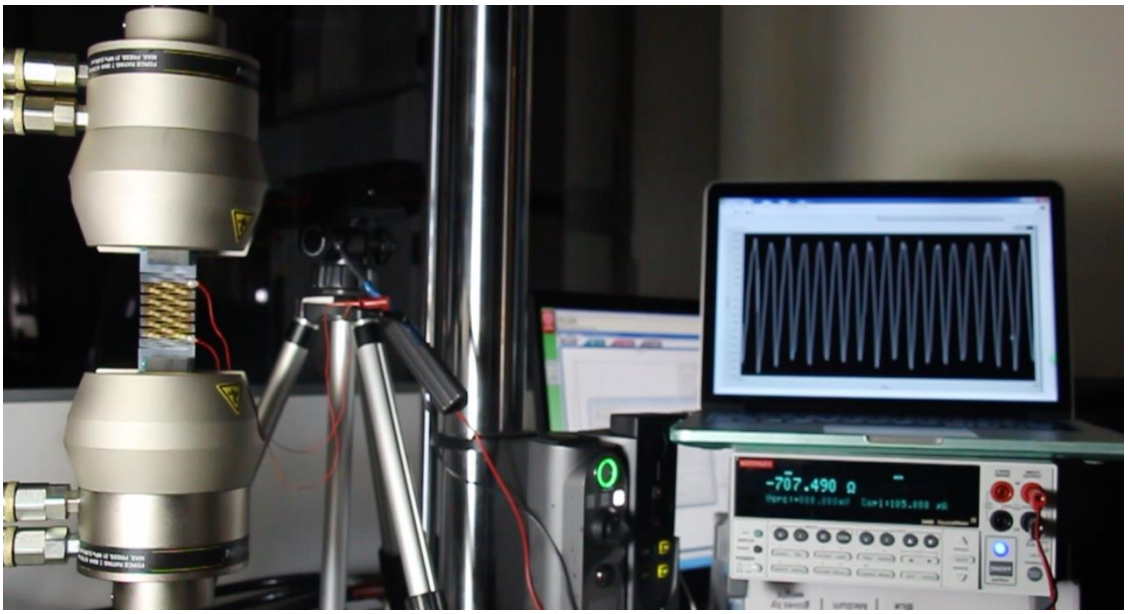

Figure 4.50 The experimental setup of the mechanical test of the sensing system to evaluate its electrical characteristics. The Instron machine was used to perform the tensile test, and the data recording was based on a LabVIEW program.

4.8.4 Electrical characterization of the sensing system

The piezoelectric sensor was characterized in a series of tests, and its energy harvesting performances were evaluated through several parameters, including the open-circuit voltage, short-circuit current, and instantaneous power.

A SourceMeter (Keithley 2400) measured the short-circuit current, and the results were recorded by a NI LabVIEW program (LabVIEW 2017). The results were stored temporarily in the buffer memory to achieve a high sampling rate. The open-circuit voltage was measured using a unity-gain

amplifier circuit with input impedance of 10^{13} Ω (Figure 4.51). An oscilloscope (PicoScope 2204A) collecting a probe with 10 MΩ impedance was used to read the output from the amplifier. For demonstration of self-powered capabilities, the AC voltage from the sensing system was rectified with a full-wave silicon bridge rectifier (HY DB107) to charge a 10 μF capacitor.

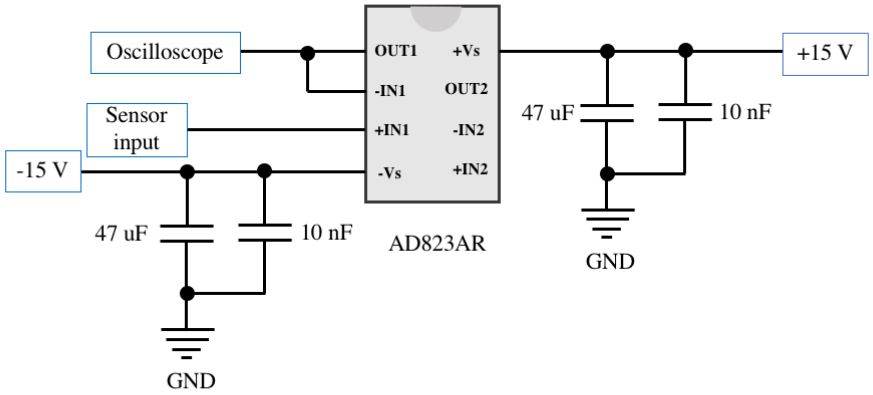

Figure 4.51 The amplified circuit for the measurement of the open circuit voltage.

4.8.5 In vitro cytotoxicity tests

To test the biocompatibility of the sensor and communication parts, 4 x 4 mm pieces of the sensor and communication devices, respectively, were sterilized by UV irradiation (40 min) and placed in wells of a 24 well plate (Corning, UK). 10^4 COS7 cells (passage 34) were placed on top of the device samples and incubated in 0.5 mL cell culture medium. Untreated controls consisting of 10^4 COS7 cells were placed in separate wells of the same 24 well plate. After 24h incubation, the culture medium was replaced with alamarBlue™ Cell Viability Reagent (Invitrogen, DAL1025) prepared as per manufacturer's instructions. Cells in each well were incubated with 0.5 ml of the reagent for 5 h. A 0.5 mL sample of the reagent was also placed in a well without cells to act as a background control. 0.1 mL aliquots of the culture supernatant of each well was placed in wells of a black 96 well plate, including the blank control and a 0.1 mL sample of fully reduced alamarBlue™ Cell Viability Reagent (obtained by autoclaving the reagent in media as instructed by the manufacturer). A Synergy Neo2 Multimode Microplate Reader (BioTek, UK) was used to

measure fluorescence intensity, at the wavelength of 550 nm and 595 nm, respectively. After this procedure, cells were kept in culture and the assay was repeated again after 48h and 72h contact with the devices. Percentage of alamarBlue™ resorufin reduction was calculated by subtracting the blank values from all readings and applying the following formula:

$$\left(\frac{AB_c}{AB_r}\right) * 100 \qquad 4.2$$

Where AB_c is the blank corrected fluorescence value measured in the cell culture supernatant and AB_r is the fluorescence value measured in the fully reduced form of the reagent.

To verify if cells were able to grow on the devices, 1 x 1 cm sensor or communication device samples were sterilized with UV irradiation (40 min) and placed in a 24 well plate. 10^4 COS7 cells were seeded on top of the devices in 0.5 mL of medium. Cells were stained with 2 μM calcein and 4 μM ethidium homodimer III (Biotium, UK) in PBS for 45 min. The stain was removed, and cell layers covered with PBS for imaging using a Leica DMI6000 epifluorescence microscope. A Leica DFC365FX digital camera was used to capture the images.

4.8.6 In vitro study

For in vitro assessment of the integrated sensing system, two platforms, air and water driven respectively, were set up to inflate the balloon dynamically (Figure 4.52).

For the air-driven setup, a 1.5 L syringe (Sealey VS405) was used to inflate the target vessel (balloon or pig heart) directly through a PVC tube. The syringe output nozzle was connected to the PVC tube through an elbow connector at the bottom. The syringe was fixed vertically on the base of the Instron machine through a designed fixture, made by 10 mm thickness Perspex sheet, allowing the Instron machine to control the syringe movement. A pressure gauge (Honeywell, HSCSAAD100MDAA5) was connected to the PVC tube through a T-shape connector to record the pressure change in the balloon. The T-connector was also connected to the PVC tube and to the balloon.

For the water driven case, a revised setup was essential to infuse water into balloon in a stable way. Due to water gravity and hydrodynamic effects, it was undesirable to directly fill the syringe with water, and extrude it into the balloon. Instead, we use an indirect way to extrude water into the balloon by adding a transfer unit. A latex cylindrical bladder was connected to the syringe output through an elbow connector and was located inside a rigid chamber fully filled with water. When the air volume of the bladder changed (controlled by the syringe), the expansion or contraction of the bladder would expel or suck in water through the outlet of the water chamber and inflate or

deflate the water-filled balloon. An ultrasonic flow meter (Cynergy3, UF08B) was spliced into the PVC tube to record the water volume that went into the balloon. A T-shape connector with valve was added after the flow meter to exhaust any air bubbles inside the system, and a balloon was then connected. All connectors were sealed with thread seal tape.

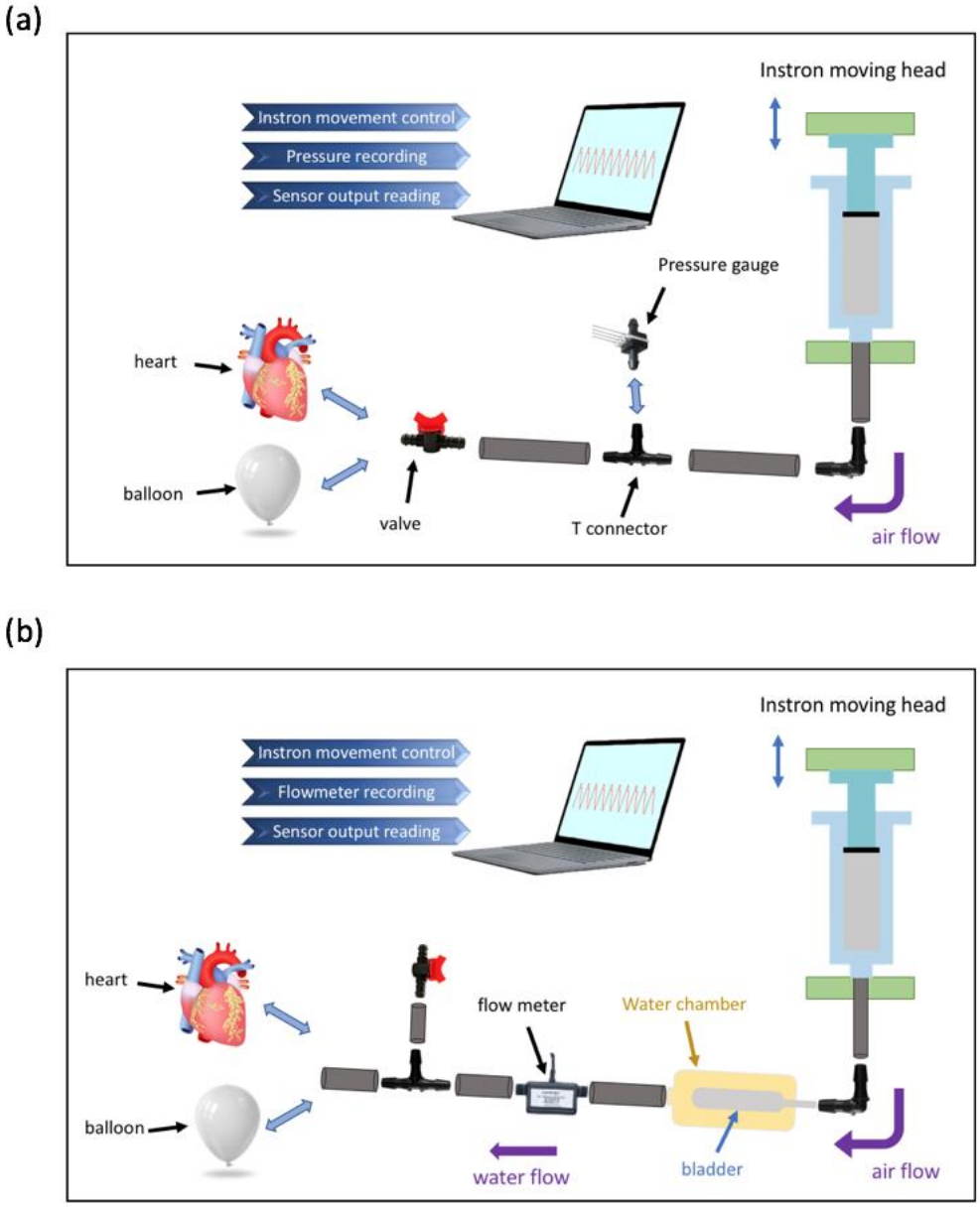

Figure 4.52 The experimental setup for the in vitro and ex vivo assessments of the sensing system on curved surfaces. (a) An air-driven platform to extrude air directly into the subject chamber from the syringe controlled by Instron machine. (b) A water-driven platform to extrude water indirectly into the subject chamber through a transfer unit.

The oscilloscope (PicoScope 2204A) has two input channels. For air-driven platform, the output of the sensing system was recorded by one channel of the oscilloscope with a 100 MΩ impedance probe, and the pressure from the analog output of the pressure gauge was recorded by the other channel with a 10 MΩ impedance probe. For water-driven setup, the reading for the sensing system was kept the same, and the second channel of the oscilloscope was used to record the NPN pulse output from the flow meter.

4.8.7 Ex vivo study

The study conformed to the protocol approved by the University of Bristol (U121458/ABP/OTHER). The pig heart was purchased directly from a local butcher's (stock certified for human consumption) and transported to the lab with a chilled container (maximum temperature lower than 8 °C). A Virkon (DuPont Virkon S Tablets) solution was made to clean the tissue surface. The sensor was then bonded onto the heart surface with a tissue adhesive (3M 1469sb Vetbond). The in vitro platforms were used in this study by substituting the balloon with the pig heart.

4.9 CONCLUSIONS

The flexible and stretchable integrated sensing system presented here represents a significant technology advance to achieve self-powered and wireless health monitoring. The structural flexibility allows this system to robustly conform to various curved surfaces, including the balloon, heart surface, and body joints. The stretchability reduces the constraints from the sensing system on the subject which could deform freely. Compared to previously reported methods for stretchability, the Kirigami technique provides a straightforward method to achieve compliance by a tailored cutting patterns, simplifying the microfabrication process. By introducing a novel inter-segment electrode design, this integrated sensing system shows advantages in both mechanical and electrical performances. Our devices are capable of differentiating various loading conditions and show robustness in cycle tests. The energy harvesting capability enables the system to potentially be a sustainable power source to other electronics.

Another attractive feature of the proposed system is the miniaturized wireless interface allowing the sensing data to be transmitted to an external device wirelessly, which is of vital importance to implantable devices. In addition to the systematic modelling of the devices, a range of practical assessments, including in vitro, ex vivo, and on body, have been performed. The deformations of the balloon and pig heart under a series of conditions, as well as three types of exercises on the body, have been successfully captured. With the integration of the NFC functionality, the collected

data are transmitted to external devices to achieve wireless and real-time health monitoring with no power needed for the sensor or the communication chip. The temperature of the subject could also be extracted by the NFC component. These features contribute to the effectiveness of the developed wireless and self-powered sensing platform and differentiate it from other sensing systems. The developed device has the potential to significantly expand the wireless monitoring of vital signs and important bio-mechanical indicators of health.

CHAPTER 5 - STRETCHABLE METASTRUCTURES WITH NON-UNIFORM KIRIGAMI

The Kirigami technique has been demonstrated to be an effective route to tune the mechanical behaviour of architected structures. Typical Kirigami-based metastructures however use well-defined topologies with uniform or periodic linear cuts. These uniform Kirigami patterns induce a homogenous spatial deformation across the entire structure, limiting the range of mechanical response and the tunability of the metastructures. In this work, we propose a novel metastructure platform with non-uniform Kirigami. Compared with conventional Kirigami structures, the presented system offers an additional non-uniformity parameter to spatially control the structural deformation, which enables to better match the deformations of biological surfaces. We present a generalized expression to describe the non-uniform characteristics and develop a series of configurations. Comprehensive studies have been performed to investigate the mechanical properties of the non-uniform Kirigami structures. Furthermore, a stretchable piezoelectric system based on the non-uniform Kirigami platform have been developed to validate the efficiency of the sensing performances and tunable sensitivity. For the first time, the feasibility of making a stretchable system with controlled spatial deformation is demonstrated, showing great potential in biomedical and healthcare areas.

5.1 INTRODUCTION

The development of material science with high-performance mechanical properties for emerging engineering applications has been a recurrent challenge during the last decades. Mechanical metamaterials [216] that change their configurations in response to external stimuli have drawn considerable attention because of their novel design principles, which allow them to achieve attractive mechanical behaviors and tunable functionality. Examples of the properties generated by mechanical metamaterials are negative Poisson's ratios [265], tunable thermal expansion [266], negative compressibility [267], and extension-to-twist transformations [268]. Recently, research in mechanical metamaterials has made it possible for potential applications in a varied range of fields, including shape morphing [238], cardiac patches [1], vibration control [269], mechanical cloak [270], soft robotics [271] and acoustic waveguides [272].

Substantial efforts have been devoted to exploring the mechanisms, designs and fabrications of mechanical metamaterials, and link them to their multiphysics performance. Amongst the different metamaterials topologies, Origami and Kirigami provide a promising route to tune the mechanical behavior of architected structures [217]. Origami involves folding a flat sheet along predefined creases [273]. Kirigami is an extension of Origami that allows the use of precision cuts to introduce additional degrees of freedom for the folded structure. The two approaches can be used as a manufacturing paradigm to transform 2D sheets into 3D structures without compromising their intrinsic properties. With their use of cuts, Kirigami-inspired techniques can improve the structural diversity and reduce the stress induced by folding. Inspired by this concept, various functional systems have been developed and their potential applications have been demonstrated in stretchable electronics [218, 256, 274], soft actuators [243, 275], deployable reflectors [222, 223], smart adhesives [276, 277], and others [219, 224, 278, 279]. Kirigami-based design and manufacturing starts with flat material substrates. This makes it possible to choose many advanced laminar materials, including inorganic semiconductors and polymers, which are difficult to process using more traditional 3D fabrications techniques, such as additive manufacturing [226]. Kirigami also allows the generation of controlled and rationally designed layouts on planar structures that can achieve sophisticated and predictable 3D configurations across a broad range of length scales, from nano to macro [225, 280]. These characteristics of predictable mechanical deformation, scalability and easy fabrication enable the creation of complex 3D structures with desirable functionalities. To date, however, almost all demonstrations of Kirigami metastructures have exploited a uniform distribution of linear cuts, thereby generating a uniform strain response across the material. However, in real world applications, such as in biological systems, the mechanical deformations are strain-dependent and spatially non-uniform. Conventional Kirigami cut patterns

are therefore unable to functionally adapt their shape with strain or in a non-uniform manner. In order to match arbitrary configurations, several improved strategies have been proposed, such as graded auxetics [281] and patterned randomness [211], hybrid Kirigami [282] and programmable Kiri-Kirigami structures [223].

In this chapter, Kirigami metastructures with non-uniform patterns of linear cuts are investigated. This engineered geometry provides additional parameters to control the mode of deformation, and to enable unique and tailorable mechanical properties. We investigate the proposed designs by first introducing cut slits into plastic films. The proposed design shows a sequential buckling deformation once stretched, which induces a non-uniform structural behavior. The relationship between the mechanical stiffness and the non-uniform geometry parameters of the patterns have been evaluated and confirmed by combined numerical and test results. The local strain on adjacent unit strips shows a linear increase with slit gap. We also demonstrate the utility of this design in stretchable sensors based on piezoelectric materials, with a gradual change of voltage output compared to the baseline uniform Kirigami topology.

5.2 NON-UNIFORM KIRIGAMI DESIGN CONCEPT

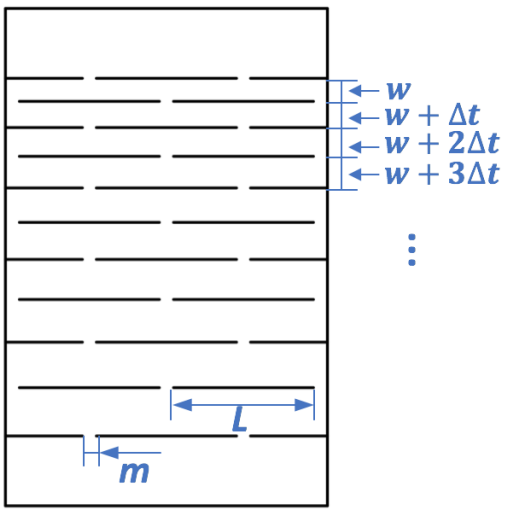

Figure 5.1 Schematic of the non-uniform Kirigami structure where L, m, w and Δt indicate slit length, hinge length, slit gap, and slit gap increment.

The proposed Kirigami design is based on a linear pattern of non-uniformly spaced linear cuts (Figure 5.1). Several parameters determine the mechanical behaviours of the resulting structure, including the slit length L, the hinge length m, the film thickness h, the slit gap w and the slit number k (defined as the minimum number of cuts across the width, with k = 2 in Figure 5.1). In a conventional Kirigami layout [256], the slit gap is constant across the entire structure, creating a uniform out-of-plane buckling deformation. Here, the slit gap varies with (in its simplest form) a fixed increment of Δt. To study its mechanical performance, this non-uniform pattern was produced in polyethylene terephthalate (PET) sheets of 125 μm in thickness, with the complete pattern defined by L = 15 mm, m = 1.5 mm, w = 2.5 mm, Δt = 0.3 mm and k = 2. A uniaxial tensile test, at a displacement control rate of 0.1 mm/s, was carried out to investigate the mechanical properties of the structure.

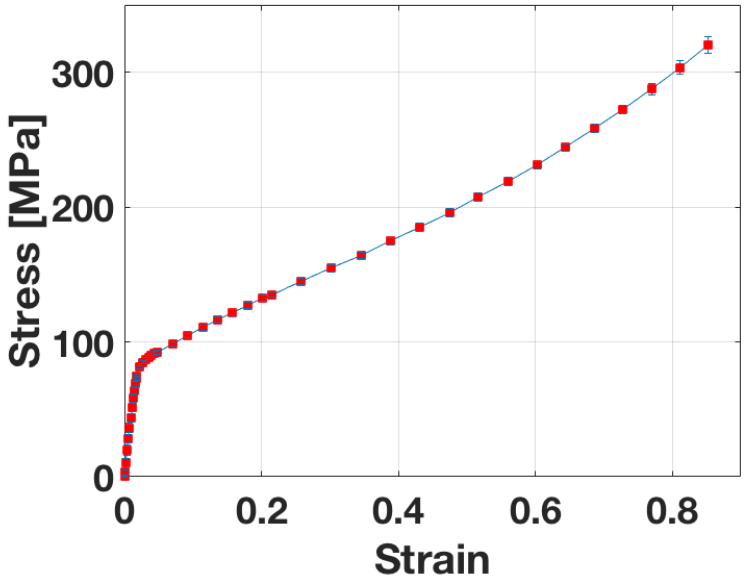

Figure 5.2 The stress-strain curves of pristine PET films (125 μm) for five samples under uniaxial tensile tests.

The material properties of this structure were obtained using standard test methods for thin plastic sheets (Figure 5.2). FEA study was carried out, and simulation results of the non-uniform Kirigami structure are compared with the results from the experiments (Figure 5.3). Three different stages of deformation are evident, as the tensile strain increases. The first features an in-plane stretching near the origin, exhibiting a large stiffness close to the underlying material modulus (PET in this case). The second stage (strain < 0.35) shows a relatively moderate stiffness due to the gradual evolution of out-of-plane buckling along the structure that acts to accommodate the presence of

further stretch. The stage separation is based on the slope of the stress-strain curve with a deviation less than 10 %. During the final third stage the stress exhibits a sharp increase, due to the transformation of the out-of-plane deformation to in-plane stretching, until material failure at a nominal strain of approximately 0.78. The effect of the slit gap increasement on the structural stiffness was analyzed through a parametric study.

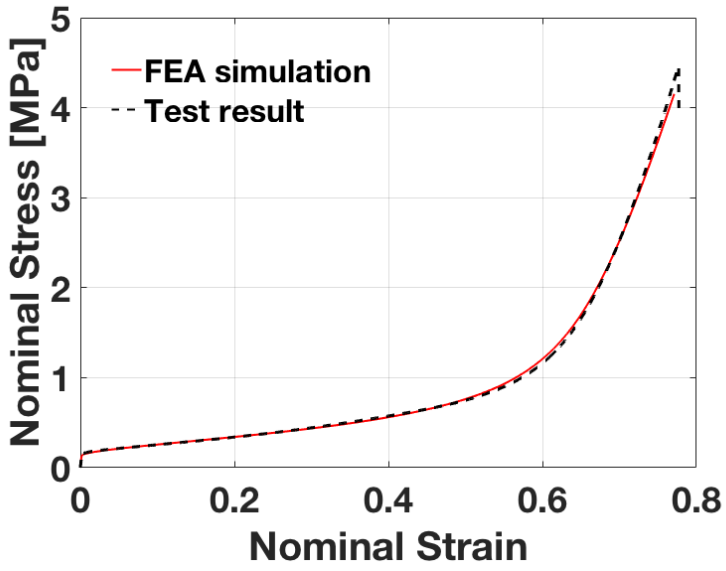

Figure 5.3 Stress-strain curves for the non-uniform Kirigami patterned film obtained by numerical simulations and experiments, where the control parameters are L = 15 mm, m = 1.5 mm, w = 2.5 mm, Δt =0.3 mm and h = 125 μm respectively.

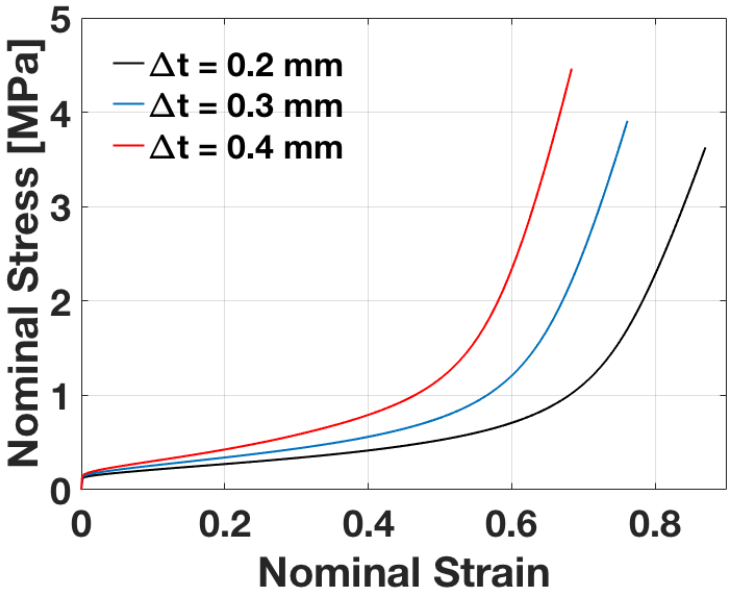

Figure 5.4 Numerically obtained stress-strain curves for the slit gap increments 0.2 mm, 0.3 mm, and 0.4 mm

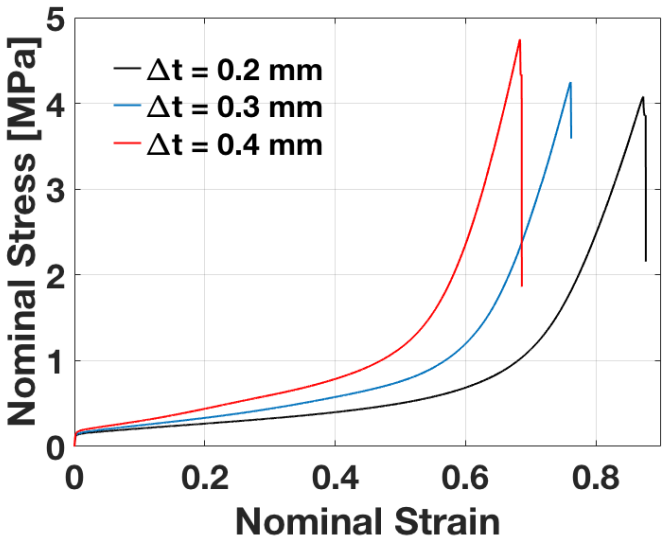

Figure 5.5 Experimentally obtained stress- strain curves by varying the slit gap increment from 0.2 mm, 0.3 mm, to 0.4 mm

As observed in Figure 5.4, as the slit gap increment Δt changes from 0.2 mm to 0.4 mm, the structure becomes more rigid. This is as one would expect since there are fewer overall cuts along the structure with increasing Δt. The experimental study was also performed to investigate the relationship between the slit gap and its mechanical properties. The results in Figure 5.5 show that consistent results can be obtained between numerical simulations and experimental tests.

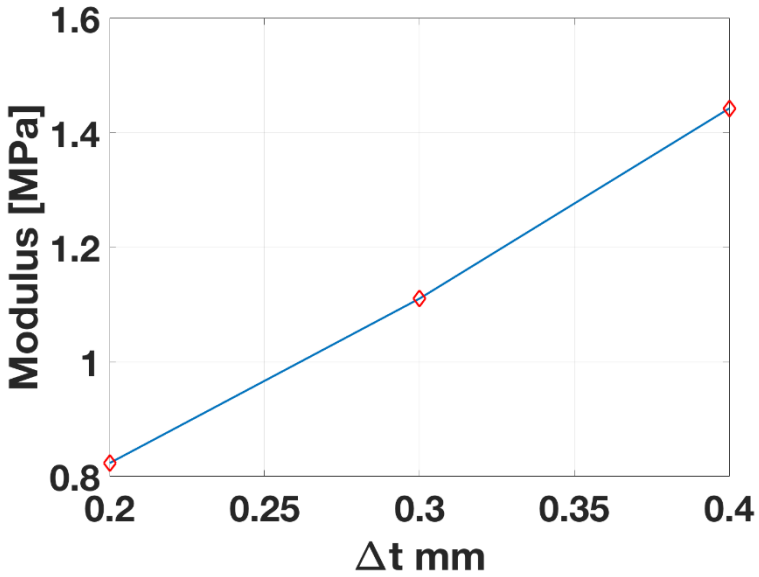

Figure 5.6 The effective modulus of the non-uniform Kirigami structures with the slit gap increment of 0.2 mm, 0.3 mm, to 0.4 mm respectively based on numerical simulations.

The effective modulus is used here to evaluate the mechanical performance of the non-uniform Kirigami patterns. The effective modulus is defined as the ratio of nominal stress and nominal strain ranging from 0.5 % to 10 % strain. The effective moduli for slit gap increments of 0.2 mm, 0.3 mm, 0.4 mm are 0.8 MPa, 1.1 MPa, and 1.4 MPa respectively. The moduli exhibit a linear relationship with slit increments (Figure 5.6). The mechanical properties of the non-uniform Kirigami structures are also compared with those from representative uniform Kirigami patterns (with uniform slit gaps of 3.1 mm, 3.7 mm, and 4.3 mm respectively) (Figure 5.7). At the beginning of the tensile deformation, the non-uniform structure is soft as out-of-plane buckling evolves at the small slits. The stress starts from lower values than those exhibited by the uniform structure with 3.7 mm slit gap. The stress then becomes equal and finally exceeds that for the uniform 3.7 mm slit gap structure as buckling of strips with large slit gaps gradually dominate the deformation. These results show that the non-uniform Kirigami design gives an added degree of freedom compared to uniform patterns for tuning the mechanical performance. As shown in Figure 5.8, the experimental tests with the same geometry parameters were also performed.

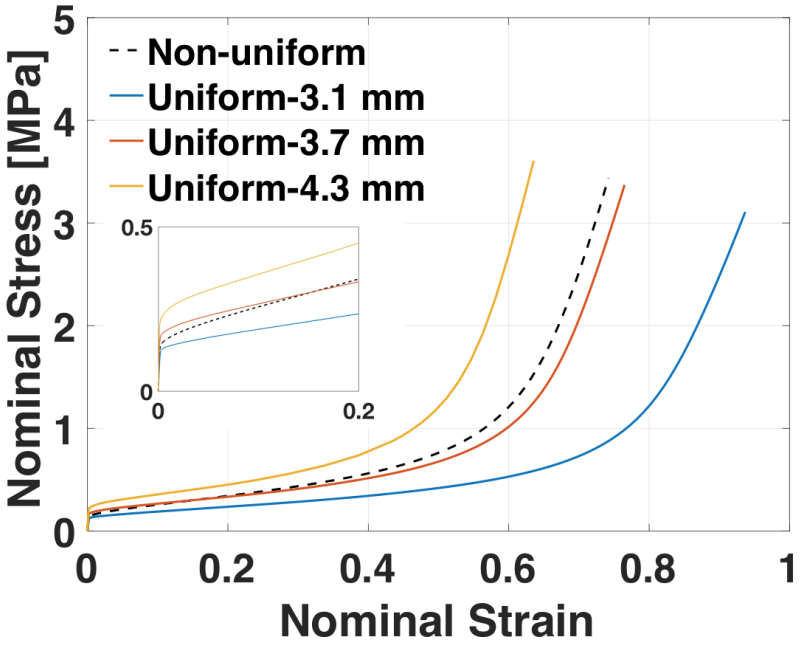

Figure 5.7 The comparison of nominal stress-strain curves of the Kirigami structures with non-uniform and three uniform patterns from numerical simulations. The inset is the stress-strain curves in the initial stage.

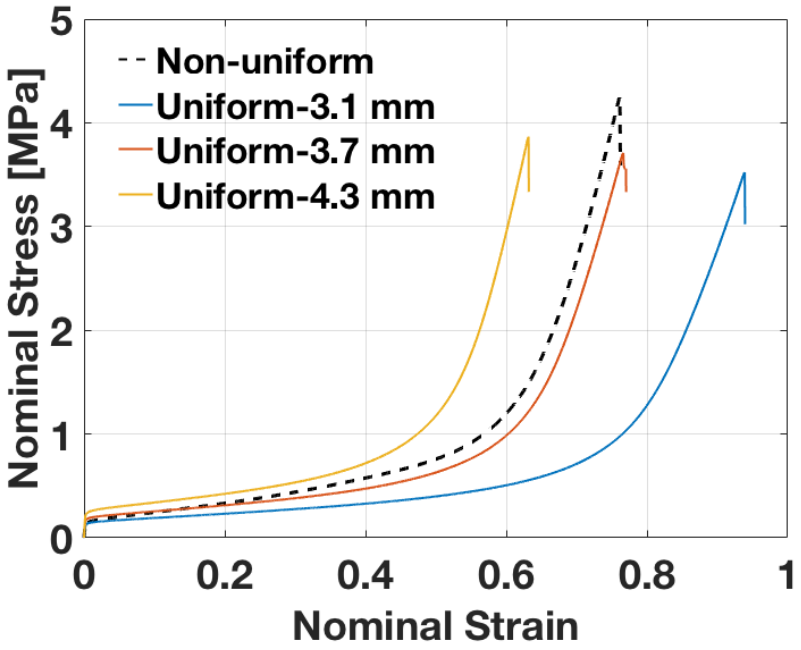

Figure 5.8 The comparison of the mechanical properties of the Kirigami structures with non-uniform and three uniform patterns from the experimental tests

5.3 MECHANICAL ANALYSIS OF DIVERSE NON-UNIFORM CONFIGURATIONS

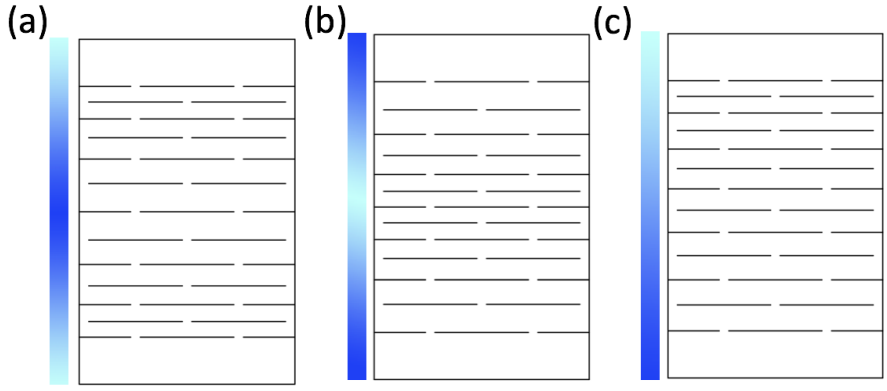

Figure 5.9 The configurations based on different non-uniform Kirigami patterns, (a)-(b) two double-graded non-uniform patterns, and (c) single-graded non-uniform pattern. The light color represents small slit gap, and the dark color means large slit gap.

Two further configurations extending the above non-uniform Kirigami patterns were investigated. As shown in Figure 5.9, the configurations feature double-graded non-uniformity. Here the gap w either increases from narrow (2.5 mm) at both ends to wide (4.5 mm) in the center or vice-versa (wide at the ends and narrow at the center). A comparative structure with single-graded non-uniformity was also studied. The configuration keeps the same number of slits and the exact global

dimensions as the double-graded non-uniform structure. The spatial deformation of the out-of-plane buckling with these two patterns is different: one starts from the edges, the other initiates from the center (Figure 5.10 and Figure 5.11).

The stress-strain relationship of the above configurations is shown in Figure 5.12. The mechanical stiffness with single-graded non-uniformity is between those with non-uniform double-grading. The directions of the patterns in the double-graded configurations slightly affect the stress-strain curves, and the narrow-wide-narrow topology shows a higher stiffness than the wide-narrow-wide design.

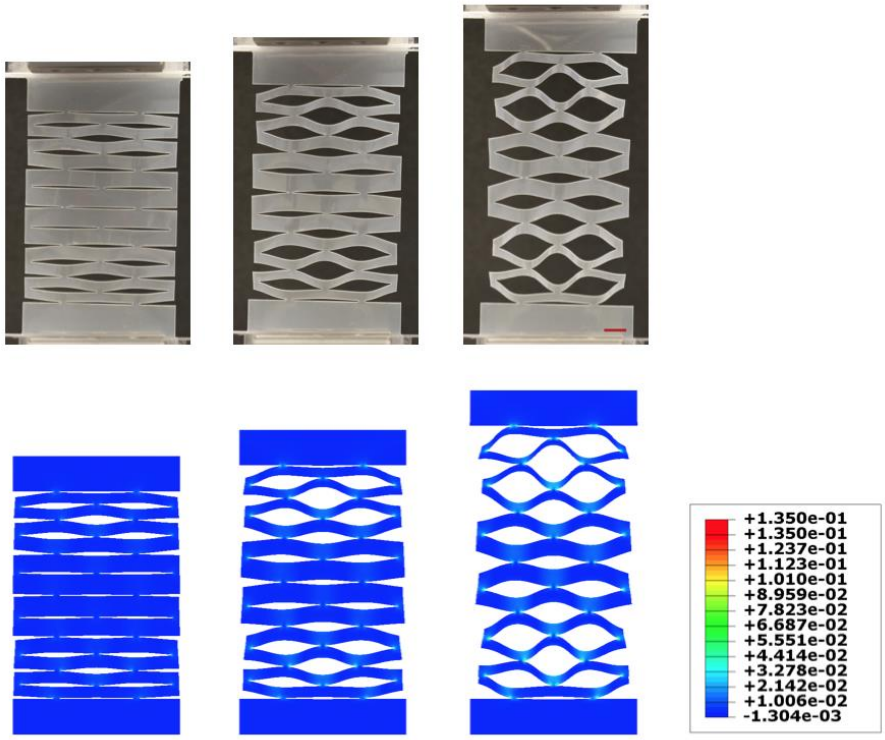

Figure 5.10 The mechanical behavior of the non-uniform Kirigami structure in Figure 5.9(a). The comparison between the test and simulation (local strain distribution) under three stages of nominal strain: 5 %, 15 % and 30 %. Scale bar: 5 cm.

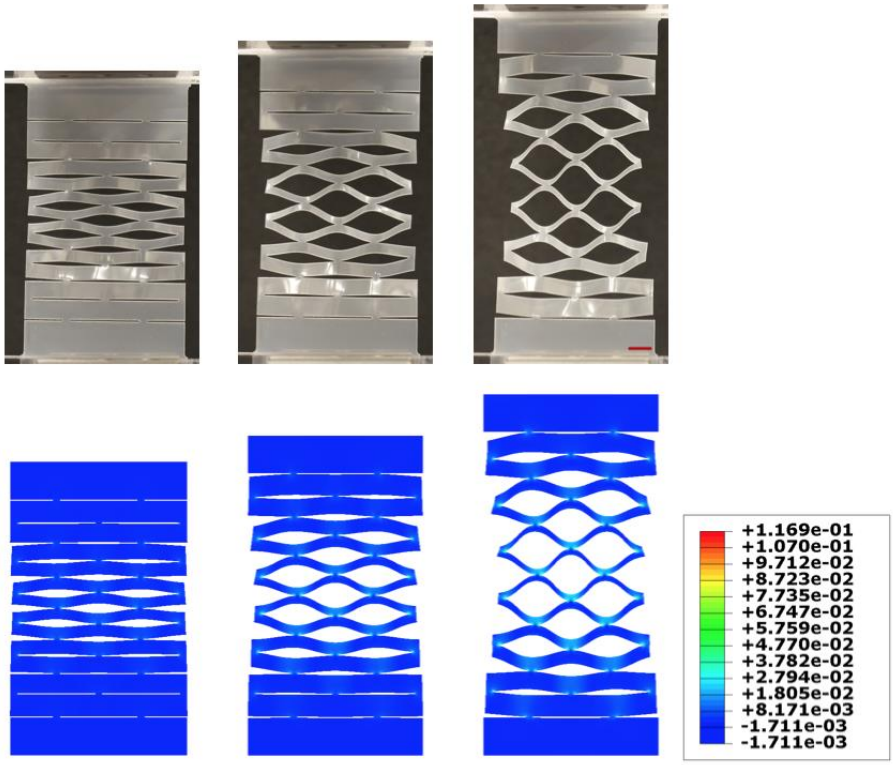

Figure 5.11 The mechanical behavior of the non-uniform Kirigami structure in Figure 5.9(b). The comparison between the test and simulation (local strain distribution) under three stages of nominal strain: 5 %, 15 % and 30 %. Scale bar: 5 cm

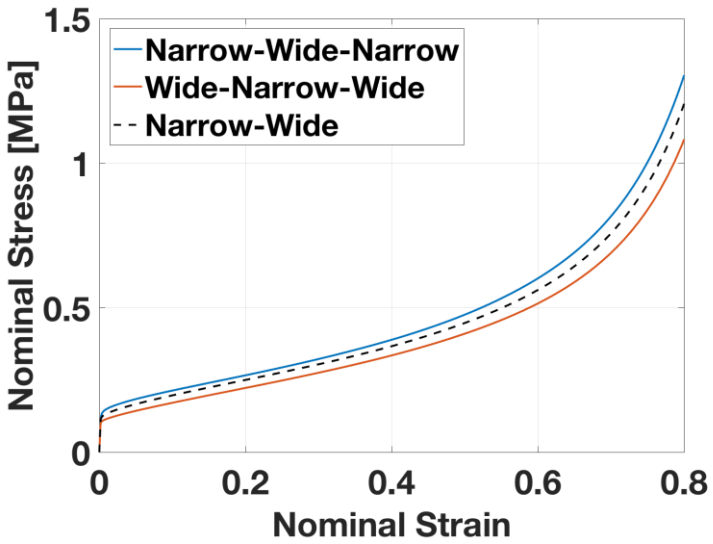

Figure 5.12 The numerically obtained stress-strain curves from the above three configurations.

Moreover, another study on the effect of varying slit number k was carried out while the non-uniformity was kept constant, for three cases $k = 1$, $k = 2$, and $k = 3$. Figure 5.13 shows the three configurations. Based on numerical simulation study, the structural properties are illustrated in Figure 5.14, which demonstrates that the slit number plays a dramatic effect on the structural stiffness, and when the slit number increases, the structure becomes much stiffer. This parametric study shows that the mechanical behaviour can be tuned through a pattern of cuts defined by parameters L, m, w, Δt and k to achieve spatially controlled deformation. This is useful in many practical applications, such as cardiac patches for dynamic surface monitoring of the heart.

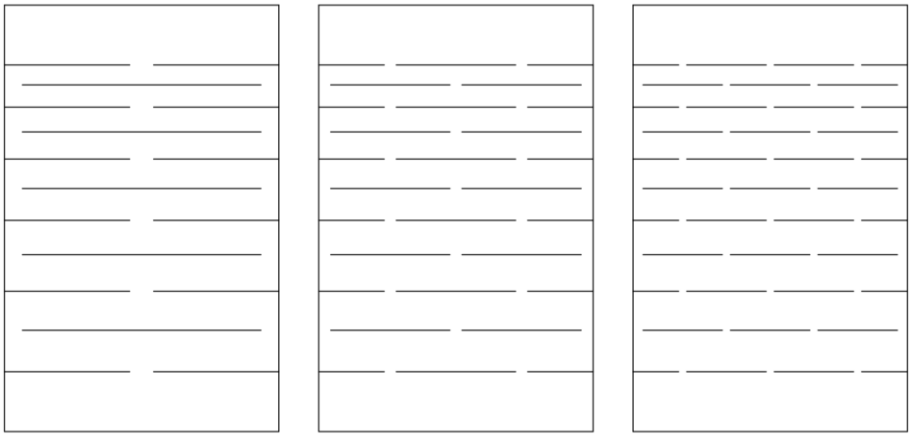

Figure 5.13 Three configurations with later characteristic of variable slit number,

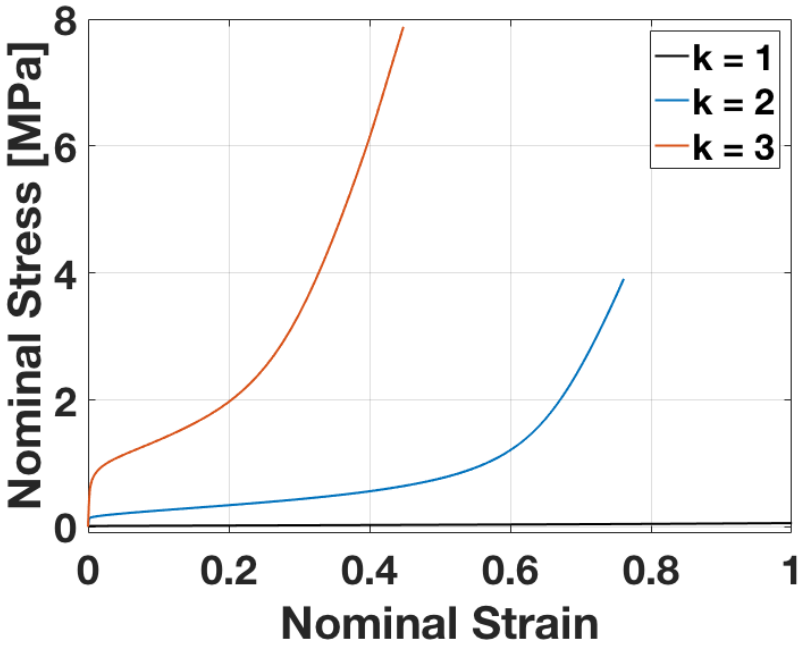

Figure 5.14 The numerically obtained stress-strain curves with diverse later characteristics

We further present a generalized equation to express the patterned non-uniformity:

$$f(x) = \beta \times x^{\alpha} + \gamma \qquad 5.1$$

where x represents the row number of the cut slits, $f(x)$ is the slip gap at the xth row and α is the degree of non-uniformity. Here, we assume $\beta = 0.3$ and $\gamma = 2.2$. When $\alpha = 1$, the corresponding configuration is shown in Figure 5.1. A parametric study was carried out to investigate the effect of varying the non-uniformity factor α on the mechanical properties of the structures. When α deviates from $\alpha = 1$, the slit gaps become more non-uniform, as shown in Figure 5.15. Variation of the α parameter generates diverse non-uniform Kirigami configurations. The stress-strain curves of these non-uniform topologies are shown in Figure 5.16. Their effective modulus is also calculated (Figure 5.17).

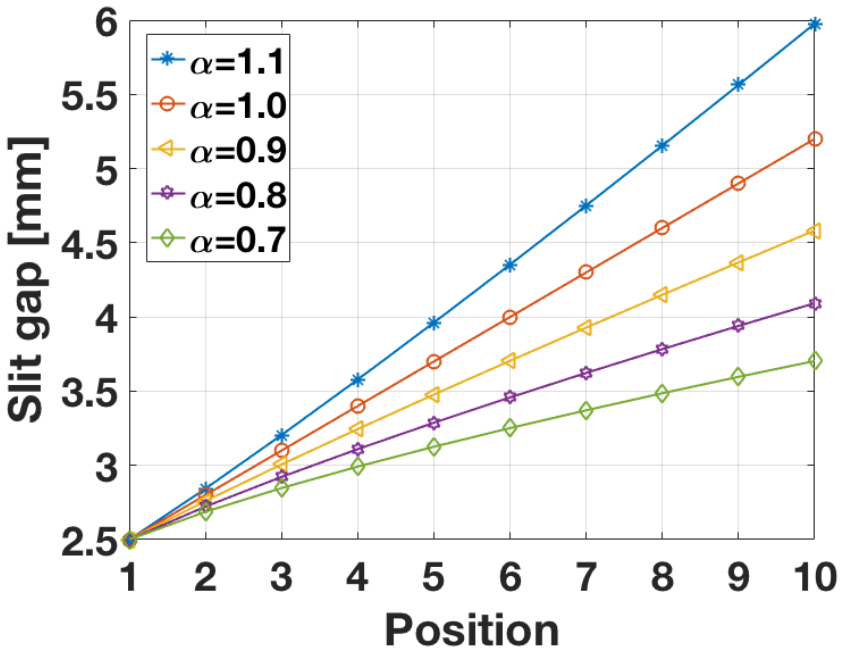

Figure 5.15 The slit gap function with changing non-uniform factor α.

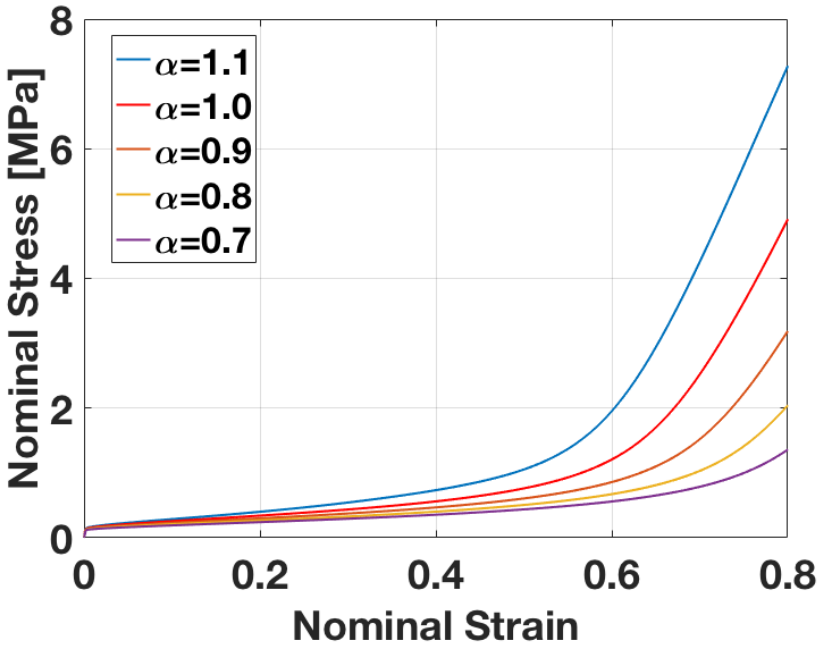

Figure 5.16 The corresponding stress-strain curves with the slit gap function

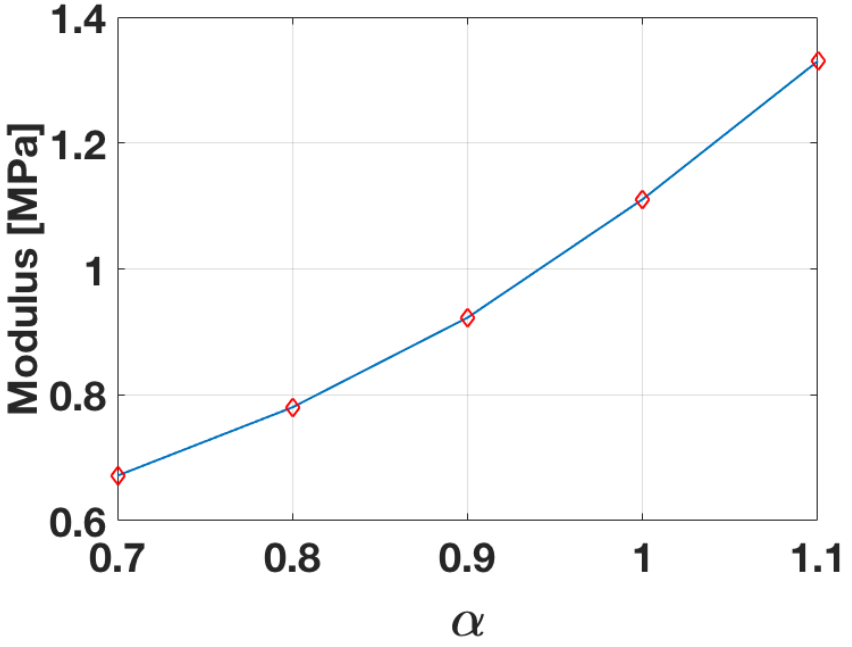

Figure 5.17 The relationship between the effective modulus and the non-uniform factor α ranging from 1.1 to 0.7 based on numerical simulations.

The Kirigami structure with single-graded non-uniformity is further investigated with a FEA simulation of the structural configuration shown in Figure 5.1. The structural deformation and the

principal strain distribution at three global nominal tensile strains (5 %, 15 % and 30 %) are shown in Figure 5.18. As replicated in the experimental tests (Figure 5.19), the out-of-plane buckling first starts from the end of the sample with the smallest slit gap, and gradually moves to the other end featuring the large slit gap.

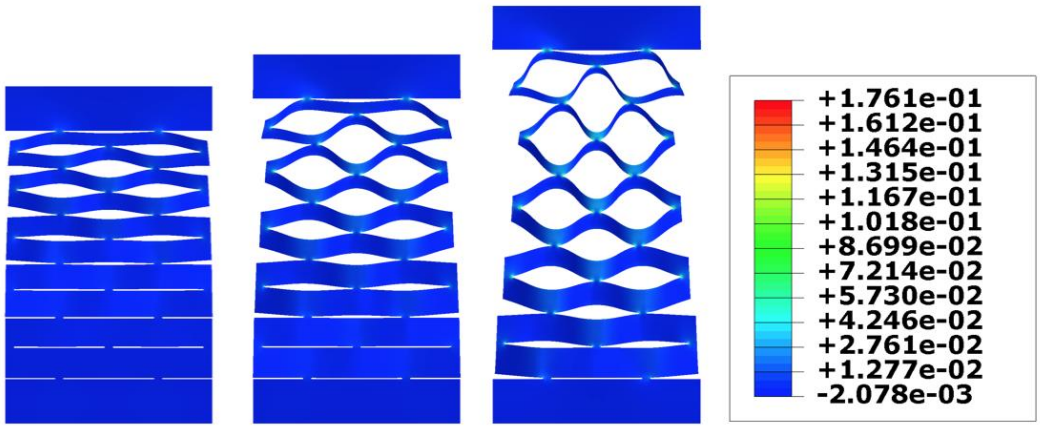

Figure 5.18 The local strain distribution under three stages of nominal strains, 5 %, 15 %, and 30 %.

Figure 5.19 The mechanical behavior of the Kirigami structure in Figure 5.18 under three stages of nominal strain: 5 %, 15 % and 30 %. Scale bar: 5 cm.

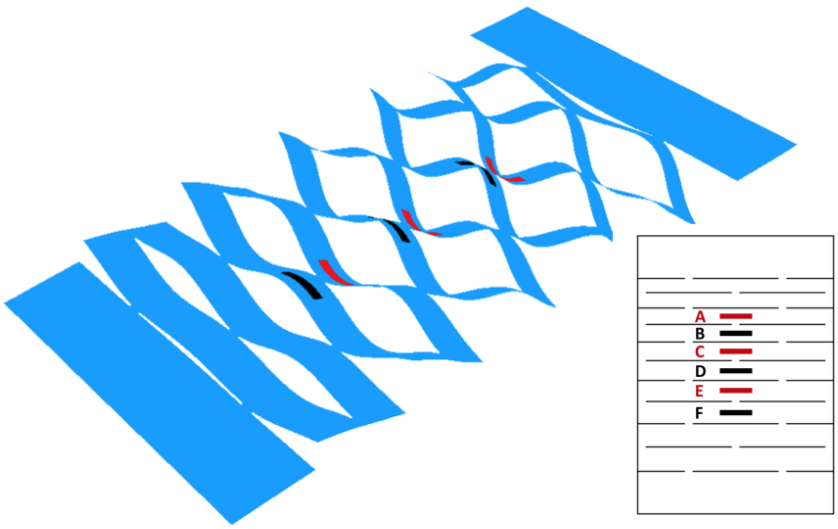

Figure 5.20 The average local strains on six rows of the unit strips

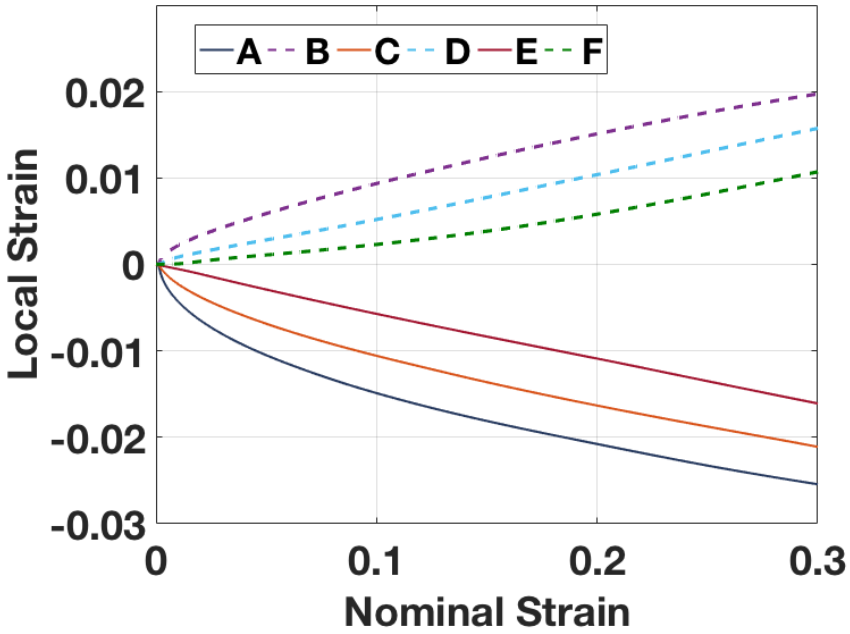

Figure 5.21 The comparison results of the local strain versus the nominal strains.

Because of the gradually changing deformation in the non-uniform Kirigami patterns of cuts, the local strain in each unit strip follows a similar trend as the global external stretching. The average local strain on a central area (5 mm × 1 mm) in each buckled unit strip was calculated and used as an indicator to compare the local strain change. Six unit-strips shown in Figure 5.20 are selected, categorized into two groups, A, C, E, and B, D, F depending on their direction of curvature. As observed in Figure 5.21, the simulation results validate the expected strain changes: the local strains

in the buckled strip with the small slit gap (A, B), either in tension or compression are higher than those with the larger slit gap (E, F). Following this analysis, a 3D solid element-based FEA study considering piezoelectric materials properties has been conducted. The structure here consists of two layers, one substrate of 125 μm thick PET bonded to a second layer of 28 μm thick PVDF. The open-circuit voltage was measured along the three positions, A, C, and E in Figure 5.20. The voltage outputs show a nonlinear relationship with the nominal strain (Figure 5.22) due to large deformations of Kirigami induced buckling, and as a result of the sequential deformation induced by the non-uniform patterns of cuts, the voltage in Position A with narrow slit gap is larger than those in Position C and E with medium and wide respective slit gaps.

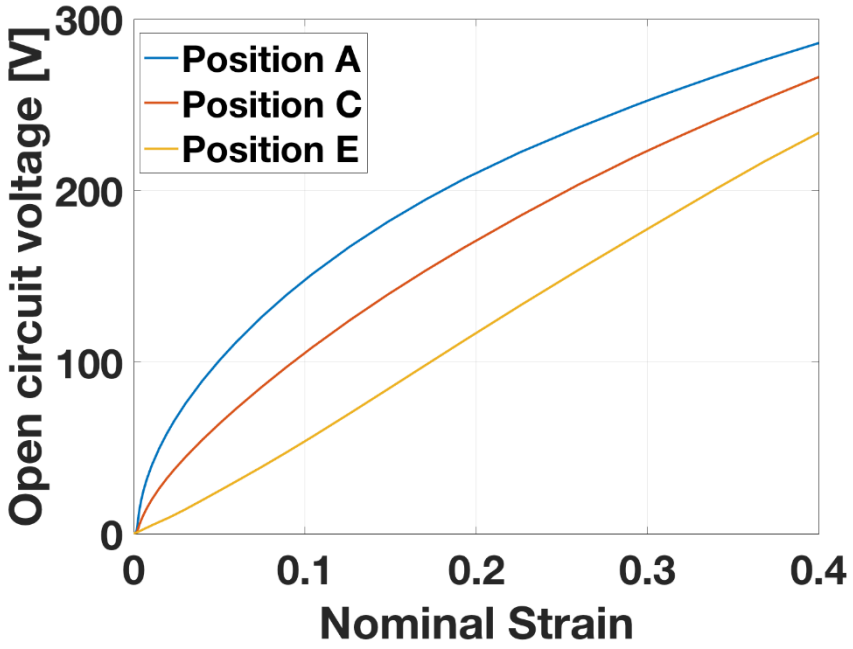

Figure 5.22 The comparison of the open circuit voltages in three positions with narrow, medium, and wide slits gaps, as shown in Figure 5.20.

5.4 EVALUATION OF NON-UNIFORM KIRIGAMI PIEZOELECTRIC STRUCTURE

The sequentially structural behavior of the non-uniform Kirigami structure has potential applications in stretchable electronics. To demonstrate this, we fabricated a non-uniform Kirigami stretch sensor by bonding thin piezoelectric films (28 μm thick PVDF) onto the above Kirigami design to study its performance under cyclic stretching. We designed and fabricated three PVDF strips with novel interconnecting electrode patterns and laminated them on the PET based Kirigami structure, as depicted in Figure 5.23. The Kirigami parameters are L = 32 mm, m = 3.2 mm, w = 6 mm, Δt = 0.6 mm, k = 2, h = 125 μm, and the corresponding non-uniformity in

Equation 5.1 are $\alpha = 1$, $\beta = 0.6$ and $\gamma = 5.4$. Based on the position of the row, these three PVDF films are integrated with the PET strips with narrow, medium, and wide slit gaps respectively. Due to the strain distribution on the buckled strip, the inter-segment electrode pattern in Figure 5.24 is adopted as the reference voltage output generator to avoid charge cancellation effects. These three PVDF strips are connected to separate oscilloscope inputs to record voltage change under cyclic straining.

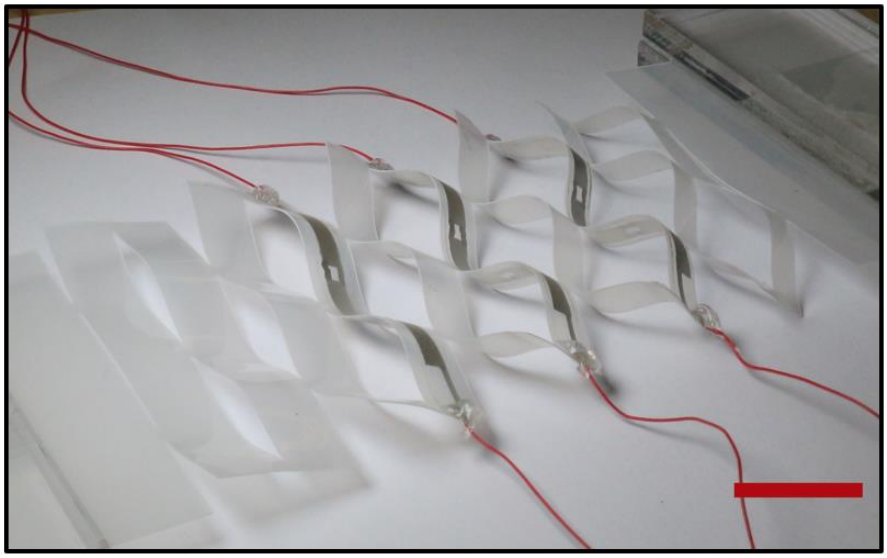

Figure 5.23 The piezoelectric sensing system based on the non-uniform Kirigami platform. Three pieces of PVDF film are bonded on the rows with slit gaps of 7.2 mm, 8.4 mm, and 9.6 mm respectively. The control parameters are L = 32 mm, m = 3.2 mm, w = 6 mm, Δt =0.6 mm, scale bar: 2 cm.

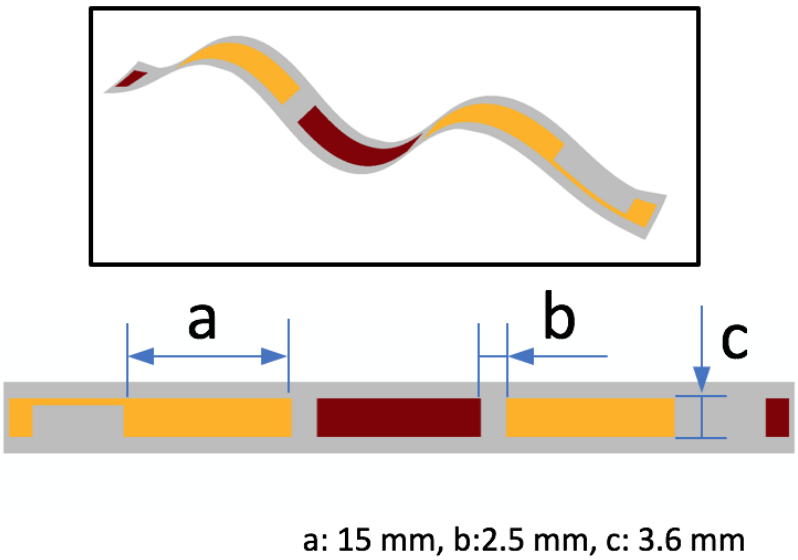

Figure 5.24 The inter-segment electrode patterns within one-unit strip of the piezoelectric films.

A series of dynamic tests using an Instron machine was performed for the evaluation of the sensing system under different loading conditions. A range of nominal global strains from 5 % to 15 % was applied to the Kirigami structure. The voltage outputs of the medium-width PVDF strip under the three nominal strains and 2 Hz are summarized in Figure 5.25(a). The voltage amplitude increases with nominal strain. A comparative study has also been performed to analyze the output of the PVDF strips in the three rows (narrow, medium and wide, Figure 5.25(b)). All three PVDF sensors provide a similar quasi-linear relationship between the voltage output and external strains. The sensing performance under 10 % tensile strain with various frequencies was also investigated at a constant nominal strain of 10 %. The amplitude of the voltage output also shows an increase as the frequency increases (medium strip, Figure 5.26(a)). For the three PVDF strips, the voltage outputs show a linear relationship with the applied frequencies ranging between 1 Hz and 3 Hz (Figure 5.26(b)). The relationship between the voltage outputs in the three PDVF strips with narrow, medium, and wide slit gaps was further investigated. The voltage output in the time domain at a strain amplitude of 5% and frequency 2 Hz is described in Figure 5.27(a). The outputs from these three areas are in phase, and one can observe a quasi-linear relationship between the voltage output and slit gaps (Figure 5.27(b)).

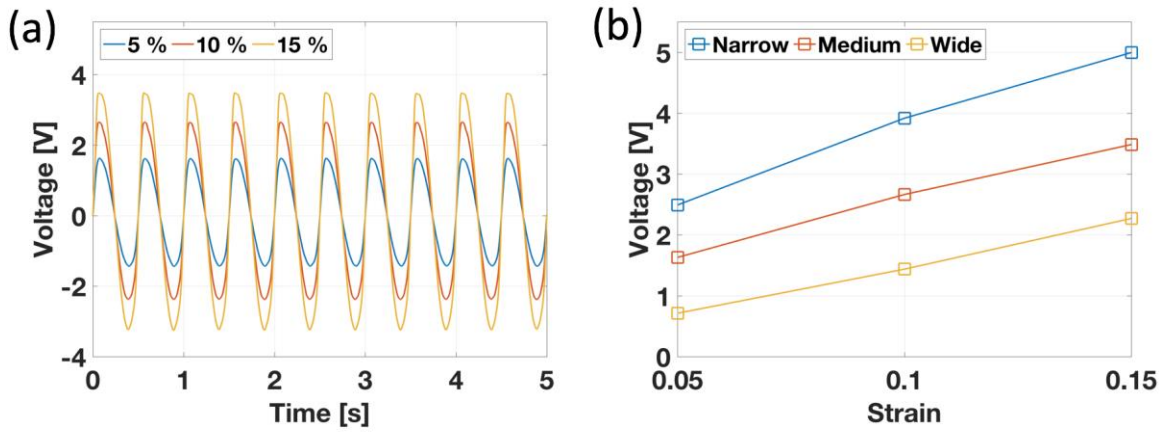

Figure 5.25 (a) The voltage response in time domain of the piezoelectric sensing system under a given frequency of 2 Hz and a nominal strain range from 5 % to 15 % for the row with medium slit gap of 8.4 mm, and (b) the effective sensitivity for the three rows with slit gaps of 7.2 mm, 8.4 mm, and 9.6 mm respectively.

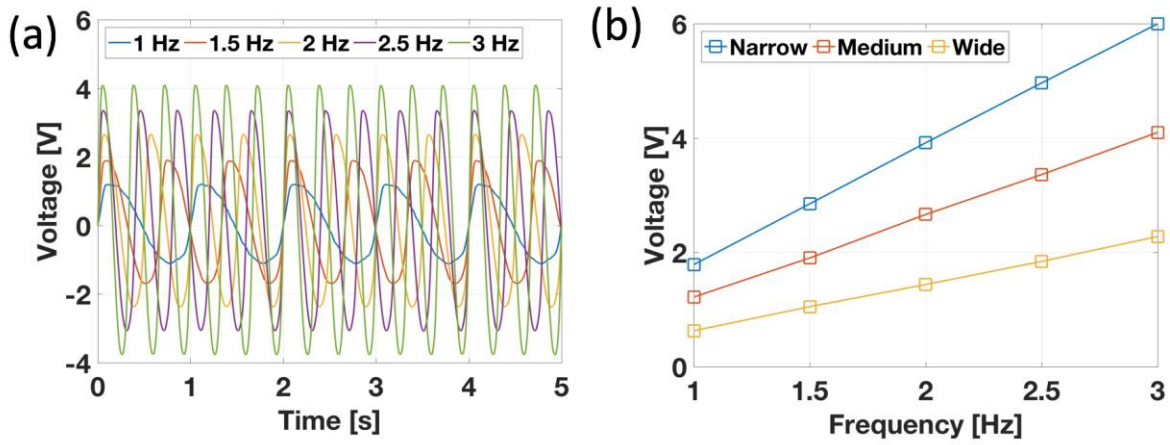

Figure 5.26 (a) The voltage response in time domain of the piezoelectric sensing system under a nominal strain of 10 % and various frequencies from 1 Hz to 3 Hz for the row with medium slit gap of 8.4 mm, and (b) the effective sensitivity for the three rows.

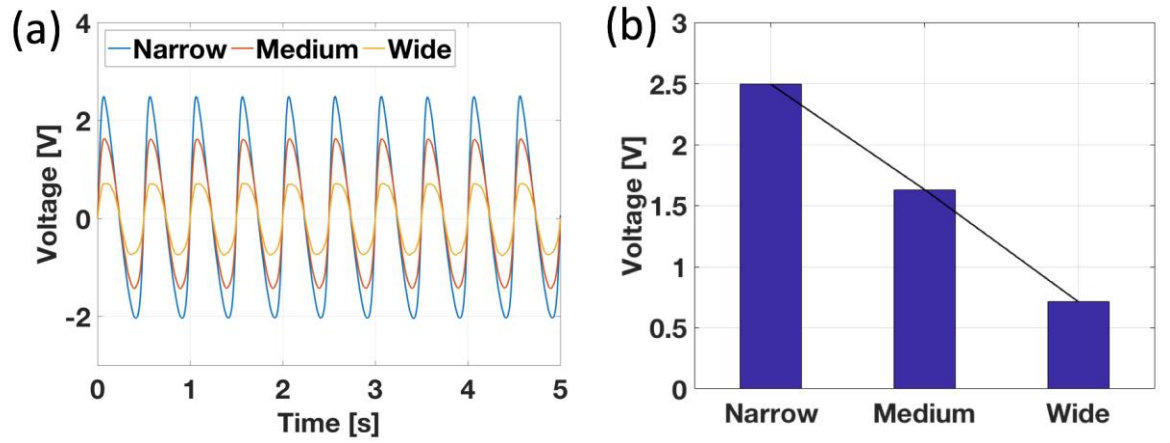

Figure 5.27 (a) The voltage response in time domain for the three rows under the nominal strain 5 % and the frequency of 2 Hz, and (b) a corresponding quasi-linear relationship between the voltage outputs and the slit gaps.

5.5 CONCLUSIONS

This chapter proposes a novel mechanical metastructural system based on non-uniform patterns of Kirigami cuts. With combined numerical and experimental analysis, the relationship between the structural behaviors and the non-uniformity of the Kirigami structure was investigated, and we demonstrated that the mechanical stiffness and spatial deformation of the non-uniform Kirigami structure could be tuned by the optimization of the configurations and parameters. Compared with conventional uniform Kirigami patterns, the non-uniform Kirigami structure provides additional non-uniformity parameters to tune the structural performance and spatially controlled deformation to match the situations where non-uniform deformation is required. This proposed platform based on simple-to-fabricate metastructures opens up new opportunities for stretchable sensing systems with tunable sensitivity covering a wide range of strains by the simple integration of sensing components at given areas within the structure. A piezoelectric sensing system was developed, validating the spatially changing properties of the non-uniform Kirigami structure through a series of dynamic tests. The current study is focused on simple linear Kirigami cuts with non-uniform patterns, and other non-uniform Kirigami cuts, such as orthogonal, diagonal and curved, are promising directions for future research.

CHAPTER 6 - TUNABLE VIBRATION ENERGY HARVESTER BASED ON 3D ARCHITECTED METASTRUCTURES

Energy harvesting from surrounding sources shows potential as an emerging technique to supply sustainable power. Vibration, a ubiquitous energy source in daily life, feature low frequency and directional randomness. Existing approaches reveal challenges to develop desirable energy harvesting systems that can efficiently scavenge the surrounding vibrations. The concepts presented in this work overcome these limitations, to establish 3D tunable systems for multi-directional vibration energy harvesting within a broad frequency range. Inspired by Kirigami-based designs, a cost-effective fabrication technique using compressive buckling is used to explore sophisticated 3D architectures and functional devices. The proposed system is capable of scavenging vibrations within wide frequency range and in multiple directions. A variety of 3D configurations and tunable dynamic performances can be easily achieved by the Kirigami technique. Successful demonstrations have shown the advantages of the proposed energy harvesting system.

6.1 INTRODUCTION

Energy harvesting techniques have been receiving tremendous attention in recent decades for promising applications in various emerging areas, including implantable biomedical devices [283], wireless sensor networks [284] and wearable electronics [285]. Various energy forms from the environment have been considered for harvesting, such as electrochemical [286], thermal [203], radio frequency [287], solar [288], and vibration sources [289]. Vibration in particular constitutes a ubiquitous source of energy, being found during human daily activity, wind flow, ambient noise, vehicle transportation and many other man-made activities. Vibration energy harvesting has been evaluated and exploited over decades to achieve vibration-to-electricity conversion. Mechanisms associated to electromagnetics [290], electrostatics [291], and piezoelectricity [292] have been used. The piezoelectric transduction effect, converting random vibration into electric voltage, is particularly adopted due to its scalability, simple architecture, and high energy generation efficiency [293]. These characteristics make piezoelectric energy harvesting appealing for wide applications in the areas of self-powered sensing systems [23].

A simple and extensively studied example of piezoelectric generator is the cantilever-type piezoelectric vibration beam [294]. This type of energy harvester relies on exploiting the dynamic deformation of the cantilever at resonance. The first bending mode of the cantilever is normally used for energy harvesting purposes, while higher-order modes are usually ignored due to low response amplitude. Environmental vibrations, however, are intrinsically random in directions and broadband. The mismatch of the resonant frequency between the energy harvesting system and the vibration drastically reduces the power output. The above singe-degree-of-freedom (SDOF) system cannot cover the frequency range of environmental vibrations because of its narrow bandwidth. To overcome this limitation, various approaches have been explored so far to increase the power output [295]. Multiple-degree-of-freedom (MDOF) concepts are promising to efficiently broaden the bandwidth. State-of-art technologies in energy harvesting can be categorized into magnetic coupling [296-298], mechanical coupling [299-303], and combinations of the two [304-306]. Although these MDOF harvesters can increase the operational bandwidth, they usually scavenge energy along a single direction only, therefore reducing energy harvesting efficiency in multi-directional environmental vibrations. There is therefore a need for more effective multi-directional and broader-bandwidth energy harvesting structures.

One route to better harvesters is through the extension or projection of planar structures into the third dimension. 3D architectures can be mechanically assembly by compressive buckling [244], and this design and manufacturing route can be used for potential applications related to soft electronics [199], microrheological devices [307], and the precise characterization of thin polymer

films [308]. Mechanically-assembled buckled systems can also offer broader bandwidth and resonance frequency tunability [309], and provide a novel type of vibration platform with potential applications into more efficient multi-directional energy harvesting.

In this chapter, we propose a 3D structurally tunable platform for multi-directional vibration energy harvesting based on 2D-to-3D assembly by compressive buckling. The 3D platform described here allows for a mechanical coupling between multiple parts of the structure, thereby delivering a multi-modal and MDOF system. The assembled 3D metastructure provides routes to improve the operational bandwidth and energy harvesting performances in the presence of multi-directional vibrations. An optional Kirigami cut pattern is applied to the buckled ribbon that is induced during compressive assembly to further enhance the dynamic performance. Modal analysis using finite element method is performed to investigate the proposed 3D metastructures, and the structural response is verified by comparing the numerical results with data from a series of vibration tests. The tunable properties are also evaluated for different pre-strains to the compressive buckling and by changing the topology of the Kirigami cut pattern. A comparative study between the proposed 3D metastructures and conventional planar systems is carried out. 3D piezoelectric energy harvesters based on the proposed metastructure design are fabricated and tested under multi-directional vibration loading. Finally, the performances of the proposed energy harvesting devices are evaluated for wind energy harvesting under a range of wind directions and air speeds.

6.2 DESIGN AND EXPERIMENTAL SETUP

6.2.1 Device design and description

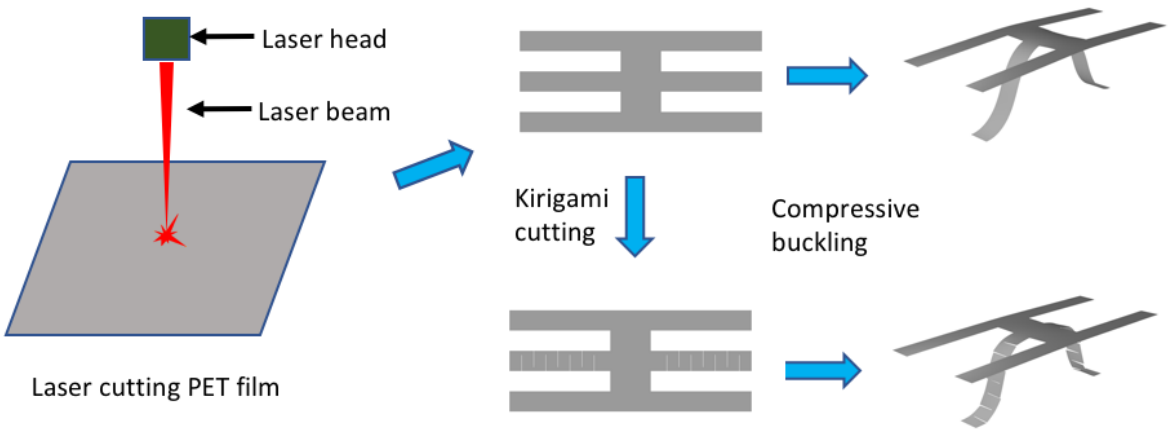

Figure 6.1 Schematic of the mechanical assembly of 3D structures through a compressive buckling process. Two types of platforms with and without Kirigami cuts on the buckled beams.

The 3D metastructures developed here are based on the mechanically assembly of 2D planar structures subjected to compressive buckling. The configuration can be designed and patterned in its 2D precursors using techniques including photolithography and laser cutting. The 2D pattern is then locally translated in the 2D plane, causing it to buckle at pre-determined points into a 3D structure. As depicted in Figure 6.1, the proposed 3D energy harvester platform is developed from patterning planar polyethylene terephthalate (PET) films by laser cutting, which is then assembled into pre-defined 3D configurations through controlled compressive buckling.

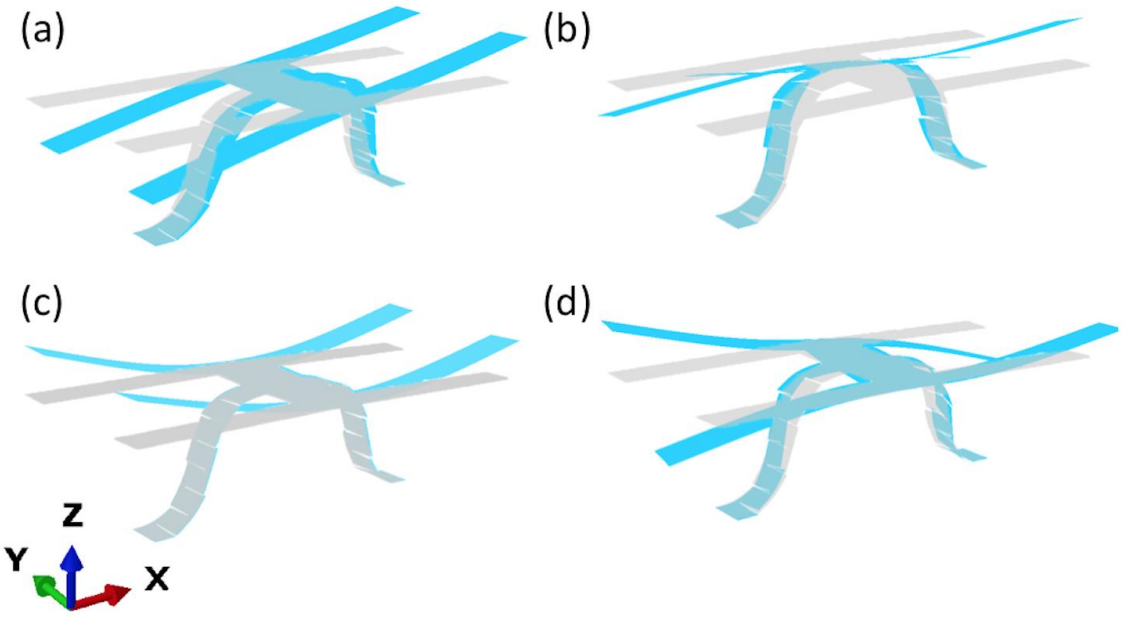

Figure 6.2 The representative mode shapes in multi-directions. (a) and (b) in-plane translational vibration in orthotropic directions, (c) vertical translational vibration, (d) torsion vibration along the vertical axis.

In our proposed configurations, four cantilever beams are mechanically coupled with each other through a central bridge which has been compressively buckled. This design enables the coupled beams to provide a compact MDOF energy harvesting system, and it also improves the broadband performance of conventional MDOF systems made from independent cantilever beams. In addition, the proposed system can also capture vibration energy from multiple directions in three dimensions due to the presence of the buckled 3D structures. Compared with planar systems, the proposed 3D structures can be designed to be particularly sensitive to multi-directional ambient vibrations. Four representative vibration modes of the 3D buckled structure with patterned Kirigami cuts on the buckled beams are presented in Figure 6.2. The three modes

in Figure 6.2(a)-(c) can be excited by vibrations from three orthogonal directions, while the mode in Figure 6.2(d) can be excited by torsion motions about the z axis. These characteristics demonstrate that the proposed 3D tunable system has the potential to be applied for multi-directional and multi-modal vibration energy harvesting.

6.2.2 Experimental setup

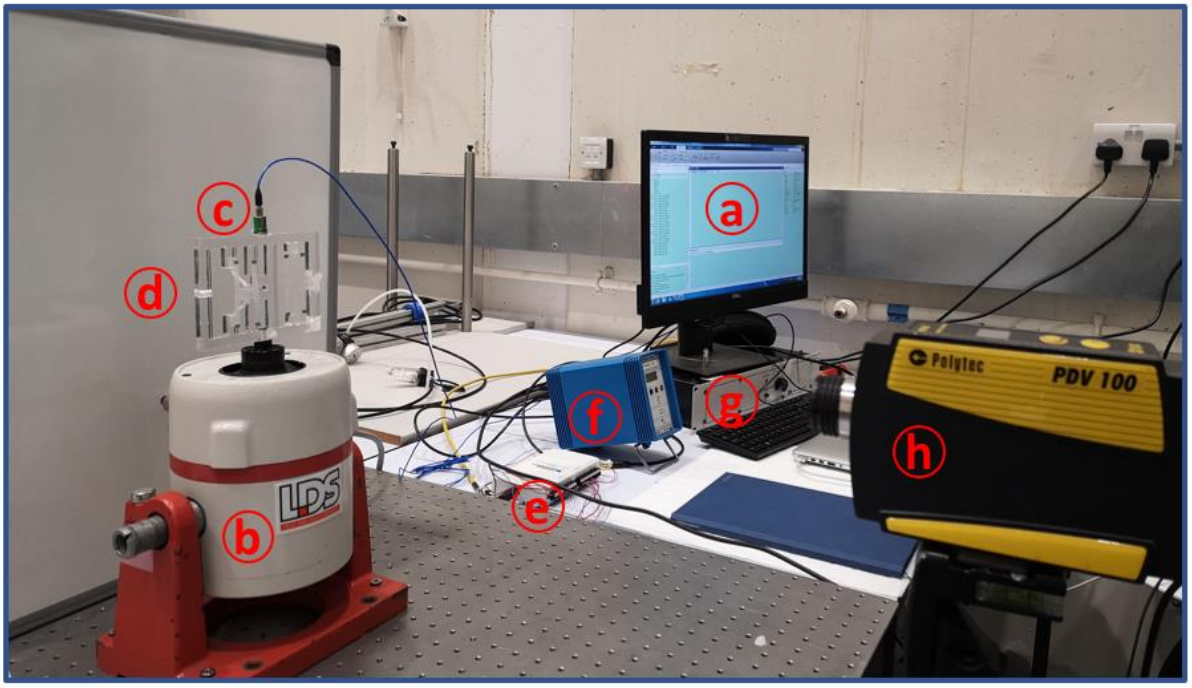

Figure 6.3 Platform setup for the vibration test of the proposed 3D tunable energy harvesting structures. (a) computer for system control and data recording, (b) vibration shaker, (c) accelerometer, (d) the acrylic base with the test structure mounted on it, (e) NI USB-6211 data acquisition device, (f) signal coupler, (g) shaker power amplifier, and (h) laser vibrometer.

A vibration platform is set up to evaluate the dynamic performances of the 3D MDOF systems and the voltage outputs of the fabricated energy harvesters, as shown in Figure 6.3. The 3D metastructures are bonded onto an acrylic base plate, which is then mounted on top of a shaker (LDS shaker system) that provides the base excitation. An accelerometer (PCB Piezotronics 333M07) is placed on the acrylic plate for the measurement of the base accelerations. The vibration shaker is controlled by the signal produced by a multifunction I/O device (NI USB-6211) and amplified by a power amplifier (LDS PA25E).

For the dynamic analysis of the 3D metastructures, a single-point vibrometer (Polytec PDV-100) is used to capture the structural velocities during the dynamic tests. The accelerometer output is

firstly processed through a signal coupler (Kistler 5134), and then measured by a data acquisition device (NI USB-6211). The signal from the laser vibrometer is directly connected to an input channel of the same card. A custom Matlab (R2017b) script is used for control and signal processing.

For the electrical performance evaluation, the generated voltage of the 3D energy harvesting system is recorded by a multi-channel oscilloscope (PicoScope 2405A). A sinusoidal waveform with controlled amplitude is generated by the NI USB-6211 card to excite the vibration shaker with sweep frequencies at different acceleration levels. The voltage outputs of the energy harvester under a frequency sweep test are investigated.

For the evaluation of wind energy harvesting, an electric fan is used to generate different levels of wind speeds, recorded by an anemometer (Sealey TA070). The voltage outputs of the system at different levels of air flow and different directions are recorded by the oscilloscope.

6.2.3 Device fabrication

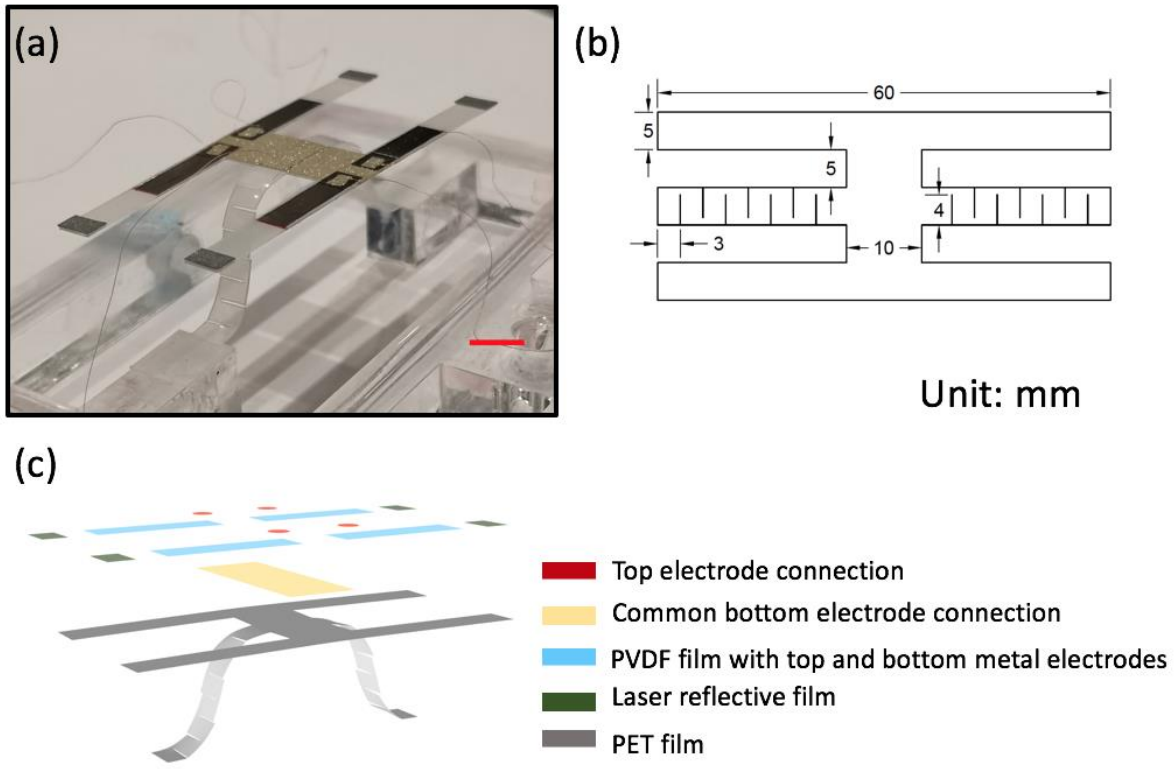

Figure 6.4 (a) the 3D vibration energy harvester with Kirigami cuts on its buckled beams. Scale bar: 10 mm. (b) the dimension of the 2D precursors. (c) the schematic illustration of the integrated energy harvesting system.

We adopt here a direct and facile method to fabricate the 3D metastructure and the energy harvester based on it. The substrate is a PET film with a thickness of 125 μm, and the 2D configuration is designed using Auto CAD (Autodesk 2018). The PET film is cut into the designed

layout by a laser engraver (Speedy 100). An acrylic plate is then cut with mounting pads for the PET film arranged such that the desired compressive buckling is induced when the film is bonded to the frame at those points. Additional Kirigami patterns can be made on the two middle of the PET beams by the laser engraver. The beams are then buckled to assemble into a 3D configuration. A piece of laser reflective film (5mm × 3mm, Testo Reflective Tape) is bonded on the tip of each of the four cantilever beams to enhance the scatter of the laser from the vibrometer.

In order to turn the PET structures into an energy harvester, an electrically conductive adhesive (3M 9707) is firstly bonded onto the middle area of the PET substrate as a common bottom electrode. Four PVDF films (28 μm of thickness, 16 mm × 4 mm, electrodes: 70 nm / 10 nm of copper / nickel, TE Connectivity) are cut using a die-cutting machine (Cricut Explore Air 2) then bonded onto each of the four cantilever arms using acrylic adhesive (3M 7952MP). Copper wires are connected with the top electrode of the PVDF film using silver conductive paint (Electrolube, SCP03B). A second wire is connected to the common bottom electrode.

The cutting of Kirigami patterns and the integration of PVDF films are performed on the 2D precursors. The planar structure is assembled into a defined 3D configuration by compressive buckling under different pre-strains and by bonding the structures onto the specified areas of the acrylic plate. Figure 6.4 shows the precursor dimensions, laminar components and fully assembled 3D structure.

6.3 Results and Discussions

6.3.1 Vibration mode analysis

In this work, we propose two types of metastructure platforms for the energy harvester: a 3D buckled structure and a modified 3D configuration with additional Kirigami cut patterns. Numerical simulations using finite element method are performed to study the dynamic characteristics of the structures. A 2D shell element (S4R) model in Abaqus (Abaqus/Standard 6.14) is used for the models with PET material properties (density 1.38 g/cm^3, modulus 6980 MPa, Poisson ratio 0.44, and thickness 125 μm). Two main steps are defined in the simulation study: a static analysis to transform the planar structure into its 3D configuration, followed by a frequency analysis of the buckled 3D structure.

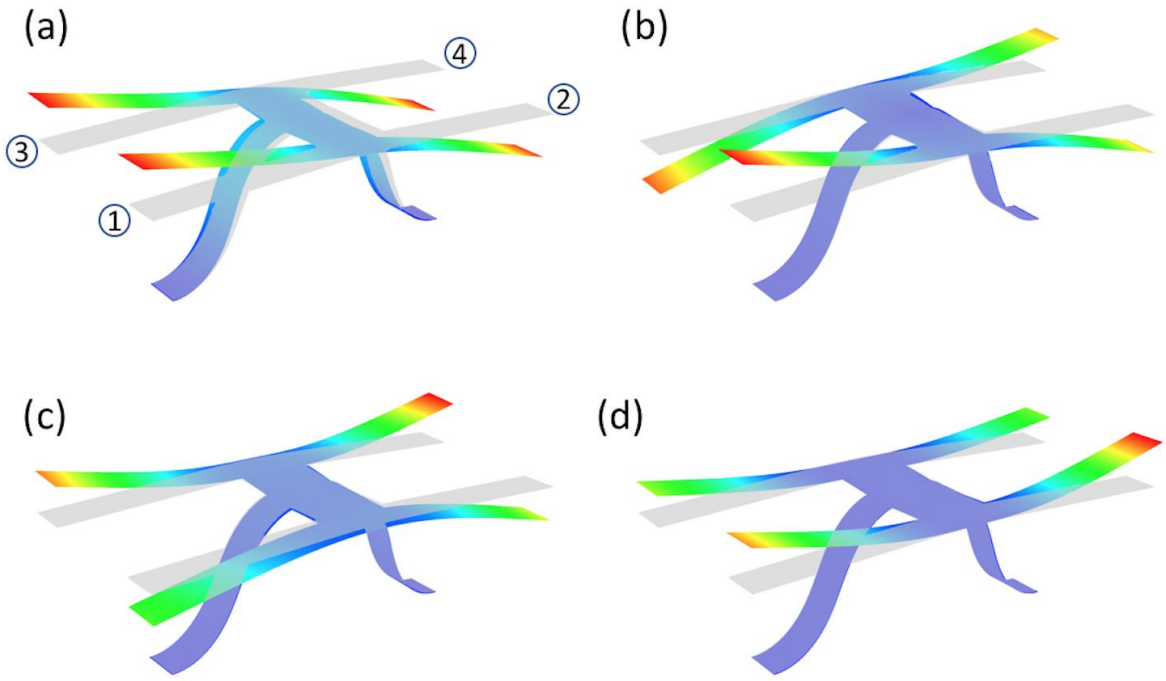

Figure 6.5 The modal analysis of the 3D bucked structure without Kirigami cuts. The four cantilever beams are mechanically coupled with each other in the first four resonant modals (a)-(d) in the low frequency range below 50 Hz.

As shown in Figure 6.5, the 3D buckled structure without Kirigami cuts possesses the first four modes at low frequency range (1 - 50 Hz). The four cantilever beams are coupled with each other, and that generates diverse vibration modes within this low frequency range. The behaviors of these coupled beams in different positions are either in phase or counter phase with each other. In the first and second modes, the beams in positions 1 and 2 deform in counter phase, while they are in phase for the third and fourth modes. However, the beams in positions 1 and 3 deform in phase in the first and fourth modes, and in counter phase in the second and third modes.

A similar study is performed on the modified 3D metastructures (Figure 6.6). We define a linear Kirigami cut pattern on the buckled beams to further tune the dynamic performances of these 3D structures. In this case six vibration modes occur within the same frequency range (1 Hz to 50 Hz). The introduction of the Kirigami cuts triggers a higher number of normal modes and reduces the resonant frequencies of the system, compared with the structure without Kirigami cuts. The modified structure also features clear vibration modes in different directions: translational modes (the 1st mode in the x axis, the 2nd and 6th modes in the y axis, and the 5th mode in the z axis) and torsion modes (the 3rd and 4th modes in the z axis). These results show that the presented 3D metastructure provides a desirable platform to harvest vibrational energy with broad frequency

bandwidth and along multiple directions. It is also evident from the modal analysis that the voltage generated from each piezoelectric film should be scavenged individually to avoid charge cancellation effect caused by the phase inconsistence in the resonant modes.

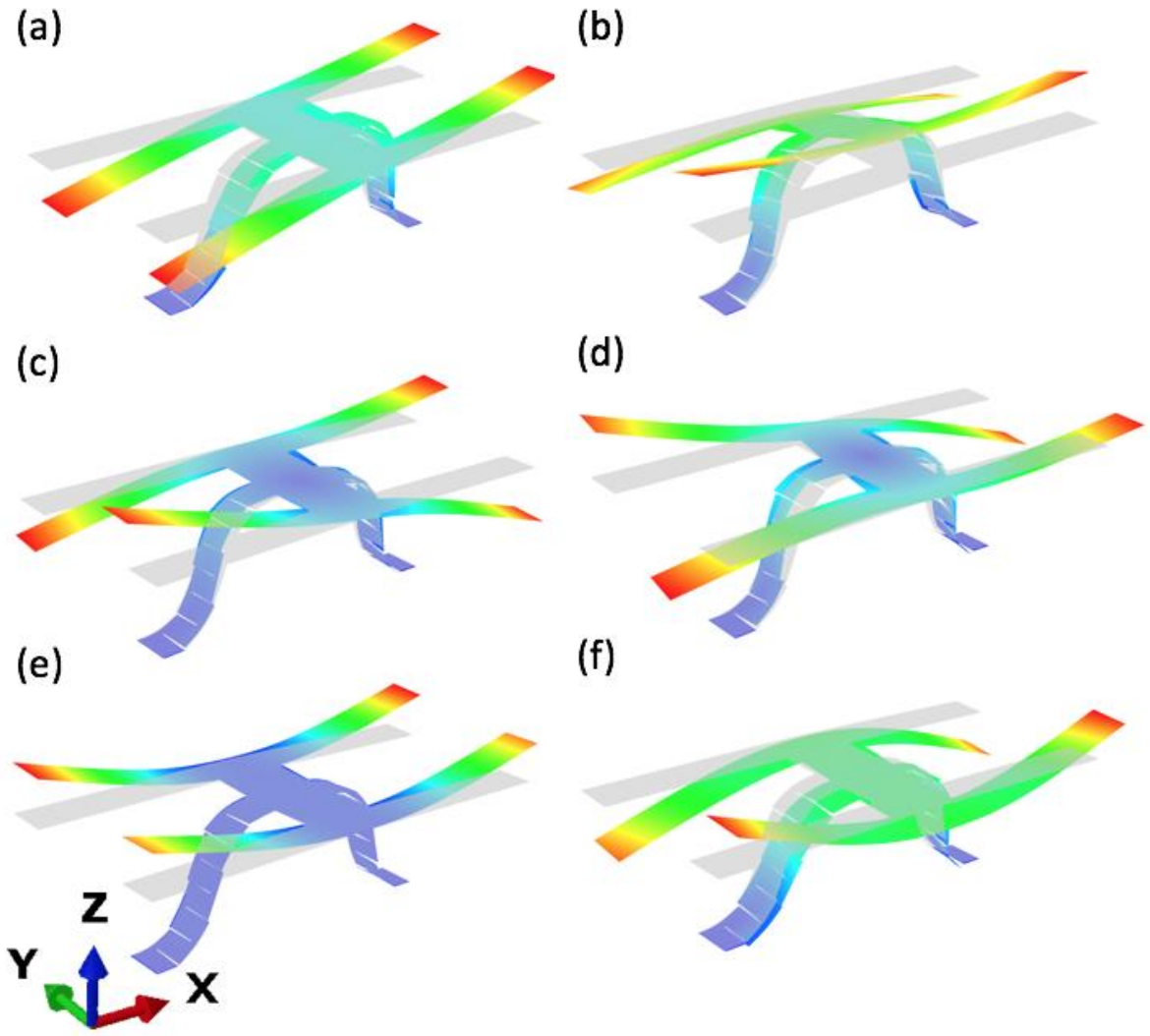

Figure 6.6 The modal analysis of the 3D bucked structure with Kirigami cuts on the buckled beams. The four cantilever beams are mechanically coupled with each other in the first six resonant modals (a)-(f) in the low frequency range below 50 Hz.

6.3.2 Measurement of structural characteristics

A series of vibration tests have been carried out to verify the simulation study and validate the feasibility of the presented designs by comparing the structural performances of the proposed 3D metastructure with those of conventional planar systems.

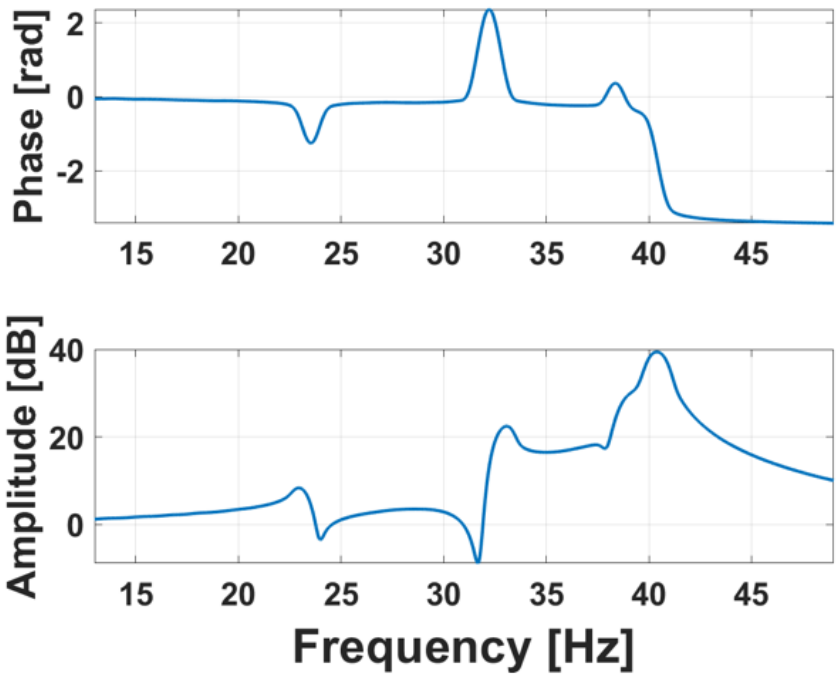

Figure 6.7 The phase and amplitude of the structural transmissibility for the 3D buckled structure without Kirigami cuts.

Table 6. 1 The comparison of natural frequencies for the buckled structure without Kirigami cuts between numerical simulation and tests. The frequency range is between 1 Hz and 50 Hz.

Mode	FEA	Test
1	24.9 Hz	24 Hz
2	33.9 Hz	32 Hz
3	38.2Hz	38 Hz
4	39.6 Hz	40 Hz

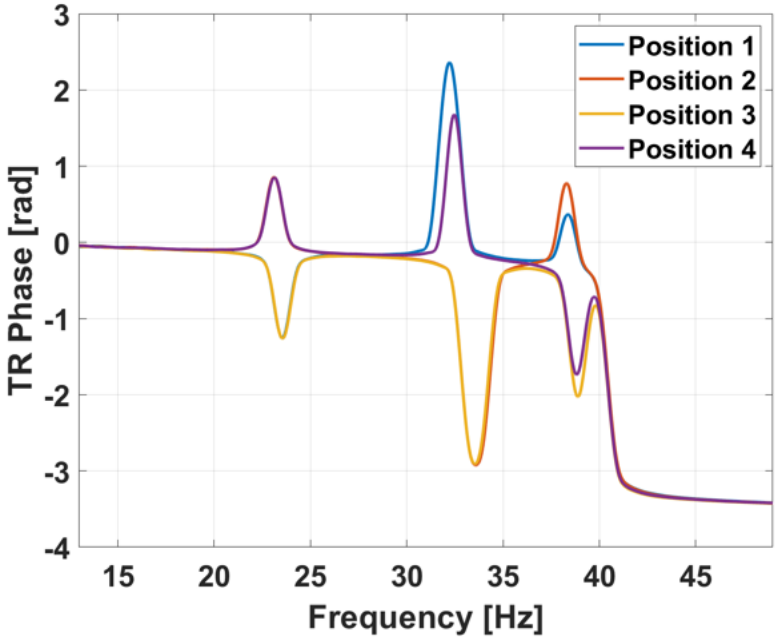

Figure 6.8 The phase of structural transmissibility in four cantilever beams for the 3D buckled structure without Kirigami cuts

We firstly evaluated the performances of the 3D buckled structure without Kirigami cuts. Modal analysis has been carried out by evaluating the vibration transmissibility (TR) of the structures. The transmissibility is measured between the accelerations of the shaker base and the beam tips. The shaker is excited by a frequency sweep from 1 to 50 Hz and an increment of 0.3 Hz/s. Its acceleration is sensed by the accelerometer placed on the shaker base. The velocity of the beam tips is measured by a laser vibrometer. It is numerically converted into acceleration before the transmissibility calculations. As shown in in Figure 6.7, the Bode plot of the transmissibility along the z direction confirms the results from the simulations: four resonant modes are present between 1 and 50 Hz, with the predicted natural frequencies comparing well with the experimental results (Table 6. 1). The phase extracted from the experimental TR (Figure 6.8) also validates the prediction from the simulations, i.e. the coupled beams deform either in phase or counter phase in the different resonant modes. To demonstrate the superior performances of our platform under multi-directional vibrations, a series of vibration tests were carried out. The position of the shaker remained the same while the acrylic base was adjusted to apply three orthogonal directional vibrations to the structures, as shown in Figure 6.9. The same input as the previous TR test (sweep frequency and amplitude) were applied on the shaker. Figure 6.10 shows the results of the structural transmissibility under the three directional vibration excitations. The 3D buckled

metastructure can generate significant output in both x and y directions, while the output along z direction dominates. For the x directional vibration, the structure also induces higher amplitudes and a lower resonant frequency compared to that along the y axis.

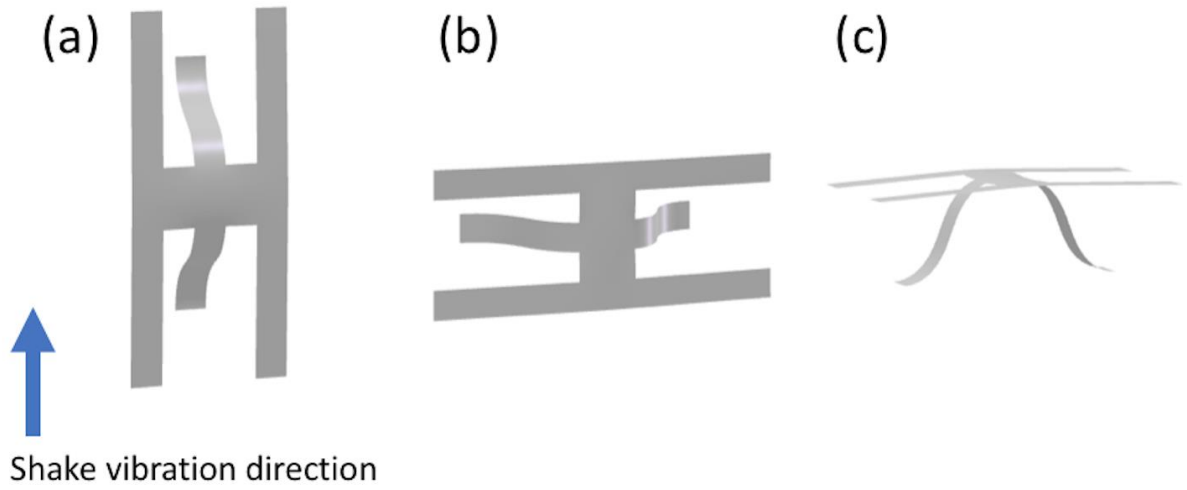

Figure 6.9 The setup for multidirectional vibration test of the 3D buckled structures. (a) x-directional vibration, (b) y-directional vibration, (c) z-directional vibration.

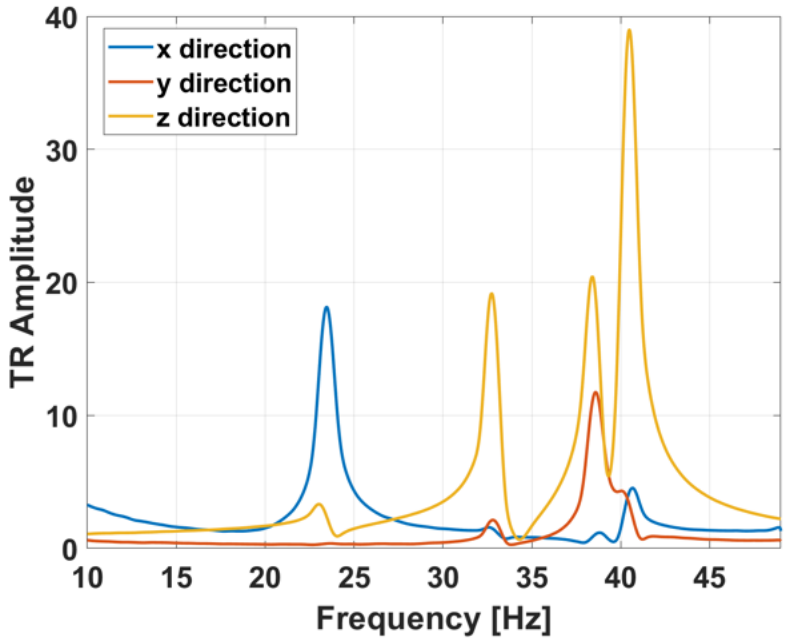

Figure 6.10 The structural characteristics of the 3D buckled structure without Kirigami cuts in multi-directional vibrations.

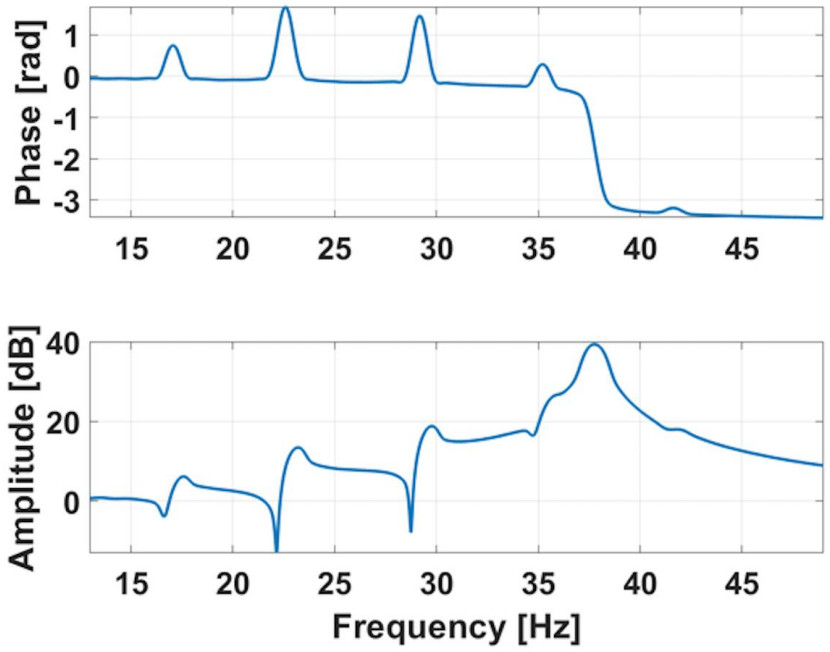

Figure 6.11 The phase and amplitude of the structural transmissibility for the 3D buckled structure with Kirigami cuts.

Table 6. 2 The comparison of natural frequencies for the buckled structure with Kirigami cuts between numerical simulation and tests. The frequency range is between 1 Hz and 50 Hz.

Mode	FEA	Test
1	18.9 Hz	17 Hz
2	24.1 Hz	23 Hz
3	30.5 Hz	29 Hz
4	37.5 Hz	35 Hz
5	37.6 Hz	38 Hz
6	43. 3 Hz	42 Hz

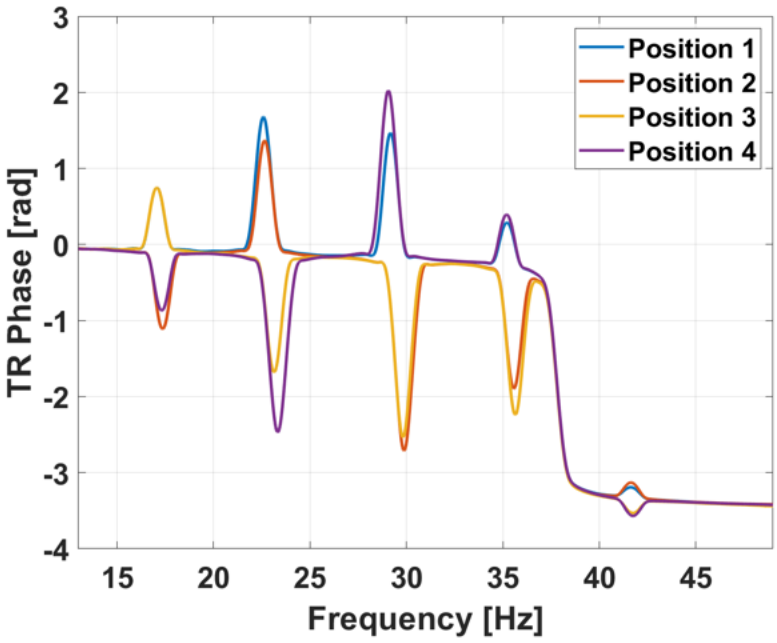

Figure 6.12 The phase of structural transmissibility in four cantilever beams for the 3D buckled structure with Kirigami cuts.

A similar study was performed on the modified 3D metastructure with additional Kirigami cuts. As demonstrated by the numerical simulations, the structural transmissibility of the modified structure exhibits a more diverse modal behavior compared to the 3D structure without Kirigami cuts. Six vibration modes are clearly present in the experimental Bode plot ((Figure 6.11). Table 6. 2 shows the comparison of natural frequencies between the tests and numerical simulations, and the results match well. The phase differences in the four beams in different modes also exhibit similar relationships, either in phase or counter phase (Figure 6.12). The modified 3D metastructure also shows advantages in terms of transmissibility, and the structure can generate comparable transmissibility magnitudes along the three directions, as shown in Figure 6.13. Vibrations along the x direction have the highest amplitudes at low frequencies. Higher amplitudes at high frequencies are observed in vibrations along the z direction, while two transmissibility peaks are observed in the y directional vibrations at the low (approx. 23 Hz) and high (approx. 42 Hz) ends of the frequency spectrum. A comparison between the 3D structure with and without the Kirigami cuts is also reported in Figure 6.14. The introduction of the Kirigami cuts not only tends to reduce the magnitude of the resonance frequencies, but it also generates more vibration modes within the same frequency range. Moreover, The Kirigami cut patterns also make the structure more compliant in the x and y axes.

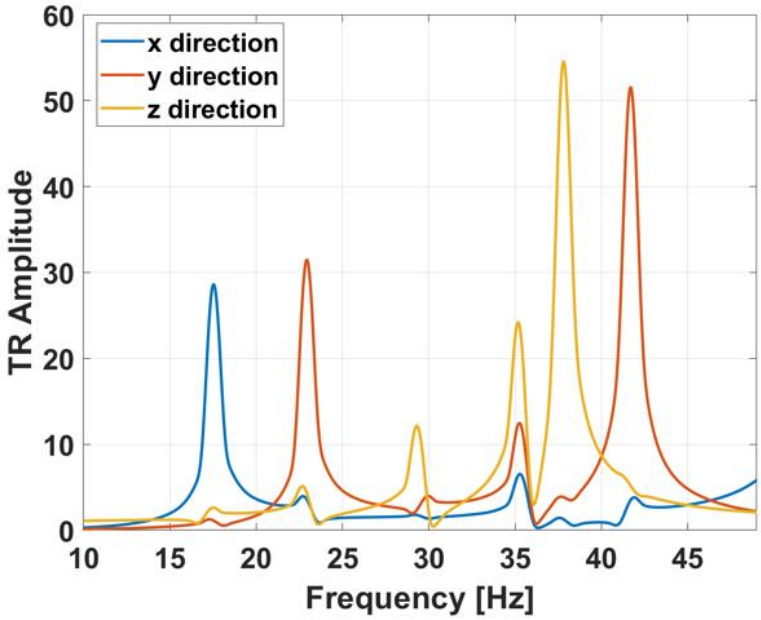

Figure 6.13 The structural characteristics of the 3D buckled structure with Kirigami cuts in multidirectional vibrations.

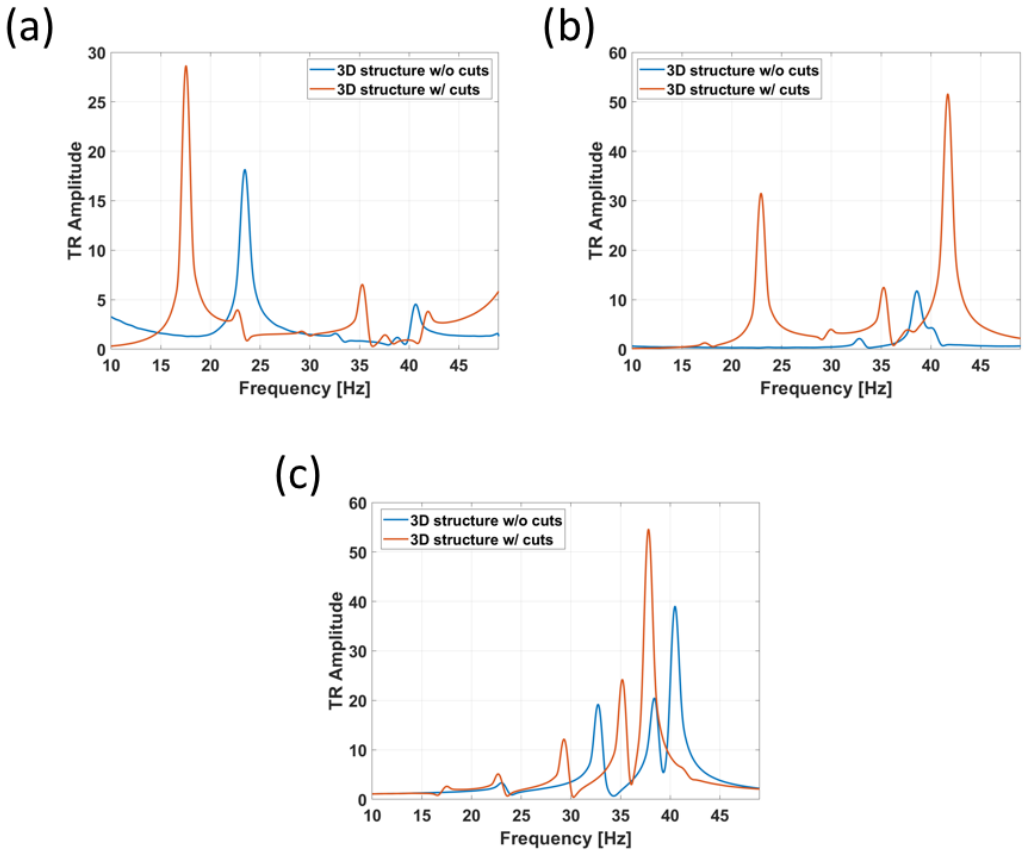

Figure 6.14 The comparison of structural transmissibility amplitude between the 3D buckled structures with and without Kirigami cuts under vibrations in (a) x, (b) y, and (c) z directions.

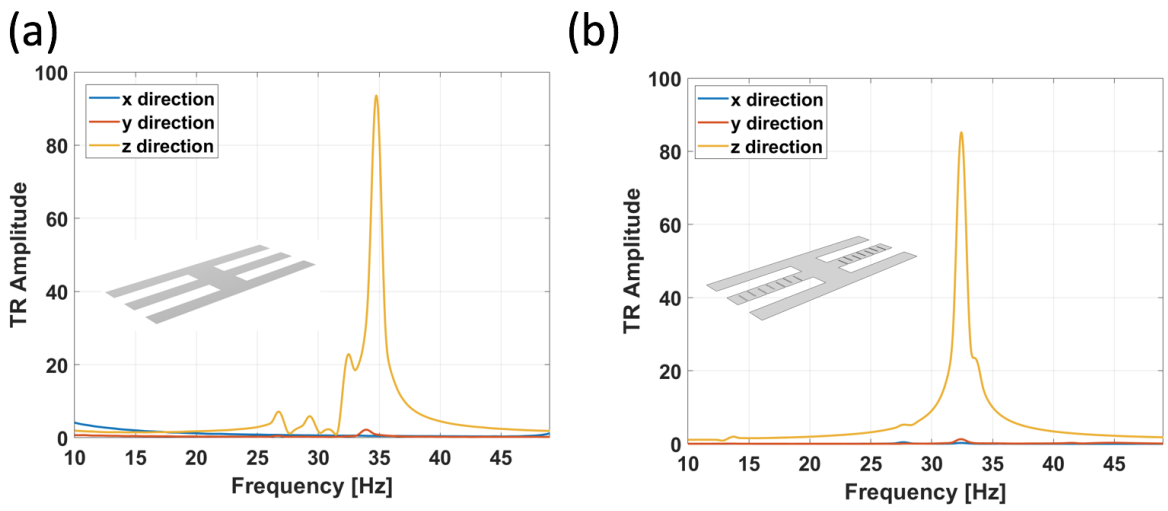

Figure 6.15 The structural characteristics of the 2D planar structure in multi-directional vibrations, (a) without and (b) with Kirigami cuts.

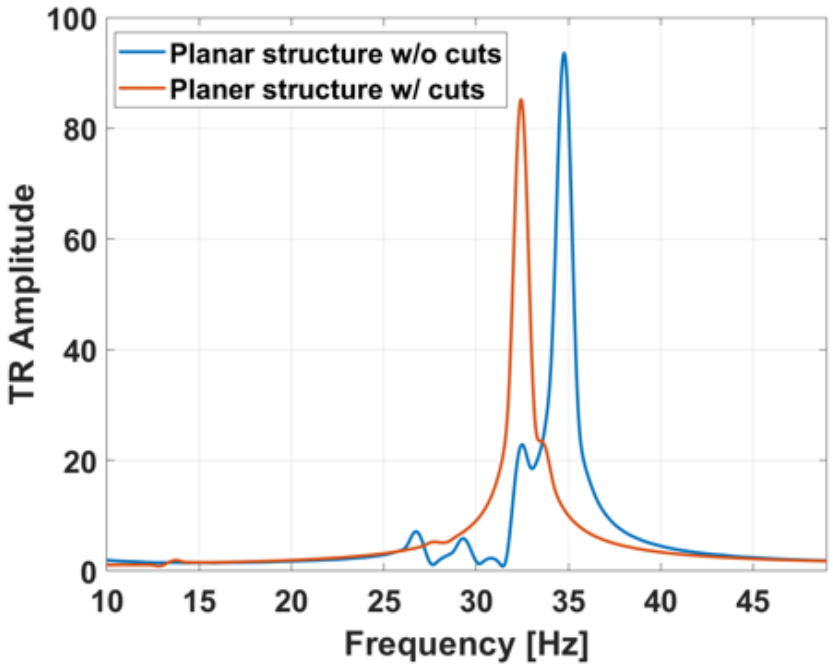

Figure 6.16 The comparison of the structural characteristics of the 2D planar structure with and without Kirigami cuts.

To demonstrate the superior characteristics of the proposed 3D metastructure, a comparative study has been performed with the conventional planar structures. Two corresponding flat structures were investigated, a planar structure with four mechanically coupled beams (Figure 6.15a) and a modified planar structure with Kirigami cuts (Figure 6.15b). Modal analysis was carried out on these two structures respectively, and the transmissibility in multi-directions was determined. Both structural configurations show that the transmissibility in x and y directions is negligible compared with the z direction, which confirms that such a type of planar design is only

suitable to the energy harvesting in one vibration direction. Similarly, as seen in Figure 6.16, the Kirigami cuts also reduce the resonance frequencies.

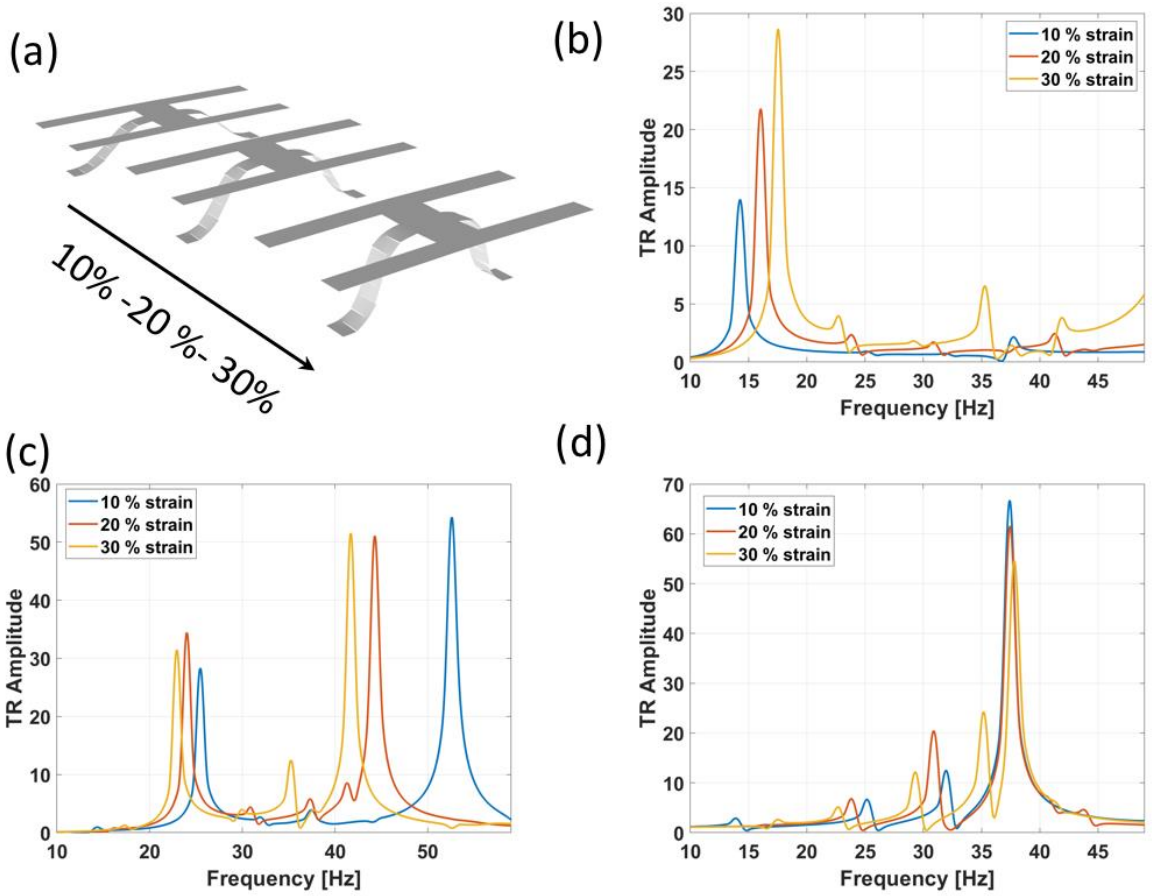

Figure 6.17 (a) The schematics of the 3D buckled structure with three pre-strains of 10 %, 20 %, and 30 %. The structure characteristics of the buckled structure with Kirigami cuts under vibrations of (b) x, (c) y, and (d) z directions.

In addition to the advantages of multi-directional vibration energy harvesting capabilities within a wide frequency range, the proposed structure can be tuned by assembly parameters, such as the pre-strain to control the buckling. We investigated the dynamic properties of the structures buckled with different pre-strains, 10 %, 20 %, and 30 %, as seen in Figure 6.17(a). Their structural transmissibility is calculated and compared, Figure 6.17(b)-(d). The increase of the pre-strain leads to an increase in resonant frequencies when the structure is subjected to the x directional vibration. The opposite however occurs when the dynamic loading is exerted along the y direction: as the pre-strain increases, the resonant frequencies decrease. The transmissibility of the metastructure does not however exhibit a clear dependence versus the level of pre-strain when subjected to the z directional vibration.

6.3.3 Energy harvesting from multi-directional vibration

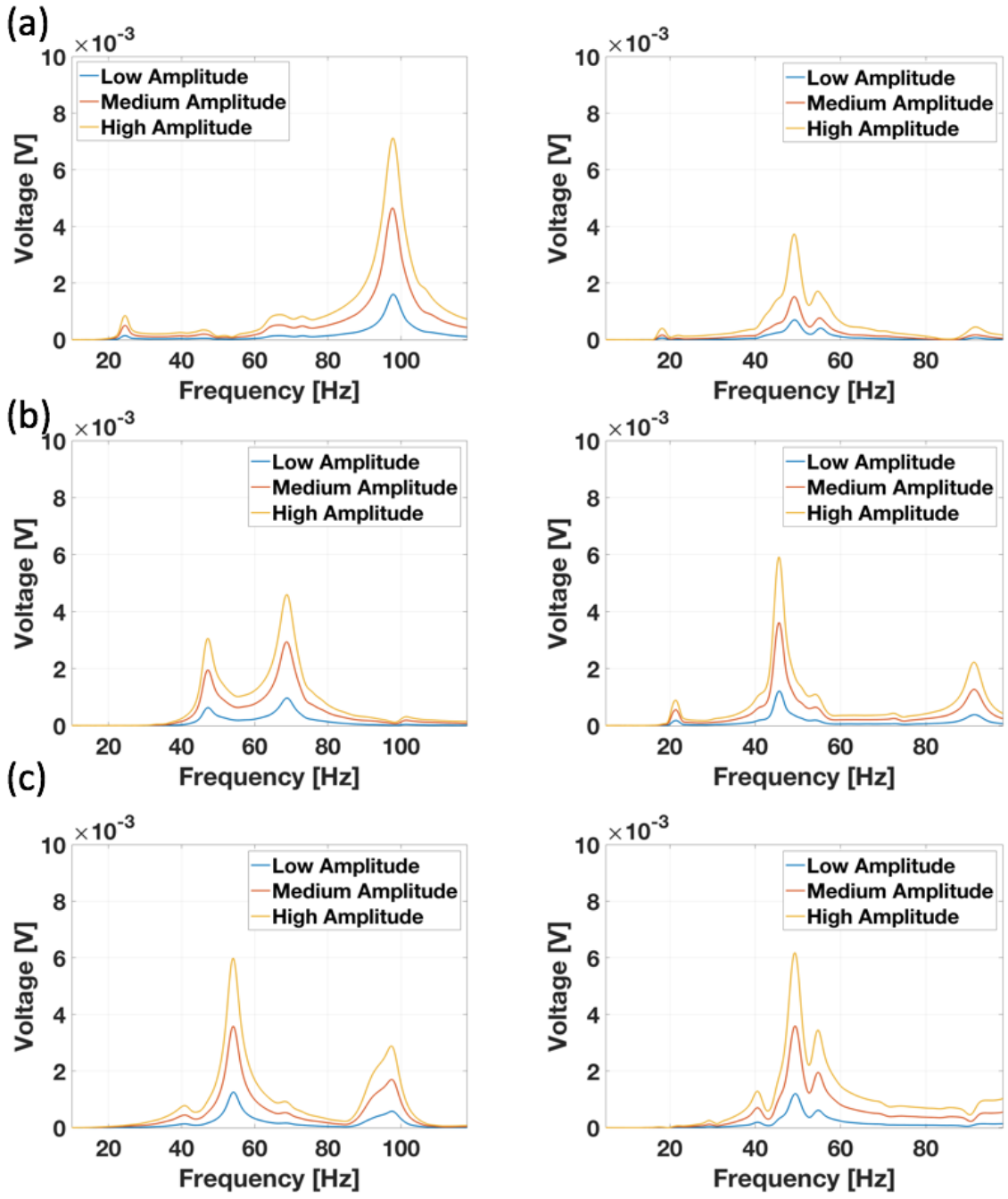

Figure 6.18 The voltage output of the buckled structure without (left) and with (right) Kirigami cuts under different vibration amplitudes in (a) x, (b) y, and (c) z directions.

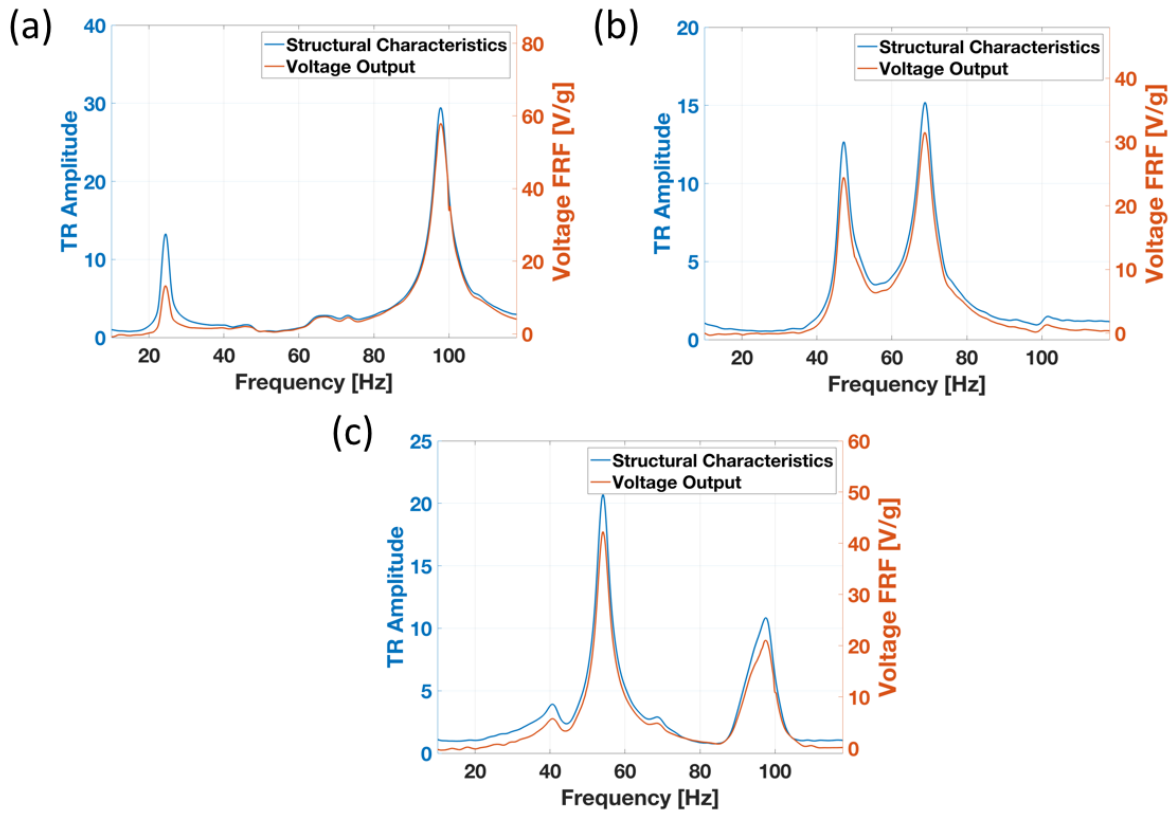

Figure 6.19 The comparison of the dynamic performances for the 3D energy harvesting system without Kirigami cuts under vibrations in (a) x, (b) y, and (c) z directions.

The vibration mode analysis has demonstrated the advantages of the presented 3D metastructures: multi-directional vibration features, broad frequency bandwidth, and tunable dynamic performances.

Following the validation of the baseline configuration of the 3D metastructures, we designed and fabricated two types of energy harvesters using the presented 3D platform. Vibration tests under various loading conditions have been performed to analyze the voltage outputs from the devices. The structures discussed herein have been buckled with a pre-strain level of 30 %. The voltage outputs along three orthogonal directions under different vibration amplitudes for the 3D structure without Kirigami cuts are shown on the left of Figure 6.18. Compared to the pure PET structure discussed in Section 6.3.2, these energy harvesting devices are stiffer overall(i.e. they have higher resonant frequencies) due to the integration of the PVDF films with the substrate. Frequency sweep tests were performed in a range from 1 Hz to 120 Hz. With an increase of the vibration amplitude, the voltage amplitudes increase accordingly. Along the x direction, the voltage outputs have a peak around 100 Hz, while for the y direction, the voltage output exhibits a wider bandwidth between 40 Hz and 80 Hz, and for the z direction vibration two peaks are seen within the ranges of 40 Hz – 60 Hz and 80 Hz – 100 Hz respectively. A comparison test was performed

to validate the generated voltage from the piezoelectric films in Figure 6.19. The laser vibrometer is used to capture the structural deformation of the device and to calculate the structural transmissibility, using a similar procedure to Section 6.3.2. The transmissibility in three directions is compared with the corresponding voltage output, and modal analysis confirms that the resonant frequencies from structural analysis and voltage output are consistent.

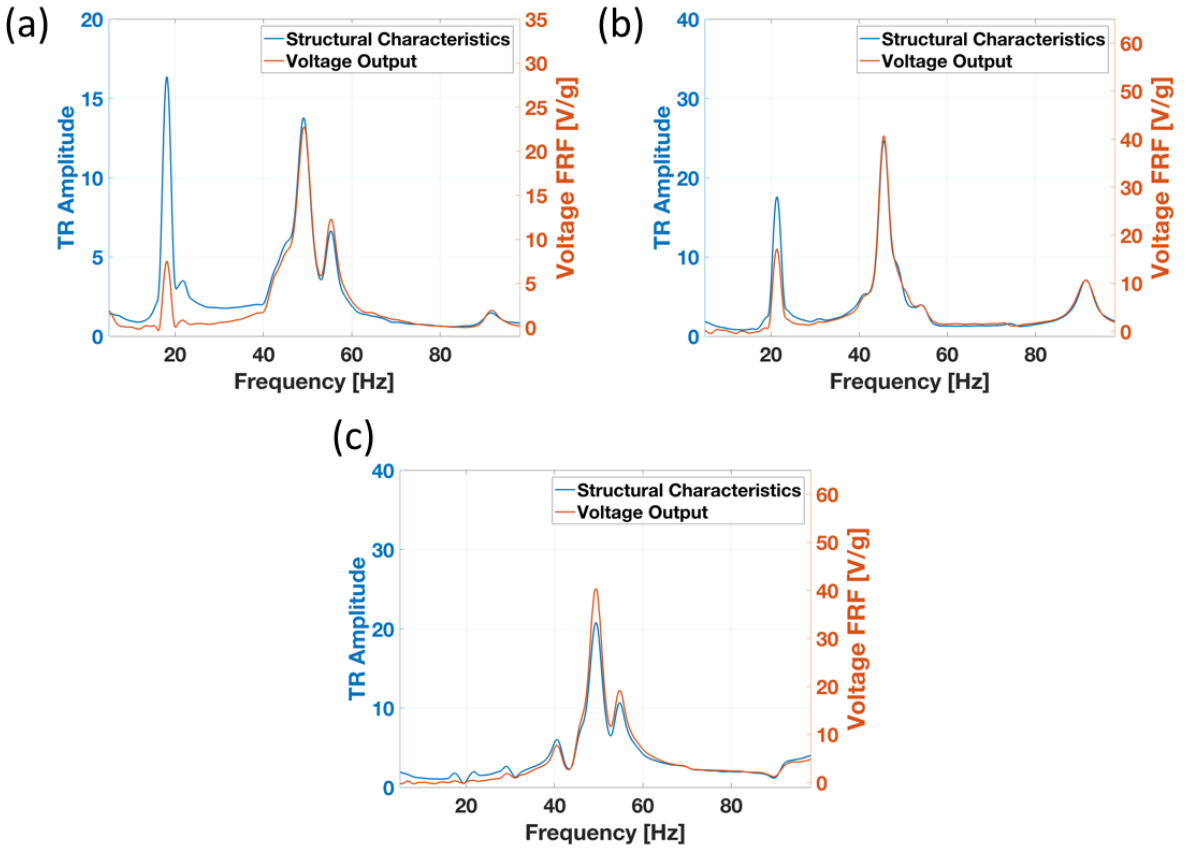

Figure 6.20 The comparison of the dynamic performances for the 3D energy harvesting system with Kirigami cuts under vibrations in (a) x, (b) y, and (c) z directions.

The voltage outputs for the modified device with Kirigami cuts are analyzed under a series of vibration tests, and shown on the right of Figure 6.18. We compared the voltage output for multi-directional vibrations and different shaker vibration amplitudes. The device can generate comparable voltage outputs in all three orthogonal directions, and the voltage amplitude increases with vibration amplitude. For x and z directional vibrations, the device has a broad bandwidth between 40 Hz and 60 Hz, and for the z directional vibration, an additional output peak is observed in the range 80 Hz to 100 Hz. A comparative study between the structural analysis and voltage output is conducted and summarized in Figure 6.20, and it is shown that the resonant frequencies based on these two measurements match well.

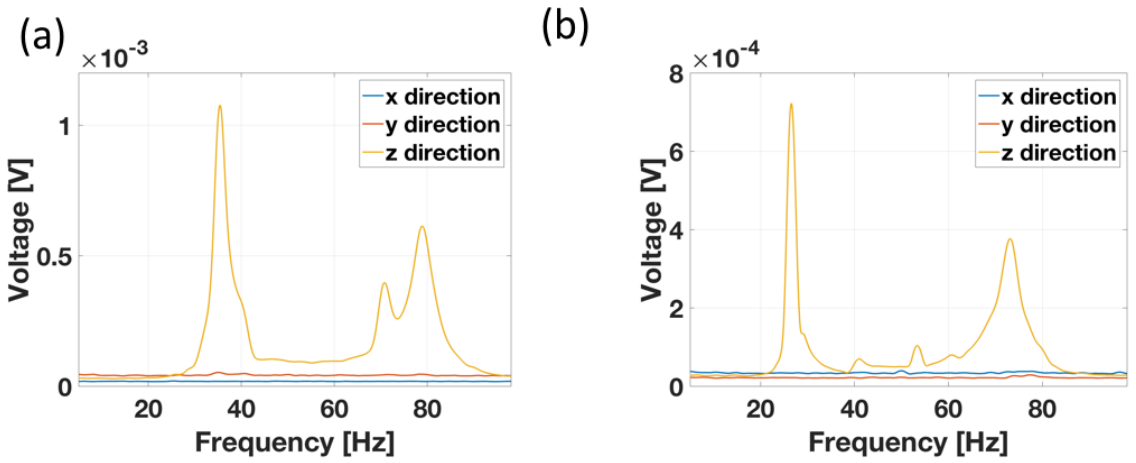

Figure 6.21 The voltage output of the planer structure (a) without and (b) with Kirigami cuts under multidirectional vibrations.

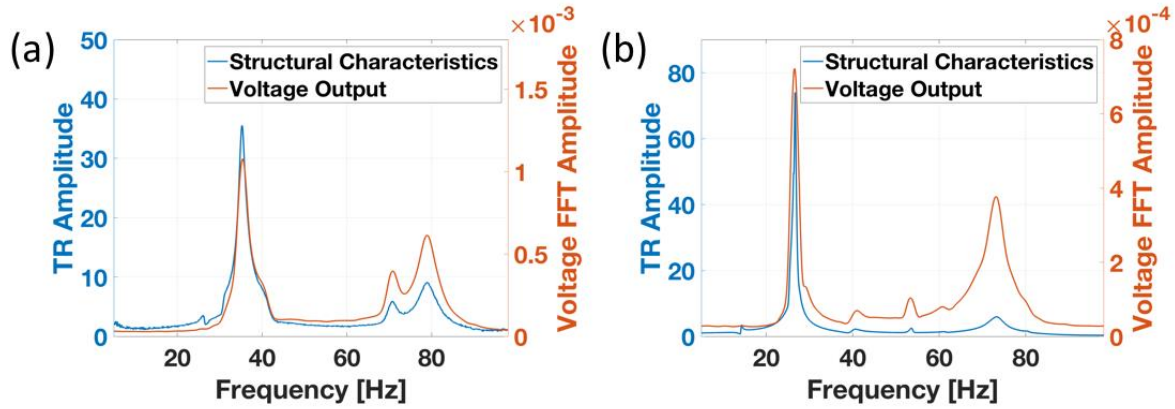

Figure 6.22 The comparison of the dynamic performances for 2D the energy harvesting system (a) without and (b) with Kirigami cuts under vibrations in z direction.

We further investigated the voltage generation performance of the conventional energy harvester based on planar configurations. Two types of planar energy harvesters were analyzed: a planar structure with four coupled piezoelectric beams; and the modified planar structure with additional Kirigami cuts on the central beams. A frequency sweep was conducted under multi-directional vibration. As seen in Figure 6.21, both planar devices show good performances in energy harvesting in the z axis, while in the x and y axes, the devices fail to transduce significant vibration. Structural analysis in the z direction confirms the frequency responses embodied in the voltage outputs (Figure 6.22). In contrast, the proposed 3D harvesting devices have been demonstrated to be promising in high-performance vibration energy harvesting systems.

6.3.4 Demonstration of wind energy harvesting

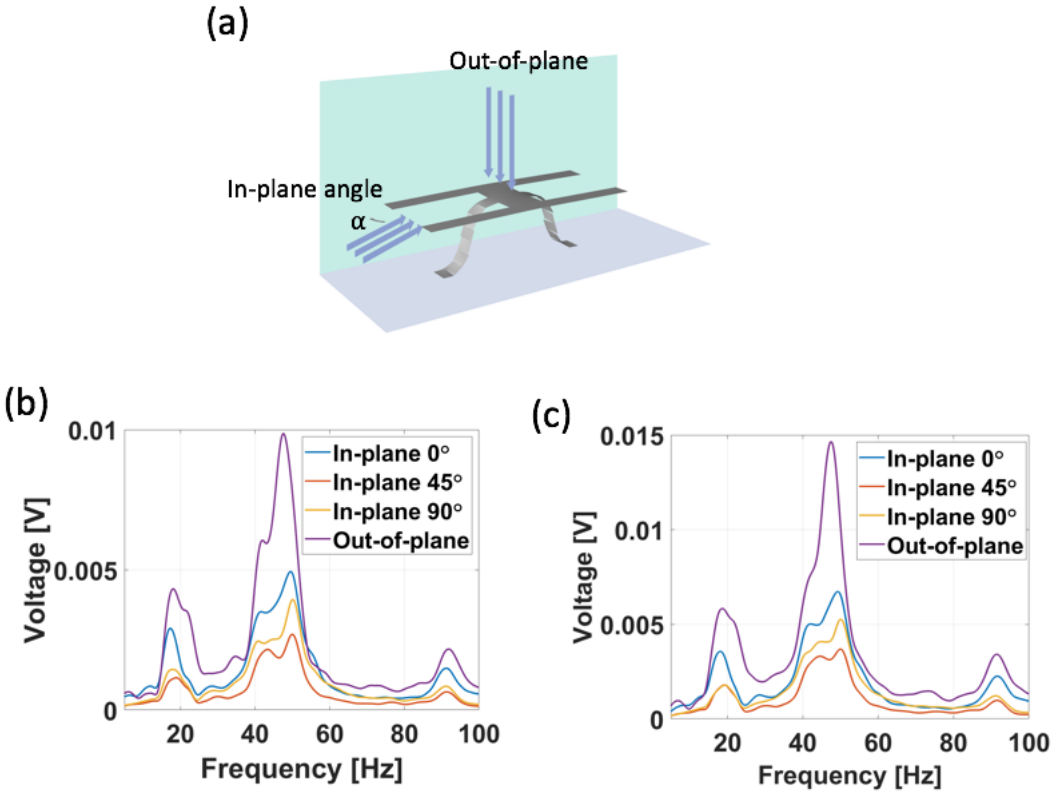

Figure 6.23 The energy harvester with Kirigami cuts and wind energy harvesting capacities. (a) the schematics of multiple wind direction applied on the harvester. The comparison of the voltage output for multidirectional wind with different levels of speed. (b) low speed, and (c) high speed.

The structural analysis and voltage outputs have validated the superior performances of the presented designs. In this section, the voltage generation capacities of the devices in a custom wind environment are evaluated. We use a commercial electric fan as the wind source, which can provide different wind speeds. In real applications, the wind direction is typically time-varying thus requiring the energy harvesting device to possess the ability to extract energy from air flow from different directions. Herein, two different wind directions were applied, in-plane and out-of-plane. Three representative angles were used for the in-plane air flow, as seen in Figure 6.23(a), where α defines the in-plane wind angle. The wind test for the 3D energy harvester with Kirigami cuts under two levels of wind speeds (low: 1.9 m/s and high: of 2.2 m/s) are summarized as frequency domain responses in Figure 6.23(b)-(c). The device has a broad low frequency bandwidth of around 60 Hz for both in-plane and out-of-plane winds. The voltage outputs from the out-of-plane wind features the largest amplitude as the wind directly acts upon the four beams lying

orthogonal to that direction. For the in-plane wind, the $\alpha = 0°$ angle wind is more efficient than the $\alpha = 90°$ angle wind in inducing vibrations, and the generated voltage under the 45° wind has a similar frequency response but with a lower amplitude. For the 3D energy harvesting system without Kirigami cuts, the results in the above wind environment are summarized in Figure 6.24.

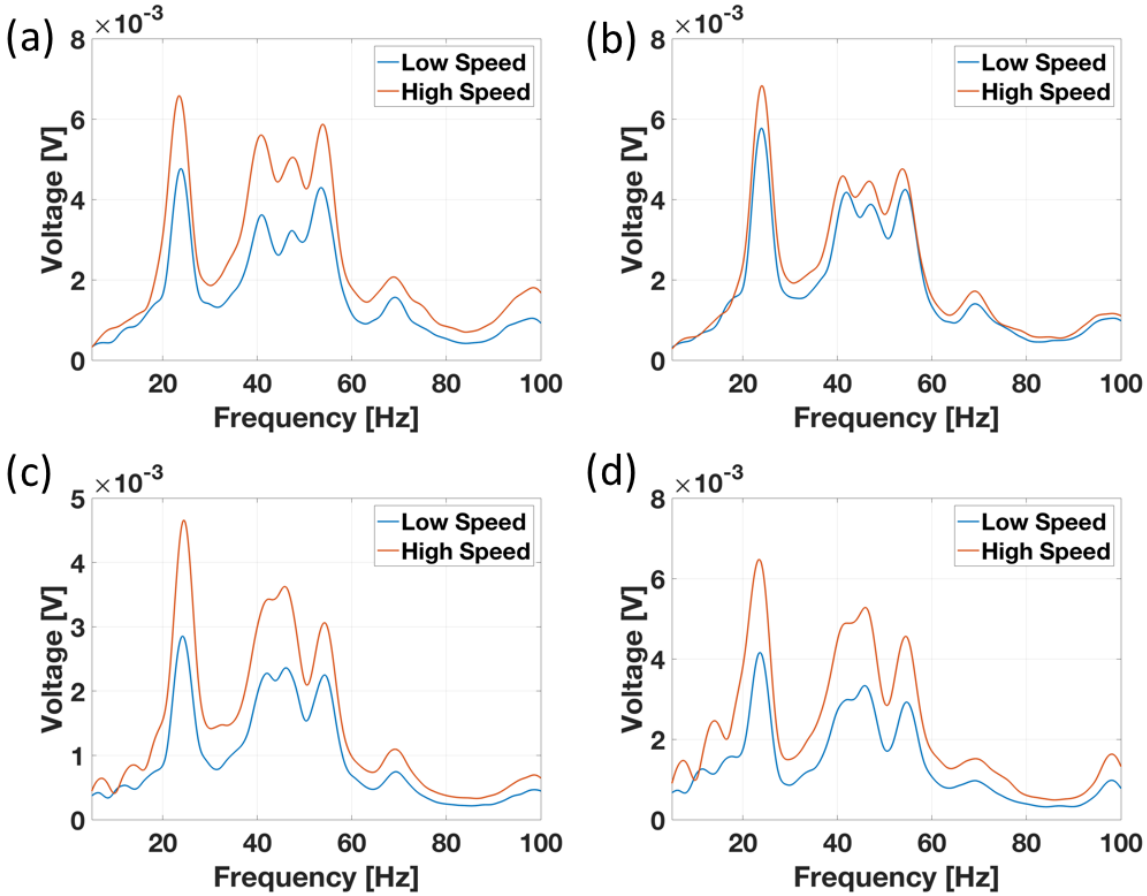

Figure 6.24 The energy harvester without Kirigami cuts and wind energy harvesting capacities. The voltage outputs in wind directions of (a) in-plane 0 degree, (b) in-plane 45 degree, (c) in-plane 90 degree, and (d) out-of-plane with two wind speeds.

6.4 CONCLUSION

A novel 3D tunable structural platform is presented for low-frequency vibration energy harvesting. Two types of 3D configurations either with or without additional Kirigami cuts have been designed and investigated, and a combined numerical and experimental study has demonstrated that this design has superior performance in multi-directional vibrations and features a broad frequency bandwidth within a low frequency range. Moreover, the dynamic properties of the proposed 3D

structure are highly tunable by changing the pre-strain of the structural buckling or through the introduction of Kirigami cut patterns. Based on the 3D structural platform, we designed and fabricated a series of energy harvesters, and dynamic tests validate that the proposed devices exhibit significant energy harvesting capacities for multi-directional low-frequency vibrations. The fabrication process of these structures is simple and allows for various geometric designs on the 2D precursor, with mechanical assembly into the defined 3D architectures. These features have been validated in a custom wind environment with effective energy harvesting from different directional winds and show frequency responses with broad bandwidths. The 3D tunable vibration systems presented in this work provide promising insights to develop high-performance and multi-functional energy harvesting devices. In future work, a series of optimized geometric designs will be investigated to maximize the dynamic energy harvesting properties and widen potential applications.

CHAPTER 7 - CONCLUSIONS AND FUTURE WORK

The work presented in this thesis has explored the technique of Kirigami-inspired design methodology to overcome several challenges remaining in bio-integrated electronics, including flexibility, stretchability, and energy harvesting/self-power. The Kirigami technique, derived from ancient paper folding and cutting, has provided new opportunities in modern material science and structural engineering. This technique features a cost-effective fabrication technique to transfer planar structures into diverse 3D configurations. By integrating functional materials, it has demonstrated the potential applications and superior advantages in stretchable sensing systems and energy harvesting devices. In this chapter, summary and conclusions of the dissertation are given, then future perspectives and potential research directions are discussed.

7.1 CONCLUSIONS

Bio-integrated electronics have received growing interests in the past decade due to potential use in healthcare monitoring and management. However, conventional electronic systems exhibit several limitations, such as the mechanical mismatch between the device and biological systems, hindering further developments for next-generation medical devices. The novelty of this work is the introduction of a facile Kirigami-based technique into the development of integrated and multi-functional electronic devices. The contributions of this thesis are summarised in this section, which includes two main areas: stretchable systems and energy harvesting.

7.1.1 Kirigami-inspired concept in stretchable systems

Stretchability is an important parameter for electronic devices which integrated with the human body. Most biological systems exhibit soft, stretchable, and dynamic surfaces, which impose challenges to conventional rigid electronic systems. Current approaches to explore the stretchability for bio-integrated electronics can be classified into either material synthesis or structural designs. Both of these typically require complicated fabrication process. Therefore, to develop an efficient method to achieve stretchability is of vital importance.

In Chapter 1, Kirigami cut patterns into planar plastic films was introduced, through which the intrinsically non-stretchable materials could be endowed with the property of ultra-stretchability. The Kirigami approach shows the characteristics of cost-effective, simple process, predictable structural behaviors, and the capacity for many different pattern designs on its planar layout. The relationship between the mechanical properties and Kirigami geometry parameters were investigated. The combined parametric studies of numerical simulations and experimental tests indicate that the mechanical properties, such as stretchability, of Kirigami structures can be easily tuned by changing the geometries of Kirigami patterns. This technique has offered a platform to develop diverse stretchable systems with variable functionalities by integrating advanced materials. Based on the proposed system with tunable mechanical properties, a preliminary demonstration was carried out using thin PVDF films as piezoelectric materials. A series of dynamic tests under various external strains and frequencies were performed to validate the high-performance as stretchable sensing systems.

A further comprehensive study based on the results in Chapter 1 was conducted to develop an integrated, stretchable, and self-powered sensing system for wireless health monitoring. The Kirigami technique has been proved to be an efficient way to introduce stretchability into intrinsically non-stretchable materials without affecting their original properties. Considering practical applications in wearable and implantable devices, a miniaturized device using piezoelectric

materials was designed using an improved fabrication process. This device shows significant advantages through flexibility, stretchability, self-power, and wireless communication. The flexible piezoelectric PVDF film can generate voltage outputs in response to an applied strain. A linear cut pattern was then introduced into PVDF films, enhancing its sretchability for intimately conforming to biological systems. NFC technology was adopted as a wireless communication interface to transmit the acquired signals to external devices, which is an essential and promising characteristic especially in implantable medical devices. By combining a novel electrode design, inter-segment electrode connections, with the Kirigami induced buckling behaviors, the proposed system exhibits improvements in both mechanical and electrical performances. A range of successful demonstrations including in vitro, ex vivo, and on body validated the superior performances of the proposed sensing systems in practical applications.

The Kirigami patterns adopted in the above research are based on uniform topologies, and the structural behaviors exhibit homogenous spatial deformations across the entire surface. It is of interest to explore the mechanical properties of non-uniform Kirigami-based structures due to their unique structural characteristics. As discussed in Section 2.4, a range of Kirigami-based metastructures have been extensively explored recently, but until now, studies on non-uniform Kirigami-based structures are limited. In Chapter 5, a non-uniform Kirigami structure based on the research in the previous chapters is proposed, and the non-uniform patterns have linear cuts with controlled non-uniform distributions. A generalized expression to describe the non-uniformity was presented, and diverse configurations with various non-uniformity factors were investigated. In comparison with the uniform Kirigami-based structures, the deformations of this type of structure exhibit a unique spatial characteristic and it can be controlled by the non-uniformity factors. This design offers an additional parameter to control the deformed behaviors which has the potential to broaden the design space in structural engineering. A representative demonstration using piezoelectric materials has been performed, and a sequential change of the voltage can be obtained due to the non-uniform properties of the Kirigami structures.

7.1.2 Kirigami-inspired concept in energy harvesting

The power supply is an essential part of any electronic system, which generally determines the lifetime of the devices. The development of a sustainable power source that can alleviate or remove the dependence on external power such as battery is quite promising and has received increasing attention. As the human body can be regarded as a biomechanical energy source, it is of significance to develop an efficient energy harvesting system to scavenge this type of energy. Vibration is ubiquitous in daily life, such as human activities (walking, running, and climbing), however this type of vibration features low frequency, broad bandwidth, and random directions,

which imposes challenges to the development of energy harvesting systems. In this work, we developed a 3D tunable dynamic system with great potential for vibration energy harvesting. The Kirigami cuts were introduced into a flexible thin film with patterned configurations on its 2D layout. With well-defined patterns, the structure was subsequently assembled into the predicted 3D architectures via compressive buckling process. The proposed platform features four cantilevers which are mechanically coupled via a buckled ribbon. Combined numerical simulation and experimental tests have demonstrated that this Kirigami-based 3D design revealed promising properties, including broadband response in a low frequency range, and multi-directional vibration, which are advantageous in energy harvesting from biomechanical energy of human body. Comprehensive experiments have been carried out to validate the performance of the proposed harvesting systems, including low-frequency range in multiple directions, and a controlled wind environment. The results demonstrate its superior capabilities in energy harvesting.

7.2 FUTURE WORK

The findings presented herein have offered new opportunities to improve the properties of bio-integrated electronics based on Kirigami-inspired concept designs. Several potential challenges and opportunities remain when moving towards practical applications in healthcare.

Optimization of Kirigami pattern. The linear cut pattern in uniform and non-uniform configurations were extensively studied and their potential applications for healthcare monitoring were demonstrated in this work. In real conditions, the properties of biological systems vary in different positions, thus requiring specific designs of electronic systems for better conformity. Currently, diverse Kirigami patterns have been explored, but mainly focusing on the mechanical properties. Functional devices based on these Kirigami patterns for bio-medical applications are limited. Comprehensive optimization designs are needed in order to precisely match the local deformation of biological systems.

The Kirigami-inspired designs together with the mechanically guided method via compressive buckling provide a promising routine to develop tunable 3D vibration systems. In this work, a 3D piezoelectric structure consisting of four mechanically coupled beams has been investigated and its high performance in multi-modal and multi-directional vibration energy harvesting has been validated. This research opens up new directions to develop highly efficient energy harvesting systems through a cost-effective fabrication process. In this type of configurations, the buckled ribbon serves as a bridge to couple different parts in the system, thereby enabling the induction of multi-modal vibrations. Due to the 3D structural characteristics, it contributes to the dynamic performance in multiple directions. A preliminary design based on cantilever beams was

investigated, and future work will focus on the optimization designs of Kirigami patterns to improve the coupling efficiency and dynamic performance in multiple directions. The complexity of vibration modes increases due to the mechanically coupling effect of 3D Kirigami-based structures, and charge cancellation would occur in a single electrode. To fully utilize the vibration energy an optimal electrode design is necessary to increase the power output. From a different perspective, the charge cancellation/amplification can also be used for a vibration switch. In the proposed 3D vibration system, the coupled beams can be excited either in phase or counter phase. When in-phase vibration beams are parallelly connected, the voltage output will be amplified, while the connection of counter-phase vibration beams would result in charge cancellation, thus reducing the voltage output. The voltage output can be used as an indicator of the vibration information and used as a vibration logic switch. Another interesting direction is device minimization. For practical applications, such as wearable devices, apart from flexibility and strechability, the device size is also an important parameter, and minimized devices using the proposed techniques promise to be more compatible with human body.

Integrated devices - Several biological systems, such as human skin and animal whiskers, exhibit advantages in detecting and distinguishing various external stimuli, such as thermal stimuli, and mechanical tactile sensation including normal, shear, stretching, and vibration forces. Mimicking the tactile and temperature sensing properties of human skin should be further investigated to achieve an integrated multi-functional sensing system. Highly integrated electronics are future research directions with tremendous opportunities. Desirable integrated capacities could possess but not be limited to, data modules for recording, storage, processing, and wireless communication capacities, power component, and actuation modules with functions, such as tactile stimulation and drug delivery. In the present work, we adopted piezoelectric materials to develop self-powered strain sensors. In the perspectives of future work, the proposed platform based on Kirigami-inspired concepts offers possibilities to integrate a range of functional materials for different practical applications. For example, by integrating electrode arrays, electrophysiological information can be recorded and modulated in a 3D environment. In addition, tailored Kirigami patterns could be introduced into textile materials, and by integrating specific electronics, functional textile with self-sensing capacity would be achievable. This system would also possess intrinsic breathability provided by the induced 3D open structure.

Bibliography

[1] Kapnisi M, Mansfield C, Marijon C, Guex AG, Perbellini F, Bardi I, et al. Auxetic Cardiac Patches with Tunable Mechanical and Conductive Properties toward Treating Myocardial Infarction. Advanced Functional Materials. 2018;28:1800618.
[2] Wessendorf AM, Newman DJ. Dynamic Understanding of Human-Skin Movement and Strain-Field Analysis. IEEE Transactions on Biomedical Engineering. 2012;59:3432-8.
[3] McEvoy MA, Correll N. Materials that couple sensing, actuation, computation, and communication. Science. 2015;347:1261689.
[4] Son D, Lee J, Lee DJ, Ghaffari R, Yun S, Kim SJ, et al. Bioresorbable Electronic Stent Integrated with Therapeutic Nanoparticles for Endovascular Diseases. ACS Nano. 2015;9:5937-46.
[5] Rogers JA. Electronics for the Human Body. JAMA. 2015;313:561-2.
[6] Heikenfeld J, Jajack A, Rogers J, Gutruf P, Tian L, Pan T, et al. Wearable sensors: modalities, challenges, and prospects. Lab on a Chip. 2018;18:217-48.
[7] Yang T, Xie D, Li Z, Zhu H. Recent advances in wearable tactile sensors: Materials, sensing mechanisms, and device performance. Materials Science and Engineering: R: Reports. 2017;115:1-37.
[8] Harada S, Kanao K, Yamamoto Y, Arie T, Akita S, Takei K. Fully Printed Flexible Fingerprint-like Three-Axis Tactile and Slip Force and Temperature Sensors for Artificial Skin. ACS Nano. 2014;8:12851-7.
[9] Xu S, Zhang Y, Cho J, Lee J, Huang X, Jia L, et al. Stretchable batteries with self-similar serpentine interconnects and integrated wireless recharging systems. Nature Communications. 2013;4:1543.
[10] Kim T-i, McCall JG, Jung YH, Huang X, Siuda ER, Li Y, et al. Injectable, Cellular-Scale Optoelectronics with Applications for Wireless Optogenetics. Science. 2013;340:211.
[11] Xu L, Gutbrod SR, Bonifas AP, Su Y, Sulkin MS, Lu N, et al. 3D multifunctional integumentary membranes for spatiotemporal cardiac measurements and stimulation across the entire epicardium. Nature Communications. 2014;5:3329.
[12] Lee SH, Jeong CK, Hwang G-T, Lee KJ. Self-powered flexible inorganic electronic system. Nano Energy. 2015;14:111-25.
[13] Mannsfeld SCB, Tee BCK, Stoltenberg RM, Chen CVHH, Barman S, Muir BVO, et al. Highly sensitive flexible pressure sensors with microstructured rubber dielectric layers. Nature Materials. 2010;9:859.
[14] Wang X, Song J, Liu J, Wang ZL. Direct-Current Nanogenerator Driven by Ultrasonic Waves. Science. 2007;316:102.
[15] Hu Y, Wang ZL. Recent progress in piezoelectric nanogenerators as a sustainable power source in self-powered systems and active sensors. Nano Energy. 2015;14:3-14.
[16] Lou Z, Li L, Wang L, Shen G. Recent Progress of Self-Powered Sensing Systems for Wearable Electronics. Small. 2017;13:1701791.
[17] Parvez Mahmud MA, Huda N, Farjana SH, Asadnia M, Lang C. Recent Advances in Nanogenerator-Driven Self-Powered Implantable Biomedical Devices. Advanced Energy Materials. 2018;8:1701210.
[18] Park K-I, Son JH, Hwang G-T, Jeong CK, Ryu J, Koo M, et al. Highly-Efficient, Flexible Piezoelectric PZT Thin Film Nanogenerator on Plastic Substrates. Advanced Materials. 2014;26:2514-20.
[19] Kim DH, Shin HJ, Lee H, Jeong CK, Park H, Hwang G-T, et al. In Vivo Self-Powered Wireless Transmission Using Biocompatible Flexible Energy Harvesters. Advanced Functional Materials. 2017;27:1700341.

[20] Park DY, Joe DJ, Kim DH, Park H, Han JH, Jeong CK, et al. Self-Powered Real-Time Arterial Pulse Monitoring Using Ultrathin Epidermal Piezoelectric Sensors. Advanced Materials. 2017;29: 1702308.
[21] Park K-I, Xu S, Liu Y, Hwang G-T, Kang S-JL, Wang ZL, et al. Piezoelectric BaTiO3 Thin Film Nanogenerator on Plastic Substrates. Nano Letters. 2010;10:4939-43.
[22] Xu S, Yeh Y-w, Poirier G, McAlpine MC, Register RA, Yao N. Flexible Piezoelectric PMN–PT Nanowire-Based Nanocomposite and Device. Nano Letters. 2013;13:2393-8.
[23] Yang Z, Zhou S, Zu J, Inman D. High-Performance Piezoelectric Energy Harvesters and Their Applications. Joule. 2018;2:642-97.
[24] Hwang G-T, Kim Y, Lee J-H, Oh S, Jeong CK, Park DY, et al. Self-powered deep brain stimulation via a flexible PIMNT energy harvester. Energy & Environmental Science. 2015;8:2677-84.
[25] Sun R, Carreira SC, Chen Y, Xiang C, Xu L, Zhang B, et al. Stretchable Piezoelectric Sensing Systems for Self-Powered and Wireless Health Monitoring. Advanced Materials Technologies. 2019;0:1900100.
[26] Wang G, Liu T, Sun X-C, Li P, Xu Y-S, Hua J-G, et al. Flexible pressure sensor based on PVDF nanofiber. Sensors and Actuators A: Physical. 2018;280:319-25.
[27] Zabek D, Taylor J, Boulbar EL, Bowen CR. Micropatterning of Flexible and Free Standing Polyvinylidene Difluoride (PVDF) Films for Enhanced Pyroelectric Energy Transformation. Advanced Energy Materials. 2015;5:1401891.
[28] Chen X, Han X, Shen Q-D. PVDF-Based Ferroelectric Polymers in Modern Flexible Electronics. Advanced Electronic Materials. 2017;3:1600460.
[29] Sharma T, Je S-S, Gill B, Zhang JXJ. Patterning piezoelectric thin film PVDF–TrFE based pressure sensor for catheter application. Sensors and Actuators A: Physical. 2012;177:87-92.
[30] Persano L, Dagdeviren C, Su Y, Zhang Y, Girardo S, Pisignano D, et al. High performance piezoelectric devices based on aligned arrays of nanofibers of poly(vinylidenefluoride-co-trifluoroethylene). Nature Communications. 2013;4:1633.
[31] Beringer LT, Xu X, Shih W, Shih W-H, Habas R, Schauer CL. An electrospun PVDF-TrFe fiber sensor platform for biological applications. Sensors and Actuators A: Physical. 2015;222:293-300.
[32] Chen X, Li X, Shao J, An N, Tian H, Wang C, et al. High-Performance Piezoelectric Nanogenerators with Imprinted P(VDF-TrFE)/BaTiO3 Nanocomposite Micropillars for Self-Powered Flexible Sensors. Small. 2017;13:1604245.
[33] Chen X, Parida K, Wang J, Xiong J, Lin M-F, Shao J, et al. A Stretchable and Transparent Nanocomposite Nanogenerator for Self-Powered Physiological Monitoring. ACS Applied Materials & Interfaces. 2017;9:42200-9.
[34] Shin K-Y, Lee JS, Jang J. Highly sensitive, wearable and wireless pressure sensor using free-standing ZnO nanoneedle/PVDF hybrid thin film for heart rate monitoring. Nano Energy. 2016;22:95-104.
[35] Yu X, Wang H, Ning X, Sun R, Albadawi H, Salomao M, et al. Needle-shaped ultrathin piezoelectric microsystem for guided tissue targeting via mechanical sensing. Nature Biomedical Engineering. 2018;2:165-72.
[36] Dagdeviren C, Javid F, Joe P, von Erlach T, Bensel T, Wei Z, et al. Flexible piezoelectric devices for gastrointestinal motility sensing. Nature Biomedical Engineering. 2017;1:807-17.
[37] Han M, Wang H, Yang Y, Liang C, Bai W, Yan Z, et al. Three-dimensional piezoelectric polymer microsystems for vibrational energy harvesting, robotic interfaces and biomedical implants. Nature Electronics. 2019;2:26-35.
[38] Hwang G-T, Park H, Lee J-H, Oh S, Park K-I, Byun M, et al. Self-Powered Cardiac Pacemaker Enabled by Flexible Single Crystalline PMN-PT Piezoelectric Energy Harvester. Advanced Materials. 2014;26:4880-7.

[39] Dagdeviren C, Yang BD, Su Y, Tran PL, Joe P, Anderson E, et al. Conformal piezoelectric energy harvesting and storage from motions of the heart, lung, and diaphragm. Proceedings of the National Academy of Sciences. 2014;111:1927.
[40] Dagdeviren C, Su Y, Joe P, Yona R, Liu Y, Kim Y-S, et al. Conformable amplified lead zirconate titanate sensors with enhanced piezoelectric response for cutaneous pressure monitoring. Nature Communications. 2014;5.
[41] Ausanio G, Barone AC, Campana C, Iannotti V, Luponio C, Pepe GP, et al. Giant resistivity change induced by strain in a composite of conducting particles in an elastomer matrix. Sensors and Actuators A: Physical. 2006;127:56-62.
[42] Chiriac H, Urse M, Rusu F, Hison C, Neagu M. Ni–Ag thin films as strain-sensitive materials for piezoresistive sensors. Sensors and Actuators A: Physical. 1999;76:376-80.
[43] Yang T, Li X, Jiang X, Lin S, Lao J, Shi J, et al. Structural engineering of gold thin films with channel cracks for ultrasensitive strain sensing. Materials Horizons. 2016;3:248-55.
[44] Lei Z, Wang Q, Sun S, Zhu W, Wu P. A Bioinspired Mineral Hydrogel as a Self-Healable, Mechanically Adaptable Ionic Skin for Highly Sensitive Pressure Sensing. Advanced Materials. 2017;29:1700321.
[45] Wang S, Xiao P, Liang Y, Zhang J, Huang Y, Wu S, et al. Network cracks-based wearable strain sensors for subtle and large strain detection of human motions. Journal of Materials Chemistry C. 2018;6:5140-7.
[46] Liu Q, Chen J, Li Y, Shi G. High-Performance Strain Sensors with Fish-Scale-Like Graphene-Sensing Layers for Full-Range Detection of Human Motions. ACS Nano. 2016;10:7901-6.
[47] Liu Y, Zhang D, Wang K, Liu Y, Shang Y. A novel strain sensor based on graphene composite films with layered structure. Composites Part A: Applied Science and Manufacturing. 2016;80:95-103.
[48] Amjadi M, Turan M, Clementson CP, Sitti M. Parallel Microcracks-based Ultrasensitive and Highly Stretchable Strain Sensors. ACS Applied Materials & Interfaces. 2016;8:5618-26.
[49] Hu N, Karube Y, Yan C, Masuda Z, Fukunaga H. Tunneling effect in a polymer/carbon nanotube nanocomposite strain sensor. Acta Materialia. 2008;56:2929-36.
[50] Shi G, Zhao Z, Pai J-H, Lee I, Zhang L, Stevenson C, et al. Highly Sensitive, Wearable, Durable Strain Sensors and Stretchable Conductors Using Graphene/Silicon Rubber Composites. Advanced Functional Materials. 2016;26:7614-25.
[51] Park J, Lee Y, Hong J, Ha M, Jung Y-D, Lim H, et al. Giant Tunneling Piezoresistance of Composite Elastomers with Interlocked Microdome Arrays for Ultrasensitive and Multimodal Electronic Skins. ACS Nano. 2014;8:4689-97.
[52] Zhao X, Hua Q, Yu R, Zhang Y, Pan C. Flexible, Stretchable and Wearable Multifunctional Sensor Array as Artificial Electronic Skin for Static and Dynamic Strain Mapping. Advanced Electronic Materials. 2015;1:1500142.
[53] Yao S, Zhu Y. Wearable multifunctional sensors using printed stretchable conductors made of silver nanowires. Nanoscale. 2014;6:2345-52.
[54] Hu W, Niu X, Zhao R, Pei Q. Elastomeric transparent capacitive sensors based on an interpenetrating composite of silver nanowires and polyurethane. Applied Physics Letters. 2013;102:083303.
[55] Choi TY, Hwang B-U, Kim B-Y, Trung TQ, Nam YH, Kim D-N, et al. Stretchable, Transparent, and Stretch-Unresponsive Capacitive Touch Sensor Array with Selectively Patterned Silver Nanowires/Reduced Graphene Oxide Electrodes. ACS Applied Materials & Interfaces. 2017;9:18022-30.
[56] Wan Y, Qiu Z, Hong Y, Wang Y, Zhang J, Liu Q, et al. A Highly Sensitive Flexible Capacitive Tactile Sensor with Sparse and High-Aspect-Ratio Microstructures. Advanced Electronic Materials. 2018;4:1700586.

[57] Green JJ, Elisseeff JH. Mimicking biological functionality with polymers for biomedical applications. Nature. 2016;540:386.
[58] Boutry CM, Nguyen A, Lawal QO, Chortos A, Rondeau-Gagné S, Bao Z. A Sensitive and Biodegradable Pressure Sensor Array for Cardiovascular Monitoring. Advanced Materials. 2015;27:6954-61.
[59] Cho SH, Lee SW, Yu S, Kim H, Chang S, Kang D, et al. Micropatterned Pyramidal Ionic Gels for Sensing Broad-Range Pressures with High Sensitivity. ACS Applied Materials & Interfaces. 2017;9:10128-35.
[60] Lee B-Y, Kim J, Kim H, Kim C, Lee S-D. Low-cost flexible pressure sensor based on dielectric elastomer film with micro-pores. Sensors and Actuators A: Physical. 2016;240:103-9.
[61] He Z, Chen W, Liang B, Liu C, Yang L, Lu D, et al. Capacitive Pressure Sensor with High Sensitivity and Fast Response to Dynamic Interaction Based on Graphene and Porous Nylon Networks. ACS Applied Materials & Interfaces. 2018;10:12816-23.
[62] Yoon SG, Park BJ, Chang ST. Highly Sensitive Piezocapacitive Sensor for Detecting Static and Dynamic Pressure Using Ion-Gel Thin Films and Conductive Elastomeric Composites. ACS Applied Materials & Interfaces. 2017;9:36206-19.
[63] Wan S, Bi H, Zhou Y, Xie X, Su S, Yin K, et al. Graphene oxide as high-performance dielectric materials for capacitive pressure sensors. Carbon. 2017;114:209-16.
[64] Yin R, Xu Z, Mei M, Chen Z, Wang K, Liu Y, et al. Soft transparent graphene contact lens electrodes for conformal full-cornea recording of electroretinogram. Nature Communications. 2018;9:2334.
[65] Jang H, Yoon H, Ko Y, Choi J, Lee S-S, Jeon I, et al. Enhanced performance in capacitive force sensors using carbon nanotube/polydimethylsiloxane nanocomposites with high dielectric properties. Nanoscale. 2016;8:5667-75.
[66] Kou H, Zhang L, Tan Q, Liu G, Lv W, Lu F, et al. Wireless flexible pressure sensor based on micro-patterned Graphene/PDMS composite. Sensors and Actuators A: Physical. 2018;277:150-6.
[67] Fan F-R, Tian Z-Q, Lin Wang Z. Flexible triboelectric generator. Nano Energy. 2012;1:328-34.
[68] Fan F-R, Lin L, Zhu G, Wu W, Zhang R, Wang ZL. Transparent Triboelectric Nanogenerators and Self-Powered Pressure Sensors Based on Micropatterned Plastic Films. Nano Letters. 2012;12:3109-14.
[69] Yu A, Chen L, Chen X, Zhang A, Fan F, Zhan Y, et al. Triboelectric sensor as self-powered signal reader for scanning probe surface topography imaging. Nanotechnology. 2015;26:165501.
[70] Yang Y, Zhang H, Lin Z-H, Zhou YS, Jing Q, Su Y, et al. Human Skin Based Triboelectric Nanogenerators for Harvesting Biomechanical Energy and as Self-Powered Active Tactile Sensor System. ACS Nano. 2013;7:9213-22.
[71] Zhang R, Hummelgård M, Örtegren J, Olsen M, Andersson H, Olin H. Interaction of the human body with triboelectric nanogenerators. Nano Energy. 2019;57:279-92.
[72] Wang S, Lin L, Wang ZL. Triboelectric nanogenerators as self-powered active sensors. Nano Energy. 2015;11:436-62.
[73] Zang Y, Huang D, Di C-a, Zhu D. Device Engineered Organic Transistors for Flexible Sensing Applications. Advanced Materials. 2016;28:4549-55.
[74] Wu X, Mao S, Chen J, Huang J. Strategies for Improving the Performance of Sensors Based on Organic Field-Effect Transistors. Advanced Materials. 2018;30:e1705642.
[75] Lee YH, Jang M, Lee MY, Kweon OY, Oh JH. Flexible Field-Effect Transistor-Type Sensors Based on Conjugated Molecules. Chem. 2017;3:724-63.
[76] Wang S, Xu J, Wang W, Wang G-JN, Rastak R, Molina-Lopez F, et al. Skin electronics from scalable fabrication of an intrinsically stretchable transistor array. Nature. 2018.

[77] Shin S-H, Ji S, Choi S, Pyo K-H, Wan An B, Park J, et al. Integrated arrays of air-dielectric graphene transistors as transparent active-matrix pressure sensors for wide pressure ranges. Nature Communications. 2017;8:14950.
[78] Yun S, Park S, Park B, Kim Y, Park SK, Nam S, et al. Polymer-Waveguide-Based Flexible Tactile Sensor Array for Dynamic Response. Advanced Materials. 2014;26:4474-80.
[79] Alfadhel A, Kosel J. Magnetic Nanocomposite Cilia Tactile Sensor. Advanced Materials. 2015;27:7888-92.
[80] Ota S, Ando A, Chiba D. A flexible giant magnetoresistive device for sensing strain direction. Nature Electronics. 2018;1:124-9.
[81] Chen LY, Tee BCK, Chortos AL, Schwartz G, Tse V, J. Lipomi D, et al. Continuous wireless pressure monitoring and mapping with ultra-small passive sensors for health monitoring and critical care. Nature Communications. 2014;5:5028.
[82] Hsu AL, Herring PK, Gabor NM, Ha S, Shin YC, Song Y, et al. Graphene-Based Thermopile for Thermal Imaging Applications. Nano Letters. 2015;15:7211-6.
[83] Jeon J, Lee H-B-R, Bao Z. Flexible Wireless Temperature Sensors Based on Ni Microparticle-Filled Binary Polymer Composites. Advanced Materials. 2013;25:850-5.
[84] Wu X, Ma Y, Zhang G, Chu Y, Du J, Zhang Y, et al. Thermally Stable, Biocompatible, and Flexible Organic Field-Effect Transistors and Their Application in Temperature Sensing Arrays for Artificial Skin. Advanced Functional Materials. 2015;25:2138-46.
[85] O'Sullivan BP, Freedman SD. Cystic fibrosis. The Lancet. 2009;373:1891-904.
[86] Feins EN, Lee Y, O'Cearbhaill ED, Vasilyev NV, Shimada S, Friehs I, et al. A growth-accommodating implant for paediatric applications. Nature Biomedical Engineering. 2017;1:818-25.
[87] Jia W, Bandodkar AJ, Valdés-Ramírez G, Windmiller JR, Yang Z, Ramírez J, et al. Electrochemical Tattoo Biosensors for Real-Time Noninvasive Lactate Monitoring in Human Perspiration. Analytical Chemistry. 2013;85:6553-60.
[88] Bandodkar AJ, Molinnus D, Mirza O, Guinovart T, Windmiller JR, Valdés-Ramírez G, et al. Epidermal tattoo potentiometric sodium sensors with wireless signal transduction for continuous non-invasive sweat monitoring. Biosensors and Bioelectronics. 2014;54:603-9.
[89] Parrilla M, Cánovas R, Jeerapan I, Andrade FJ, Wang J. A Textile-Based Stretchable Multi-Ion Potentiometric Sensor. Advanced Healthcare Materials. 2016;5:996-1001.
[90] Kim J, de Araujo WR, Samek IA, Bandodkar AJ, Jia W, Brunetti B, et al. Wearable temporary tattoo sensor for real-time trace metal monitoring in human sweat. Electrochemistry Communications. 2015;51:41-5.
[91] Nyein HYY, Gao W, Shahpar Z, Emaminejad S, Challa S, Chen K, et al. A Wearable Electrochemical Platform for Noninvasive Simultaneous Monitoring of Ca2+ and pH. ACS Nano. 2016;10:7216-24.
[92] Bandodkar AJ, Jeang WJ, Ghaffari R, Rogers JA. Wearable Sensors for Biochemical Sweat Analysis. Annual Review of Analytical Chemistry. 2019;12:1-22.
[93] Yang Y, Gao W. Wearable and flexible electronics for continuous molecular monitoring. Chemical Society Reviews. 2019;48:1465-91.
[94] Gao W, Emaminejad S, Nyein HYY, Challa S, Chen K, Peck A, et al. Fully integrated wearable sensor arrays for multiplexed in situ perspiration analysis. Nature. 2016;529:509.
[95] Koh A, Kang D, Xue Y, Lee S, Pielak RM, Kim J, et al. A soft, wearable microfluidic device for the capture, storage, and colorimetric sensing of sweat. Science Translational Medicine. 2016;8:366ra165.
[96] Bandodkar AJ, Gutruf P, Choi J, Lee K, Sekine Y, Reeder JT, et al. Battery-free, skin-interfaced microfluidic/electronic systems for simultaneous electrochemical, colorimetric, and volumetric analysis of sweat. Science Advances. 2019;5:eaav3294.
[97] Liu Y, Pharr M, Salvatore GA. Lab-on-Skin: A Review of Flexible and Stretchable Electronics for Wearable Health Monitoring. ACS Nano. 2017;11:9614-35.

[98] Jeong J-W, Kim MK, Cheng H, Yeo W-H, Huang X, Liu Y, et al. Capacitive Epidermal Electronics for Electrically Safe, Long-Term Electrophysiological Measurements. Advanced Healthcare Materials. 2014;3:642-8.
[99] Norton JJS, Lee DS, Lee JW, Lee W, Kwon O, Won P, et al. Soft, curved electrode systems capable of integration on the auricle as a persistent brain–computer interface. Proceedings of the National Academy of Sciences. 2015;112:3920.
[100] Fang H, Yu KJ, Gloschat C, Yang Z, Song E, Chiang C-H, et al. Capacitively coupled arrays of multiplexed flexible silicon transistors for long-term cardiac electrophysiology. Nature Biomedical Engineering. 2017;1:0038.
[101] Huang X, Liu Y, Cheng H, Shin W-J, Fan JA, Liu Z, et al. Materials and Designs for Wireless Epidermal Sensors of Hydration and Strain. Advanced Functional Materials. 2014;24:3846-54.
[102] Zhang F, Zang Y, Huang D, Di C-a, Zhu D. Flexible and self-powered temperature–pressure dual-parameter sensors using microstructure-frame-supported organic thermoelectric materials. Nature Communications. 2015;6:8356.
[103] Park J, Kim M, Lee Y, Lee HS, Ko H. Fingertip skin–inspired microstructured ferroelectric skins discriminate static/dynamic pressure and temperature stimuli. Science Advances. 2015;1:e1500661.
[104] Hua Q, Sun J, Liu H, Bao R, Yu R, Zhai J, et al. Skin-inspired highly stretchable and conformable matrix networks for multifunctional sensing. Nature Communications. 2018;9:244.
[105] Jung S, Kim JH, Kim J, Choi S, Lee J, Park I, et al. Reverse-Micelle-Induced Porous Pressure-Sensitive Rubber for Wearable Human–Machine Interfaces. Advanced Materials. 2014;26:4825-30.
[106] Mao Y, Zhao P, McConohy G, Yang H, Tong Y, Wang X. Sponge-Like Piezoelectric Polymer Films for Scalable and Integratable Nanogenerators and Self-Powered Electronic Systems. Advanced Energy Materials. 2014;4:1301624.
[107] Lee KY, Chun J, Lee J-H, Kim KN, Kang N-R, Kim J-Y, et al. Hydrophobic Sponge Structure-Based Triboelectric Nanogenerator. Advanced Materials. 2014;26:5037-42.
[108] Vandeparre H, Watson D, Lacour SP. Extremely robust and conformable capacitive pressure sensors based on flexible polyurethane foams and stretchable metallization. Applied Physics Letters. 2013;103:204103.
[109] Yao H-B, Ge J, Wang C-F, Wang X, Hu W, Zheng Z-J, et al. A Flexible and Highly Pressure-Sensitive Graphene–Polyurethane Sponge Based on Fractured Microstructure Design. Advanced Materials. 2013;25:6692-8.
[110] Jeong YR, Park H, Jin SW, Hong SY, Lee S-S, Ha JS. Highly Stretchable and Sensitive Strain Sensors Using Fragmentized Graphene Foam. Adv Funct Mater. 2015;25:4228-36.
[111] Samad YA, Li Y, Alhassan SM, Liao K. Novel Graphene Foam Composite with Adjustable Sensitivity for Sensor Applications. ACS Applied Materials & Interfaces. 2015;7:9195-202.
[112] Samad YA, Li Y, Schiffer A, Alhassan SM, Liao K. Graphene Foam Developed with a Novel Two-Step Technique for Low and High Strains and Pressure-Sensing Applications. Small. 2015;11:2380-5.
[113] Zhao S, Zhang G, Gao Y, Deng L, Li J, Sun R, et al. Strain-Driven and Ultrasensitive Resistive Sensor/Switch Based on Conductive Alginate/Nitrogen-Doped Carbon-Nanotube-Supported Ag Hybrid Aerogels with Pyramid Design. ACS Applied Materials & Interfaces. 2014;6:22823-9.
[114] He W, Li G, Zhang S, Wei Y, Wang J, Li Q, et al. Polypyrrole/Silver Coaxial Nanowire Aero-Sponges for Temperature-Independent Stress Sensing and Stress-Triggered Joule Heating. ACS Nano. 2015;9:4244-51.
[115] Park J, Lee Y, Hong J, Lee Y, Ha M, Jung Y, et al. Tactile-Direction-Sensitive and Stretchable Electronic Skins Based on Human-Skin-Inspired Interlocked Microstructures. ACS Nano. 2014;8:12020-9.

[116] Pang C, Lee G-Y, Kim T-i, Kim SM, Kim HN, Ahn S-H, et al. A flexible and highly sensitive strain-gauge sensor using reversible interlocking of nanofibres. Nature Materials. 2012;11:795.
[117] Ha M, Lim S, Park J, Um D-S, Lee Y, Ko H. Bioinspired Interlocked and Hierarchical Design of ZnO Nanowire Arrays for Static and Dynamic Pressure-Sensitive Electronic Skins. Advanced Functional Materials. 2015;25:2841-9.
[118] Su B, Gong S, Ma Z, Yap LW, Cheng W. Mimosa-Inspired Design of a Flexible Pressure Sensor with Touch Sensitivity. Small. 2015;11:1886-91.
[119] Wei Y, Chen S, Lin Y, Yang Z, Liu L. Cu-Ag core-shell nanowires for electronic skin with a petal molded microstructure. Journal of Materials Chemistry C. 2015;3:9594-602.
[120] Takei K, Yu Z, Zheng M, Ota H, Takahashi T, Javey A. Highly sensitive electronic whiskers based on patterned carbon nanotube and silver nanoparticle composite films. Proceedings of the National Academy of Sciences. 2014;111:1703.
[121] Harada S, Honda W, Arie T, Akita S, Takei K. Fully Printed, Highly Sensitive Multifunctional Artificial Electronic Whisker Arrays Integrated with Strain and Temperature Sensors. ACS Nano. 2014;8:3921-7.
[122] Reeder JT, Kang T, Rains S, Voit W. 3D, Reconfigurable, Multimodal Electronic Whiskers via Directed Air Assembly. Advanced Materials. 2018;30:1706733.
[123] Kang D, Pikhitsa PV, Choi YW, Lee C, Shin SS, Piao L, et al. Ultrasensitive mechanical crack-based sensor inspired by the spider sensory system. Nature. 2014;516:222.
[124] Pang C, Koo JH, Nguyen A, Caves JM, Kim M-G, Chortos A, et al. Highly Skin-Conformal Microhairy Sensor for Pulse Signal Amplification. Advanced Materials. 2015;27:634-40.
[125] Tee BCK, Chortos A, Dunn RR, Schwartz G, Eason E, Bao Z. Tunable Flexible Pressure Sensors using Microstructured Elastomer Geometries for Intuitive Electronics. Advanced Functional Materials. 2014;24:5427-34.
[126] Choong C-L, Shim M-B, Lee B-S, Jeon S, Ko D-S, Kang T-H, et al. Highly Stretchable Resistive Pressure Sensors Using a Conductive Elastomeric Composite on a Micropyramid Array. Advanced Materials. 2014;26:3451-8.
[127] Dhakar L, Pitchappa P, Tay FEH, Lee C. An intelligent skin based self-powered finger motion sensor integrated with triboelectric nanogenerator. Nano Energy. 2016;19:532-40.
[128] Luo C, Liu N, Zhang H, Liu W, Yue Y, Wang S, et al. A new approach for ultrahigh-performance piezoresistive sensor based on wrinkled PPy film with electrospun PVA nanowires as spacer. Nano Energy. 2017;41:527-34.
[129] Park S-J, Kim J, Chu M, Khine M. Flexible Piezoresistive Pressure Sensor Using Wrinkled Carbon Nanotube Thin Films for Human Physiological Signals. Advanced Materials Technologies. 2018;3:1700158.
[130] Gao Y, Yu G, Tan J, Xuan F. Sandpaper-molded wearable pressure sensor for electronic skins. Sensors and Actuators A: Physical. 2018;280:205-9.
[131] Sun Q-J, Zhuang J, Venkatesh S, Zhou Y, Han S-T, Wu W, et al. Highly Sensitive and Ultrastable Skin Sensors for Biopressure and Bioforce Measurements Based on Hierarchical Microstructures. ACS Applied Materials & Interfaces. 2018;10:4086-94.
[132] Pang Y, Zhang K, Yang Z, Jiang S, Ju Z, Li Y, et al. Epidermis Microstructure Inspired Graphene Pressure Sensor with Random Distributed Spinosum for High Sensitivity and Large Linearity. ACS Nano. 2018;12:2346-54.
[133] Rasel MSU, Park J-Y. A sandpaper assisted micro-structured polydimethylsiloxane fabrication for human skin based triboelectric energy harvesting application. Applied Energy. 2017;206:150-8.
[134] Rogers JA, Someya T, Huang Y. Materials and Mechanics for Stretchable Electronics. Science. 2010;327:1603.

[135] Zhang Y, Huang Y, Rogers JA. Mechanics of stretchable batteries and supercapacitors. Current Opinion in Solid State and Materials Science. 2015;19:190-9.
[136] Khang D-Y, Jiang H, Huang Y, Rogers JA. A Stretchable Form of Single-Crystal Silicon for High-Performance Electronics on Rubber Substrates. Science. 2006;311:208.
[137] Fan JA, Yeo W-H, Su Y, Hattori Y, Lee W, Jung S-Y, et al. Fractal design concepts for stretchable electronics. Nature Communications. 2014;5:3266.
[138] Xu F, Wang X, Zhu Y, Zhu Y. Wavy Ribbons of Carbon Nanotubes for Stretchable Conductors. Advanced Functional Materials. 2012;22:1279-83.
[139] Yu C, Masarapu C, Rong J, Wei B, Jiang H. Stretchable Supercapacitors Based on Buckled Single-Walled Carbon-Nanotube Macrofilms. Advanced Materials. 2009;21:4793-7.
[140] Feng X, Yang BD, Liu Y, Wang Y, Dagdeviren C, Liu Z, et al. Stretchable Ferroelectric Nanoribbons with Wavy Configurations on Elastomeric Substrates. ACS Nano. 2011;5:3326-32.
[141] Xu S, Yan Z, Jang K-I, Huang W, Fu H, Kim J, et al. Assembly of micro/nanomaterials into complex, three-dimensional architectures by compressive buckling. Science. 2015;347:154.
[142] Gao L, Zhang Y, Zhang H, Doshay S, Xie X, Luo H, et al. Optics and Nonlinear Buckling Mechanics in Large-Area, Highly Stretchable Arrays of Plasmonic Nanostructures. ACS Nano. 2015;9:5968-75.
[143] Zhang Y, Xu S, Fu H, Lee J, Su J, Hwang K-C, et al. Buckling in serpentine microstructures and applications in elastomer-supported ultra-stretchable electronics with high areal coverage. Soft Matter. 2013;9:8062-70.
[144] Widlund T, Yang S, Hsu Y-Y, Lu N. Stretchability and compliance of freestanding serpentine-shaped ribbons. International Journal of Solids and Structures. 2014;51:4026-37.
[145] Zhang Y, Wang S, Li X, Fan JA, Xu S, Song YM, et al. Experimental and Theoretical Studies of Serpentine Microstructures Bonded To Prestrained Elastomers for Stretchable Electronics. Adv Funct Mater. 2014;24:2028-37.
[146] Xu R, Jang K-I, Ma Y, Jung HN, Yang Y, Cho M, et al. Fabric-based stretchable electronics with mechanically optimized designs and prestrained composite substrates. Extreme Mechanics Letters. 2014;1:120-6.
[147] Webb RC, Bonifas AP, Behnaz A, Zhang Y, Yu KJ, Cheng H, et al. Ultrathin conformal devices for precise and continuous thermal characterization of human skin. Nature Materials. 2013;12:938.
[148] Son D, Koo JH, Song J-K, Kim J, Lee M, Shim HJ, et al. Stretchable Carbon Nanotube Charge-Trap Floating-Gate Memory and Logic Devices for Wearable Electronics. ACS Nano. 2015;9:5585-93.
[149] Sharma T, Aroom K, Naik S, Gill B, Zhang JXJ. Flexible Thin-Film PVDF-TrFE Based Pressure Sensor for Smart Catheter Applications. Annals of Biomedical Engineering. 2013;41:744-51.
[150] Zhang Y, Fu H, Xu S, Fan JA, Hwang K-C, Jiang J, et al. A hierarchical computational model for stretchable interconnects with fractal-inspired designs. Journal of the Mechanics and Physics of Solids. 2014;72:115-30.
[151] Fu H, Xu S, Xu R, Jiang J, Zhang Y, Rogers JA, et al. Lateral buckling and mechanical stretchability of fractal interconnects partially bonded onto an elastomeric substrate. Applied Physics Letters. 2015;106:091902.
[152] Su Y, Wang S, Huang Y, Luan H, Dong W, Fan JA, et al. Elasticity of Fractal Inspired Interconnects. Small. 2015;11:367-73.
[153] Kim J, Lee M, Shim HJ, Ghaffari R, Cho HR, Son D, et al. Stretchable silicon nanoribbon electronics for skin prosthesis. Nature Communications. 2014;5:5747.
[154] Xu L, Gutbrod SR, Ma Y, Petrossians A, Liu Y, Webb RC, et al. Materials and Fractal Designs for 3D Multifunctional Integumentary Membranes with Capabilities in Cardiac Electrotherapy. Advanced Materials. 2015;27:1731-7.

[155] Lv C, Yu H, Jiang H. Archimedean spiral design for extremely stretchable interconnects. Extreme Mechanics Letters. 2014;1:29-34.
[156] Jang K-I, Chung HU, Xu S, Lee CH, Luan H, Jeong J, et al. Soft network composite materials with deterministic and bio-inspired designs. Nature Communications. 2015;6:6566.
[157] Lee CH, Ma Y, Jang K-I, Banks A, Pan T, Feng X, et al. Soft Core/Shell Packages for Stretchable Electronics. Advanced Functional Materials. 2015;25:3698-704.
[158] Lanzara G, Salowitz N, Guo Z, Chang F-K. A Spider-Web-Like Highly Expandable Sensor Network for Multifunctional Materials. Advanced Materials. 2010;22:4643-8.
[159] Yang P-K, Lin L, Yi F, Li X, Pradel KC, Zi Y, et al. A Flexible, Stretchable and Shape-Adaptive Approach for Versatile Energy Conversion and Self-Powered Biomedical Monitoring. Advanced Materials. 2015;27:3817-24.
[160] Trung TQ, Lee N-E. Recent Progress on Stretchable Electronic Devices with Intrinsically Stretchable Components. Advanced Materials. 2017;29:1603167.
[161] Dickey MD, Chiechi RC, Larsen RJ, Weiss EA, Weitz DA, Whitesides GM. Eutectic Gallium-Indium (EGaIn): A Liquid Metal Alloy for the Formation of Stable Structures in Microchannels at Room Temperature. Advanced Functional Materials. 2008;18:1097-104.
[162] Boley JW, White EL, Kramer RK. Mechanically Sintered Gallium–Indium Nanoparticles. Advanced Materials. 2015;27:2355-60.
[163] Yoon J, Hong SY, Lim Y, Lee S-J, Zi G, Ha JS. Design and Fabrication of Novel Stretchable Device Arrays on a Deformable Polymer Substrate with Embedded Liquid-Metal Interconnections. Advanced Materials. 2014;26:6580-6.
[164] Overvelde JTB, Mengüç Y, Polygerinos P, Wang Y, Wang Z, Walsh CJ, et al. Mechanical and electrical numerical analysis of soft liquid-embedded deformation sensors analysis. Extreme Mechanics Letters. 2014;1:42-6.
[165] Matsuzaki R, Tabayashi K. Highly Stretchable, Global, and Distributed Local Strain Sensing Line Using GaInSn Electrodes for Wearable Electronics. Advanced Functional Materials. 2015;25:3806-13.
[166] Ota H, Chen K, Lin Y, Kiriya D, Shiraki H, Yu Z, et al. Highly deformable liquid-state heterojunction sensors. Nature Communications. 2014;5:5032.
[167] An BW, Hyun BG, Kim S-Y, Kim M, Lee M-S, Lee K, et al. Stretchable and Transparent Electrodes using Hybrid Structures of Graphene–Metal Nanotrough Networks with High Performances and Ultimate Uniformity. Nano Letters. 2014;14:6322-8.
[168] Kim KS, Zhao Y, Jang H, Lee SY, Kim JM, Kim KS, et al. Large-scale pattern growth of graphene films for stretchable transparent electrodes. Nature. 2009;457:706.
[169] Cheng T, Zhang Y-Z, Lai W-Y, Chen Y, Zeng W-J, Huang W. High-performance stretchable transparent electrodes based on silver nanowires synthesized via an eco-friendly halogen-free method. Journal of Materials Chemistry C. 2014;2:10369-76.
[170] Yamada T, Hayamizu Y, Yamamoto Y, Yomogida Y, Izadi-Najafabadi A, Futaba DN, et al. A stretchable carbon nanotube strain sensor for human-motion detection. Nature Nanotechnology. 2011;6:296.
[171] Roh E, Hwang B-U, Kim D, Kim B-Y, Lee N-E. Stretchable, Transparent, Ultrasensitive, and Patchable Strain Sensor for Human–Machine Interfaces Comprising a Nanohybrid of Carbon Nanotubes and Conductive Elastomers. ACS Nano. 2015;9:6252-61.
[172] Amjadi M, Pichitpajongkit A, Lee S, Ryu S, Park I. Highly Stretchable and Sensitive Strain Sensor Based on Silver Nanowire–Elastomer Nanocomposite. ACS Nano. 2014;8:5154-63.
[173] Han S, Hong S, Ham J, Yeo J, Lee J, Kang B, et al. Fast Plasmonic Laser Nanowelding for a Cu-Nanowire Percolation Network for Flexible Transparent Conductors and Stretchable Electronics. Advanced Materials. 2014;26:5808-14.
[174] Hu W, Wang R, Lu Y, Pei Q. An elastomeric transparent composite electrode based on copper nanowires and polyurethane. Journal of Materials Chemistry C. 2014;2:1298-305.

[175] Savagatrup S, Printz AD, O'Connor TF, Zaretski AV, Lipomi DJ. Molecularly Stretchable Electronics. Chemistry of Materials. 2014;26:3028-41.
[176] Savagatrup S, Printz AD, Rodriquez D, Lipomi DJ. Best of Both Worlds: Conjugated Polymers Exhibiting Good Photovoltaic Behavior and High Tensile Elasticity. Macromolecules. 2014;47:1981-92.
[177] Libanori R, Erb RM, Reiser A, Le Ferrand H, Süess MJ, Spolenak R, et al. Stretchable heterogeneous composites with extreme mechanical gradients. Nature Communications. 2012;3:1265.
[178] Xu S, Zhang Y, Jia L, Mathewson KE, Jang K-I, Kim J, et al. Soft Microfluidic Assemblies of Sensors, Circuits, and Radios for the Skin. Science. 2014;344:70.
[179] Liang J, Li L, Niu X, Yu Z, Pei Q. Elastomeric polymer light-emitting devices and displays. Nature Photonics. 2013;7:817.
[180] Wang J, Yan C, Chee KJ, Lee PS. Highly Stretchable and Self-Deformable Alternating Current Electroluminescent Devices. Advanced Materials. 2015;27:2876-82.
[181] Wang S, Xu J, Wang W, Wang G-JN, Rastak R, Molina-Lopez F, et al. Skin electronics from scalable fabrication of an intrinsically stretchable transistor array. Nature. 2018;555:83.
[182] Oh JY, Rondeau-Gagné S, Chiu Y-C, Chortos A, Lissel F, Wang G-JN, et al. Intrinsically stretchable and healable semiconducting polymer for organic transistors. Nature. 2016;539:411.
[183] Yanju L, Haiyang D, Liwu L, Jinsong L. Shape memory polymers and their composites in aerospace applications: a review. Smart Materials and Structures. 2014;23:023001.
[184] Wang J, Yan C, Kang W, Lee PS. High-efficiency transfer of percolating nanowire films for stretchable and transparent photodetectors. Nanoscale. 2014;6:10734-9.
[185] Kettlgruber G, Kaltenbrunner M, Siket CM, Moser R, Graz IM, Schwödiauer R, et al. Intrinsically stretchable and rechargeable batteries for self-powered stretchable electronics. Journal of Materials Chemistry A. 2013;1:5505-8.
[186] Song L, Myers AC, Adams JJ, Zhu Y. Stretchable and Reversibly Deformable Radio Frequency Antennas Based on Silver Nanowires. ACS Applied Materials & Interfaces. 2014;6:4248-53.
[187] Hong S, Lee H, Lee J, Kwon J, Han S, Suh YD, et al. Highly Stretchable and Transparent Metal Nanowire Heater for Wearable Electronics Applications. Advanced Materials. 2015;27:4744-51.
[188] Kassal P, Steinberg MD, Steinberg IM. Wireless chemical sensors and biosensors: A review. Sensors and Actuators B: Chemical. 2018;266:228-45.
[189] Kim J, Salvatore GA, Araki H, Chiarelli AM, Xie Z, Banks A, et al. Battery-free, stretchable optoelectronic systems for wireless optical characterization of the skin. Science Advances. 2016;2:e1600418.
[190] Kim J, Gutruf P, Chiarelli AM, Heo SY, Cho K, Xie Z, et al. Miniaturized Battery-Free Wireless Systems for Wearable Pulse Oximetry. Adv Funct Mater. 2017;27:1604373.
[191] Kang S-K, Murphy RKJ, Hwang S-W, Lee SM, Harburg DV, Krueger NA, et al. Bioresorbable silicon electronic sensors for the brain. Nature. 2016;530:71.
[192] Shin G, Gomez AM, Al-Hasani R, Jeong YR, Kim J, Xie Z, et al. Flexible Near-Field Wireless Optoelectronics as Subdermal Implants for Broad Applications in Optogenetics. Neuron. 2017;93:509-21.e3.
[193] Lee CH, Jeong J-W, Liu Y, Zhang Y, Shi Y, Kang S-K, et al. Materials and Wireless Microfluidic Systems for Electronics Capable of Chemical Dissolution on Demand. Advanced Functional Materials. 2015;25:1338-43.
[194] Han S, Kim J, Won SM, Ma Y, Kang D, Xie Z, et al. Battery-free, wireless sensors for full-body pressure and temperature mapping. Science Translational Medicine. 2018;10:eaan4950.
[195] Krishnan SR, Su C-J, Xie Z, Patel M, Madhvapathy SR, Xu Y, et al. Wireless, Battery-Free Epidermal Electronics for Continuous, Quantitative, Multimodal Thermal Characterization of Skin. Small. 2018;14:1803192.

[196] Kim J, Imani S, de Araujo WR, Warchall J, Valdés-Ramírez G, Paixão TRLC, et al. Wearable salivary uric acid mouthguard biosensor with integrated wireless electronics. Biosensors and Bioelectronics. 2015;74:1061-8.
[197] Lee Y, Howe C, Mishra S, Lee DS, Mahmood M, Piper M, et al. Wireless, intraoral hybrid electronics for real-time quantification of sodium intake toward hypertension management. Proceedings of the National Academy of Sciences. 2018;115:5377.
[198] Krishnan SR, Ray TR, Ayer AB, Ma Y, Gutruf P, Lee K, et al. Epidermal electronics for noninvasive, wireless, quantitative assessment of ventricular shunt function in patients with hydrocephalus. Science Translational Medicine. 2018;10:eaat8437.
[199] Jang K-I, Li K, Chung HU, Xu S, Jung HN, Yang Y, et al. Self-assembled three dimensional network designs for soft electronics. Nature Communications. 2017;8:15894.
[200] Chung HU, Kim BH, Lee JY, Lee J, Xie Z, Ibler EM, et al. Binodal, wireless epidermal electronic systems with in-sensor analytics for neonatal intensive care. Science. 2019;363:eaau0780.
[201] Pu X, Liu M, Chen X, Sun J, Du C, Zhang Y, et al. Ultrastretchable, transparent triboelectric nanogenerator as electronic skin for biomechanical energy harvesting and tactile sensing. Science Advances. 2017;3:e1700015.
[202] Lai Y-C, Deng J, Liu R, Hsiao Y-C, Zhang SL, Peng W, et al. Actively Perceiving and Responsive Soft Robots Enabled by Self-Powered, Highly Extensible, and Highly Sensitive Triboelectric Proximity- and Pressure-Sensing Skins. Advanced Materials. 2018;30:1801114.
[203] Nan K, Kang SD, Li K, Yu KJ, Zhu F, Wang J, et al. Compliant and stretchable thermoelectric coils for energy harvesting in miniature flexible devices. Science Advances. 2018;4:eaau5849.
[204] Bandodkar AJ, Wang J. Wearable Biofuel Cells: A Review. Electroanalysis. 2016;28:1188-200.
[205] Jia W, Valdés-Ramírez G, Bandodkar AJ, Windmiller JR, Wang J. Epidermal Biofuel Cells: Energy Harvesting from Human Perspiration. Angewandte Chemie International Edition. 2013;52:7233-6.
[206] Bandodkar AJ, You J-M, Kim N-H, Gu Y, Kumar R, Mohan AMV, et al. Soft, stretchable, high power density electronic skin-based biofuel cells for scavenging energy from human sweat. Energy & Environmental Science. 2017;10:1581-9.
[207] Jeerapan I, Sempionatto JR, Pavinatto A, You J-M, Wang J. Stretchable biofuel cells as wearable textile-based self-powered sensors. Journal of Materials Chemistry A. 2016;4:18342-53.
[208] Jia W, Wang X, Imani S, Bandodkar AJ, Ramírez J, Mercier PP, et al. Wearable textile biofuel cells for powering electronics. Journal of Materials Chemistry A. 2014;2:18184-9.
[209] Zadpoor AA. Mechanical meta-materials. Materials Horizons. 2016;3:371-81.
[210] Kolken HMA, Zadpoor AA. Auxetic mechanical metamaterials. RSC Advances. 2017;7:5111-29.
[211] Mirzaali MJ, Hedayati R, Vena P, Vergani L, Strano M, Zadpoor AA. Rational design of soft mechanical metamaterials: Independent tailoring of elastic properties with randomness. Applied Physics Letters. 2017;111:051903.
[212] Mirzaali MJ, Caracciolo A, Pahlavani H, Janbaz S, Vergani L, Zadpoor AA. Multi-material 3D printed mechanical metamaterials: Rational design of elastic properties through spatial distribution of hard and soft phases. Applied Physics Letters. 2018;113:241903.
[213] Mirzaali MJ, Janbaz S, Strano M, Vergani L, Zadpoor AA. Shape-matching soft mechanical metamaterials. Scientific Reports. 2018;8:965.
[214] Kolken HMA, Janbaz S, Leeflang SMA, Lietaert K, Weinans HH, Zadpoor AA. Rationally designed meta-implants: a combination of auxetic and conventional meta-biomaterials. Materials Horizons. 2018;5:28-35.

[215] Jiang Y, Liu Z, Matsuhisa N, Qi D, Leow WR, Yang H, et al. Auxetic Mechanical Metamaterials to Enhance Sensitivity of Stretchable Strain Sensors. Advanced Materials. 2018;30:1706589.
[216] Bertoldi K, Vitelli V, Christensen J, van Hecke M. Flexible mechanical metamaterials. Nature Reviews Materials. 2017;2:17066.
[217] Callens SJP, Zadpoor AA. From flat sheets to curved geometries: Origami and kirigami approaches. Materials Today. 2018;21:241-64.
[218] Shyu TC, Damasceno PF, Dodd PM, Lamoureux A, Xu L, Shlian M, et al. A kirigami approach to engineering elasticity in nanocomposites through patterned defects. Nature Materials. 2015;14:785.
[219] Lyu J, Hammig MD, Liu L, Xu L, Chi H, Uher C, et al. Stretchable conductors by kirigami patterning of aramid-silver nanocomposites with zero conductance gradient. Applied Physics Letters. 2017;111:161901.
[220] Guo H, Yeh M-H, Lai Y-C, Zi Y, Wu C, Wen Z, et al. All-in-One Shape-Adaptive Self-Charging Power Package for Wearable Electronics. ACS Nano. 2016;10:10580-8.
[221] Lamoureux A, Lee K, Shlian M, Forrest SR, Shtein M. Dynamic kirigami structures for integrated solar tracking. Nature Communications. 2015;6:8092.
[222] Wang W, Li C, Rodrigue H, Yuan F, Han M-W, Cho M, et al. Kirigami/Origami-Based Soft Deployable Reflector for Optical Beam Steering. Advanced Functional Materials. 2017;27:1604214.
[223] Tang Y, Lin G, Yang S, Yi YK, Kamien RD, Yin J. Programmable Kiri-Kirigami Metamaterials. Advanced Materials. 2017;29:1604262.
[224] Morikawa Y, Yamagiwa S, Sawahata H, Numano R, Koida K, Ishida M, et al. Ultrastretchable Kirigami Bioprobes. Advanced Healthcare Materials. 2018;7:1701100.
[225] Blees MK, Barnard AW, Rose PA, Roberts SP, McGill KL, Huang PY, et al. Graphene kirigami. Nature. 2015;524:204.
[226] Zhang Y, Yan Z, Nan K, Xiao D, Liu Y, Luan H, et al. A mechanically driven form of Kirigami as a route to 3D mesostructures in micro/nanomembranes. Proceedings of the National Academy of Sciences. 2015;112:11757.
[227] Cho Y, Park JB, Kim B-S, Lee J, Hong W-K, Park I-K, et al. Enhanced energy harvesting based on surface morphology engineering of P(VDF-TrFE) film. Nano Energy. 2015;16:524-32.
[228] Zheng Q, Shi B, Li Z, Wang ZL. Recent Progress on Piezoelectric and Triboelectric Energy Harvesters in Biomedical Systems. Advanced Science. 2017;4:1700029.
[229] Wang ZL, Song J. Piezoelectric Nanogenerators Based on Zinc Oxide Nanowire Arrays. Science. 2006;312:242.
[230] Xu S, Qin Y, Xu C, Wei Y, Yang R, Wang ZL. Self-powered nanowire devices. Nature Nanotechnology. 2010;5:366.
[231] Yu Y, Sun H, Orbay H, Chen F, England CG, Cai W, et al. Biocompatibility and in vivo operation of implantable mesoporous PVDF-based nanogenerators. Nano Energy. 2016;27:275-81.
[232] Fu J, Hou Y, Zheng M, Wei Q, Zhu M, Yan H. Improving Dielectric Properties of PVDF Composites by Employing Surface Modified Strong Polarized BaTiO3 Particles Derived by Molten Salt Method. ACS Applied Materials & Interfaces. 2015;7:24480-91.
[233] Lund A, Gustafsson C, Bertilsson H, Rychwalski RW. Enhancement of β phase crystals formation with the use of nanofillers in PVDF films and fibres. Composites Science and Technology. 2011;71:222-9.
[234] Yang L, Ji H, Zhu K, Wang J, Qiu J. Dramatically improved piezoelectric properties of poly(vinylidene fluoride) composites by incorporating aligned TiO2@MWCNTs. Composites Science and Technology. 2016;123:259-67.
[235] Xu L, Shyu TC, Kotov NA. Origami and Kirigami Nanocomposites. ACS Nano. 2017;11:7587-99.

[236] Tang Y, Yin J. Design of cut unit geometry in hierarchical kirigami-based auxetic metamaterials for high stretchability and compressibility. Extreme Mechanics Letters. 2017;12:77-85.
[237] Tang Y, Lin G, Han L, Qiu S, Yang S, Yin J. Design of Hierarchically Cut Hinges for Highly Stretchable and Reconfigurable Metamaterials with Enhanced Strength. Advanced Materials. 2015;27:7181-90.
[238] Cho Y, Shin J-H, Costa A, Kim TA, Kunin V, Li J, et al. Engineering the shape and structure of materials by fractal cut. Proceedings of the National Academy of Sciences. 2014;111:17390.
[239] Rafsanjani A, Bertoldi K. Buckling-Induced Kirigami. Physical Review Letters. 2017;118:084301.
[240] Isobe M, Okumura K. Initial rigid response and softening transition of highly stretchable kirigami sheet materials. Scientific Reports. 2016;6:24758.
[241] Han T, Scarpa F, Allan NL. Super stretchable hexagonal boron nitride Kirigami. Thin Solid Films. 2017;632:35-43.
[242] Wang Z, Zhang L, Duan S, Jiang H, Shen J, Li C. Kirigami-patterned highly stretchable conductors from flexible carbon nanotube-embedded polymer films. Journal of Materials Chemistry C. 2017;5:8714-22.
[243] Dias MA, McCarron MP, Rayneau-Kirkhope D, Hanakata PZ, Campbell DK, Park HS, et al. Kirigami actuators. Soft Matter. 2017;13:9087-92.
[244] Song Z, Wang X, Lv C, An Y, Liang M, Ma T, et al. Kirigami-based stretchable lithium-ion batteries. Scientific Reports. 2015;5:10988.
[245] Rossiter JM, Stoimenov BL, Mukai T. A linear actuator from a single ionic polymer-metal composite (IPMC) strip: SPIE; 2007.
[246] Kim D-H, Lu N, Ma R, Kim Y-S, Kim R-H, Wang S, et al. Epidermal Electronics. Science. 2011;333:838.
[247] Son D, Lee J, Qiao S, Ghaffari R, Kim J, Lee JE, et al. Multifunctional wearable devices for diagnosis and therapy of movement disorders. Nature Nanotechnology. 2014;9:397.
[248] Xu J, Wang S, Wang G-JN, Zhu C, Luo S, Jin L, et al. Highly stretchable polymer semiconductor films through the nanoconfinement effect. Science. 2017;355:59.
[249] Lipomi DJ, Vosgueritchian M, Tee BCK, Hellstrom SL, Lee JA, Fox CH, et al. Skin-like pressure and strain sensors based on transparent elastic films of carbon nanotubes. Nature Nanotechnology. 2011;6:788.
[250] Someya T, Kato Y, Sekitani T, Iba S, Noguchi Y, Murase Y, et al. Conformable, flexible, large-area networks of pressure and thermal sensors with organic transistor active matrixes. Proceedings of the National Academy of Sciences of the United States of America. 2005;102:12321.
[251] Kim D-H, Song J, Choi WM, Kim H-S, Kim R-H, Liu Z, et al. Materials and noncoplanar mesh designs for integrated circuits with linear elastic responses to extreme mechanical deformations. Proceedings of the National Academy of Sciences. 2008;105:18675.
[252] Lu N, Lu C, Yang S, Rogers J. Highly Sensitive Skin-Mountable Strain Gauges Based Entirely on Elastomers. Advanced Functional Materials. 2012;22:4044-50.
[253] Han D, Pal S, Liu Y, Yan H. Folding and cutting DNA into reconfigurable topological nanostructures. Nature Nanotechnology. 2010;5:712.
[254] Wang X, Guo X, Ye J, Zheng N, Kohli P, Choi D, et al. Freestanding 3D Mesostructures, Functional Devices, and Shape-Programmable Systems Based on Mechanically Induced Assembly with Shape Memory Polymers. Advanced Materials. 2019;31:1805615.
[255] Neville RM, Scarpa F, Pirrera A. Shape morphing Kirigami mechanical metamaterials. Scientific Reports. 2016;6:31067.

[256] Sun R, Zhang B, Yang L, Zhang W, Farrow I, Scarpa F, et al. Kirigami stretchable strain sensors with enhanced piezoelectricity induced by topological electrodes. Applied Physics Letters. 2018;112:251904.
[257] Proto A, Penhaker M, Conforto S, Schmid M. Nanogenerators for Human Body Energy Harvesting. Trends in Biotechnology. 2017;35:610-24.
[258] Dagdeviren C, Li Z, Wang ZL. Energy Harvesting from the Animal/Human Body for Self-Powered Electronics. Annual Review of Biomedical Engineering. 2017;19:85-108.
[259] Zhang H, Zhang X-S, Cheng X, Liu Y, Han M, Xue X, et al. A flexible and implantable piezoelectric generator harvesting energy from the pulsation of ascending aorta: in vitro and in vivo studies. Nano Energy. 2015;12:296-304.
[260] Xu B, Lin X, Li W, Wang Z, Zhang W, Shi P. Cell Generator: A Self-Sustaining Biohybrid System Based on Energy Harvesting from Engineered Cardiac Microtissues. Advanced Functional Materials. 2017;27:1606169.
[261] Zheng Q, Zhang H, Shi B, Xue X, Liu Z, Jin Y, et al. In Vivo Self-Powered Wireless Cardiac Monitoring via Implantable Triboelectric Nanogenerator. ACS Nano. 2016;10:6510-8.
[262] Ma Y, Zheng Q, Liu Y, Shi B, Xue X, Ji W, et al. Self-Powered, One-Stop, and Multifunctional Implantable Triboelectric Active Sensor for Real-Time Biomedical Monitoring. Nano Letters. 2016;16:6042-51.
[263] Zheng Q, Shi B, Fan F, Wang X, Yan L, Yuan W, et al. In Vivo Powering of Pacemaker by Breathing-Driven Implanted Triboelectric Nanogenerator. Advanced Materials. 2014;26:5851-6.
[264] Kim SH, Moon J-H, Kim JH, Jeong SM, Lee S-H. Flexible, stretchable and implantable PDMS encapsulated cable for implantable medical device. Biomedical Engineering Letters. 2011;1:199.
[265] Hewage TAM, Alderson KL, Alderson A, Scarpa F. Double-Negative Mechanical Metamaterials Displaying Simultaneous Negative Stiffness and Negative Poisson's Ratio Properties. Advanced Materials. 2016;28:10323-32.
[266] Boatti E, Vasios N, Bertoldi K. Origami Metamaterials for Tunable Thermal Expansion. Advanced Materials. 2017;29:1700360.
[267] Nicolaou ZG, Motter AE. Mechanical metamaterials with negative compressibility transitions. Nature Materials. 2012;11:608.
[268] Frenzel T, Kadic M, Wegener M. Three-dimensional mechanical metamaterials with a twist. Science. 2017;358:1072.
[269] Chen Y, Li T, Scarpa F, Wang L. Lattice Metamaterials with Mechanically Tunable Poisson's Ratio for Vibration Control. Physical Review Applied. 2017;7:024012.
[270] Bückmann T, Thiel M, Kadic M, Schittny R, Wegener M. An elasto-mechanical unfeelability cloak made of pentamode metamaterials. Nature Communications. 2014;5:4130.
[271] Taghavi M, Helps T, Rossiter J. Electro-ribbon actuators and electro-origami robots. Science Robotics. 2018;3:eaau9795.
[272] Babaee S, Overvelde JTB, Chen ER, Tournat V, Bertoldi K. Reconfigurable origami-inspired acoustic waveguides. Science Advances. 2016;2:e1601019.
[273] Tang R, Huang H, Tu H, Liang H, Liang M, Song Z, et al. Origami-enabled deformable silicon solar cells. Applied Physics Letters. 2014;104:083501.
[274] Kim T, Price JS, Grede A, Lee S, Choi G, Guan W, et al. Kirigami-Inspired 3D Organic Light-Emitting Diode (OLED) Lighting Concepts. Advanced Materials Technologies. 2018;3:1800067.
[275] Rafsanjani A, Zhang Y, Liu B, Rubinstein SM, Bertoldi K. Kirigami skins make a simple soft actuator crawl. Science Robotics. 2018;3:eaar7555.
[276] Hwang D-G, Trent K, Bartlett MD. Kirigami-Inspired Structures for Smart Adhesion. ACS Appl Mater Interfaces. 2018;10:6747-54.
[277] Zhao R, Lin S, Yuk H, Zhao X. Kirigami enhances film adhesion. Soft Matter. 2018;14:2515-25.

[278] Yang C, Zhang H, Liu Y, Yu Z, Wei X, Hu Y. Kirigami-Inspired Deformable 3D Structures Conformable to Curved Biological Surface. Advanced Science. 2018;5:1801070.
[279] Wu C, Wang X, Lin L, Guo H, Wang ZL. Paper-Based Triboelectric Nanogenerators Made of Stretchable Interlocking Kirigami Patterns. ACS Nano. 2016;10:4652-9.
[280] Liu Z, Du H, Li J, Lu L, Li Z-Y, Fang NX. Nano-kirigami with giant optical chirality. Science Advances. 2018;4:eaat4436.
[281] Hedayati R, Mirzaali MJ, Vergani L, Zadpoor AA. Action-at-a-distance metamaterials: Distributed local actuation through far-field global forces. APL Mater. 2018;6:036101.
[282] Hwang D-G, Bartlett MD. Tunable Mechanical Metamaterials through Hybrid Kirigami Structures. Scientific Reports. 2018;8:3378.
[283] Shi B, Li Z, Fan Y. Implantable Energy-Harvesting Devices. Advanced Materials. 2018;30:1801511.
[284] Shaikh FK, Zeadally S. Energy harvesting in wireless sensor networks: A comprehensive review. Renewable and Sustainable Energy Reviews. 2016;55:1041-54.
[285] Wang J, Li S, Yi F, Zi Y, Lin J, Wang X, et al. Sustainably powering wearable electronics solely by biomechanical energy. Nature Communications. 2016;7:12744.
[286] Lee H, Choi TK, Lee YB, Cho HR, Ghaffari R, Wang L, et al. A graphene-based electrochemical device with thermoresponsive microneedles for diabetes monitoring and therapy. Nature Nanotechnology. 2016;11:566.
[287] Le T, Mayaram K, Fiez T. Efficient Far-Field Radio Frequency Energy Harvesting for Passively Powered Sensor Networks. IEEE Journal of Solid-State Circuits. 2008;43:1287-302.
[288] Scholes GD, Fleming GR, Olaya-Castro A, van Grondelle R. Lessons from nature about solar light harvesting. Nature Chemistry. 2011;3:763.
[289] Wei C, Jing X. A comprehensive review on vibration energy harvesting: Modelling and realization. Renewable and Sustainable Energy Reviews. 2017;74:1-18.
[290] Beeby SP, Torah RN, Tudor MJ, Glynne-Jones P, O'Donnell T, Saha CR, et al. A micro electromagnetic generator for vibration energy harvesting. Journal of Micromechanics and Microengineering. 2007;17:1257-65.
[291] Mitcheson PD, Miao P, Stark BH, Yeatman EM, Holmes AS, Green TC. MEMS electrostatic micropower generator for low frequency operation. Sensors and Actuators A: Physical. 2004;115:523-9.
[292] Toprak A, Tigli O. Piezoelectric energy harvesting: State-of-the-art and challenges. Applied Physics Reviews. 2014;1:031104.
[293] Priya S. Advances in energy harvesting using low profile piezoelectric transducers. Journal of Electroceramics. 2007;19:167-84.
[294] Erturk A, Inman DJ. An experimentally validated bimorph cantilever model for piezoelectric energy harvesting from base excitations. Smart Materials and Structures. 2009;18:025009.
[295] Tang L, Yang Y, Soh CK. Toward Broadband Vibration-based Energy Harvesting. Journal of Intelligent Material Systems and Structures. 2010;21:1867-97.
[296] Lu Q, Scarpa F, Liu L, Leng J, Liu Y. An E-shape broadband piezoelectric energy harvester induced by magnets. Journal of Intelligent Material Systems and Structures. 2018;29:2477-91.
[297] Song H-C, Kumar P, Sriramdas R, Lee H, Sharpes N, Kang M-G, et al. Broadband dual phase energy harvester: Vibration and magnetic field. Applied Energy. 2018;225:1132-42.
[298] Zou H-X, Zhang W-M, Li W-B, Wei K-X, Hu K-M, Peng Z-K, et al. Magnetically coupled flextensional transducer for wideband vibration energy harvesting: Design, modeling and experiments. Journal of Sound and Vibration. 2018;416:55-79.
[299] Sun S, Tse PW. Modeling of a horizontal asymmetric U-shaped vibration-based piezoelectric energy harvester (U-VPEH). Mechanical Systems and Signal Processing. 2019;114:467-85.

[300] Sun S, Tse PW. Design and performance of a multimodal vibration-based energy harvester model for machine rotational frequencies. Applied Physics Letters. 2017;110:243902.
[301] Deng H, Du Y, Wang Z, Zhang J, Ma M, Zhong X. A multimodal and multidirectional vibrational energy harvester using a double-branched beam. Applied Physics Letters. 2018;112:213901.
[302] Kim I-H, Jung H-J, Lee BM, Jang S-J. Broadband energy-harvesting using a two degree-of-freedom vibrating body. Applied Physics Letters. 2011;98:214102.
[303] Wu Y, Qiu J, Zhou S, Ji H, Chen Y, Li S. A piezoelectric spring pendulum oscillator used for multi-directional and ultra-low frequency vibration energy harvesting. Applied Energy. 2018;231:600-14.
[304] Toyabur RM, Salauddin M, Cho H, Park JY. A multimodal hybrid energy harvester based on piezoelectric-electromagnetic mechanisms for low-frequency ambient vibrations. Energy Conversion and Management. 2018;168:454-66.
[305] Deng H, Wang Z, Du Y, Zhang J, Ma M, Zhong X. A seesaw-type approach for enhancing nonlinear energy harvesting. Applied Physics Letters. 2018;112:213902.
[306] He Q, Dong C, Li K, Wang J, Xu D, Li X. A multiple energy-harvester combination for pattern-recognizable power-free wireless sensing to vibration event. Sensors and Actuators A: Physical. 2018;279:229-39.
[307] Ning X, Yu X, Wang H, Sun R, Corman RE, Li H, et al. Mechanically active materials in three-dimensional mesostructures. Science Advances. 2018;4:eaat8313.
[308] Nan K, Wang H, Ning X, Miller KA, Wei C, Liu Y, et al. Soft Three-Dimensional Microscale Vibratory Platforms for Characterization of Nano-Thin Polymer Films. ACS Nano. 2019;13:449-57.
[309] Ning X, Wang H, Yu X, Soares JANT, Yan Z, Nan K, et al. 3D Tunable, Multiscale, and Multistable Vibrational Micro-Platforms Assembled by Compressive Buckling. Advanced Functional Materials. 2017;27:1605914.